Porosity of Concrete

Morphological Study of Model Concrete

Porosity of Concrete
Morphological Study of Model Concrete

Proefschrift

ter verkrijging van de graad van doctor
aan de Technische Universiteit Delft,
op gezag van de Rector Magnificus prof.dr.ir. J.T. Fokkema,
voorzitter van het College voor Promoties,
in het openbaar te verdedigen
op maandag 15 november 2004 om 10:30 uur
door

Jing HU

Master of Engineering aan de Wuhan University of Technology
geboren te Danjiangkou, Hubei Province, P.R. China

Dit proefschrift is goedgekeurd door de promotor:
Prof.dr.ir. Ch.F. Hendriks

Samenstelling promotiecommissie

Rector Magnificus	Voorzitter
Prof.dr.ir. Ch. F. Hendriks	Technische Universiteit Delft, promotor
Prof.dr.ir. R. de Borst	Technische Universiteit Delft
Prof. P.J.M. Bartos	University of Paisley, UK
Prof.dr.ir. M.G.D. Geers	Technische Universiteit Eindhoven
Prof. K.L. Scrivener	École Polytechnique Fédérale de Lausanne, Switzerland
Prof.dr.ir. P. Stroeven	Technische Universiteit Delft Hoogleraar: Northern Jiaotong University, China
Dr.ir. L.J. Sluys	Technische Universiteit Delft

Prof.dr.ir. P. Stroeven heeft als begeleider in belangrijke mate aan de totstandkoming van het proefschrift bijgedragen.

Published and distributed by: OPTIMA Grafische Communicatie

ISBN 90-77595-99-6

Keywords: cement permeability, mathematical morphology, pore structure, quantitative image analysis, SPACE system, stereological theory.

Printed in the Netherlands

Acknowledgements

The research project reported in this thesis forms an integral part of the cooperation program 'Technology of Modern Concrete Composites', conducted by Delft University of Technology and three universities in China, among which my home-institute Wuhan University of Technology. Financial support is partly provided by the Royal Netherlands Academy of Arts and Sciences (KNAW). This support is gratefully acknowledged. This study is carried out partly in the Materials Science and Sustainable Construction Section and partly in the Structural Mechanics Section at the Faculty of Civil Engineering and Geosciences, Delft University of Technology.

I am grateful to my promotor, Prof.dr.ir. Ch.F. Hendriks for his support and guidance during my study. In particular, I would like to express my sincere gratitude to my supervisor, Prof.dr.ir. P. Stroeven, who gave me the chance to study at TUDelft and offered me the valuable encouragement, inspiring discussions and continuous support throughout the whole period of four years. I am deeply moved by his active involvement in international science cooperation, his enthusiastic approach to scientific research and optimistic attitude towards life. I cherish our friendship, and highly appreciate the interesting social communications and his patient help in my language study. I am obliged to Prof. D. Jeulin (Centre de Morphologie Mathématique, École des Mines de Paris) for providing me the opportunity to follow the courses 'Models of Random Structures' and 'Mathematical Morphology' and to use the software Micromorph for mathematical morphological measurements. I am also grateful to Prof.dr.ir. K. van Breugel for initiating cooperation research between the author and his former Ph.D. student, Dr. G. Ye. In addition, I would like to thank Dr. L.J. Sluys for his comments and suggestions about the manuscript.

My special thanks go to Dr. G. Ye (Ghent University) for his valuable cooperation and instructive discussions during my study, for his consent to use some of his microscopic images of cement pastes for this study, and for his positive attitude in getting me acquainted with and applying the OPTIMAS software for image analysis. I would like to thank Dr. H. Chen for providing the packing structure of model cements generated by the SPACE system, and for his significant contributions to the interesting joint publications. I wish to thank Dr. M. Stroeven for his assistance to get familiar with the SPACE system, and his support at finding solutions for specific problems. I am also grateful to Ir. Z. Guo for his encouragement and help. Also, I would like to thank all staff members of the Materials Science and Sustainable Construction Section, and of the Structural Mechanics Section, as well as my Chinese friends in Delft for their cooperation and support during my stay.

Sincere gratitude is also given to the CICAT staff members, Drs. P. Althuis, Mr. D. Jellema and Ms. T. Olsder for their efforts in the arrangement of my stay.

Last but not least, I wish to thank my family for their long-distance encouragement and support throughout my study.

Jing Hu
Delft, October 2004

Table of contents

List of Abbreviations

1D	One-dimensional
2D	Two-dimensional
3D	Three-dimensional
w/c	Water to cement ratio
BSE	Backscattered electron
CH	Calcium hydroxides
C-S-H	Calcium silicate hydrates
CV	Coefficient of variation
EN	Equal number fraction mixture
EV	Equal volume fraction mixture
GEM	General effective media theory
HPC	High performance concrete
HYMOSTRUC	HYdration, MOrphology and STRUCture formation
ITZ	Interfacial transition zone
IUR	Isotropic uniform random
LPT	Local porosity theory
LPD	Local porosity distribution
MIP	Mercury intrusion porosimetry
NIST	National Institute of Standards and Technology, USA
NND	Nearest neighbour distance
OPC	Ordinary Portland cement
PC	Portland cement
PDD	Pore distribution density
PSD	Particle size distribution
PSI	Point-sampled intercept
RG	Random generator
RHA	Rice husk ash
RAE	Representative area element
RVE	Representative volume element
SEM	Scanning electronic microscopy
SPACE	Software Package for the Assessment of Compositional Evolution
VUR	Vertical uniform random
WMIP	Wood’s metal intrusion porosimetry

Chapter 1

General Introduction

Relevant to the design of high performance concrete, insight into the microstructure of cement-based materials and its relationship with concrete properties are of paramount importance. Specifically for early age concrete, the structural evolution of solid phases is of high relevance to the prediction of concrete strength. On the other hand, geometrical characteristics of the pore space determine the rate at which fluids penetrates into concrete and to what extent causes damage to the material. Hence, porosity and details of pore structure are of paramount importance for mechanical and durability properties of cementitious materials. The micro-structural development of cementitious materials and the relationship between structure and material properties have been extensively studied by experimental techniques and in computer modelling approaches.

However, an accurate quantitative characterisation of the geometrical aspects of pore structure remains a challenge due to the complex and interconnected nature of pore network in cement pastes and concretes, which has been recently visualized by computer simulation approaches based on simplified modelling concepts. The reliability of most experimental techniques (such as mercury intrusion porosimetry) is limited since the interpretation of experimental data is based on assumptions of pore geometry that are largely deviating from reality. Moreover, the numerical modelling of cement paste and concrete, when starting from a non-realistic simulation of the particle packing structure, cannot yield correct information on material structure. This situation is pertinent to all commonly used systems that are making use of random generators. This inevitably leads to dramatic biases in the spatial dispersion of generated particles at densities relevant for cement and concrete.

In contrast, microscopical visualisation techniques allows for direct observation and basic quantitative characterisation of pore structure, without any assumption on pore geometry. X-ray computer microtomography can provide three-dimensional (3D) images of cement paste microstructure with a satisfactory quality [Bentz *et al*., 2002]. Unfortunately, this technique is not suitable for routine application to pore space because the resolution is insufficient to detect part of size ranges of the capillary pores. It is impossible to apply conventional observation techniques directly to cementitious materials due to their opaque nature. Only two-dimensional (2D) sections of material specimens are available for microscopic observations and quantitative image analysis. However, the conventional approach based on size characterisation of individual pore features (pore areas) observed on 2D section image cannot yield reliable 3D structural information on material structure.

In this case, the stereological theory and mathematical morphological measurements can be employed as challenging alternatives for characterising pore structure in cementitious materials. Stereological theory provides geometrical statistical tools for unbiased estimation of the 3D geometrical parameters of the state of aggregation on the basis of one-dimensional (1D) or 2D observations. These methods will be combined with quantitative image analysis techniques and applied to 2D section images of actual cement pastes for 3D characterisation of pores structure, which constitutes the main experimental part of this study. Parallel to the experimental research, use is made of the SAPCE system for computer simulation of cements/ concretes structure and morphological study of model concretes. The SPACE system replies on a so-called dynamic mixing strategy instead of random-generator (RG) procedures for the simulation of cement particle packing. This realistic modelling approach, although based on simplified concepts, allows for a representation of the structural evolution of the solid phase and pore space during the hydration process.

In this chapter, the fundamentals of concrete as a particulate material will be emphasized at first (section 1.1). This is highly relevant to experimental design and structural analysis of materials in concrete technology. Evolution of pore space during the hydration process and the involved technical parameters will be briefly discussed in section 1.2. Section 1.3 presents a short introduction of representative models for simulating the microstructural development of cementitious materials. The advantages of the SPACE system compared with other simulation models will be highlighted. Section 1.4 (state-of-the-art) reviews the experimental or modelling outcomes of other researchers in this field. In view of the deficiencies and the labour-intensive nature of conventional experimental techniques for characterising pore structure, a research strategy largely replying on proper and more efficient characterisation methods is adopted in this study. Section 1.5 gives some basics of these stereological and mathematical morphological approaches. The last section presents the aim and outline of this study.

1.1 Fundamentals: concrete as a particulate material

Concrete is a particulate composite material on different levels of the microstructure. It is also referred to as a macroscopically heterogeneous quasi-brittle material. Already in early 1960s research efforts demonstrated virgin concrete to contain myriads of tiny cracks resulting from stress due to shrinkage and differential settlements [Stroeven, 1973]. They are not visible by naked eye, though. Gravel grains (and eventually macro-fibres) are aggregated on meso-level in a cementitious matrix. Sand grains become discernable upon further increase of resolution in the aggregated mass of particles dispersed in the cement paste. An even more sensitive approach would allow detecting the very particles of this paste in the fresh state, or the hydrate structure of the hardened material. The molecular structure is situated at the lowest micro-structural level. A particulate composite material reveals size segregation of particles near surfaces at a higher level of the microstructure, ranging from boundary effects in structural elements to interfacial transition zones around aggregate grains [Stroeven, 2003].

1.1.1 Three levels of aggregation

The underlying concept of the three discrete levels of aggregation, denoted by macro-, meso- and micro-level in concrete technology, has been recognized for a long period of time in the physics and mechanics of deformable bodies. For this purpose see, *e.g*. Freudenthal's [1950] book with the name of 'The inelastic behaviour of engineering materials and structure'. This way of emphasizing material structure can also be found in Holliday's book on 'Composite materials' [Holliday, 1966]. Stroeven [1973] introduced the ideas in concrete technology more explicitly, referring to the various connotations attributed to the three levels in different material technologies. The three levels defined by Freudenthal [1950] are:

- The macro-level or *phenomenological* (engineering) level at which the material is considered to be continuous and homogeneous, being made up of identical volume elements of finite dimensions;
- The meso-level or *structural* level at which the material is still considered to be continuous but non-homogeneous, consisting of elements of different properties and of finite (macroscopically or microscopically observable) dimensions, which fill the space continuously. These elements can be made optically visible. These elements, usually of different size, are considered to be individually homogeneous and isotropic, but are distributed and oriented at random, that is, so that all positions and orientations are equally probable.
- The micro-level (*atomic* or *molecular* level) at which the material is considered to be discontinuous, made up of discrete particles of atomic or molecular size.

Roughly speaking, in this sequence the dimensions are measured in the units, mm-m, μm-mm, and Å, respectively. Of course, a continuous linear range of microscopical (microstructural) dimensions exists. The morphological study of pore structure in cementitious materials is generally on the meso-level (structural level), thus, the materials are accepted to be inhomogeneous. This necessitates a short introduction to some fundamental terminology, *i.e.*, heterogeneity and representative volume element (RVE).

1.1.2 Heterogeneity and the Representative Volume Element

The concepts of homogeneity and isotropy in relation to real materials can only be justified on a statistical basis, considering the average shape and material properties of the elements making up the body. It is evident that in the case of such statistical homogeneity and isotropy, the relations between the quantities describing average behaviour and properties of the body and those describing the individual behaviour and properties of the constituent elements can only be statistical relations [Freudenthal, 1950].

If we assume cement paste to be a two-phase material (which is a suitable model for a structural approach), the material body is transformed into a dispersion of pores in a matrix of solid phase. The distribution of pores describes the extent to which the two phases are mixed and is the most important single measure of the homogeneity of the system. Increasing the sample size decreases the scatter in porosity values of the separate samples of similar size. By accepting a particular value for the coefficient of variation of the porosity values, the size of the sample is fixed. ‘This volume can be called the representative cell, and is the imaginary unit which represents the heterogeneity of the actual material to a defined and arbitrary probability. In an isotropic material the representative cell can be imagined as a cube’ [Freudenthal, 1950]. This defines the representative volume element (RVE). In the case of quantitative image analysis, the area element is referred to as the representative area element (RAE).

Hence, heterogeneity is not a material property, but *a stochastic concept*. Homogeneity of a geometric parameter or of the associated material property can only be achieved for volume elements that are large enough to reduce the between-samples scatter in the relevant parameter or property to an acceptable level. Scatter in the estimated global geometric parameters of material structure can be theoretically estimated and expressed as standard deviation or coefficient of variation. By definition the RVE/RAE is homogeneous as to the relevant parameter (or property). ‘It should be noted that if there are n independent geometrical parameters (such as concentration, particle size, orientation, etc.), there will be n

values for the representative cells since each geometrical parameter has an independent scale of homogeneity with its corresponding size of RVE' [Freudenthal, 1950]. To put this in another way, heterogeneity cannot be uniquely described by a single geometrical variable [Stroeven, 1973].

Engineering properties are supposed to reflect certain aspects of the behaviour of material elements of at least representative dimensions. That is to say, unbiased estimation should be based on the so-called RVE/RAE. Heterogeneity of the selected parameter will increase inside the RVE/RAE with a decline of the micro-structural level taken into consideration and defined by the selected resolution of observations (*e.g.* scanning electronic microscopy) or measurement equipment (*e.g.* strain gauges). When the experimental design is based on the volume or area elements of sub-representative size as to the property or geometric feature of interest, the associated amount of heterogeneity is a function of the size ratio of the sample and the RVE/RAE (this ratio is defined as probing sensitivity). This implies the biases to be similar when this size ratio is similar in comparative studies on cementitious materials with different RVE sizes (because of, *e.g.*, different maximum grain size in concrete or different maturity of cement paste). The bridge to the engineering level can only be taken when the experimental design is based on RVEs or RAEs. However, in most cases this is impossible. In engineering testing (employing volume elements), as well as in materials investigations (based on area elements), all results should therefore be corrected to obtain unbiased engineering estimates. These correlations should be either obtained experimentally or analytically, based on material models of the material in which heterogeneity is a continuous function of the size ratio of the sample and the RVA/RAE.

1.1.3 Composition and configuration aspects of material structure

The morphological aspects of solid phase can also provide structural information on pore space since it is complementary to pore space in the two-phase material concept. In the fresh state of packing, solid phase consists of discrete cement particles conforming to a specific size distribution. A comment must be made on the degree of cooperation of the individual cement particles. The cement particles are defining a group pattern that includes the effects of geometrical and material properties. The configuration aspect of material structure is dependent on the group pattern of relevant particles with respect to size, shape and dispersion. Hence, particle size and spacing (spatial dispersion) are involved in the configuration aspect of material structure.

Material behaviour under forces is the reflection of material characteristics and of material structure. This behaviour is defined in terms of properties, such as mechanical ones. It is possible to distinguish between two fundamentally different types of properties, those which are not affected by the group pattern, denoted as structure-insensitive properties, and those which are essentially affected by the group pattern, the structure-sensitive properties. The *structure-insensitive properties* are the result of *additive* contribution of all constitutional elements to the average behaviour of the group, whereas the *structure-sensitive ones* depend on the *selective* contribution of a small group of anomalous or anomalously located element within the whole group of elements [Freudenthal, 1950]. Hence, structure-insensitive properties are solely governed by material *composition*, *e.g.* mass and Young's modulus; however, structure-sensitive properties such as the crack initiation strength are affected by the so-called *configuration* aspect of material structure.

Geometric parameters can reflect different aspects of material structure. When it is not dependent on material configuration, the parameter is defined as a *composition parameter*. In the other extreme case, we deal with a *configuration-sensitive parameter*. The size of the RVE/RAE is a direct reflection of the degree of sensitivity to configuration of the geometric parameter, or to structure of the material property. This implies each geometric parameter and each material property to have its own homogeneous RVE/RAE with dimensions specific for that parameter/property.

Since a structure-sensitive property depends on the behaviour of a small group of selected elements, the fluctuation of the values of this property, according to statistical principles, will necessarily be considerable wider than that of a structure-insensitive property that depends on the interaction of all elements. Hence, RVEs of structure-sensitive properties will exceed those of structure-insensitive ones to a considerable degree. This implies that the dimensions of the RVE/RAE can fluctuate within wide boundaries. For example, when dealing with concrete, the linear dimensions of the representative element might be between, say, one decimetre and one meter [Brown, 1965; Stroeven, 1973].

1.1.4 Size sampling strategy in experimental design

A theoretical concept underlying the dispersion of one phase in a second (in the present case, pores in the cement paste matrix) that is generally accepted in modelling and experimental approaches is isotropic uniform randomness (IUR). This implies that *sufficiently* large samples can provide *representative* information when drawn at an arbitrary location and orientation in bulk of the material. Mostly, this concept is (seriously) violated in practice, however. Care should therefore be bestowed on how to sample (as to location and orientation), since the quality of the estimate can never be better than the quality of the sample.

Ordinary cement paste is assumed and demonstrated to be isotropic [Hu and Stroeven, 2002], so orientation sampling is not of interest in this study. Hence, the sample size is what governs the representativeness of the derived structural information. Samples for structural analysis in concrete technology are mostly not designed for size, because standardized specimens or specimens designed for material performance are used. So, sample size is insufficient in many cases (revealed by too large scatter); outcomes will be biased. This inevitably reduces the efficiency of experimental design.

The rule of thumb in concrete technology is to have a linear dimension of sample exceeding 4~5 times the maximum structural dimension [Cooke and Seddon, 1956]. However, this is a proper approach when interested in structure-insensitive properties. When micro-mechanical or microphysical modelling pursues an estimation of the structure-sensitive global properties, and the structural information is as a consequence required on configuration instead of on composition, sample sizes should be significantly larger. A factor of 5~10 should be considered [Stroeven, 1973]. This principle in size sampling strategy should be kept in mind in experimental design.

1.1.5 Law of similar level of microstructure in comparison study

The aforementioned continuity in aggregation levels has significant implications for size sampling strategy in comparison study of pore structure in cement pastes with different degrees of maturity. The engineering level might be looked upon as that level at which material structure is invisible, because observation sensitivity is too low. At first, the larger elements in concrete will become discernable when the resolution level is somewhat increased. This is the start of a continuous process of revealing more and more geometric details on a declining level of the microstructure. Of course, the 'micro-level' should be associated with the geometric parameter defining the level of the RVE. Hence, this microstructural level is intimately linked up with that of the RVE.

This law of similar level of microstructure is also referred to as the continuous scaling problem. Continuous scaling plays an important role when dealing with the amount of damage or the total (or specific) crack surface area as in the case of studying shrinkage cracks. The closer the observation, the more heterogeneous and the more extensive the damage structure will appear. Hence, observations on different levels of the microstructure will systematically produce different information on density (extension) and on dispersion (degree of heterogeneity).

Hydration will gradually transfer cement paste into a matured material with lower porosity. When the structure of cement paste is modified by hydration, a similar level of the microstructure should be adapted for comparison purposes in experimental designs pursuing a study of the effects of such changes on porosity. Unless this is properly arranged, artificial effects will be mixed with fundamental ones. Hence, a proper comparative study requires that the size ratio of the sample and the RVE/RAE (*i.e.*, probing sensitivity) is similar. This requirement results in an experimental design encompassing different sample sizes (volume or area) adapted to the range of RVE/RAE sizes involved. In discussing the fundamentals underlying the experimental and modelling approaches to cementitious materials, sampling will receive proper attention in this study, in the light of the continuous range of microscopic dimensions.

1.2 Evolution of pore structure during hydration

The inherent pore system affects the most important properties of concrete, notably its strength and durability. Abrams argued that 'The strongest cements should be made without water' [van Breugel, 1991], which points to the distinct relationship between the strength and porosity of cement-based materials. The durability of cementitious materials largely depends on the possibilities of penetration of hazardous ions into the porous material with water as medium. Therefore, the water permeability of cementitious materials is very crucial to its durability. Porosity and pore structure are generally accepted to exert significant influences on the permeability of cementitious materials. Hence, insight into porosity and pore structure is of paramount importance. In this study, particular attention is given to the morphological (geometrical) aspects of pore space in cement pastes and concretes.

1.2.1 Definition of pore structure

The pore system in cement-based materials consists of four types of pores, namely, gel pores, capillary pores, macro-pores due to deliberately entrained air, and macro-pores due to inadequate compaction. Of particular interest for ordinary cement paste is the capillary porosity. The pore volume is generally defined as the initial paste volume minus the volume of solid phases (the total volume of remaining unhydrated cement particles and the hydration products). Porosity p is defined as the ratio between the pore volume V_{pore} and the initial paste volume.

The pore sizes in cement-based materials range between nanometres to millimetres (for a scheme of pore size ranges, van Breugel [1991] can be referred to). Several researchers assume a continuous pore size distribution. There is a general agreement concerning a subdivision of pores into different classes, viz. gel pores, capillary pores and air voids. Pores with a diameter larger than 10 μm can be associated with air voids, whereas capillary pores are assumed to cover a range of 0.001 to 10 μm.

1.2.2 Factors affecting pore structure

Cement hydration modifies pore structure in continuous stages, in which cement chemical composition, cement particle size distribution (PSD), cement fineness, water cement (w/c) ratio, temperature, etc are involved. Cement fineness level is usually represented by Blaine specific surface area, expressed in m^2/kg. Porosity and pore size distribution are functions of w/c ratio and degree of hydration and are strongly influenced by curing conditions and cement composition. In this study, only the most important technical parameters, *i.e.*, the degree of hydration, the w/c ratio and the cement PSD are taken into consideration.

<u>Degree of hydration</u>

The total porosity decreases during the hydration process since hydration products gradually fill in the available space in cement paste. A general trend is that the volume of the large pores significantly declines, whereas the volume proportion of small pores (<100Å) in the total porosity dramatically increases [van Breugel, 1991]. The reduction in volume of the large pores is predominant in the early stage of hydration. It is explained that, at first, the hydration products are formed in larger pores and later on in the smaller ones, thus leaving the volume of the small pores more or less constant. Once the larger voids are filled, further hydration would affect the entire pore size distribution. It has been experimentally shown that the shape of the pore size distribution curve plotted versus the hydration degree remains fairly constant throughout the hydration process.

<u>Water to cement ratio</u>

It is expected that a high w/c ratio will result in a higher volume of porosity in all size ranges. An increase of the w/c ratio leads to an increase in the portion of the larger pores, and hence an increase in the mean pore size.

<u>Cement particle size distribution</u>

The cement fineness and PSD are expected to exert significant influence on cement microstructure since smaller cement particles react faster during hydration. It is found that the volume of smaller pores is higher in finer cement. Moreover, the packing structure of cement particles is more important than the cement fineness. The pore volume decreases with denser packing of cement particles. Experimental researches reveal that the addition of fine silica fume results in a denser paste, a reduction of the volume of large pores and hence a reduction of the average pore size. The decline in pore size and the densification of the cement paste can be partly attributed to a denser packing of the cement particles. In view of the chemical reaction during the hydration process, this can be accounted for by the fact that the silica fume acts as nucleation centres in the water-rich spaces [van Breugel, 1991]. In this study, special emphasis will be given to the packing structure of cement particles in the fresh state of model cements and concretes. A relatively realistic packing structure can be realised by the SPACE system that is used in this study for computer simulation. In what follows, the representative simulation models of cementitious materials will be briefly reviewed.

1.3 Computer simulation of cementitious materials

Direct observations and quantitative measurements of 2D section images of cementitious materials allow for deriving part of the important structural information. Although certain microstructural aspects of cement paste such as porosity are statistically the same in 2D and 3D, other structure features are considerably different, including the connectivity or depercolation of porosity. Characterisation of the porosity connectivity and depercolation threshold of capillary porosity relies on a realistic 3D representation of the pore structure. It is extremely difficult to reconstruct an accurate 3D microstructure from successive 2D images [Scrivener, 1989a].

Hence, computer simulation provides a promising alternative for this purpose. Modelling of the microstructure and its application for studying the transport properties and durability of cement-based materials has meanwhile been studied for a few decades. These models, categorized as continuum-based models or digital-image-based models, provide important structural information of cement-bases materials during the hydration process, and thereby allow predicting part of the mechanical and transport properties of the materials.

1.3.1 Overview of different simulation models

Pioneering work on computer simulation of cementitious materials dated to Wittmann *et al.* [1984], who proposed the concept of 'numerical concrete' consisting of aggregates in a cement paste matrix. Their model mapped each aggregate grain onto a finite-element grid, allowing for the computation of mechanical stress distributions.

Jennings and Johnson [1986] established the foundation for continuum-based models by representing cement particles (tricalcium silicate, C_3S) with spherical particles enveloped by calcium silicate hydrate (C-S-H) shells of increasing thickness during the hydration process. In their model, calcium hydroxide (CH) crystals were allowed to nucleate and grow in the continuous pore space. The fundamental of the continuum-based model is that each particle can be described by its centre location and a set of radii, corresponding to the unhydrated cement core and shells of the hydration products (representing inner and outer C-S-H product). In this approach the cement hydration process is controlled by different mechanisms at different hydration stages.

Representative among this category are the HYMOSTRUC system (HYdration, MOrphology and STRUCture formation) invented by van Breugel [1991], another continuum model formulated by Navi and Pignat [1996, 1999], and the SPACE system (Software Package for the Assessment of Compositional Evolution) developed by Stroeven [1999]. These models are based on similar approaches, but focus on different aspects of the cement microstructure development. HYMOSTRUC takes the influences of technical parameters into consideration including the w/c ratio, temperature, particle size distribution and chemical composition of the cement. After further development by Koenders [1997] and Ye [2003], the model relates the volumes of embedded cement particles to cement strength, and is able to predict the permeability of cement paste.

An integrated particle kinetics model was reported by Navi and Pignat [1996, 1999]. In this simulation of the microstructural evolution, morphological thinning and partitioning of the pore phase was adopted to characterise the three-dimensional features, including pore size distribution, volume-to-surface ratio as well as connectivity of capillary porosity (defined as the fraction of connected porosity), but the limited size range of the cement particles prevents it from offering a realistic simulation of cement productions. More recently, Stroeven [1999] developed the SPACE system, also based on the continuum approach of numerical simulation. One advantage of this model is that, when used to simulate cement paste, the cement particles are not distributed in a random way, but according to an algorithm of dynamic mixing. In this way, the particles offer a more realistic packing system with structure-sensitive configuration.

An alternative approach to the continuum-based models is the so-called digital-image-based model developed by Bentz and Garboczi [1989] from National Institute of Standards and Technology (NIST, USA). This model operates on the sub-particle level as each cement particle is represented as a collection of elements (pixels). The advantage of digital-image-based models is that it allows the direct representation of multi-phase, multi-size, and non-spherical cement particles. The simulation procedure starts from a digital image of cement particles obtained by backscattered electrons (BSE) and X-rays imaging techniques. By placing digitised particles at random locations in the 3D computational volume according to the measured cement particle size distribution, the desired w/c ratio is obtained [Bentz, 1997].

Unlike the continuum-based models it does not consider the different kinetics involved in the hydration process. Based on the reconstructed fresh state of cement microstructure, a cellular automation algorithm is applied to simulate the dissolution, diffusion and reaction of cement components [Bentz and Garboczi, 1992]. The NIST model has been significantly upgraded in the past decade and utilised to simulate cement hydration and microstructural development of cement pastes with different technical parameters. The technical parameters involved in their study are the w/c ratio, the cement PSD, the replacement level of mineral admixture (fly ash and silica fume) and the fineness of the mineral admixture. A percolation theory of pore/solid phase was employed to analyse the connected fractions of different phases in three dimensions [Bentz and Garboczi, 1991]. It should be noted that the digital resolution exerts significant influences on the simulation results of the percolation and transport properties of model cements generated by this NIST model. This issue is elaborated in a recent publication of Garboczi and Bentz [2001].

Another critical difference between the aforementioned models is the location in which the hydration products are deposited. The cellular automation algorithm of NIST model allows the deposition of products on the surfaces of the cement grain and in the pore space, as does the Navi's model. In contrast, all the hydration products are placed around the grains in the HYMOSTRUC modelling approach.

1.3.2 Advantages of SPACE system

The SPACE system is based on similar algorithms as the HYMOSTRUC system for the simulation of cement hydration. However, two features of this system deserve special emphasis. In the field of cementitious materials, the aforementioned simulation models usually start from a random generation procedure. In contrast, the SPACE system offers a 3D simulation of the properly packed cement particles in the fresh state, and the aggregated state of the model cement during the hydration process. The simulation part of this study is therefore based on the SPACE system.

Dynamic mixing procedure for packing simulation

The development of high performance concrete (HPC) has shown the particle-packing phenomenon to be of major importance, since it governs significant contributions to the strength. A realistic representation of the initial packing structure of cement is an important start for a realistic simulation of cement paste. The common approach to simulating particle packing is the application of so-called random-generator (RG) as in the case of the HYMOSTRUC simulation, where particles of a certain range of particles sizes are sequentially positioned inside a container. Each location is randomly generated. With such high densities encountered in this category, 'overlap' will occur to an increasing degree during the generation process. The solution is to reject such overlap, whereby the generation process is continued. Obviously, dense random packing cannot easily be generated in this way.

Based on a dynamic mixing procedure, the SPACE simulation offers a more realistic representation of the particle packing structure reflecting the production conditions of concrete. For the details of the generation system can be referred to [Stroeven, 1999]. The SPACE system's versatile and powerful potentialities are illustrated by the assessment of the packing structure of aggregates gains in model concrete [Stroeven and Stroeven, 1999]. The result of dynamic mixing is, however, not dependent on scale. So, size can also be taken to be micro-level, suitable for simulating the initial packing of cement particles. The system is more suitable for studying the structure-sensitive properties of cementitious materials. A more detailed description of the modelling concepts will be given in Chapter 2.

Incorporation of stereological estimation

Bentz [1997] argued that although continuum models can provide valuable quantitative information, such as the effects of PSD on hydration kinetics, but it is difficult to analyse such a microstructure and directly compute transport and elastic properties. Ye [2003] developed a serial sectioning algorithm to characterise the pore network in cement paste; however, if the stereological theory is incorporated, the computing intensity can be reduced to a dramatic extent.

It is not only the unsolved difficulties of a physico-chemical nature that pushes research towards a more stereological-oriented approach. The evident effects of the particle size distribution on the structural formation, *i.e.*, of the spatial position of hydrating particles and hydration products relative to each other, also calls for increased attention to stereological considerations. Henk even explicitly states that strength development is, in essence, a geometrical problem. His statement can be substantiated by the strength development of low porosity pastes. The fact that in these pastes high strength values are reached at relatively low degrees of hydration can be attributed to the initial dense packing of the cement particles which results in only small amounts of gel required for 'gluing' the hydration particles together [van Breugel, 1991].

Therefore, some important stereological estimations are integrated into the SPACE system, allowing for quantitative characterisation of solid phase and pore space in the fresh state of cement particle packing. Technical parameters like the cement particle size distribution and the w/c ratio exert significant influences on the packing structure, and thereby on the microstructural development of cement. Their influences on the packing structure will be explored in Chapter 2 with stereological parameters.

1.4 State-of-the-art on this subject

Porosity is arguably the most important component of the microstructure of cement paste that affects important engineering properties such as strength and permeability. It is known that the total porosity has a strong link to strength and other engineering properties. Porosity may be of primary importance, but alone it does not offer insight into pore size and pore structure. Lange *et al.* [1989] demonstrated that the details of pore structure also exert important influences on cement paste strength when the total porosity is constant. Compared to the total porosity, it is much more difficult to accurately characterise pore structure.

1.4.1 Experimental approach

The conventional characterisation of pore structure involves the porosity and pore size distribution, which can be determined by mercury intrusion porosimetry (MIP). For many years, it has been customary to evaluate pore size distribution in cement pastes, mortars, and occasionally concretes, using MIP. However, the interpretations of MIP data are restricted by assumptions about pore shape that are known to be a poor approximation of the complex, tortuous network of capillary pores in cement paste. Another major deficiency of MIP is associated with the inkbottle-effect offering misleading representations of the porosity and pore size.

Mercury intrusion porosimetry (MIP)

The mercury intrusion data by itself provides no information whatsoever on the distribution of pore sizes in the specimen. For such information to be generated, an appropriate model must first be invoked. The usual model is that of a system of cylindrical pores each of which is entirely and equally accessible to the outer surface of the specimen, and thus to the surrounding mercury [Diamond, 2000]. For porous systems that conform to such a model, the well-known Washburn equation may be applied to estimate the diameter of cylindrical pores intruded at each pressuring step. However, it has become increasingly apparent that the intrinsic pores in hydrated cement systems fail to conform to the requirements of the model [Willis *et al*., 1998].

The pores are clearly not cylindrical, and the boundaries of most of them are visibly convoluted. Pore shapes in cement pastes were quantitatively evaluated by Wang and Diamond [1995] using image analysis, and were found to have a high degree of convolution as measured by standard form factor measurements, and to be significantly elongated. Furthermore, Wang [1995] found that the pore profiles exhibit an appreciably fractal character when examined for this feature using a standard progressive dilation technique. These deviations of pore shape from that assumed model undoubtedly influence the output of MIP pore size distribution measurements. However, their effect appears to be less important than the accessibility effect (the so-called ink bottle effect).

This issue of accessibility to mercury appears to be at the root of the failure of MIP to provide realistic pore size distributions. It arises from the fact that only a small proportion of the pores in hydrated cement specimens undergoing MIP are open directly to the outside of the specimen, *i.e*. are in contact with the surrounding mercury. Nearly all of the pores are in the interior of the specimen, and most of them can be reached by mercury only through a long percolation chain of intermediate pores of varying sizes and shapes. This problem is explicitly explained and illustrated in Diamond [2000]. The aforementioned deficiencies of the MIP technique have been extensively discussed and at least partly believed in cement research; as an alternative, quantitative image analysis of specimen sections is increasingly accepted for the characterisation of pore structure in cementitious materials.

The nature of this failure is such that the putative pore size distribution calculated from the Washburn equation from MIP data differs largely from reality. Diamond and Leeman [1995] conducted a comparison of the pore size distribution obtained by the MIP technique and by image analysis for a 28-day-old paste (w/c=0.4) containing air voids (deliberately designed in experiment). It is clearly revealed that the MIP data includes the air void volume as part of the measured porosity, but *disguises* the air void space by not intruding the air voids until the threshold diameter pressure is reached. Contrary, the image analysis technique shows the air void space at appropriate diameters and therefore, reveals a more realistic picture of the actual pore size distribution in cement systems.

Conventional section image analysis

Direct observations of material structure through scanning electronic microscopy (SEM) provide a useful and reliable alternative. During the past 20 years, image analysis has become an important tool for microscopic studies of cement-based materials. SEM images have been widely used to study porosity and pore structure in cement and concrete. Scrivener and Pratt [1984] processed images of polished sections to analyse the distribution of unhydrated phase, calcium hydroxide (CH), and calcium silicate hydrate (C-S-H). This technique can also be used to visualize and observe pore structure in cement pastes and concretes. The individual pore areas observed on 2D section images are defined as pore features. The amount and distribution of the pore features can be characterised by quantitative image analysis of binary section images (reflecting pore space).

The routine applications measure the area fraction of porosity and determine the pore size distribution on the basis of area classification of the pore features. This approach to pore size distribution belongs to the conventional area histogram. Considering each pore area as an individual feature, Lange *et al*. [1994] directly measured the area-based cumulative pore size distribution. The distribution curve in their study was similar in shape as the curve obtained by MIP. A scale difference of about three orders of magnitude was found, however. In their study, the pore features with an area smaller than 10 μm^2 are truncated from the data set, based on the argument that the largest pore features are those most likely to be significant in the mechanical behaviour of the material. This selective method of pore features is not suitable for study relevant to the durability aspect of cement paste.

Image-based characterisation by Wood’s metal intrusion (WMIP)

Due to the aforementioned limitations of the MIP technique, some researchers used alternatives of mercury for measurement and visualization purposes. Willis *et al*. [1998] investigated pore structure in an experimental approach similar to MIP, but by means of intruding molten Wood's metal into mortars under various pressures. The molten Wood’s metal solidifies within the pore structure of the sample, allowing for the visualisation of pore space on section images of cement paste specimens. Scrivener and Nemati [1995] also employed Wood's metal for studying the percolation of pore space in the interfacial transition zone (ITZ) in concretes.

It was found that molten Wood's metal has a contact angle on hydrated cement that is similar to that of mercury, and that its pressure vs. volume intrusion curve into a mortar was essentially identical to that of mercury into the same mortar. However, with Wood's metal, the pressure applied can be stopped at any given value, and if the sample is cooled, the location of the solidified Wood's metal within the specimen can be determined. By substituting Wood's metal for mercury as the intruding liquid, SEM and quantitative image analysis can be applied to cement paste samples after intrusion for characterisation of the pore structure, *e.g.* pore size distribution. This approach is, in fact, a combination of intrusion and quantitative image analysis techniques.

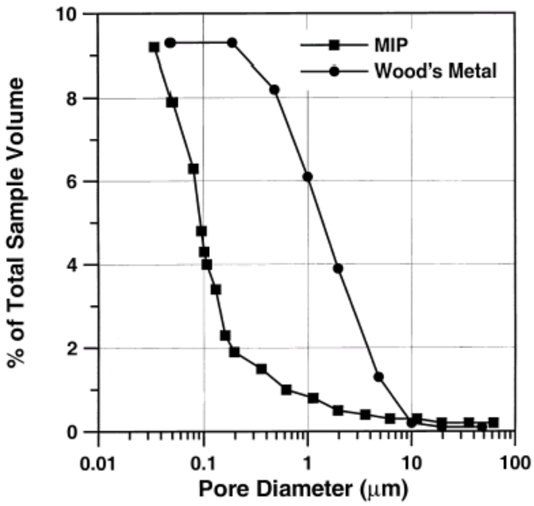

Figure 1.1 *Comparison of plots of image analysis size distribution of Wood's metal-filled pores and MIP results for the same 14-day-old mortar (w/c=0.4). After Willis et al. [1998].*

Fig. 1.1 provides the results obtained by conventional MIP and section image analysis of Wood's metal intruded mortar. The intrinsic non-air void pores, shown to be present by virtue of their being filled with Wood's metal, are mostly in sizes between 1 and 10 μm. It is clear that MIP data reveal incorrect information about pore size distribution because it measures pore size on the basis of the diameter of the access throat through which the mercury penetrates the microstructure to reach internal pores. As a result of the ink-bottle effect, the MIP pore size distribution curve shifts towards smaller size ranges by two or three orders of magnitude. The results obtained by Wood's metal intrusion and image analysis can be considered representative of the actual pore structure in cement pastes and mortars.

1.4.2 Computer simulation approach

Parallel to the experimental approaches, quantitative characterisation of pore structure in model cement paste is also pursued by different researchers, on the basis of aforementioned models (section 1.3). Most of the simulation work focuses on determination of pore size distribution and connectivity. The connectivity in their simulation study is usually defined as the fraction of connected porosity, *i.e.*, porosity connectivity.

<u>Navi and Pignat's simulation</u>

Based on their continuum-based model, Navi and Pignat [1999] applied thinning erosion method (a basic operation of mathematical morphology) to digitised pore space to partition the pore space into a well-defined collection of individual 3D pores. Each individual pore consists of a site bounded by interfaces with solid matrix, and by pore necks. A pore neck is defined as a plane in which the hydraulic radius (area divided by its perimeter) has a local minimum. The pore size distribution curve and volume-to-surface ratio can be obtained from the segmented pores. Their research outcomes revealed a much smaller percentage of small pores than suggested by MIP. The pattern of pore size distribution curve is strikingly different from MIP curve, regardless of the shift in order of magnitude.

In addition, Navi and Pignat calculated the connectivity of the pore space, defined as the fraction of connected porosity. The results revealed that, in cement paste with a porosity of lower than 10%, almost 95% of the capillary pores are connected. Although Navi and Pignat stated that using a voxel of 0.5 μm allows a reasonably accurate determination of the pore size distribution and the connectivity of pore space, the concept underlying the measurements – the collection of *individual* pores – prevents a realistic representation of the interconnected pore structure and therefore leads to misleading data.

Ye's simulation work with HYMOSTRUC

Ye [2003] developed a program to directly derive 3D pore size distribution on the basis of the RG-based HYMOSTRUC model. The pore structure in simulated cement paste is the free space between expanding cement particles during the hydration process. The pore size distribution can be determined by calculating the volumes of the pore space that are accessible to imaginary testing spheres of increasing radius *r*. Let $\rho(r)$ be the volume fraction of pore space accessible to testing spheres of radius r; it can be expected that $\rho(r)$ is a monotonically decreasing function of *r*. A 2D description of the algorithm can be found in Ye [2003], whereas the computation program is conducted directly in 3D pore space. The volume fraction $\rho(r)$ can be computed by gradually filling testing spheres of radius *r* into pore space and densely packing of the testing spheres

$$\rho_{(r)} = \frac{4k_0\pi}{3}Nr^3 \qquad r_{\max} \geq r \geq r_{\min} \tag{1.1}$$

where *N* is the number of testing spheres of radius *r* that can be accommodated in the pore space; $r_{\min}$, $r_{\max}$ are the minimum and maximum radius of testing spheres, respectively. In numerical models of cement paste, the value of $r_{\min}$ is largely dependant on the computer capacity. $k_0 = 1.83$ is a geometrical coefficient to convert the volume of void from spherical-based volume to cubic-based volume.

It should be noted that the calculation of pore volume at a certain value of *r* is no more than lower bound estimation. However, if the minimum radius and the interval between radii of testing spheres are small enough at the specified resolution, this method can provide reasonable results. In addition, the calculation results also depend on the starting point of the testing sphere. However, if the calculation starts from any vertex of the cube, the results can be consistent. The derivative $-d\rho(r)/dr$ represents the fraction of pore space accessible to spheres of radius *r* but not to spheres of radius *r*+d*r*. The cumulative pore size distribution curve is obtained by directly plotting $\rho(r)$ versus r. The pore size distribution curve can be represented by derivative of the cumulative curve, as shown in Fig. 1.2.

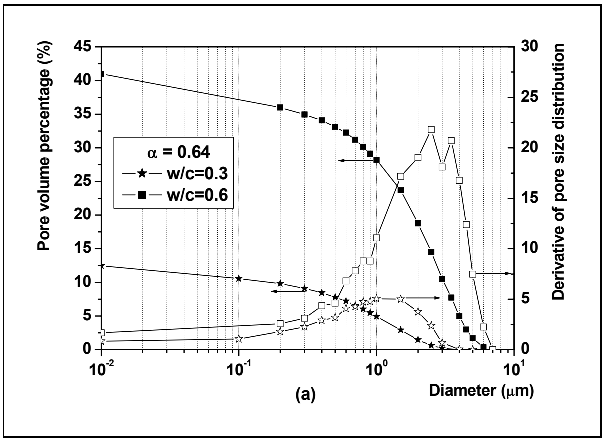

Figure 1.2 Pore size distributions of simulated cement pastes with w/c ratios of 0.3 and 0.6 at a degree of hydration of 0.64 (Blain fineness of cement is 420 m^2/kg). After Ye [2003].

Also based on the HYMOSTRUC model, Ye [2003] developed a serial sectioning algorithm with a so-called overlap criterion to characterise the geometrical and topological properties of pore space in cement paste. His method is a straightforward reconstruction of the pore network on the basis of closely spaced sections. Based on the same definition of porosity connectivity, he reported a depercolation threshold of porosity at about 3%. It is found in his study that the pore space is still completely interconnected at a hydration degree of 80%. Only when the hydration degree reaches about 90%, the individual pores become actually separate [Ye *et al*., 2003]. He attributed this finding to the high digital resolution (0.25 μm/pixel, hence tiny capillary pore pathways can be detected) and the assumption of spherical cement particles in the HYMOSTRUC model. In the pixel-based NIST model, various cement components are simulated by different sets of pixels without any constraints on the shape of these components. In contrast, HYMOSTRUC starts from a random packing of spherical cement particles.

<u>NIST model</u>

Garboczi and Bentz [1991; 1996; 2001] performed an extensive study on the porosity connectivity and the depercolation threshold of capillary porosity on the basis of their digital-image-based model. They reported a depercolation threshold of porosity between 18~21% for cement paste on moderate fineness levels and studied the influences of w/c ratio, cement PSD, digital resolution on the threshold value. They found that cement PSD exerts more significant influences than w/c ratio. In their study, the depercolation threshold of the capillary porosity changed from 24% to 18% and 12% in a cement paste with w/c ratio of 0.3 when the digital resolution shifted from 1 to 0.5 and 0.25 μm/pixel, respectively. So, even at the same resolution as HYMOSTRUC (0.25 μm/pixel), the NIST model and the HYMOSTRUC model revealed striking differences in the depercolation threshold of porosity. In fact, the extremely low depercolation threshold reported by Ye can be at least partially attributed to the modelling concept of HYMOSTRUC that hydration products can deposit only on the surface of cement particles, whereas the NIST model allows the deposition of hydration products as well as in the pore space.

The determination of pore size distribution and depercolation threshold of porosity will also be explored in this study, although based on different approaches. The pore size distribution will be derived from section image by means of a so-called opening distribution technique (Chapter 3), which is a basic operation of mathematical morphology. A brief introduction of mathematical morphology measurements will be given in section 1.5. In this study, the depercolation threshold will be approached by morphological evolution of pore structure during hydration (Chapter 5). The simulation work on depercolation threshold conducted by the NIST group provides good reference to this study; hence, the details of their research outcomes will be elaborated in Chapter 5.

Either based on experimental or modelling approaches, the derived characterisations of the pore structure will become of particular interest provided that they can be linked to physical properties of cementitious materials, such as mechanical and transport properties. Lange *et al*. [1994] indeed revealed a linear relationship between the mean perimeter length of large pore features with the fracture toughness of cement pastes and mortars. On the other hand, there also exist various empirical relationships between cement paste permeability and characterising parameters of the pore structure.

1.4.3 Empirical relationship between permeability and pore structure

Water permeability is very crucial to the durability of cementitious materials. There are several methods to measure water permeability directly. However, these methods are time-consuming especially for low-permeability concrete, mortar or cement paste at final stage of cement hydration. As an alternative, many models have been developed to relate water permeability to pore structure of cementitious materials. Among them representative are the Katz-Thompson equation [Katz and Thompson, 1986] and the Carman-Kozeny relationship [Carman, 1939]. In addition, Hughes [1985] used parallel models to relate water permeability to second intrusion data of MIP.

The Katz-Thompson equation is generally used to predict the permeability of porous materials. Christensen *et al*. [1996] directly applied the Katz-Thompson permeability theory to predict the water permeability (k) of ordinary Portland cement (OPC) paste by

$$k = \frac{1}{226} l_c^2 \frac{\vartheta}{\vartheta_0} \tag{1.2}$$

where l_c is the critical pore diameter. ϑ is the electrical conductivity of the sample, and ϑ_0 is the electrical conductivity of pore solution in the sample.

According to the Carman-Kozeny model, permeability k of cement paste can be predicted on the basis of the geometrical properties of pore space by

$$k = -\frac{p(V_{pore} / S_{pore})^2}{2\beta} \tag{1.3}$$

where p is the porosity, V_{pore} and S_{pore} are the volume and the surface area of pore space, and β is the tortuosity of the transport route in the cement.

Many researchers have tried to apply the Katz-Thompson theory to cementitious materials. Christensen *et al*. [1996] has used the theory to predict the water permeability of *very porous* cement paste and measured the relative conductivity directly. They found that the predicted permeability was in good agreement with the measurement. However, the results are not as good as those for rock and stone. El-Dieb and Hooton [1994] measured the water permeability and pore structure of both OPC and blended cement pastes but did not measure their relative conductivity directly. The porosity of the samples was very low. The experimental results were very different from the results obtained by using the Katz-Thompson equation. They concluded that the Katz-Thompson equation could not be applied to cementitious materials. Tumidajski and Lin [1998] applied the theory to predict the water permeability of concrete and found that the Katz-Thompson equation cannot be directly used in concrete systems. This implies that further improvement and refinement of the Katz-Thompson equation is necessary for the purpose of predicting permeability of cementitious materials on the basis of more efficient characterising parameters other than critical pore diameter. This issue has been explored in this study and will be presented in Chapter 7.

In view of the deficiencies of the Katz-Thompson equation, Cui and Cahyadi [2001] employed the General Effective Media (GEM) theory to predict the permeability of cement paste, based on pore structure data obtained by MIP. This theory takes the influences of capillary pores as well as gel pores on the cement paste permeability into consideration and reveals satisfactory results. In the present study, this theory will be adopted in a similar approach for permeability prediction (Chapter 7), but based on the structural information derived from section image analysis.

1.5 Proper characterisation approaches

Cement particles react with water and form a porous solid with micro-pores of a wide size range. Understanding of the microstructure-property relationships of cement-based materials necessitates knowledge of the microstructure at different levels. Hence, a comprehensive understanding of the pore structure is of significant importance in view of improving the mechanical performance and durability properties of cement-based materials. This requires *proper characterisation approaches* to the complex pore space.

It has been emphasized that all methods for the determination of porosity and pore size distribution suffer from different kinds of experimental difficulties. Simplifications in the interpretations of experimental data of MIP, *e.g.* the assumption of cylindrical pore shapes, result in the need for caution with respect to the measurement of pore size distribution by this technique [Lange *et al*., 1994]. Moreover, MIP measurement would significantly damage and coarsen the pore structure [Diamond, 2000; Olson *et al*., 1997]. In contrast, quantitative image analysis provides direct observation and representation of pore space in cementitious materials, without any assumption on pore shape. However, the reliability of data obtained by conventional quantitative image analysis (*e.g.* area histogram of pore features) is limited by the 2D nature of section images.

Particulate materials like cement and concrete are 3D aggregation of particles on different structural levels. Observations should therefore provide 3D information on material structure. Opaque materials like the cementitious ones do not allow easy access to the 3D material structure. Hence, geometrical statistical (*i.e.* stereological) tools should be applied for this purpose, since they provide means for unbiased estimation of the 3D geometrical parameters of the state of aggregation on the basis of 1D or 2D observations [Underwood, 1968].

In order to overcome the deficiencies and labour-intensive nature of aforementioned experimental and modelling approaches, a new research strategy is proposed in this study, which is replying on more efficient and practical methodology for characterisation of pore structure, *i.e.*, stereological and mathematical morphology tools. The combination of image analysis technique with these useful tools is expected to provide reliable 3D structural information on the pore structure in cementitious materials. A general introduction to the stereological and mathematical morphological theories will be given in this section. Details of the characterising parameters and measurement procedures will be described in the relevant chapters.

1.5.1 Stereological parameters

The pore areas observed on 2D section image are denoted as pore features. A quantitative description of these pore features by quantitative image analysis involves expressing the structural information of pore space in parametric or functional form. Stereological theory expresses the 3D structural information in the former form; hence, stereological parameters are involved in the characterisation of phase of interest in material structure. Relevant characteristics can be classified according to several criteria: ratio, size, shape, and dispersion of observed features representing the phase of interest (either solid phase or pore space).

Ratio (area/volume fraction of porosity)

Stereological parameters verify a certain number of properties, which can easily be explained, particularly in the case of stationary systems. Although the pore structure is continuously changing during the hydration process, it can be considered as a stationary system at a specified degree of hydration. A stationary system conforms to the rule of invariance under translations and rotations (*i.e.*, measurement independent of position), and the rule of compatibility with similarities (*i.e.*, measurement independent of magnification). The measurement of the area fraction of porosity is straightforward, and it is an unbiased estimator of the volume fraction of porosity [Underwood, 1968].

Size characterisation of pore features

Measurements of size and shape can be performed on pore features on section images. In view of the interconnected pore network of high tortuosity and irregularity, shape characterisation of pore features does not make much sense. However, various size characterisations of pore structure, although measured on 2D sections, can be assigned 3D stereological character. For example, the perimeter length of pore features per unit test area (L_A), allows for estimating the specific surface area (S_V) of pore space in cement paste.

Spacing (mean free spacing)

The w/c ratio determines the volume fraction of cement particles, *i.e.*, the compositional aspect of the material. However, varying the particle size distribution changes the structural configuration. Different stereological spacing parameters are available when the configuration is at issue. The most common ones are the nearest neighbour distance, Δ_3, and the free inter-particle spacing, λ. Their global values are directly correlated with the global density values of geometrical parameters. Measurement of spatial dispersion of solid phase in the stereological theory relies on these spacing parameters. Pore space is considered to be complementary to solid phase in cement paste. So, the mean free spacing between solid clusters reflects information on the average pore size.

1.5.2 Mathematical morphology measurements

In some cases, mean stereological parameters (like porosity, specific surface area) are insufficient to access a precise evaluation of the morphological characteristics because very different structures can give a similar mean value. Hence, mathematical morphology approaches are combined with stereological estimation in this study. Mathematical morphology techniques are based on measuring the changes produced when a binary image (reflecting phase of interest, pore space in this case) is transformed. The simplest mathematical morphological transformations are erosion, dilation, opening and closing. For a detailed description of these morphological operators, see [Serra, 1982]. Mathematical morphology measures material structure in a functional form.

Granulometric distribution functions (size distribution)

Granulometric distribution functions are the most useful methods to characterise the *size distribution* of a specific phase of interest. Two main categories of granulometric distribution methods exist: measurement by individual analysis or by morphological opening.

Individual granulometric analysis is well known: the size of each pore feature in the binary image is measured. Then they are classified according to their size to establish the distribution. To perform such an analysis, each pore area (feature) must be totally visible. One is constrained to eliminate objects intersecting the frame of measurement, which inevitably introduces a bias. To correct this bias, a counting coefficient is assigned, which is nothing else than the reciprocal probability of inclusion of the object in the frame. This probability is easily obtained from the area ratio of the frame to the objects. However, as emphasized by Scrivener [1989a] and visualized by numerical models of the hydrated cement microstructure, the pore structure is a complex interconnected network of irregular shape. It is therefore inappropriate to consider the profiles of pore features (areas) as individual objects and the pore size distribution obtained by the area histogram is incorrect.

In contrast to individual granulometric analysis, morphological opening distribution is a more suitable approach since it can be used independently on the nature of set X reflecting the phase of interest (pore space in this study). On the basis of mathematical morphology transformations, various distributions of pore phase can be obtained by using a sequence of similarly shaped structuring elements of increasing size. The *opening distribution* curve of pore space is obtained by plotting the pore area fraction after an opening operation against the linear dimension of the structuring element. This gives a type of *size classification* in the case of an interconnected structure, in contrast to single features as in the case of individual granulometric analysis. This measure is a 2D analogue of the type of size distribution obtained by gas or methanol absorption or by low temperature calorimetry [Scrivener, 1989a]. This opening distribution technique will be employed in this study for characterising pore size distribution in actual cement pastes.

Covariance function (phase dispersion)

The covariance function is obtained by erosion of the structure by a bi-point h. The simplest covariance function measures the intersection of a specific phase and its translation by vector

h. Relevant to pore space, the value at the origin is equal to the area fraction of porosity. For $h \to \infty$, the covariance tends toward a horizontal asymptote. Between the origin and the value at the infinite, the behaviour of covariance is related to the state of dispersion of the pore space. Perfectly random structures without attraction or dispersion effects will give a regular and smoothly decreasing curve. For a periodic structure, the covariance curve will oscillate.

1.6 Aim and outline of this research work

This study aims at developing a comprehensive methodological framework for characterising the geometrical and morphological aspects of pore space in cementitious materials and exploring its application to actual cement pastes and model cement pastes/concretes for the purpose of predicting mechanical and transport properties of cementitious materials. The relevance of this study is derived from the impact a methodologically sound approach to pore structure analysis of concrete will have on durability studies.

In this study, the morphological changes of the pore structure during the hydration are studied as a function of the technological parameters, including cement fineness (particle size distribution), water cement (w/c) ratio and degree of hydration. This problem is approached by quantitative image analysis techniques, stereological estimation, and by application of mathematical morphology methods. Stereological tools are adopted in this study to overcome the deficiencies of conventional structural analysis associated with the 2D nature of section images. Mathematical morphological measurements will be applied to section images for *properly characterising* pore size distribution and critical pore size.

The application of stereological theory and mathematical morphology measurements is an important aspect in the present study, dramatically reducing the labour intensity of serial sectioning. In addition, the relationship between cement paste permeability and pore structure will be reviewed and a proposal will be formulated for upgrading this relationship on the basis of the proper characterisations of pore geometry (morphology) obtained by means of the developed methodology in this study.

Relatively realistic simulations of cements and concretes are realized by the SPACE system, parallel to the experimental approach applied to section images of actual cement specimens. Stereological estimations are also applied to model cements and concretes, allowing the assessment of the depercolation threshold of porosity and the influences of the technical parameters thereupon. This morphological approach to the depercolation process, different from conventional methods based on connected fraction of porosity, is associated with a stereological spacing parameter representing the spatial dispersion of the solid phases and thereby reflecting an average pore size.

The outcomes of this study are presented in eight chapters, in accordance with the flowchart presented in Fig. 1.3.

Chapter 2 explores the morphological aspects of the solid phase and pore space in the fresh state of model cement/concrete and in hardened materials. This chapter deals with the characterisation methods applied to *model cements/concrete* generated with the SPACE system. The dynamic mixing procedure and the hydration algorithms employed in the SPACE system will be introduced in the beginning of this chapter, followed by a brief description of the technical parameters of the representative model cements/concretes used in this study. The rest of this chapter presents the results of stereological analysis and mathematical morphology measurements conducted on these model cements/concretes.

Parallel to the simulation study, stereological and mathematical morphology tools are also applied to 2D *section images of actual specimens* for structural analysis of pore space in cement pastes with various w/c ratios and at different hydration stages. The derived 3D structural information, including porosity, pore size distribution, and pore distribution density (a new characterising parameter proposed in this study) will be presented in Chapter 3.

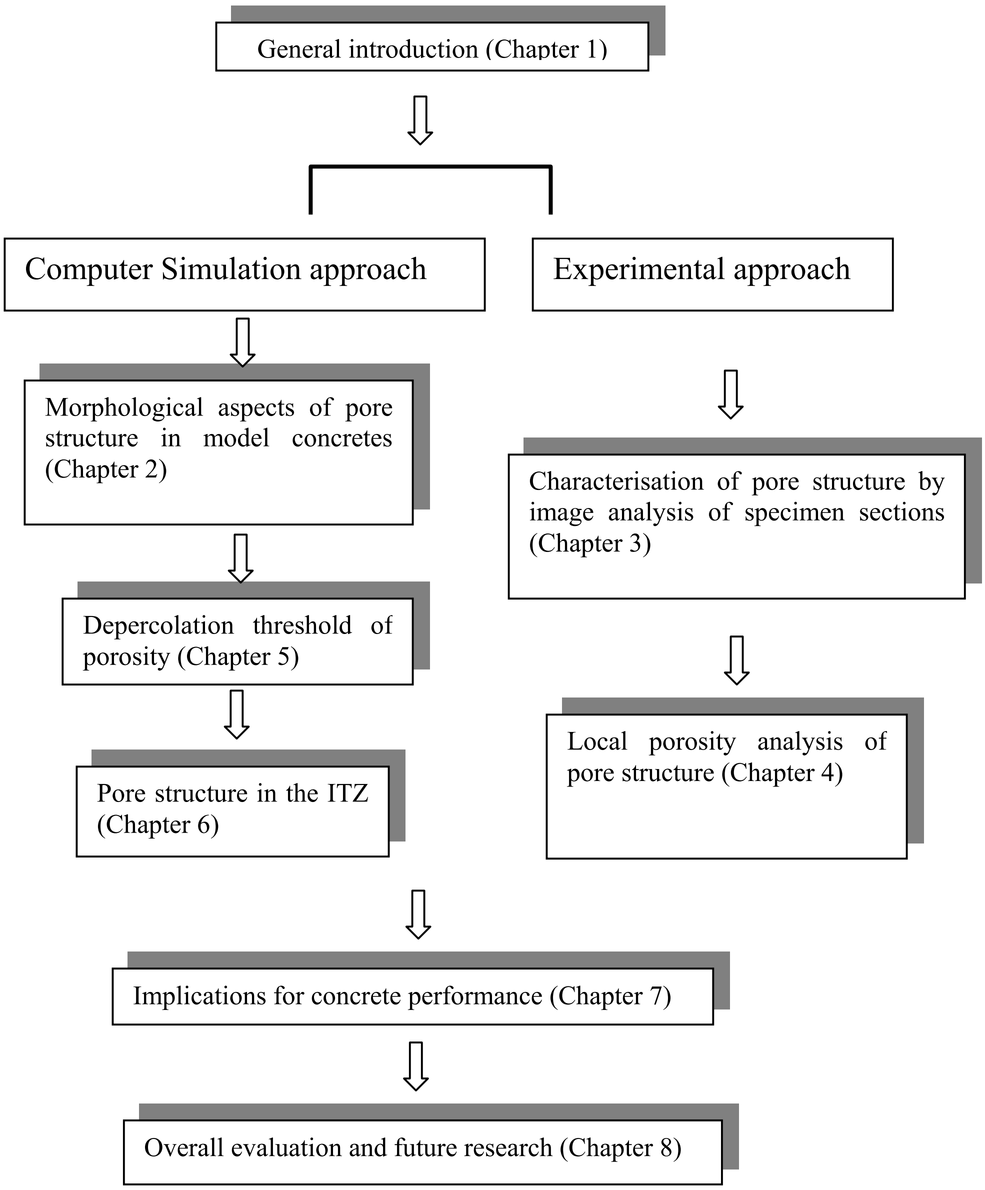

Figure 1.3 Flowchart of this thesis.

Another highlight in this study is the application of local porosity theory (LPT) to 2D section images (Chapter 4). The original LPT was proposed by Hilfer [1991] for studying the fluctuations of porosity distribution and the percolation probabilities of sandstones. His approach is readily applicable to *3D structure models* of porous materials, thus largely relying on reliability of the reconstruction model. In this study, the LPT approach is upgraded into a 2D alternative, and applied directly to the section images of actual cement paste specimens used in Chapter 3. The local porosity distribution data (obtained by the upgraded approach) are associated with the composition heterogeneity of cement paste structure modified by hydration. The implications of the statistical concept of heterogeneity for experimental design, as discussed in section 1.1, is demonstrated by a comparison study of cement pastes with different degrees of maturity.

The depercolation threshold of capillary porosity is of significant importance for the transport systems in cementitious materials. Computer simulation of the 3D cement microstructure is the only access to this phenomenon. In Chapter 5, the threshold values for model cements with different w/c ratios and fineness levels are estimated in the viewpoint of the morphological evolutions of pore space during the hydration process.

Relevant to the application of HPC, the interfacial transition zone (ITZ) between cement paste and aggregate is a crucial element in mechanical system. The extent of the ITZ is found to be dependent not only on technical parameters, but also on the configuration-sensitivity of the characterising parameter. This problem will be approached by the SPACE simulation in Chapter 6 by means of various configuration parameters. In addition, the structural evolution of the ITZ during the hydration process is explored on the basis of the stereological theory. A conventional way to improve the ITZ microstructure is by blending cement with fine mineral admixtures. The underlying physical mechanism, *i.e.*, gap grading, is revealed by computer simulation in this chapter.

The purpose for studying the pore structure is to efficiently estimate the properties of cementitious materials. The implications of the derived structural information are discussed for concrete performance in Chapter 7. Relevant to the durability aspects of cementitious materials, the discussion focuses on permeability predictions of cement paste since experimental measurements of permeability are tedious and time-consuming, especially for more matured cement and concrete. When porosity and critical pore size are known, the water permeability of cement paste can be predicted by means of the widely used Katz-Thompson equation. However, the results are not satisfactory enough when the calculation is based on porosity and critical pore size alone. Hence, more comprehensive parameters should be pursued for a better characterisation of the pore structure. The degree of correlation between characterising parameters and permeability of cement paste are studied with the Grey System theory in this chapter and the results are used to refine the Katz-Thompson equation. The refined equation incorporates another stereological parameter - 3D pore distribution density containing information on pore size and pore connectivity, and therefore provides better prediction quality.

Morphological Aspects of Cementitious Material in Model Concretes

The SPACE system will be used in this study for computer simulation of cement particle packing and structural evolution of the model cement/concretes during cement hydration. This chapter will present the results of morphological study (by means of stereological analysis and mathematical morphological measurements) obtained for representative model materials. Section 2.1 will give a brief introduction of the algorithms for the dynamic mixing procedure in the packing process and for simulation of cement hydration. Section 2.2 describes the model cements/concretes used for structural analysis in this study. A detailed description of the stereological parameters for characterising the morphological aspects of materials will be given in section 2.3. Sections 2.4 and 2.5 present the results of stereological analysis and discuss the influences of technical parameters (w/c ratio, cement PSD) on the packing structure of cement particles. The relevance of this part is derived from the importance of cement packing structure (in the fresh state) for microstructural development of cement pastes/concretes and for mechanical and transport properties of the materials. The results of some basic mathematical morphology measurements obtained on model concretes will be presented in section 2.6.

2.1 SPACE simulation system

Various computer models (see section 1.3) have been developed to simulate particle packing in cementitious materials. A common approach is using RG, where particles of a certain size range are sequentially generated at random positions inside a container (reference frame). However, *dense random packing* cannot easily be generated in this way due to dramatic increase in the number of rejections. Moreover, as an inevitable consequence of the rejection operation, a structure is obtained with a relatively high degree of order, underestimating the natural phenomenon of particle clustering [Stroeven and Stroeven, 1999]. The biased character of simulations by RG-based systems rapidly increases with volume fraction. The degree of bias is already unacceptable at only moderate values of volume fraction. The SPACE system has been developed to assess the characteristics of dense packing situations in materials by a *realistic* structure simulation.

2.1.1 Simulation of cement particle packing

The simulation approach is based on a non-continuous representation of the internal material structure. The non-homogeneous or granular nature of the internal material structure is represented by a set of distinct elements. Each element corresponds to characteristic phase in the material. For example, concrete is modelled as a set of elements that represent the aggregate particles. The elements are dispersed in a presumably homogeneous mortar matrix moulded in a cubic container. The parameters that describe a static situation of the internal structure are the location, orientation and shape of the various elements. Since the elements represent real physical phases in the material, physical properties can be assigned to each element along with their shapes, at least in principle [Stroeven and Stroeven, 1996]. The distribution of location and orientation of these non-overlapping elements is more difficult to derive, however. To be able to simulate effects such as clustering (flocculation) and to reach high volume density, element motion and inter-element collision [Brach, 1991] are modelled, which leads to effective ingredient mixing. This stage is referred to as the *dynamic mixing* process.

Thus, the general simulation concept can be described as follows. For a detailed description of the system, see [Stroeven, 1999; Stroeven and Stroeven, 1996].

- Initially a structured or random 3D dilute distribution of elements with predefined shape and size distribution is generated within the boundaries of a cubical container. Fig. 2.1a presents an example of the starting situation of a multi-sized dilute mixture of spherical particles inside the cubic container.
- The second step, the actual dynamic stage, is an iterative procedure in which location and orientation of all elements are changed at each time step according to a Newtonian motion model [Stroeven, 1999]. This motion model relates the element's linear and angular displacement to a set of conditions enforced on the element (*e.g.*, gravity, friction, etc). The friction coefficient is denoted as *f*; the restitution coefficient *e* is a parameter representing the energy dispassion during the motion process. When elements meet during this time interval, a 'contact model' defines the effect of contact on the motion/rotation update. Inter-particle influences are obviously revealed by the contact model. Higher densities are obtained by gradual reduction in the size of the container.
- The iteration stops when certain conditions are reached (such as the required volume fraction, corresponding to the water cement ratio). Fig. 2.1b reveals such a final situation, concerning the example of Fig. 2.1a. The resulted structure in Fig. 2.1b is photographically magnified for visual purposes.

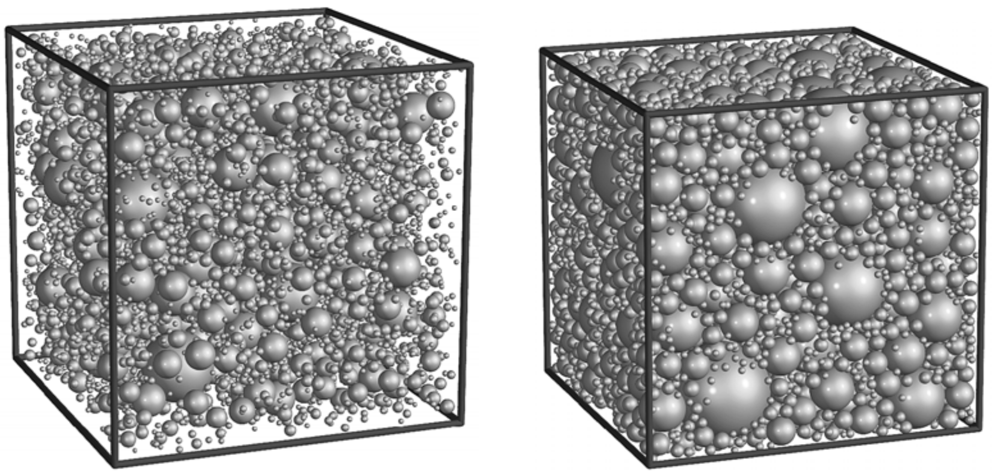

(a) (b)

Figure 2.1 Schematic of dynamic mixing method adopted in SPACE simulation: (a) initial dilute system of cement particles; (b) fresh state of model cement, after dynamic densification process. After Stroeven [1999].

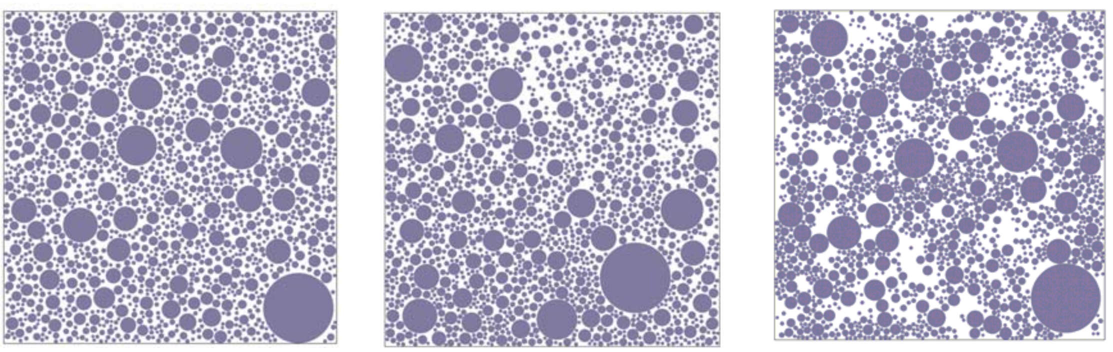

(a) Sequential random distribution | (b) Dynamic mixing procedure (f=0.0, e=1.0) | (c) Particle flocculation (f=0.1, e=0.1)

Figure 2.2 Comparison between the cement particle packing in fresh state obtained by sequential random distribution and dynamic mixing approach. After Chen [2002].

By assigning proper mixing parameters to cement particles, different production conditions of cement and concrete can be simulated. The flocculation phenomenon can be realistically simulated and explicitly visualized (Fig. 2.2) by this system [Stroeven, 1999; Chen, 2002; Hu *et al*., 2003]. The value of restitution coefficient e can be associated with the dosage of superplasticizer. The coefficient f reflects the extent of friction between the particles.

2.1.2 Simulation of cement hydration

The hydration process of a single cement particle as a set of concentric spheres largely follows the hydration description presented by van Breugel [1991]. The algorithm will be clarified on the basis of a schematic description [Stroeven and Stroeven, 2001]. The more complicated situation of multiple merging particles will be evaluated afterwards.

The kinetic hydration process of a single particle consists of two subsequent stages in time. The first stage, in which a phase boundary mechanism controls the hydration rate, is followed by a stage in which the reaction rate is controlled by a diffusion mechanism. The transition between the two stages is assumed to occur when the thickness of the layer of the reaction product $d(t)$, precipitated on the cement particle at time t, equals a transition thickness δ_{tr}. The inward growth or decrease of the unhydrated cement surface Δr_{in} for a sufficiently small time period Δt is then given by

$$\Delta r_{in} = \Delta t K_0 ((\frac{\delta_{tr}}{d(t)})^{\beta})^{\gamma} \qquad (2.1)$$

where K_0 is the rate constant, $\gamma = 0$ as long as $\delta_{tr} > d(t)$ and $\gamma = 1$ otherwise. The constant β regulates the diffusion process. The chemical reaction between cement and water results in a gel-product. The relationship between the volume change ΔV_{in} of the hydrated cement and the volume change ΔV_{out} of the gel or outer product is given by

$$\Delta V_{out} = v \Delta V_{in} \tag{2.2}$$

with constant $v = 2.2$ [van Breugel, 1991]. A volume ΔV_{in} of the reaction product is used to fill the space of the reacted cement. The remaining volume precipitates equally on the existing gel surface of the particle thereby introducing an outward growth.

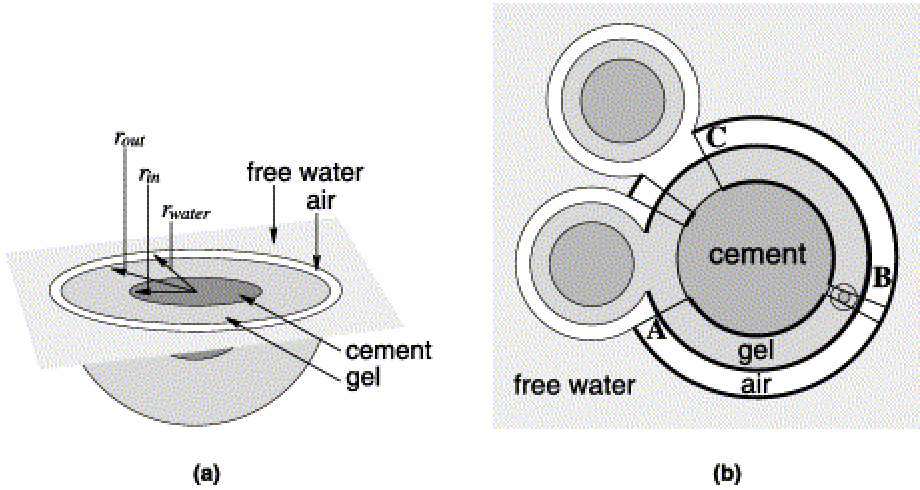

Figure 2.3 (a) Geometric representation of hydrated cement and (b) various contact situations between cement particles. After Stroeven and Stroeven [2001].

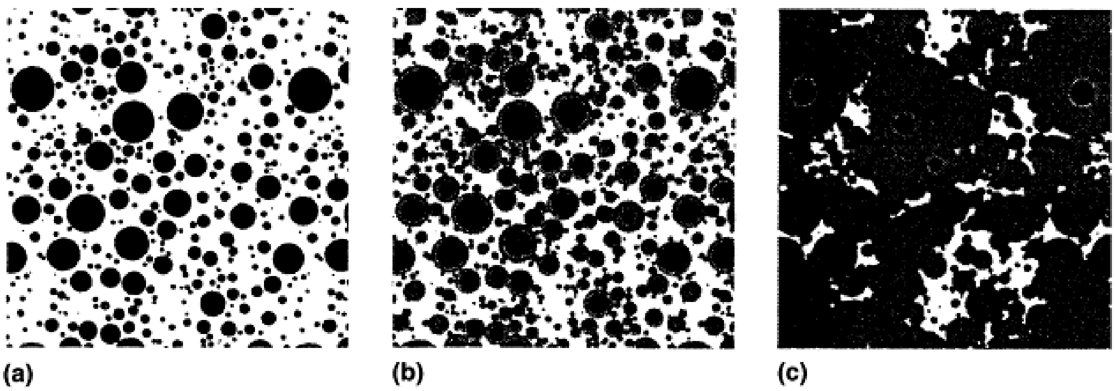

Figure 2.4 Sections of bulk paste with w/c =0.5 during hydration: (a) initial stage; (b) after 3 days, and (c) after 10 years of hydration (white areas indicate water/air and black areas represent solid phase including unhydrated cement and hydration products. After [Stroeven, 1999].

In this simulation the water will appear in three forms, *i.e.*, chemical bound water, which is chemically bound to the cement by the hydration reaction, physical water that is adsorbed in the pores of the gel, and free water that is supposed to be the only form available for hydration. The deposition of the gel product and consumption of cement and free water are assumed equally divided over the entire free surface. Thus, the cement-gel interface, gel-air and air-water interfaces remain located on concentric spheres throughout the hydration process (see Fig. 2.3a). This is particularly convenient for modelling purposes [Stroeven and Stroeven, 2001].

However, the simultaneous expansion of other particles in the vicinity will lead to growing contact areas between the gel products of neighbouring particles, which diminishes the surface area that is available for production deposition. Fig. 2.3b illustrates a 2D representation of this situation, whereby the thick line at the gel-air interface represents the free surface onto which the gel product may precipitate. A particle embedded in the gel layer, as illustrated by case B in Fig. 2.3b, prevents part of the gel surface to be active in the diffusion process. The different contact situations (Fig. 2.3b) and their influences on the hydration rate are taken into consideration in the simulation by the SPACE system. A detailed description of the hydration algorithms is available in Stroeven [1999]. A section example of the cement paste is given in Fig. 2.4 for different hydration stages. Relevant to this study, the cement paste is considered composed of two phases, *i.e.*, solid phase and pore space.

2.2 Model cements of different particle size distribution

Fresh state of model cements with different size distributions and/or different Blaine specific surface areas (S_G, expressed in m^2/kg) were designed and generated by Chen [2002] with the SPACE system. This author applies stereological analysis and mathematical morphological measurements to these model cements for structural analysis of cement packing in the fresh state and of the hardened materials. The involved w/c ratio ranges between 0.3 and 0.6. Relevant to this study, three model cements were selected representing different fineness levels. The Blaine specific surface areas are 167 m^2/kg (cement C167), 342 m^2/kg (cement C342) and 605 m^2/kg (cement C605), corresponding to coarse, ordinary and fine cement, respectively. These three representative samples are subjected to all structural analysis (Chapter 2) and are used to study the influence of cement fineness on the depercolation threshold of porosity (Chapter 5).

In addition, six samples with different size ranges and size distributions at the intermediate cement fineness level of about 350 m^2/kg (typically produced by the cement industry today) were selected exclusively for investigating the influence of PSD on cement packing structure (*e.g.* particle flocculation phenomenon). This reflects the impact of cement packing on microstructural development of cementitious materials. PSD parameters of a major part of the model cements are shown in Table 2.1. The PSD of the model cements is made in accordance with the so-called Rosin-Rammler size distribution function. The percentage of the particles by mass retained on the various sieves is plotted on a logarithmic scale. The mass (volume) fraction of particles passing a sieve of diameter *d*, is given by

$$G(d) = 1 - \exp(-bd^a) \tag{2.3}$$

where *a* and *b* are constants for a certain particle system; *a* representing the degree of uniformity in the size distribution of the cement particles. The minimum and maximum sizes of particles (denoted as d_0 and d_m) are incorporated in these two constants. The Rosin-Rammler distribution is generally accepted as a relatively accurate approximation of the actual system of cement particles [Taylor, 1997; van Breugel, 1991].

The cumulative size distribution curves of the model cements are shown in Figs. 2.5 and 2.6. Note that this graph contains more information on the particle mixtures than a sieve curve, which is based on a very limited number of sieve-opening sizes. The mixtures were compacted to volume fractions of 51%, 44%, 39%, and 35%, corresponding to w/c ratios of 0.3, 0.4, 0.5 and 0.6, respectively. The compacted structure is the starting point for applying the hydration algorithm to the fresh model cement. The hydration process is implemented according to the kinetics of cement hydration (see section 2.1.2).

Table 2.1 Size range and fineness of cement particle systems

Sample	Size range (μm)	Mean diameter (by volume, μm)	S_G (m^2/kg)
C167	1~45	18.86	166.67
C188	1~35	16.23	188.06
C317	1~20	10.73	317.71
C332	1~20	10.10	331.87
C334	1~20	10.11	334.43
C342	1~45	14.37	342.15
C605	1~20	6.07	605.28

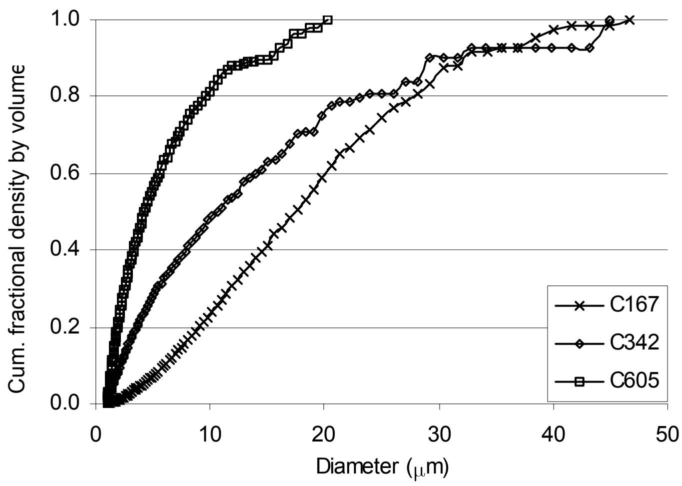

Figure 2.5 *Cumulative particle size distribution curves for model cements C167, C342 and C605. The mixtures were generated with the SPACE system.*

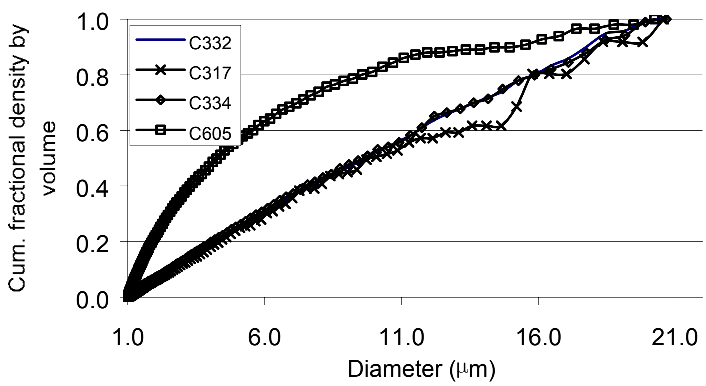

Figure 2.6 *Cumulative particle size distribution for model cements with size range between 1~20 μm, with different values of specific surface area.*

The model cements were hydrated for up to 100,000 hours. The degree of hydration at time t is defined as the mass (volume) ratio of hydrated cement and the initial amount of cement. The morphological aspects of solid phase and pore space are measured by the integrated stereological estimation in the system. This allows deriving 3D structural information of the microstructure in the fresh state and in hardened materials. The stereological parameters used for characterising material structure will be introduced in what follows.

2.3 Stereological descriptors

Different stereological parameters can be associated with the composition and configuration aspects of material structure. When material composition is at issue, stereological parameters like volume fraction can be employed in the analysis of material structure. When one is interested in the configuration aspect of materials, various spacing parameters are available.

2.3.1 Definition of relevant stereological parameters

Underwood's [1968] classical book is one of the very limited stereological literature sources to which researchers in concrete technology refer. Unfortunately, for experimental methodology, this book is at least partly outdated. New and far more powerful approaches have been developed in the last 20 years [Gundersen, 1988]. But for the basic set up of the stereological theory, the book is very useful. Certain important relationships exist connecting the stereological parameters for 2D measurement and the ones for 3D structure. Underwood [1968] presents the various stereological parameters and the associated correlations in a single table. The definitions of the relevant stereological parameters are given in Table 2.2. Relevant for this study are the following relationships:

$$V_V = \overline{A}_A = \overline{L}_L = \overline{P}_P \tag{2.4}$$

$$S_V = \frac{4}{\pi}\overline{L}_A = 2\overline{P}_L \tag{2.5}$$

Note that in the standardized stereological notation $P_L = P/L$. The bar on top of the expressions implies an averaging operation realized by a proper sampling strategy. The first sequence of formulas represents a complete historical development in volume fraction (V_V) analysis (of pores, aggregate grains, etc). The oldest approach from 1848 is based on experimental determination of area fractions (A_A) and is due to Delesse [1848]. Half a century later, Rosiwall [1898] introduced the lineal analysis. The method involves coverage of the section image by a randomly oriented or directed line grid, whereupon the line fraction (L_L) is determined that covers the sections of the pores or aggregate grains. The last development dates back three-quarters of a century [Thomson, 1930; Glagolev, 1934], and is referred to as the point counting method; instead of lines, a random (or systematic) point grid is superimposed and the point fraction (P_P) covering the pore or grain sections is determined. The second set of equations is relevant for quantitative damage (*e.g.* crack extension) analysis. Introduced by Saltikov [1945], this is referred to as the method of random (or directed) secants on a plane. It allows by simple intersection point counting (P_L) to assess the 2D trace extension (L_A) of linear features on a plane, or the 3D surface area density (S_V) of linear features in space. All relationships require random sampling strategies unless one is confronted with the extremely rare situation of an IUR structure. A schematic description of the point counting method and the linear analysis is shown in Figs. 2.7 and 2.8, respectively.

Table 2.2 Definition of stereological parameters

Symbol	Dimensions*	Definition
L_A	mm/mm^2	Length of linear elements per unit test area
P_L	mm^{-1}	Number of intersections per unit test line
$\overline{L}_3$	mm	Mean intercept length
A_A	mm^2/mm^2	Area fraction, *i.e.*, area of intercepted features per unit test area
V_V	mm^3/mm^3	Volume fraction, volume of features per unit test volume
S_V	mm^2/mm^3	Surface area per unit test volume
N_V	mm^{-3}	Number of features per unit test volume
$\overline{S}$	mm^2	Average surface area, S_V/ N_V
$\overline{V}$	mm^3	Average volume, V_V/ N_V
Δ_2	mm	Centre-to-centre distance between a pair of nearest neighbouring particles on a section plane
Δ_3	mm	Centre-to-centre distance between a pair of nearest neighbouring particles in space
λ	mm	Mean free spacing, *i.e.*, average of uninterrupted distance between all particle pairs

*Arbitrarily shown in millimetres

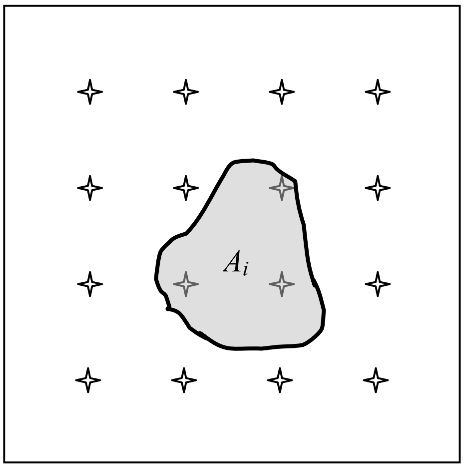

Figure 2.7 A schematic description of point counting method. The number ratio of points situated inside the phase of interest (grey area) and the test points (denoted as P_P) is an unbiased estimation of the area fraction A_A.

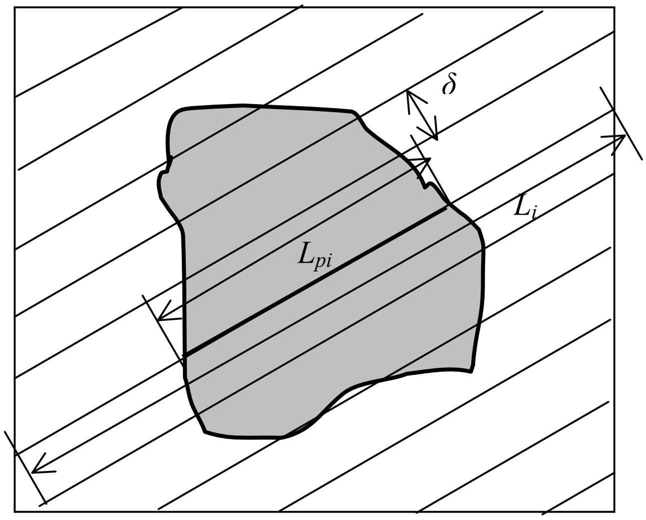

Figure 2.8 A schematic description of linear analysis method. The ratio of total intercept length and total length of the test lines, denoted as L_L, is an unbiased estimation of area fraction A_A. The concept can be expressed as $\dfrac{\sum L_{pi}}{\sum L_i} = L_L = A_A$.

When pore space is at issue, V_V means the volume fraction of pore phase in a sample (*i.e.*, porosity *p*), A_A is the area fraction of pore features on a section, L_A is the total perimeter length of pore features on a section per unit test area, S_V is the total surface area of pores per unit test volume. The same interpretations hold for the solid phase in cement paste. Eq. (2.4) implies that the volume fraction of porosity can be determined with probes of a dimension lower than 3 (including point counting, linear analysis, and area fraction of porosity on 2D section). The advantage is that, for instance, the mathematical evaluation of P_P is in general easier than the mathematical evaluation of V_V because it only involves a simple algorithm to check whether points are situated inside a phase or not (Fig. 2.7). Eq. (2.5) applies to systems of surfaces with any configuration. In order to evaluate the specific surface area of a certain phase in space, one only needs to perform a simple intersection (P_L) count on a test section.

The most common spacing parameters are the nearest neighbour distance (NND, defined as the smallest distance between the particle of interest and other particles in the structure) and the free inter-particle spacing (also denoted as mean free distance or mean free distance). The mean free spacing, denoted as λ, is defined as the mean value of uninterrupted surface-to-surface distances between all neighbouring particles. During the measurement, a test line system is swept over the material structure in different directions. The measurement is conducted in 3D, although a 2D schematic description is shown in Fig. 2.9. The NND only involves centre-to-centre or surface-to-surface distances between the nearest neighbouring particle pairs as shown in Fig. 2.10 (the measurement is also conducted in 3D). Their global values are directly correlated with global density values of geometrical parameters by

$$\lambda = 4\frac{1-V_V}{S_V} \tag{2.6}$$

$$\overline{\Delta}_3 = \frac{0.554}{\sqrt[3]{N_V}} \tag{2.7}$$

Configuration homogeneity can be based on representative information as to the distribution of either one (or both) of these spacing parameters. This is not the focus of this study; thus a simple example of configuration homogeneity will be discussed in Chapter 4 in the context of composition homogeneity based on local porosity distribution data.

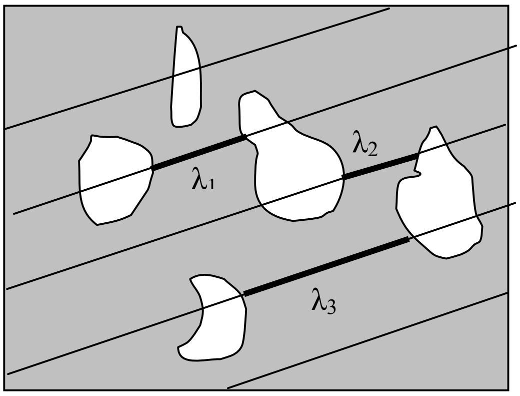

Figure 2.9 A schematic description of the mean free spacing in a plane. The uninterrupted distances between all particles in the frame are measured and averaged to yield λ.

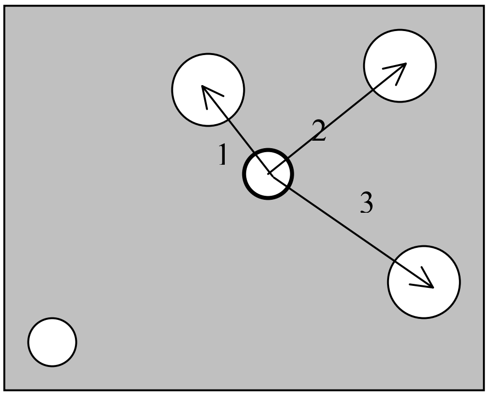

Figure 2.10 A schematic description of the nearest neighbour distance in a plane. Centre-to-centre distance between the investigated particle and its nearest neighbouring particle is marked as 1.The measured NND are averaged over all particles in the frame to yield $\overline{\Delta}_3$.

2.3.2 Stereological estimation integrated in SPACE system

One important advantage of the SPACE system is the integration of relevant stereological estimates. In addition to the basic parameters like V_V, A_A, L_A and S_V, the system is able to calculate the mean free spacing (λ) between cement particles in model cements (or aggregate grains in model concretes). By measuring the probability distribution density of the NND between the cement particles or aggregate grains, the average value ($\overline{\Delta_3}$) of this spacing parameter can be derived. Another important spacing parameter, the *surface-to-surface* distance between *a pair of nearest neighbouring particles* in space (Δ_{3S}), although not defined in the stereological theory, is also available in the SPACE system.

As for structural analysis of material structure, a relevant 2D parameter reflecting the composition aspect is the area fraction of phase of interest (A_A), which can be accurately determined from a full section of the structure. A_A is an unbiased estimator of V_V for the phase of interest (unhydrated cement, hydration products, or pore space). With respect to cement particles, this statement holds for either a part of the particle system within a specific range of size, or for the full size range of the particles.

The mean free spacing λ is linked to the 3D structural information accessible in a section by Eq. (2.6), in which S_V is related to the total parameter length of the cross-sectional features (of the phase of interest) per unit of area in the section plane (L_A) by Eq. (2.5). This allows for an unbiased and exact estimation of λ. The mean free spacing λ can be associated with mechanical properties, like global bonding strength. On the other hand, this parameter is a representation of pore size in hydrated cement paste, and therefore can be associated with the permeability of cementitious materials. This implies the possibility of predicting material properties on the basis of the morphological aspects (represented by stereological parameters) of the material structure. This will be discussed in Chapter 7.

2.4 Influence of technical parameters on cement packing structure

Insight into the fresh state of cement particle packing is of significant importance because it is the starting status of cement hydration. The insufficiency of research in this field can be attributed to its complicated nature. Actually, the packing structure is not random. It is clear that packing depends on the particle size distribution and on boundary conditions. Among various additional influences that determine the ultimate particle dispersion the continuous inter-particle forces are of great significance. The intensity and direction of inter-particle forces depend on the geometrical inter-particle configuration. In other words, the packing structure of cement particles will be governed partly by deterministic and partly by stochastic influences [Stroeven and Stroeven, 1999].

Therefore, the packing of cement particles is not easily accessible by theoretical approaches. The conventional RG-based systems will produce a relatively uniform packing structure, which underestimates natural phenomena such as the clustering of particles (particle flocculation). The SPACE system, based on a so-called dynamic mixing process instead of the conventional RG procedures, provides a realistic simulation of the *packing structure* in the fresh state of model cement. The integrated measurements of the stereological spacing parameters allow for characterising the packing structure of cement particles and assessing the influence of technical parameters thereupon.

Flocculation of cement particles is an intrinsic phenomenon in the fresh state of cement particle packing. Forces of van der Waals type between particles are the main reason for this phenomenon. For two spherical particles of 1 μm (diameter) at a surface-to-surface distance of 0.01 μm, the attractive force between the two particles is about 4×10^{-12} N, which exceeds the inter-particle gravity force by two orders of magnitude [Lu, 1993]. The PSD and cement fineness exert significant influences on particle flocculation. However, a quantitative relationship remains to be established between geometric characteristics of cement particles and degree of flocculation.

In this study, the degree of particle flocculation is evaluated by aforementioned spacing parameters ($\overline{\Delta}_3$) and average coordination number C_1. Average coordination number C_1 is defined as the average number of inter-particle contacts per particle measured within a reference frame of the material structure. The degree of flocculation is associated with the coordination number. A schematic description of this parameter is available in Fig. 2.11.

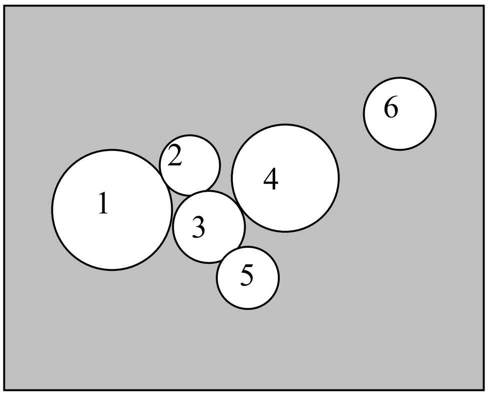

Particle no.	1	2	3	4	5	6	Average
Coordination number	2	2	4	1	1	0	C_1=1.67

Figure 2.11 A schematic description of the average coordination number C_1 in a plane. The measurement is conducted in 3D material structure. This parameter reflects to a certain extent the degree of flocculation in the packing structure of cement particles.

The values of $\overline{\Delta}_3$ for cements with different w/c ratios are given in Fig. 2.12. It can be expected that $\overline{\Delta}_3$ increases with w/c ratio, because higher w/c ratio corresponds to a less densely packed structure. The values of $\overline{\Delta}_3$ for w/c=0.3 mixtures are plotted in Fig. 2.13, as function of cement fineness. The picture reveals a clear trend that $\overline{\Delta}_3$ decreases with increasing cement fineness. The mean free spacing is related to the specific surface area of cement particles, S_G (surface area per unit mass of cement, in m^2/kg), by the following equations

$$\lambda = 4\frac{1-(V_V)_{cem}}{(S_V)_{cem}} \tag{2.8}$$

$$(S_V)_{cem} = \frac{S_{cem}}{V_{test}} = \frac{S_{cem}}{V_{cem}}(V_V)_{cem} = S_G \cdot \rho_{cem}(V_V)_{cem} \tag{2.9}$$

where $(V_V)_{cem}$ is the volume fraction of cement particles in the reference frame (cubic container), and $(S_V)_{cem}$ is the surface area of cement particles per unit test volume (the cubic container), ρ_{cem} (3.15×10^3 kg/m^3) is the density of fresh cement. For a given w/c ratio, $(V_V)_{cem}$ is constant. Combining Eqs. (2.8) and (2.9) reveals a reciprocal relation between λ and cement fineness S_G. In the case of a w/c ratio of 0.3, the mean free spacing can be expressed as $\lambda=1200/S_G$ (in μm). Hence, at a given w/c ratio, λ is exclusively associated with the specific surface area of cement.

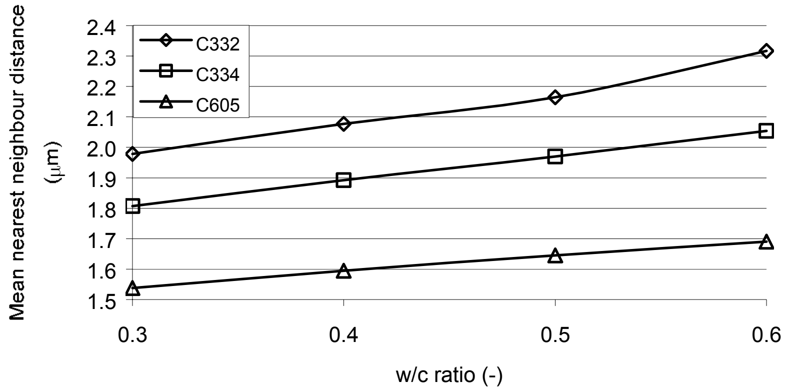

Figure 2.12 Mean nearest neighbour distance for cements with different w/c ratios.

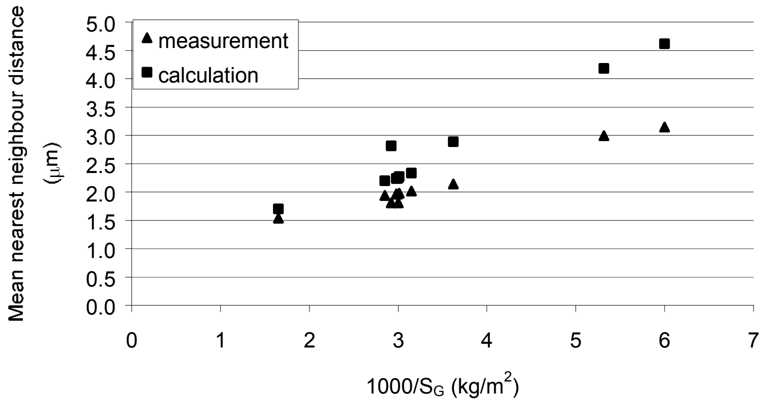

Figure 2.13 Mean nearest neighbour distance $\overline{\Delta_3}$ for cements with different values of specific surface area S_G, w/c ratio involved is 0.3.

In this study, the value of $\overline{\Delta_3}$ is found to be reciprocal to S_G (Fig. 2.13). The theoretical value of $\overline{\Delta_3}$ for spherical particles (with a diameter of $2r$) distributed in a random uniform manner is approximately $0.554(\pi r^2\lambda)^{1/3}$ [Underwood, 1968]. The estimates according to this equation are also plotted in Fig. 2.13. The calculation results are 10~40% higher than the measurements. This indicates that a randomly distributed structure of particles underestimates the flocculation phenomenon in actual cement systems. There seems to be no direct correlation between $\overline{\Delta_3}$ and particle size range: C334 (size range 1~20 μm) and C342 (size range 1~45 μm) reveal similar values of $\overline{\Delta_3}$. This is in agreement with the stereological estimation in a stochastic approach.

However, C_1 reveals a relatively complicated profile. Although C_1 shows a global trend of increase with cement fineness, it is also related to the particle size distribution. C334 and

C332 are similar in all structure parameters. This demonstrates that particle systems of certain fineness level and size distribution would follow an intrinsic pattern during packing process, instead of being a random phenomenon of poor repetition. All the mixtures in Fig. 2.13 have the same w/c ratio (0.3) and thus the same volume fraction (51%) of cement particles in the cubic container. In this case, the average coordination number effectively represents the degree of flocculation between the cement particles.

Comparison between sample C334 and C342 revealed that particles of wider size range are more reliable to flocculate, and thereby lead to a higher value of the average coordination number. In terms of the size distribution, a more sensitive index is proposed in this study to represent the uniformity of the size distribution. This parameter u is defined as the ratio between the mean diameter of cement particles by number and the mean diameter by volume.

$$u = \frac{\sum N_i d_i}{\sum N_i} / \frac{\sum N_i d_i^4}{\sum N_i d_i^3} \qquad (2.10)$$

where N_i is the number of particles with a diameter of d_i. For a mono-sized particle system, the value of u equals 1. For C342, u=0.1183, and for C334, u=0.1831.

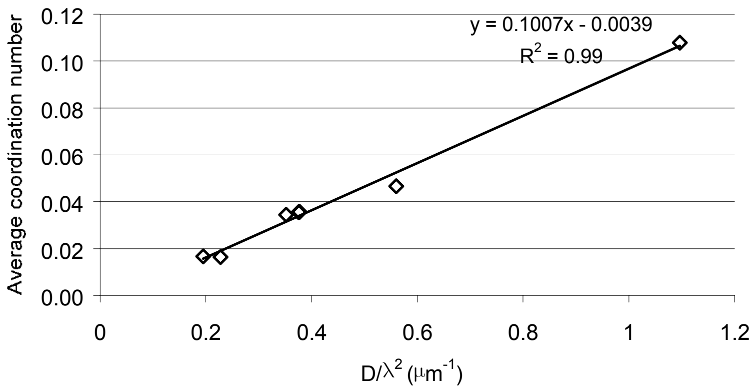

Figure 2.14 *Linear relationship between C_1 and D/λ^2. D is the mean diameter of cement particles, and λ is the mean free spacing of the particles. The solid line is the linear regression of the measurement results. R is the correlation coefficient between C_1 and D/λ^2.*

At a given fineness, the model cement of a wider size range (smaller u) reveals a higher coordination number, corresponding to a higher extent of flocculation. Based on the theoretical calculation of bimodal mixture of spherical particles, Johnson and Anderson [1991] stated that particle systems with a lower u can lead to a denser packing structure. However, the effect of cement fineness is more pronounced than the size range. According to Lu [1993], the inter-particle attraction F between two spherical particles can be expresses as

$$F = -\frac{AD}{24a^2} \qquad (2.11)$$

where D is particle diameter, a is the surface-to-surface distance between the particles, and A is the Hamakar constant. When the application of this equation is extended to actual cement systems of multi-sized particles, the mean free spacing λ can be loosely associated with the global average of the various distances governing attraction in a multi-particle system. As mentioned above, at a certain w/c ratio, $\lambda \sim S_G^{-1}$. Hence, the overall attraction between the cement particles (F) is proportional to the second power of the cement fineness, *i.e.*, $F \sim S_G^2$. This accounts for the observation that the coordination number is more strongly influenced by the cement fineness than by the cement size range. This also demonstrates that particle flocculation is mainly governed by van der Waals forces (as demonstrated by the linear relationship between C_1 and D/λ^2 in Fig. 2.14). This conclusion is supported by experimental observations of a similar mechanical effect obtained by improving the interfacial transition zone (ITZ) with either fine-ground silica fume (pozzolanic particles) or with inert carbon black particles of the same fineness [Detwiler and Metha, 1989].

The average coordination number of model cements is plotted in Fig. 2.15 as a function of the w/c ratio. An approximate negative exponential relationship is found. Smith experimentally studied the packing characteristics of mono-sized rigid particles and reported a similar relationship between void fraction (corresponding to the w/c ratio in this study) and average coordination number [Lu, 1993]. Theoretical calculations also support this observation. Fig. 2.15 reveals that at a low w/c ratio (0.3), C_1 increases sharply with an increase in cement fineness. This means that particle flocculation is strongly stimulated at higher level of cement fineness, requiring higher dosages of superplasticizer. Portland cement fineness has generally increased over the years because of considerations of high early strength. It has recently been argued that in high-performance concrete, a coarser type of cement would offer equivalent long-term performance as finer cement [Bentz *et al*., 1999]. Costs associated with reducing flocculation would support this argument that for lower w/c ratio systems, the use of coarser cements may offer an equivalent or superior performance, as well as reducing production costs for the manufacturer.

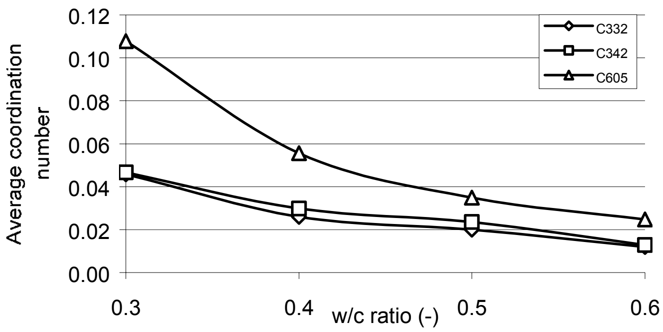

Figure 2.15 Average coordination number C_1 for model cements with different w/c ratios.

2.5 Analytical approach to the relationship between PSD and packing structure

The size distribution and spatial dispersion of Portland cement particles in the fresh state have significant influences on hydration, microstructure development and ultimate properties of cement-based materials. The packing structure is also dependent on size and spatial dispersion of cement particles. The influences of w/c ratio and cement fineness on packing structure have been investigated by stereological measurements in section 2.4, among which the λ and $\overline{\Delta}_3$ have been adopted to represent the spatial dispersion of cement particles in model cements.

In this section, the relationship between cement PSD and the spatial dispersion of cement particles will be elaborated in an analytical approach by means of stereological tools and verified by computer simulation. This quantitative relationship is discussed for four kinds of PSD functions, *i.e.* the Rosin-Rammler distribution (generally accepted as an approximation of cement particle size distribution), the Fuller distribution function (generally accepted for approximating aggregate size distribution), the equal volume (EV) fraction and the equal number (EN) fraction mixtures.

Stereological parameters for size characterisation will be involved for this purpose. The mean intercept length through the particles ($\overline{L}_3$) is the mean value of line length intersecting with particles of grids randomly positioned as well as oriented. This parameter is directly related to the specific surface area (S_G) of cement. It appears that average value rather than maximum value of the intercept length across the cement particles is an important quantity when considering bulk properties of a cement system [Myers, 1963]. On the other hand, λ in cement systems is actually an estimation of *pore size*. The parameters can be calculated as follows:

$$\overline{L}_3 = 4\frac{V_V}{S_V} = 4\frac{N_V \frac{1}{6}\pi \overline{d^3}}{N_V \pi \overline{d^2}} = \frac{2\overline{d^3}}{3\overline{d^2}} \tag{2.12}$$

$$\lambda = 4\frac{1-V_V}{S_V} = \overline{L}_3 \frac{1-V_V}{V_V} \tag{2.13}$$

where $\overline{d^3}$ and $\overline{d^2}$ are the third and second moments, respectively, of the PSD.

For a uniformly random distribution of point particles in a test volume $\overline{\Delta}_3$ is well defined in Underwood [1968] and can be transformed to the following expression:

$$\overline{\Delta}_3 = 0.554\frac{1}{\sqrt[3]{N_V}} = 0.554\sqrt[3]{\frac{\pi}{6V_V}\overline{d^3}} \tag{2.14}$$

Strictly speaking, the derived expression pertains to point particles only, but it should apply to aggregates of small, randomly dispersed particles [Underwood, 1968]. The most important geometric characteristics of cement particles can be derived from the moments of PSD function, which can be calculated according to the specific PSD function. In the previous section, $\overline{\Delta}_3$ and C_1 were directly measured and employed to characterise the degree of flocculation of cement particles in model cements. In this section, $\overline{\Delta}_3$ is calculated from the PSD of cement (or aggregate) particles and compared with the measurement results.

2.5.1 The Rosin-Rammler distribution function

The Rosin-Rammler distribution is generally accepted as a relatively accurate approximation of the actual system of cement particles. The percentage of the particles by weight retained on the various sieves is plotted on a logarithmic scale. The mass (volume-based) fraction of particles passing a sieve is given by:

$$F(V_{pi}) = 1 - \exp(-bd_i^{\,a}) \tag{2.15}$$

where d_i stands for particle size, a and b are constants for a certain particle system, a representing the degree of uniformity in size distribution of the cement particles. The values of a and b can be calculated from the measured cumulative PSD curve. The maximum and minimum sizes of particles are incorporated in these two constants. The density distribution function for V_{pi} follows upon differentiation. Hence,

$$f(V_{pi}) = abd_i^{a-1}\exp(-bd_i^{\,a}) \tag{2.16}$$

The density distribution function can be transformed into particle size distribution (PSD) function using the transformation rule:

$$V_{pi} = \frac{1}{6}\pi d_i^{\,3} N_{pi} \tag{2.17}$$

where N_{pi} is the number of particles in size range i per unit of volume. The resulting particle size distribution function (number-based) is

$$f(d_i) = \frac{6}{\pi} abd_i^{a-4}\exp(-bd_i^{\,a}) \tag{2.18}$$

The n-th moment of $f(d_i)$ is defined as

$$\overline{d_i^{\,n}} = \int_{d_0}^{d_m} d_i^{\,n} f(d_i) d(d_i) \tag{2.19}$$

where d_0 and d_m are the minimum and maximum diameters of the cement particles, respectively.

Direct integration of this equation is not possible. In case of a>1 (generally a>1 for actual cement), the moments of the Rosin-Rammler PSD can be approximated by means of a Gamma function

$$\frac{\overline{d^3}}{\overline{d^2}} = \frac{b^{-\frac{1}{a}}}{\Gamma(1-\frac{1}{a}) - \frac{(bd_0^{\,a})^{1-\frac{1}{a}}}{1-\frac{1}{a}}} \tag{2.20}$$

In case of a<1, Eq. (2.21) is suggested as an approximation [Lu, 1993]:

$$\frac{\overline{d^3}}{\overline{d^2}} = \frac{b^{-\frac{1}{a}}}{1.065\exp(\frac{1.795}{a^2})} \tag{2.21}$$

For an actual cement with a=1.249 and b=0.045 (calculated from the cumulative PSD curve obtained by laser granulometer), the direct calculation revealed $\overline{d^3}$ and $\overline{d^2}$ to be 129.70 μm^3 and 17.86 μm^2, respectively. Thus, the mean intercept length $\overline{L}_3$ is 4.84 μm. The estimation by the Gamma function resulted in a value of 4.82 μm. The comparison between the Gamma approximation and the direct calculation reveals that the estimation of moments by means of the Gamma function provides satisfactory results for the Rosin-Rammler PSD.

2.5.2 Other PSD functions

The calculation for the Fuller distribution, EV and EN fractions are relatively easy because their PSD functions are simple. The PSDs and expressions for different moments are listed in Table 2.3.

Table 2.3 Moments of different PSD functions

PSD type	Fuller	Equal volume	Equal number
$f(d_i)$	$5d_0^{2.5}/(2d_i^{3.5})$	$3d_0^3/d_i^4$	$1/(d_m-d_0)$
$\overline{d}$	$5d_0/3$	$3d_0/2$	$\frac{d_m^2-d_0^2}{2(d_m-d_0)}$
$\overline{d^2}$	$5d_0^2$	$3d_0^2$	$\frac{d_m^3-d_0^3}{3(d_m-d_0)}$
$\overline{d^3}$	$5d_0^{2.5}d_m^{0.5}$	$3d_0^3\ln(d_m/d_0)$	$\frac{d_m^4-d_0^4}{4(d_m-d_0)}$

2.5.3 Experimental verification

Three particle systems were generated by the SPACE system with Fuller size distribution. The volume fraction of particles is 51%. $\overline{\Delta}_3$ is calculated according to Table 2.3 and Eq. (2.14). To verify the reliability of calculation by stereological theory, $\overline{\Delta}_3$ was also measured by SPACE (Table 2.4). The measurements slightly exceed the calculation. This is attributed to increased order in model cements. C=0.554 in Eq. (2.14) is suitable for a randomly dispersed system of particles. However, the packing structure of particles in actual cement will be governed partly by deterministic and partly by stochastic influences. Therefore, at higher volume fraction of cement particles, order will start to overrule the influences of random positioning during the packing process. On the other hand, the higher measurement values demonstrate that SPACE offers a more realistic simulation of the packing structure than those based on the concept of the RG-based models.

Table 2.4 Comparison between calculations and measurements of $\overline{\Delta}_3$

Size range μm	$\overline{d^2}$ μm^2	$\overline{d^3}$ μm^3	$\overline{L}_3$ μm	λ μm	$\overline{\Delta}_3$, μm Calculation	Measurement
1~20	5	22.36	2.98	2.82	1.57	1.74
1~30	5	27.39	3.65	3.45	1.70	1.77
3~20	45	348.57	5.16	4.88	3.97	4.62

The mean free spacing λ represents the uninterrupted inter-particle distance averaged over all possible particle pairs, while $\overline{\Delta}_3$ refers to the average distance between nearest neighbour pairs only. Therefore, $\overline{L}_3$ and λ are more suitable to characterise the morphological evolution of solid phase (unhydrated cement and hydration products) and pore space, respectively, during the hydration process. In the case of actual cements, the aforementioned geometric (stereological) parameters can be directly estimated from moments of the PSD functions, for the four types of PSD functions discussed in this section.

2.6 Mathematical morphology measurements

Size and spatial dispersion of phase in material microstructure can be characterised on the basis of granulometric distribution functions (see section 1.5.2). Granulometric distribution functions are general and useful methods for characterising the size of a specific phase, since it can be used independently of the nature of set *X* reflecting the phase of interest. The granulometric distribution (the so-called opening distribution) in measure on 2D section image is given by

$$G(\omega) = \frac{A_A(X \cap (Z\Theta B(2\omega))) - A_A(X_{B(\omega)} \cap (Z\Theta B(2\omega)))}{A_A(X \cap (Z\Theta B(2\omega)))} \tag{2.22}$$

where $B(\omega)$ is a convex structuring element of size ω, it can be a square, a hexagon, a segment, etc. $G(\omega)$ measures the change of area fraction A_A of set *X* incurred by the opening operation with structuring element $B(\omega)$. The use of a linear structuring element (*l*) leads to linear granulometries that are particularly interesting since the estimate in 2D remains valid for 3D. Opening granulometry allows using linear erosion, denoted as '*Psegbin*(*l*)', to directly obtain granulometry in that it represents the probability of a segment *l* to be included in the phase of interest. Of course, erosion by a segment is sensitive to orientation of the segment. Hence, measurement of linear granulometry in different directions allows evaluating the isotropy of the phase of interest with respect to the degree of orientation in phase dispersion.

2.6.1 Measurement procedures

A simple approach with mono-sized (particle radius denoted as *r*) cement system is used in this section for illustration purpose. Six serial sections were produced with a spacing of *r*/2 at five hydration stages (series 1~5 corresponding to a increasing maturity) and subjected to morphological measurements after being transformed into binary images (by a segmentation process). The morphological evolution of solid phase and pore space during the hydration process can be quantitatively characterised by means of measurements of covariance *C*(*h*) (the probability of two points $\{x, x+h\}$ to remain in phase of interest, *h* is defined as lag), 'Psegbin' (probability of a segment *l* to be inserted into phase of interest) and 'Phexbin' (probability of a hexagon fitting into phase of interest) with Micromorph (a software package of mathematical morphology, see Jeulin [2001]).

Spatial distribution (dispersion) of a specific phase is very important to account for the presence of scales in material structure [Jeulin, 2000]. Scales and their superimposition can be quantified from second order statistics based on covariance function, from which nested structures such as clusters, repulsion effects, as well as periodicity in images are easily detected [Serra, 1982]. In this study, covariance and 'Psegbin' and 'Phexbin' measurements were performed on all the section images, and the results for different hydration stages were averaged over the six sections to improve accuracy. The field size corresponds to the whole sampled image (800x800 pixels).

2.6.2 Results of morphological measurements

Fig. 2.16 explicitly illustrates the porosity decline during the hydration process. The value of the covariance function at *h*=0 is a direct measure of A_A of the phase of interest. The covariance decreases gradually with length of lag h, because the possibility of overlapping between the phase of interest and its translation with lag h declines. When h reaches a threshold value, the covariance turns to be relatively constant. This stable value $(A_A)^2$ is defined as the asymptotic value of the covariance curve, whereas the threshold value of h defined as correlation length. At this length scale, the events {x belonging to phase of interest} and {$x+h$ belonging to phase of interest} become statistically independent. This length scale is in fact associated with the average pore size. It is clear from Fig. 2.16 that the correlation length is decreasing during the hydration process, corresponding to the declining pore size.

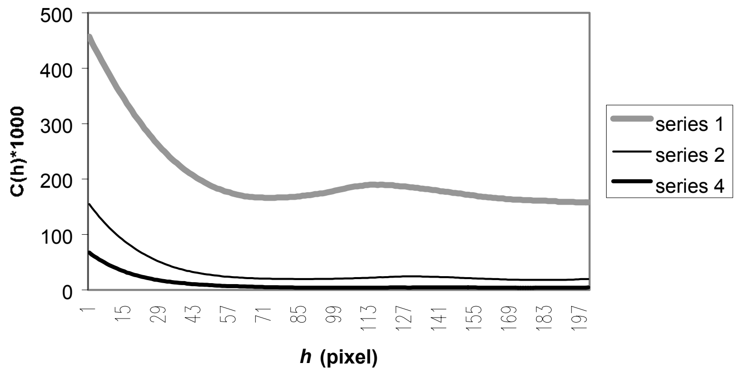

Figure 2.16 Covariance functions of the pore space measured for series 1, 2 and 4. For example, the covariance of pore space for series 2 declines from porosity p =0.155 (for h=0) to p^2 =0.024 at a distance of 50 pixels.

Covariance function is also known as two-point correlation function; it is instrumental for obtaining statistics of material microstructure, and has been used to estimate fluid permeability of sandstones [Berryman and Blair, 1987]. It should be noted, however, that the size characterisation approach by Berryman and Blair contains some imperfections. They proposed a *characteristic pore size* R_c, defined as the intersection of the tangent of the covariance function of pore space at lag 0 and the horizontal line given by the asymptotic value p^2:

$$R_c = 4(p - p^2)/S_V = 4R_{hv}(1-p) = 4R_{hs}p \qquad (2.23)$$

where R_{hv} and R_{hs} are hydraulic radius of pore space and solid phase, respectively. The hydraulic radius of pore space is defined by Dullien [1992] as the pore volume divided by wetted area. In the case of full saturation, R_{hv} can be defined as the ratio of porosity p and specific surface area S_V. Since the surface areas of solid phase and pore space are the same, the hydraulic radius of solid phase R_{hs} should be $(1\text{-}p)/S_V$. Hence, the stereological parameters characterising the size of solid phase ($\overline{L}_3$) and pore space (λ) are associated with the hydraulic radii of solid phase and pore space by a constant factor of 4, see Eqs. (2.12) and (2.13).

It follows that R_c is identical for the pore space and the solid phase, but a slight difference is observed (see Fig. 2.17), mainly due to statistical fluctuations of the experimental curve. However, it is not a characterisation of pore size, but a length scale proportional to the linear dimension of the RVE/RAE. The RVE is the statistically homogeneous sub-volume of the material representative for a certain bulk property. The value of R_c is increasing during the hydration process, corresponding to the increasing size of the RVE/RAE for porosity distribution with maturing cement pastes. Hydration induces continuous changes in the cement microstructure, yielding an RVE for more matured cement paste exceeding in size the one for young cement. The statistic concept of heterogeneity and the RVE/RAE will be elaborated in Chapter 4. Hence, R_c defined by Berryman and Blair is obviously not a size characterisation of pore structure, since average pore size is decreasing during the hydration process. Pore size can be assessed properly by the mean free spacing or by the correctly defined hydraulic radius.

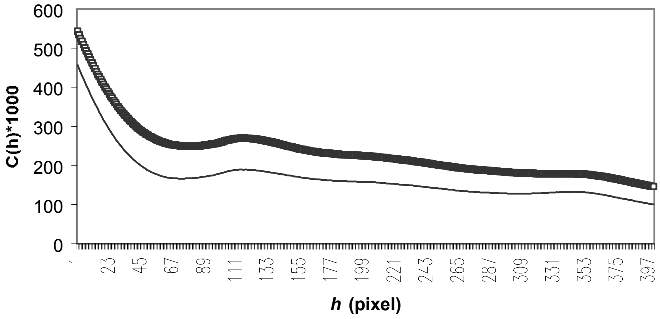

Figure 2.17 Covariance of pore space (thin line) and solid phase (thick line) for series 1.

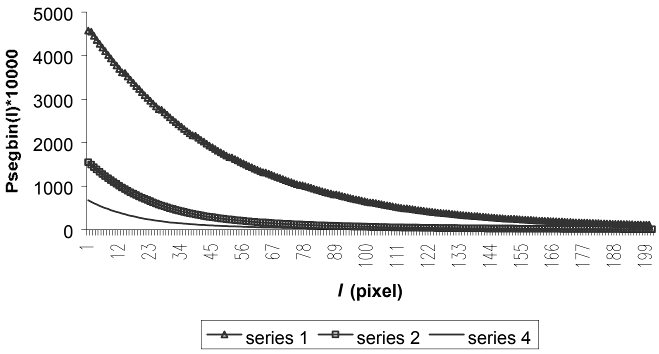

Figure 2.18 Psegbin curves of pore space for series 1, 2 and 4.

Fig. 2.18 presents the Psegbin curves for series 1, 2 and 4. The sharp decline with l is expected in view of the decrease in porosity and pore size during the hydration process. These measurements can also be applied to section images of actual cementitious materials. For illustration purpose, the same morphological approach was applied to a SEM image (Fig. 2.19) of a mortar (w/c=0.4) showing dense C-S-H around unhydrated grains with less dense outer products. The unhydrated cement phase was extracted by means of image segmentation according to a 'maximization of the average global contrast' proposed by Kolher [1981].

Figs. 2.20 and 2.21 present the measurements on unhydrated cement phase and pore space. The covariance $C(h)$ and probability function $Psegbin(l)$ reflect anisotropy of the material structure, since they depend on the orientation of vector h and segment l. Anisotropy can be accessed from directional measurements of covariance and the 'Psegbin' function. In this study, the measurements were performed in six directions (defined from coding the neighbours of a pixel in the hexagonal grid) and no significant anisotropy was observed for the cement microstructure.

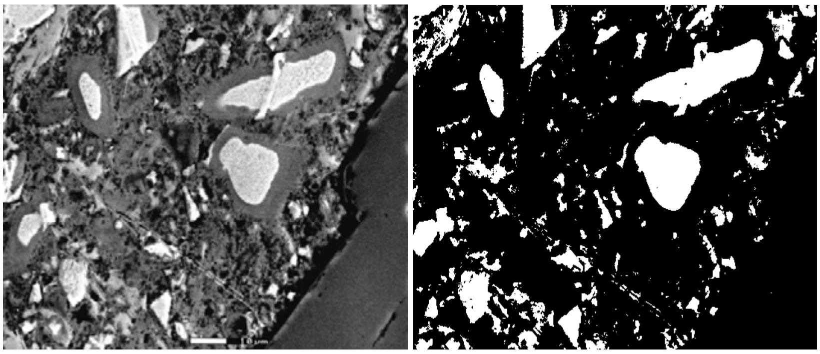

Figure 2.19 *Original SEM image (left) and the corresponding binary image (right) of a mortar, imaging by Lange D, Jennings H and Shah SP, Northwest University, available on the website of Concrete Microscopy Library [Lange, 1999]. The field width is 115 μm.*

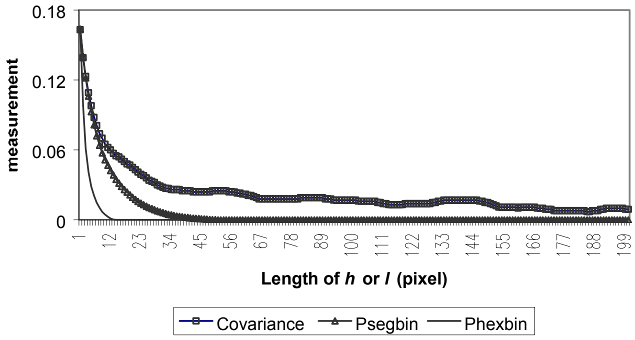

Figure 2.20 *Measurement results of SEM image of hydrated cement structure*

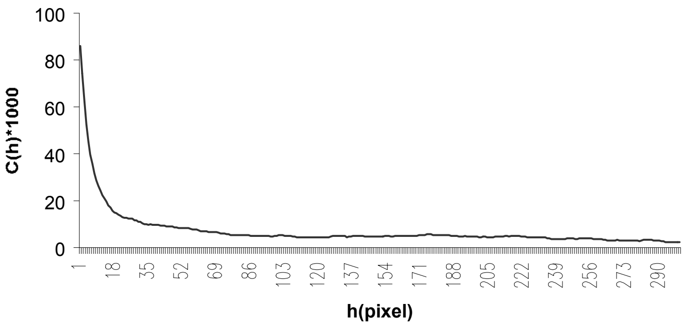

Figure 2.21 *Covariance of pore space in mortar (w/c=0.4, see Fig. 2.19), porosity is 8.5%.*

The example discussed here is only an illustration of the application of mathematical morphology measurements to SEM images. A more specific mathematic morphology measurement, the so-called opening distribution technique, will be applied to 2D section images of actual cement pastes for characterising pore size distribution. This will be the subject of Chapter 3. The measurement of pore size distribution in cement pastes with different w/c ratios and degrees of maturity allows a *systematic investigation* of the evolving pore structure during hydration process. The derived structural information includes porosity, pore size distribution, critical pore size; they can be directly used to predict mechanical and transport properties of cementitious materials.

2.7 Summary

The SPACE system provides reliable and realistic simulation of cement particle packing. The packing structure can be characterised by stereological parameters describing the size distribution and the spatial dispersion of cement particles. Basic stereological parameters can be associated with composition and configuration aspects of material structure. The most important spacing parameters, mean free spacing and mean nearest neighbour distance have been successfully employed to characterise the spatial dispersion of cement particles (or aggregate grains) in the fresh state of particle packing of cementitious materials.

In combination with the average coordination number, the mean nearest neighbour distance is used to evaluate the degree of particle flocculation in packing structure of cement system. The influences of the w/c ratio and PSD on the packing structure are explored by means of computer simulation with the SPACE system. The influence of uniformity in PSD, of specific surface area (fineness) on cement particle flocculation was studied. A lower specific surface area and a more uniform PSD leads to a lower average coordination number and a larger mean nearest neighbour distance (corresponding to a lower degree of flocculation). In view of the disproportionately increased flocculation at higher fineness levels, the application of coarser cements is recommended for HPC with a low w/c ratio.

For Rosin-Rammler distribution, Fuller distribution function, the equal volume (EV) fraction and the equal number (EN) fraction mixtures, the size-characterising and spacing parameters can be calculated according to the specific PSD function of cement particles (or aggregate grains). This allows investigating the influence of PSD on packing structure and microstructural development of the materials in an analytical approach and in a quantitative manner.

In addition, some basic mathematical morphological measurements are applied to model cements at different hydration stages to illustrate the capability of this method for characterising material structure. The results reveal that morphological functions are useful tools for characterising the structural evolution of solid phase and pore space during the hydration process.

Characterisation of Pore Structure by Image Analysis of Specimen Sections

Two major obstacles to successfully correlate pore structure and material properties are the accuracy of total porosity measurements and, especially, the characterisation of the extremely complex pore structure. Several techniques have been developed and employed to determine the porosity and pore structure morphology in cement-based materials. They can be categorised as indirect experiment methods (MIP, BET surface area, nitrogen absorption, low temperature calorimetry, etc.) or as direct ones based on quantitative image analysis. The reliability of experimental results such as MIP data is restricted by assumptions about pore geometry that are not supported by microscopic evidences. The deficiencies of MIP technique have been discussed in Chapter 1. In contrast, image analysis is drawing increasing attention due to the fact that it can provide direct observations of pore space.

The use of backscattered electron (BSE) imaging to study the pore structure in cement paste and concrete is a comparatively new technique. The amount and distribution of the pore features can be quantified by image analysis. Based on area classification of the pore features, the pore size distribution can be derived. This is the conventional approach in image analysis for characterising pore size distribution. However, the pore features seen on a section are interconnected above and below the section plane. It is therefore inappropriate to consider the profiles of pore features as individual objects. Scrivener [1989a] stated that far more suitable are the techniques of mathematical morphology. In this study, pore size distribution is characterised by this mathematical morphology approach, the so-called opening distribution technique.

The stereological theory (introduced in Chapter 2) can help to derive 3D structural information from 2D observations. This chapter deals with the application of stereological analysis and opening distribution technique to section images of *actual cement paste specimens* with various w/c ratio and degrees of hydration. Porosity, pore size distribution and critical pore size will be determined by the opening distribution technique. In addition to these ordinary characterising parameters, a new 3D characterising parameter, the so-called pore distribution density, is proposed in this study with the aid of the stereological theory.

Sections 3.1 and 3.2 give a brief introduction to the sample preparation of cement pastes and the image acquisition procedures. Section 3.3 presents the results of basic stereological analysis performed on section images of cement paste specimens, followed by a comparison between the analysis results obtained for real cement pastes and model cements. The most important part in this chapter is section 3.4, dealing with the opening distribution technique and the research findings. Section 3.5 explores the fractal dimension of cement paste on the basis of image analysis. The new characterising parameter (pore distribution density) is proposed in Section 3.6.

3.1 Sample preparation

SEM imaging with a BSE detector requires a highly polished surface because improper preparation methods may obscure features, and even create artefacts that may be misinterpreted [Struble and Stutzman, 1989]. Proper preparation includes casting of cement paste, drying of the specimen, epoxy impregnation, cutting, and polishing of the section surface. The cement pastes and SEM images used in this chapter are selected from the section images of cement pastes made by Ye in an extensive experimental program for his PhD study. This author applies mathematical morphological and stereological methods, as well as the local porosity theory (see Chapter 4) to the section images for the characterisation of pore space. The sample preparation procedures are briefly introduced in this section; for the experimental details refer to Ye [2003]. Cement pastes with w/c ratios of 0.4, 0.5 and 0.6 were cast in $40 \times 40 \times 160$ mm^3 prism and de-moulded after one day. The specimens were cured in a chamber at 20 °C and at a 90% humidity level until the day of testing (3, 7 and 14 days, respectively). Then the specimen pieces were subjected to vacuum drying until a constant weight of the samples was reached before epoxy impregnation with a type of epoxy-resin of very low viscosity. After cutting, the samples were polished by hand at a moderate pressure on the middle-speed lap wheel with sand papers of p320, p500 and p1200, respectively.

It is well known that pores exist in cement paste over a wide range of scales from ~1 nm to >1 mm. Small capillary pores play a very important role with respect to the permeability of cement paste. A digital image for quantitative analysis of pore structure must have an adequate resolution so that it can display the relevant range of length scales. Therefore, a rather high optical resolution of the SEM image is required to ensure the detection of small capillary pores. On the other hand, a single section image, if large enough to contain a statistically significant number of features, may suffice to obtain valid results. Hence, it is also necessary for each SEM image to cover an area element as large as possible with sufficient features of pore space. It is suggested by Lange *et al*. [1994] that a magnification of around 400x (corresponding to a resolution about 0.5 μm/pixel) is adequate for routine measurement of porosity from BSE images. In this study, the physical size of the reference region of each SEM image is 263 μm in length and 186 μm in width (1424×968 pixels). The magnification is 500x corresponding to a resolution of 0.185 μm/pixel. 12 BSE images of different parts of each specimen section are taken and the image analysis results are averaged to guarantee a satisfactory accuracy. Lange *et al*. [1994] proved that 12-image sets for cement paste provide a value for pore area fraction within a relative error of 15% of the true value at a 95% confidence level. Ye [2003] also stated that a total area of about 5×10^5 μm^2 (corresponding to 10 images of 263×186 μm) needed to be investigated for reliable estimation of porosity at a confidence level of 95%.

3.2 Image acquisition and segmentation of pore space

A BSE detector in the water vapour mode was used for image acquisition. The principle of BSE imaging is that the intensity at which electrons are backscattered depends on the local atomic number and topography of the specimen. For a polished section of paste specimen, the unhydrated cement appears bright, the calcium hydroxide (CH) light grey and the other hydration products dark grey. The pore space (being an absence of solid) does not scatter electrons and therefore appears uniformly black. The technical parameters were constant during the imaging process; the water vapour pressure at 4.0 Torr and temperature at 5^{o}C. The relative humidity was around 61%. For imaging details, see Ye *et al*. [2002] or Ye [2003]. Fig. 3.1 provides an example of BSE image for cement paste and the corresponding grey level histogram.

It is not easy to define the boundary between C-S-H gel and pore space directly from the BSE image. Since the average atomic number of epoxy is much lower than that of cement hydration products, pores impregnated by epoxy can be distinguished as black areas in BSE images. The unhydrated cement and CH have fairly uniform grey levels, resulting in sharp peaks in the grey level histogram. Due to variation in composition, the grey levels of other hydration products (basically C-S-H gel) form a relatively shallow, but still clearly identifiable peak in the histogram. Scrivener [1989a] suggested to choose a threshold value of grey level for segmentation of pore space from the lower slope of the peak produced by C-S-H hydration products in image histogram (see Fig. 3.1). The pore areas observed on a section image are defined as pore features of which the perimeters are defined as profiles in image analysis. In this way, the original BSE image can be segmented to create a binary image reflecting the pore features in the field image of the specimen section. It has been demonstrated by Scrivener [1989a] that consistent results can be obtained by such segmentation techniques with a grey level threshold. Fig. 3.2 presents the corresponding binary image reflecting the pore space (phase of interest) for the cement paste shown in Fig. 3.1 (with a w/c ratio of 0.4 at 1 day of hydration). The binary images were then subjected to stereological analysis and opening distribution technique. In this chapter, use is made of the stereological theory and mathematical morphology techniques for assessment of the pore size distribution, the pore distribution density, as well as the porosity distribution.

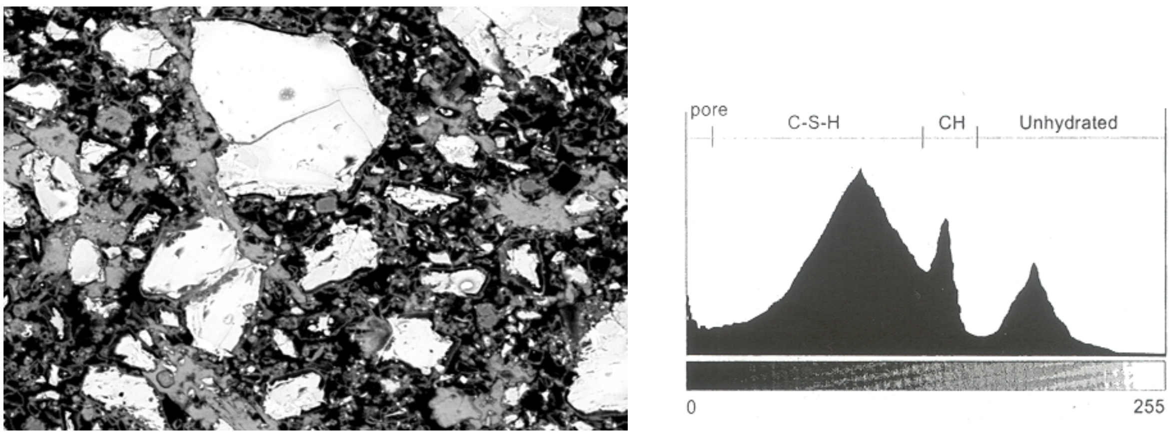

Figure 3.1 An example of SEM image (with BSE detector, left) and corresponding grey level histogram (right). After Ye [2003].

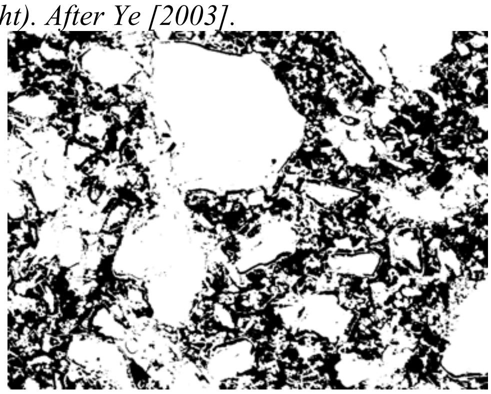

Figure 3.2 The binary image of cement paste with w/c ratio of 0.4 at 1-day hydration (black area representing pore space, the rest constituents of cement paste set to white background). The original SEM image is given in Fig. 3.1.

3.3 Stereological analysis of SEM images

One important stereological parameter to characterise the pore structure in hydrated cement is the surface area per unit of test volume (sample), S_V. For model cements, this parameter can be measured by tessellation on the surface of solid phase (or pore space) and recorded as a function of the hydration time. It can also be calculated from the perimeter length of pore features per unit of test area L_A (that can be determined by edge detection in section image analysis) applying the relationship $S_V = 4L_A/\pi$ [Underwood, 1968]. Although the former approach is only applicable to 3D model cement, the latter technique is applicable to both model cements and SEM section images of actual cement pastes.

The total perimeter length of pore features observed on SEM images was measured and divided by area of the section image, yielding L_A. Then, the surface area of pore space per unit test volume (denoted as S_V) can be derived according to Eq. (2.5). This is a standard stereological parameter, the value of which is the same for solid phase and for pore space because they are complementary to each other. A better-known parameter is the specific surface area of pore space, denoted as $(S_V)_{pore}$. It is defined as S_{pore} / V_{pore}, herein S_{pore} and V_{pore} means the total surface area of pore space (in μm^2) and total volume of pore space (in μm^3). It is obvious that $(S_V)_{pore} = S_{pore} / V_{pore} = S_V / p$, where p is the global porosity.

The stereological measurements are performed on section images of cement pastes with w/c ratios of 0.5 and 0.6, at hydration stages of 3, 7 and 14 days, respectively. The results of stereological analysis are presented in Table 3.1. The area fraction of porosity on section images is an unbiased estimator of the global porosity (p) in cement paste. As hydration progresses, the porosity of cement paste decreases as expected, and the pore size also exhibits an obvious decline (reflected by a decline in L_A during the hydration process). This is due to the fact that cement hydration products (light grey and dark grey as indicated in the SEM image) gradually fill up the available space. The decline of porosity and L_A follows a similar pattern for cement pastes with different w/c ratios. At a given hydration stage, the porosity of cement paste with a w/c ratio of 0.6 is higher than the paste with a w/c ratio of 0.5; this is a natural result of the higher water content at the initial state of cement hydration.

Table 3.1 Stereological estimation based on SEM image analysis

Hydration time (days)		A_A %	S_V μm^2/μm^3	$(S_V)_{pore}$ μm^2/μm^3	L_A μm/μm^2
w/c = 0.5	3	32.18	0.358	1.113	0.281
	7	26.64	0.302	1.135	0.238
	14	18.61	0.195	1.048	0.153
w/c = 0.6	3	39.67	0.523	1.318	0.411
	7	32.48	0.399	1.227	0.313
	14	21.62	0.236	1.090	0.185

The stereological analysis of cement pastes at different degrees of hydration allows exploring the morphological changes of the pore structure during the hydration process. For model cements generated by SPACE system, the integrated stereological analysis can provide the structural information such as p, L_A and S_V. In mode cement, the solid phase is complementary to pore space. Therefore, the morphological (geometrical) properties of the solid phase introduced in Chapter 2 are indirect representations of the morphology of the pore structure.

The results of stereological analysis obtained for the actual cement pastes and model cement C342 under comparable conditions will be compared in this section. Fig. 3.3 provides a comparison of the stereological parameters, including the specific surface area of pore space, denoted as $(S_V)_{pore}$, as well as the perimeter length per unit test area L_A, derived from SEM images of actual specimens and from model cement C342. Due to the sub-representative sampling strategy as discussed in Chapter 1, a good agreement between the numerical results and the experimental data cannot be claimed.

However, it should be emphasized that the results obtained from experimental and computer simulation approaches reveal quite similar values, especially for the specific surface area. This implies that a proper computer simulation approach, although based on a simplified modelling concept, allows for a reliable characterisation of the microstructure development in cement paste. The divergence in L_A data can be attributed to the higher fineness level of the cement (420 m^2/kg) used in experiments. The experimental cement hydrated faster than the model cement, resulting in a much lower porosity compared to the model cement. For example, at 14 days of hydration (w/c=0.6), the model cement reveals a porosity of 36%, whereas the porosity in the actual cement paste is 22%. According to the relationship

$$L_A = \frac{\pi}{4} S_V = \frac{\pi}{4} p \cdot (S_V)_{pore} \tag{3.1}$$

The low value of L_A for the experimental cement is associated with the lower porosity, and is further stimulated at the late stage of cement hydration, as shown in Fig 3.3.

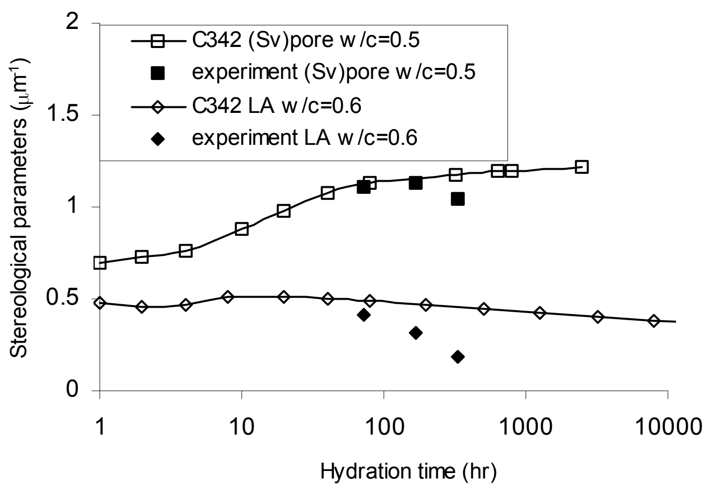

Figure 3.3 *Comparison of stereological analysis results (specifically, specific surface area and L_A) obtained for actual cement paste specimens (indicated as 'experiment') and for model cement C342. The w/c ratios involved are 0.5 and 0.6, respectively.*

3.4 Pore size distribution by opening distribution technique

As mentioned earlier in this chapter, a so-called opening distribution technique has been suggested for characterising pore size distribution in cement pastes. However, a systematic study of the capability of this technique has not been carried out in concrete technology. In this study, the pore size distribution will be measured by means of this approach for cement pastes with various w/c ratios and degrees of maturity. The study is expected to yield a relatively accurate characterisation of pore size distribution and to reveal the influences of technical parameters on the evolution of pore structure during the hydration process.

3.4.1 Opening distribution technique

Opening distribution is a type of granulometric analysis by measuring changes in amount of phase of interest after an opening operation. It is defined as granulometric distribution functions in mathematical morphology (see section 1.5). The clustering of objects in space can be studied by volume fraction measurements (of phase of interest) after a dilation operation with structural elements of increasing size [Jeulin, 2000]. In a similar approach, the pore size distribution in cement paste can be determined by means of area fraction measurements after the opening operation on pore space with structural elements of increasing size. This formulates the foundations of applying opening distribution technique to section images for deriving pore size distribution. The structuring element used in this study is square; the size of structuring element is represented by linear dimension of the square. The *opening distribution curve* (pore size distribution) is obtained by plotting the area fraction of pore space after each step of opening operation versus the linear dimension of the structuring element. The obtained curve can be considered as cumulative pore size distribution. It is a monotonously decreasing function of size of the structuring element.

3.4.2 Determination of critical pore size

The critical pore diameter is an important parameter since it is associated with the percolation threshold of porosity. It is defined as the diameter of the pore that completes the first connected pore pathway if the pores are added to the network one by one in a descending order (from largest to smallest). It is generally accepted that the smaller the critical pore size, the finer the pore structure. The critical pore size is a unique transport length scale of major significance for the permeability properties. The conventional way to determine the critical pore diameter is by way of the inflection point of the cumulative pore size distribution curve obtained by MIP.

Katz and Thompson [1986] supported the conjecture that mercury injection is of percolation geometry and considered the characteristic length l_c as corresponding to the percolation threshold. A typical mercury injection curve (as shown in Fig. 3.4), reflecting the volume percentage of mercury intruded as a function of the applied pressure, is S-shaped; after a gradual increase under rising pressure, a rapid rise in volume percentage of mercury intrusion occurs at a certain pressure, whereupon gradually a plateau value is reached. This stage of rapid rise is interpreted as the moment when the intruded mercury has formed the first connected cluster spanning the sample. The inflection point of the rapidly rising portion of the curve can be seen as the percolation threshold, expressed by the threshold pressure P_t. Next, the characteristic length l_c is derived from the Washburn equation: $l_c = -4\gamma \cos\theta / P_t$, where γ is the surface tension (=485 dyn/cm), and θ is the contact angle (130°). So, the critical pore size l_c can be associated with the *inflection point* of the cumulative pore size distribution curve.

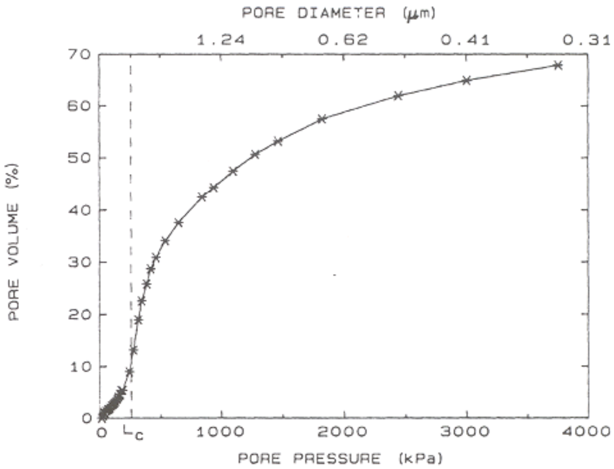

Figure 3.4 *Typical mercury injection curve taken on a quartz cemented sandstone from eastern Utah. The characteristic length is labelled l_c. The pore diameters are calculated from the pore pressures using the Washburn equation. After Katz and Thompson [1986].*

In this study, the critical pore size is determined in a similar way, on the basis of the pore size distribution curve obtained by the opening distribution technique instead of MIP. The size of structuring element corresponding to the inflection point of the opening distribution curve is defined as critical pore size. The inflection point is reflected by the peak of the derivative curve of the opening distribution curve (pore area fraction after opening operation vs. size of structuring element).

3.4.3 Influence of image resolution

The optical magnification required for visualization of the material microstructure at the level of the researcher's interest defines both the micro-structural level displayed by the field, and the geometric structure of the RVE. Hence, *optical resolution* and observed *level of the microstructure* are intimately connected: higher densities of geometric parameters will be observed under higher optical resolution. Hence, image resolution (optical resolution) has significant impact on the results of section image analysis, and thereby also on the accuracy of critical pore size obtained from the opening distribution curve.

Fig. 3.5 and Table 3.2 reveal the influence of image resolution on the accuracy of determining critical pore size. The curves are derivatives of the opening distribution curves (*i.e.* pore size distribution), whereby peaks arise at inflection points of the pore size distribution curves. The BSE images of cement paste (with a w/c ratio of 0.35) at different resolutions are downloaded from the Internet [Stutzman, 1999]. A resolution of 0.49 μm/pixel fails to differentiate the pore structure between 7 and 28 days of hydration. Although at the highest magnification (2000x) trivial as well as subtle changes of the pore structure were revealed, resolutions of 0.293 and 0.146 μm per pixel result in similar values of the critical pore size.

Some doubt exists as to the potentials of image analysis to study cement permeability that is generally associated with small capillary pores. Bágel and Zivica [1997] investigated the relationship between pore structure (determined by MIP) and permeability of pastes and mortars. He concluded that the fraction of pores between 100~10000 nm (*i.e.* 0.1~10 μm) is highly correlated with cement permeability (correlation coefficient of 0.953). For smaller pores in the 3.7~7500 nm range, the correlation coefficient declines to 0.883. Therefore, it is reasonable to study cement permeability with image analysis techniques, as long as a satisfactory resolution of about 0.15~0.20 μm per pixel is ensured. The resolution in this study is 0.185 μm/pixel.

Table 3.2 Value of critical pore size at different hydration times (in μm)

Resolution (μm/pixel)	1 day	7 days	28 days
0.488 (600x)	1.953	0.976	0.976
0.293 (1000x)	2.344	0.879	0.586
0.146 (2000x)	1.904	0.879	0.586

Note: the number indicated in parenthesis is magnification.

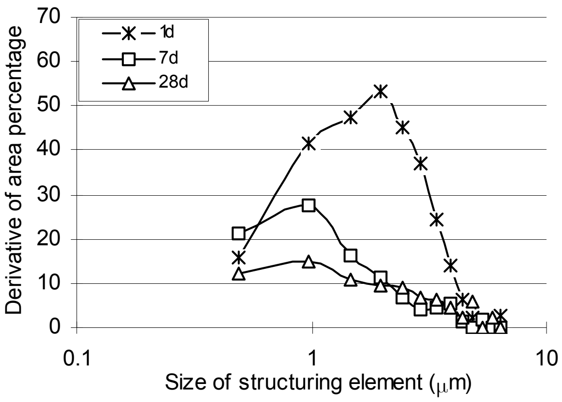

(a) Resolution: 0.488 μm per pixel

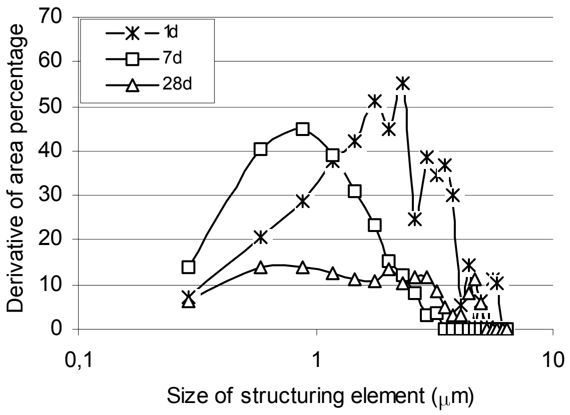

(b) Resolution: 0.293 μm per pixel

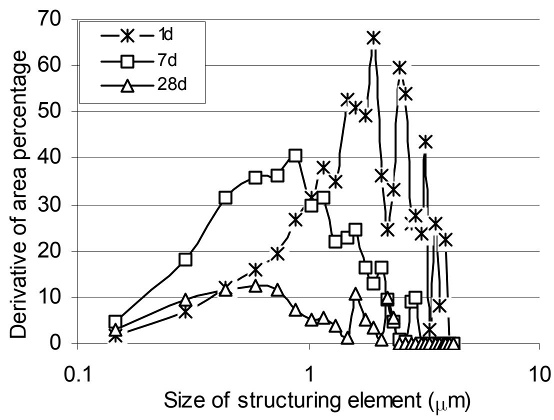

(c) Resolution: 0.146 μm per pixel

Figure 3.5 *Influence of resolution on the accuracy of determination of critical pore size by means of opening distribution curve, for cement paste with a w/c ratio of 0.35 at 1, 7, 28 days of hydration.*

3.4.4 Results and discussions

Overall measurement of the porosity p is fairly straightforward as the average area fraction measured on 2D sections is an unbiased estimate of the volume fraction. The area fraction of porosity is equal to the value of the *opening distribution curve* when the size of structuring element is zero (Fig. 3.6). Since the curves of the *opening distribution* change with hydration time in a similar manner for different w/c ratios, only the curves for w/c=0.6 paste are presented in Fig. 3.6. The critical pore size l_c is determined as shown in Fig. 3.7. The results for pastes of various w/c ratios at different hydration times are presented in Table 3.3. The values of critical pore size are striking different from the experimental results of Cui and Cahyadi [2001]. Based on MIP for pore size distribution, they reported a critical diameter of 0.069 and 0.010 μm for w/c=0.3 pastes at the age of 7 and 210 days, respectively. The values for w/c=0.4 pastes are 0.045 μm at 7 days, 0.036 μm at 35 days, and 0.010 μm at the age of 210 days. In view of the ink-bottle effect, the results obtained by MIP can be expected to yield much lower values for the critical pore size than in the case of results obtained by image analysis.

Although the two techniques revealed different orders of magnification for l_c, the same trend is found. The critical pore size decreases with hydration time. The higher the w/c ratio, the larger is the critical pore size. Hence, this approach allows studying the evolution of pore structure in cement paste with different w/c ratios. The critical pore size reduces rapidly in the first 7 days (or so) of hydration, and then gradually decreases to a stable value. It is not possible to convert the opening distribution to a direct representation of 3D pore size distribution, but it is useful, nevertheless, to measure the degree of difference between pore structures in cement pastes.

Pore size distribution obtained by various experimental or numerical modelling approaches has been reviewed in section 1.4. The direct calculation of pore size distribution in 3D model cement, developed by Ye [2003] provides a rather straightforward measurement of pore size distribution. For a model cement paste with a w/c ratio of 0.6, Ye's data of pore size distribution, revealed a critical pore size of about 3 μm at 4 days of hydration (corresponding to a degree of hydration of 0.64). The value for cement paste with a w/c ratio of 0.3 is 1.5 μm at this degree of hydration. This is in good agreement with the data obtained by opening distribution on section images of actual paste specimens (see Table 3.3). This demonstrates that, although based on image analysis of 2D sections, the opening distribution technique reveals realistic 3D structural information on pore size distribution in cement pastes.

However, a comment has to be made on Ye's modelling approach to pore size distribution by filling testing spheres of increasing sizes. As a straightforward 3D measurement, it can be expected to be time consuming. One accessible definition of size for a connected phase such as pore space in hydrated cement pastes is the mean volume-based star volume, $\bar{v}^*_V$. This is defined as the average volume of the phase that can be seen unobscured from a random point within the phase [Serra, 1982]. The star volume can be estimated for a 3D system from either isotropic uniform random (IUR) or vertical uniform random (VUR) sections using the point-samples intercepts (PSI) method developed by Gundersen and Jensen [1985]. This method allows more efficient derivation of the pore size distribution for model cements, based on classification of the so-called star sizes.

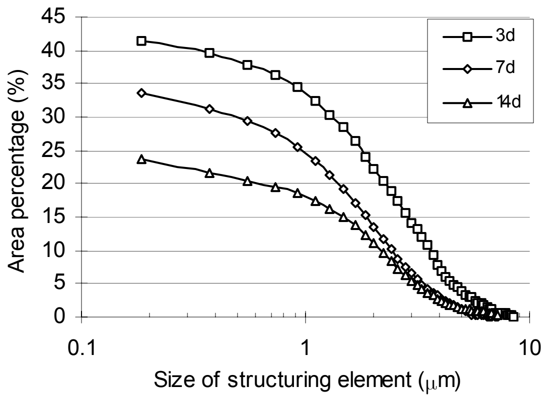

Figure 3.6 Pore size distribution (opening distribution) curves for cement paste with a w/c ratio of 0.6 at 3, 7, 14 days of hydration, respectively.

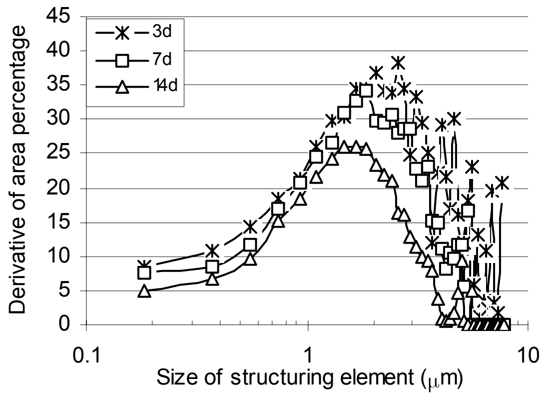

Figure 3.7 Determination of critical pore size from derivatives of pore size distribution curves for cement paste with a w/c ratio of 0.5 at 3, 7, 14 days of hydration, respectively. The maximum peak point corresponds to the inflection point on the pore size distribution curve.

Table 3.3 Porosity and critical pore size obtained by opening distribution

w/c	Age (days)	Porosity p (%)	Critical size l_c (μm)
0.4	3	34.50	1.847
	7	24.85	1.293
	14	15.53	1.108
0.5	3	33.18	2.586
	7	25.41	1.847
	14	18.46	1.478
0.6	3	41.40	3.694
	7	33.46	2.401
	14	23.68	2.032

The conventional way to derive pore size distribution from section image analysis is a direct area histogram, *i.e.*, the pore features revealed on section images are classified according to their areas and the pore size distribution curve is obtained by plotting the area fraction of porosity versus the equivalent *pore diameter*, usually converted from the equation $A = \pi d^2 / 4$. It has been discussed earlier that area histogram provides incorrect results since the pore features are considered as individual objects for size classification. Fig. 3.8 presents a comparison between pore size distribution curves obtained by means of the opening distribution and by the conventional area histogram. Since the structuring element used in the opening distribution technique is square, the pore size (x-axis) in Fig. 3.8 is converted by $l = \sqrt{A}$. It is clear that the shape of the pore distribution curve and the size range of the pores obtained by opening distribution resemble the results of the WMIP (a proper experimental technique, see section 1.4) to a much better extent. This confirms that area histogram is not suitable for characterising the size distribution of such a highly interconnected structure like pore space in cement systems. In contrast, the mathematical morphology technique (opening distribution) can provide far more realistic structural information of pore space. The area-based pore size distribution can be corrected by the opening distribution data.

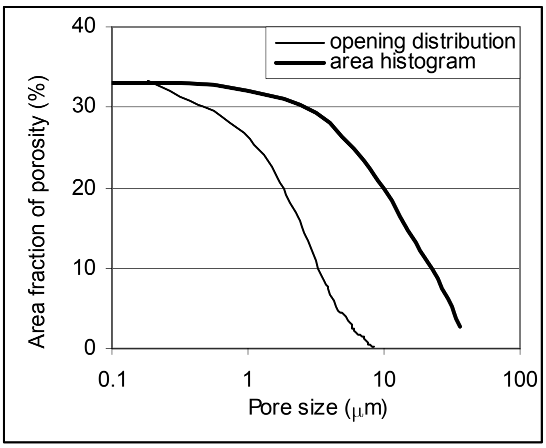

Figure 3.8 *Pore size distribution curve obtained by opening distribution technique and by area histogram, for cement paste with a w/c ratio of 0.5 at 3 days hydration.*

3.4.5 Number-based pore size distribution

Two histograms can be drawn from the fundamental sorting on the basis of pore volume, *i.e.*, volume-based pore size distribution (volume fraction of pores in a specific size range) and number-based distribution (how many pore features in a specific size range). The general definition of pore size distribution, as in the cases of opening distribution and MIP data, refers to the former catalogue. The area histogram is a 2D analogue of volume-based distribution with respect to pore features on section images. Note that both volume- and number-based histograms represent the same raw data, but they focus on different aspects of the pore size distribution. Number-based distribution assigns equal statistical 'weight' to each pore feature regardless of its area. The number-based pore size distribution of pore features on section image, can be assigned 3D character when corrected according to a method introduced in DeHoff and Rhines [1968]. Fig. 3.9 provides comparison between the 2D number-based pore size distribution and the corresponding 3D distribution, it can be seen that direct 2D representation of number-based histogram significantly underestimates the number fraction (number-based portion) of pores smaller than 2 μm.

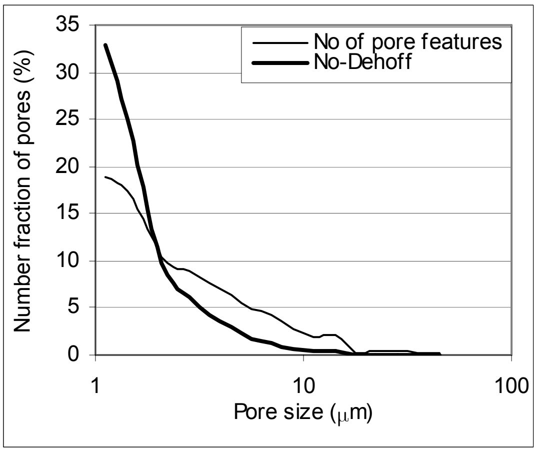

Figure 3.9 Number-based pore size distribution (frequency, in %) derived from number of pore features on section image.

3.5 Fractal dimension of cement pastes

A special structural feature linked up with the continuous scaling phenomenon is *fractality* [Stroeven, 1991a]. This should be considered highly relevant when researchers are *e.g.* interested in the geometric parameters of cracking. Geometric parameters of cracking would change at a lower level of aggregation. Myriads of tiny cracks can be visualized in areas where the naked eye would be incapable of doing so. Hence, intuitively we accept geometric parameters of cracking (density, length, spacing) to *depend on sensitivity*. This is what is meant by the "coastline of Britain" effect: the coastline's length will increase steadily starting from observations by satellite, thereupon by plane, and ending up by walking (and measuring!) along the beach [Stroeven, 1991b].

Carpinteri *et al*. [1999] are actively involved in fractal analysis of fracture surfaces in concrete. Tensile properties can be defined with physical dimensions depending on the fractal dimension of the damaged microstructure, which turns out to be scale-invariant material constants. Obviously, length in sections and surface area in space cannot be measured unambiguously. When dealing with (near) fractal properties, the scaling effect can be quantitatively estimated. The researcher should acknowledge that experimental findings are indeed fundamentally dependent on the scaling level. This section will explore the fractal dimension of cement paste on the basis of image analysis technique.

The values of fractal dimension range from 2.4~3.0 for the volume-based methods and from 1.1~1.4 for the area-based method according to the individual studies on the scaling nature of cement microstructure [Lange *et al.*, 1994]. It is often necessary to consider several orders of magnitude of scaling when dealing with the direct measurement of fractal dimension [Carpinteri *et al.*, 2000]. New techniques need to be applied to cement-based systems to estimate the fractal relationship from single images, rather than from a long series of images acquired at different magnifications. A number of different image processing techniques can be used to perform fractal analysis on section images.

One of the most convenient methods is the dilation technique simulating the coarsening of resolution of irregular profiles of pore features on section images. The measurement of the perimeter of the profiles at each stage of dilation, plotted against the magnitude of the dilation, yields the fractal dimension of the profiles of pore features. At each step of dilation, the perimeter of pore features can be estimated by measuring the area of the contour image and dividing the area value by its thickness. A log-log plot of the normalised measure of the perimeter against the contour thickness, can be used to compute the fractal dimension, D_f. The fractal dimension is related to the slope of the Richardson plot by the relation D_f = 1-Slope. This is indeed an analogue to the well-defined bi-logarithmic diagram log (number of boxes) ~ log (box size) in box counting method [Carpinteri *et al.*, 1999] for the fractal analysis of concrete. At a coarse resolution, the fractal behaviour at small scales cannot be revealed.

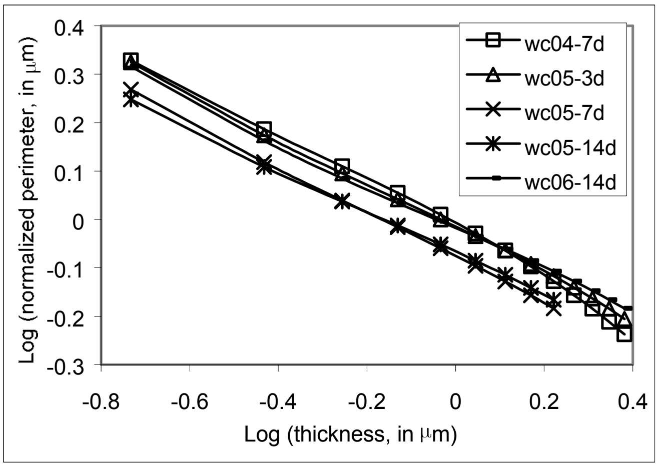

Figure 3.10 *Fractal dimension of pore structure in cement pastes determined by dilation technique. The legend for cement paste indicates the w/c ratio and hydration stage.*

Fig. 3.10 reveals a nearly constant value of D_f within the narrow range of 1.42~1.48 for cement pastes with different w/c ratios at different degrees of maturity. Based on a similar approach, Lange *et al.* [1994] also reported a constant value of 1.25 for the fractal dimension of pore structure in cement paste. The difference may be attributed to different shape of the structuring elements in the dilation operation of pore space. However, in both cases a constant value was observed for the fractal dimension. Hence, fractal analysis is not useful as a means of differentiating pore structure using section images. On the other hand, the consistency of D_f across distinctly different specimens suggests that a *universal* value of D_f may apply to the pore structure in cement pastes. The fractal analysis allows correlating the research outcomes obtained on different scaling (structural) levels of the materials.

3.6 Pore distribution density

Lange *et al*. [1989] studied the influence of pore structure on the properties of cement paste by altering the pore structure with the use of a superplasticizer. It was found that pore structure affected material properties when total porosity was held constant. Therefore, in addition to the accurate measurement of the total porosity, it is important as well to characterise the pore structure in an effective way. Up to now, the attempts to characterise pore structure mostly focus on the determination of porosity, the pore size distribution and on the critical pore diameter. The pores in 3D space can be divided into isolated pores, dead-end pores and effective pores. Relevant to the permeability and durability aspect of cementitious materials, connected effective pores provide the transport route for the fluid. Therefore, pore size, porosity connectivity and total length of the connected pore space are of the utmost importance.

Although image analysis is very helpful for characterising pore structure, it is severely limited by the fact that only 2D sections can be examined. Scrivener [1989a] stated that it would be impossible to reconstruct the pore network in a representative volume by serial sectioning because of its labour intensity. In this case, the stereological theory and mathematical morphology measurements are very useful to derive the 3D structural information from quantitative image analysis of 2D sections. Porosity and pore size distribution can be relatively accurately determined from section images by means of the mathematical morphology technique, as demonstrated in the previous section.

In this section, a concept of 3D *pore distribution density* (PDD) is proposed. It is based on quantitative image analysis of 2D sections using stereological methods. This parameter contains information about the size of pore clusters and their spatial distribution density. It is impossible to assess the 3D distribution density directly from image analysis of 2D sections. An alternative is to determine the 2D distribution density from specimen sections and to calculate the 3D distribution density on the basis of the stereological theory.

3.6.1 Definition of pore distribution density

A plane section of a cement specimen reveals pore areas and pore clusters. The measurement and calculation of 2D pore distribution density is fairly straightforward. When an appropriate binary image (with pores as phase of interest) is obtained, pore clusters are skeletonised and the length of each skeleton segment is recorded. The 2D distribution density Γ_{2D} of pore phase in an image with area A encompassing N skeleton segments of length l_i, is defined by

$$\Gamma_{2D} = \frac{\sum_{i=1}^{N} l_i^2}{A} \tag{3.2}$$

Γ_{2D} should be converted to the 3D pore distribution density for applications to transport studies. The relationship between the length of a skeleton segment in 3D, denoted as l_{act}, and l_i is given by

$$l_i = l_{act} \int_0^{\pi/2} \sin\theta^2 d\theta = \frac{\pi}{4} l_{act} \quad \text{or} \quad l_{act} = \frac{4}{\pi} l_i \tag{3.3}$$

Eq. (3.3) yields the actual length of a skeleton segment in 3D space. The relationship between 2D and 3D pore distribution density is provided by stereological theory, as explained in [Nemati, 1994; Underwood, 1968]

$$\Gamma_{3D} = \frac{2}{\pi} N_A l_{act}{}^2 = \frac{2}{\pi} N_A (\frac{4}{\pi})^2 l_i{}^2 = \frac{32}{\pi^3} \Gamma_{2D} \tag{3.4}$$

where N_A represents the number of skeleton segments per unit area of the test image in 2D. Herewith, the 2D pore distribution density is converted to 3D.

3.6.2 Results and discussions

Garboczi and Bentz [1991] studied the percolation evolution of cement paste during the hydration process in a modelling approach, and proposed a parameter υ containing information about the connectivity of the pore network, *i.e.*, $v = 1.8(p - p_c)^2$. Here p is the porosity, $p_c = 0.18$ is usually adopted as the threshold value of capillary porosity for the depercolation of pore space in ordinary cement paste. Although this parameter is demonstrated to be useful for predicting the permeability of cement paste, it considers the connectivity of pore space in terms of total porosity only, ignoring size and spatial distribution of pore features. Γ_{3D} (Table 3.4) is a direct representation of pore size, and contains information about pore connectivity. It is expected that Γ_{3D} increases with w/c ratio, and declines during the hydration process at a given w/c ratio.

When it comes to the transport properties of cement paste, pore size, pore connectivity and tortuosity are highly relevant. Pore connectivity will be increased in systems with larger pores. On the other hand, pore tortuosity will be decreased in systems with larger pores. Γ_{3D} will have a higher value for cement paste with larger pores and higher pore connectivity. The correlation between these characterising parameters of pore structure and permeability of cement paste will be analysed by the grey system theory in Chapter 7.

Table 3.4 Pore distribution density

w/c ratio	w/c=0.5			w/c=0.6		
Hydration age (days)	3d	7d	14d	3d	7d	14d
Γ_{3D}	1.80	1.26	0.93	2.68	1.49	1.26

3.7 Summary

In this chapter, stereological and mathematical morphological methods are applied to binary section images of actual cement paste specimens of with various w/c ratios and at different hydration stages. The structural parameters derived by stereological includes porosity, specific surface area of pore space and perimeter length of pore features. These stereological parameters can help to characterise the morphological aspect of pore structure in cement paste. In addition, a new characterising parameter, pore distribution density, is proposed in this study on the basis of stereological theory; this parameter contains information about both pore size and connectivity of the pore network in cement paste. The correlation between this parameter and cement paste permeability will be explored in Chapter 7. The incorporation of this new parameter into empirical relationships for estimating cement paste permeability is expected to improve the quality of prediction.

An important application of mathematical morphology theory in this chapter is the opening distribution technique. Important structural information including porosity, pore size distribution and critical pore size can be properly determined. This method can overcome the deficiencies of experimental techniques such as MIP, and represent more accurate structural information of pore space (compared to area histogram and MIP). It has been demonstrated that the results of opening distribution approximate the findings of proper experimental method (WMIP), and provides a realistic picture of pore structure in actual cement pastes. The critical pore size is a useful index relevant to the depercolation threshold of porosity, and thereby associated with permeability and ion diffusion in cement systems. Total porosity varies with w/c ratio and hydration time in a similar way as the critical pore size. Although limited in size range (by image resolution), the image analysis technique, when combined with mathematical morphology tools, provides realistic structural information of 3D pore space.

Chapter 4

Local Porosity Analysis of Pore Structure in Cement Pastes

The study of porous and heterogeneous media is involved in many fields of science, including materials science, environmental technology, geology, hydrology and petroleum engineering. The essential problem is the specification (quantitative characterisation) of the material microstructure that is necessary for predicting the macroscopic properties of the material. Conventional geometric characterisations of pore structure in experimental as well as in simulation studies, particularly focus on porosity, specific pore surface area, pore size distribution, and sometimes on correlation functions. Extensive literature is available on such approaches.

Although the pore size distribution function is a traditional and widely used way to describe the geometry of pore space, Scheidegger [1974] pointed out that the pore size distribution is mathematically ill defined. It depends on an arbitrary identification of cylindrical pores and their *diameters*. For example, it is now well accepted that the results of MIP cannot be interpreted without a trustworthy geometrical model of the pore space, which itself requires knowledge of the pore size distribution. Without such a model, no reliable geometrical information such as pore size distribution can be extracted from the MIP measurements. The opening distribution techniques discussed in Chapter 3, although being able to provide much more realistic representations of pore structure than MIP, remains in the catalogue of *size classification*.

A complete specification of the microstructure is both impractical and unnecessary. It is therefore important to describe the microstructure in a general statistical manner. Such a description should meet four criteria: a) well-defined in terms of geometrical quantities; b) involve only experimentally accessible parameters; c) being of economical size and d) usable in exact or approximate solutions of the underlying equations of motion [Virgin *et al*., 1996]. Currently there are only two statistical methodologies available fulfilling these requirements, *i.e*., correlation functions (see *e.g*. [Jeulin, 2000; Berryman and Blair, 1986]) and local geometry distributions [Hilfer, 1991; 1992; 1996].

Instead of considering different *sizes of pores* as the fundamental source of randomness in porous media, the local porosity theory (LPT) proposed by Hilfer [1991] suggested to consider porosity itself as the fundamental random variable. This immediately leads to suggest local porosity distribution and local percolation probabilities as partial geometric characterisations of the complex pore space. The original LPT is a 3D measurement, so it can only be applied to a reconstructed structure model of porous material.

This author proposed a modified 2D approach analogue to the 3D LPT and applied it directly to section images of actual cement pastes used in Chapter 3. Local porosity distribution (LPD) and percolation probability in the cement pastes are explored based on this adapted 2D approach. The 2D LPT analysis constitutes a comparative study of *local porosity distribution* in cement pastes with different w/c ratios and at different degree of maturities. Section 4.1

describes the theoretical background of LPT. The measurement results obtained by 2D LPT analysis are presented in section 4.2. Based on this, the composition heterogeneity of cement pastes, the structure of which is continuously modified by cement hydration, is discussed in section 4.3. The results of this comparative study are presented in section 4.4, reflecting the natural law of statistic concept of heterogeneity.

4.1 Local porosity theory analysis

The LPT encompasses two geometric characteristics, *i.e*. the *local porosity distribution* and the *local percolation probability*. In doing so, the fluctuations in porosity as well as in connectivity are recorded. The local geometry distributions are a functional generalisation of the correlation-function approach. This theory has been used by Biswal *et al*. [1998] to assess the heterogeneity of porosity in model sandstones. For the details of this theory and some examples of application to porous media refer to Hilfer [1992, 1996]. Local geometry distributions can be used in mean field theory calculations of the dielectric and transport properties of various porous media, for instance porous rock filled with brine. Preliminary comparisons of the theory with experimental results have already been carried out, and show good agreement [Hilfer *et al*., 1994].

However, direct characterisation by LPT is only possible on the basis of a *reliable* 3D structure model (3D reconstruction) of porous media. For actual cement pastes such models cannot be easily derived from the available 2D section images. Hence, 3D LPT is not directly applicable to SEM images. The practical applicability of local geometry distributions will be extended to section images in this study. Interest in these distributions arises from their potential use in distinguishing different microstructures and in estimating transport properties of porous materials. In this chapter, 2D local porosity analysis is therefore proposed as an analogue of 3D LPT. It simplifies computation and maintains the characteristics of the pore structure directly obtained from cement paste. The information on LPD is acquired by quantitative image analysis of polished sections of the actual cement pastes. Stereology allows for 3D interpretation of such data. The reliability of this 2D alternative approach will be discussed.

4.1.1 3D local porosity theory (LPT)

LPT measures porosity and other geometric observable within a bounded (compact) volume of the porous medium. These measurements are collected into various histograms (empirical probability density) by means of a δ-function (delta function). It is a generalised function defined as the limit of a class of delta sequences. In engineering contexts, the functional nature of the delta function is often suppressed, and δ is instead viewed as a special kind of function, resulting in the useful notation [Bracewell, 1999]. The type of δ-function used in this study will be described later in section 4.1.2.

The sample set S contains two disjoint subsets, pore space P and solid matrix M (composed of unhydrated cement and hydration products). Let $K(x, L)$ denote a cube of side length L centred at the lattice vector x in discretised model sample. The set $K(x, L)$ defines a measurement cell inside which local geometric properties such as porosity can be measured. The local porosity in this measurement cell is denoted as $\phi(x, L)$.

The local porosity distribution $\mu(\phi, L)$ is defined as

$$\mu(\phi, L) = \frac{1}{m}\sum_{x}\delta(\phi - \phi(x, L)) \tag{4.1}$$

with δ-function: $\delta(\phi - \phi(x,L)) = 0 \quad for \quad \phi \neq \phi(x,L)$

where m is the number of placements of the measurement cell. The function $\mu(\phi, L)$ measures the probability to find the local porosity ϕ in the range from ϕ to ϕ+dϕ in a cell of linear dimension L.

The second geometric property to characterise local geometry indicates whether pore space percolates or not. A cell $K(x, L)$ is called 'percolating in the x-direction' if a path exists inside the pore space connecting those two faces of the measurement cell that are perpendicular to the x-axis. The definition is similar for other directions.

Let

$$\Lambda_\alpha(x,L) = \begin{cases} 1 \quad if \quad K(x,L) \quad percolates \quad in \quad \alpha \quad direction \\ 0 \quad otherwise \end{cases} \tag{4.2}$$

be an indicator for percolation. The definition of 'α' direction is given in Table 4.1. Thus Λ_3=1 indicates that the cell can be traversed along all three directions, while Λ_1=1 indicates that there exists at least one direction along which the cell is percolating. Λ_0=1 indicates a blocking cell.

The local percolation probability in the 'α'-direction is now defined through

$$\lambda_\alpha(\phi, L) = \frac{\sum_x \Lambda_\alpha(x,L)\cdot\delta(\phi - \phi(x,L))}{\sum_x \delta(\phi - \phi(x,L))} \tag{4.3}$$

Thus $\lambda_\alpha(\phi, L)$ denotes the fraction of cells (with side length L and local porosity ϕ) percolating in the 'α'-direction. Pore space in cement paste is fully connected at λ_3=1. It is an important geometric quantity for physical properties of porous media such as permeability. The calculation of $\mu(\phi, L)$ and $\lambda_\alpha(\phi, L)$ is fairly straightforward.

Table 4.1 Definition of 'α' direction

Index α	Meaning
x	x-direction
y	y-direction
z	z-direction
3	$(x \wedge y \wedge z)$-direction
1	$(x \vee y \vee z)$-direction
0	$(\neg(x \vee y \vee z))$-direction

4.1.2 Conversion to 2D LPT

The area fraction of pore space A_A in a measurement square (2D) is an unbiased estimator of the volume fraction of pores V_V, *i.e.* porosity in a measurement cell (3D). The local porosity in a measurement square of linear dimension L on a section image can be easily determined. The local porosity distribution curve of $\mu(\phi, L)$ can be obtained in a similar way as in the 3D case. The δ-function can take different forms. In this study, the following δ function is used:

$$\delta(t) = \frac{\zeta}{\pi(\zeta^2 + t^2)} \quad \text{with} \quad \zeta=0.001 \tag{4.4}$$

The δ-function plotted against t appears like a very tall and narrow spike (at t=0) of height $1/\pi\zeta$ and width of about $\pi\zeta$. The δ-curve vanishes outside a very narrow range symmetric around t=0. This operation conveniently collects the measured data of local porosity into a histogram and yields a continuous curve of the porosity density distribution.

The local percolation probability in a measurement square makes little sense because the percolation probability is much lower in two-dimensions than in three-dimensions. Scher and Zallen [1970] proposed *universal* values for the percolation threshold at 45% in 2D, and 16% in 3D. This means that the 3D porosity is still highly connected at a total porosity of 45% while appearing to be blocked in 2D porosity. Scher and Zallen's results also qualitatively confirm the general observation that in cements the pore space appears discontinuous in 2D micrographs far earlier than it actually becomes discontinuous in 3D. Bentz and Garboczi [1991] proposed an approximately 18% porosity as the depercolation threshold; this means that the porosity network will depercolate when the porosity falls below 18%. This statement is in reasonable agreement with the *universal* value of Scher and Zallen. Recent publications of the NIST group revealed that the depercolation threshold of porosity in ordinary cement is also dependent on cement fineness [Bentz *et al.*, 1999], *i.e.*, coarser cement has a lower depercolation threshold of porosity than finer cement.

The depercolation threshold of porosity is around 18~21% for cement paste with *ordinary fineness*. Garboczi and Bentz [1996] stated that knowledge of the 3D percolation threshold can be utilized by researchers working on 2D micrographs of a hydrated cement paste. For example, if the capillary porosity quantified by image analysis is 25%, it is likely that the capillary porosity is still connected in three dimensions. *In this study, the indicator for percolation of a measurement cell is determined in view of the local porosity instead of considering whether there exists a connecting path in the pore space*. This approach simplifies the computation required for the determination of percolating or blocking for a measurement cell as accomplished in the three-dimensional LPT analysis. Since the local porosity in a measurement square can be easily determined, the indicator for 3D percolation can be defined as follows:

$$\Lambda_3(x, L) = \begin{cases} 1 & \text{if } 0.45 \le \phi \\ 1.8(\phi - 0.18)^2 & \text{if } 0.18 < \phi < 0.45 \\ 0 & \text{if } \phi \le 0.18 \end{cases} \tag{4.5}$$

where $1.8(\phi\text{-}0.18)^2$ is the 3D connectivity of porosity proposed by Garboczi and Bentz [1996]. It should be noted that this equation is valid for cement with moderate value of specific surface area (300~400 m^2/kg). When the percolation indicator is determined by Eq. (4.5), the local percolation probability λ_3 can be calculated according to Eq. (4.3).

Directional measurements based on the covariance function (covariance measurements reflect the anisotropy of the structure, see [Hu and Stroeven, 2002] for details) of model cement pastes suggested that ordinary cement paste can be considered as an isotropic structure on a sufficiently high level of the microstructure. For a presumably isotropic structure like ordinary cement pastes, the percolation probability should be identical in *x*, *y* and *z* directions. In this case, the following relations should hold for the percolation probability.

$$\lambda_x = \lambda_y = \lambda_z$$

$$\lambda_3 = \lambda_x^3$$

$$\lambda_0 = (1-\lambda_x)^3$$

$$\lambda_1 = 1-\lambda_0 = 1-(1-\lambda_x)^3 \tag{4.6}$$

Hence, local percolation functions in particular directions can be derived from λ_3. Of course, Eq. (4.6) basically only holds for RVE/RAE sized samples, since percolation probability is sensitive to configuration. Hence, all λ values of smaller units will yield biased estimates of engineering values. This relatively small effect (with respect to possible depercolation threshold values) is neglected in this study.

4.2 Materials and measurements

The SEM images used in this section are selected from the images for opening distribution measurements in Chapter 3. Section images of cement paste specimens with two extreme w/c ratios (0.4 and 0.6, respectively) are involved in the LPT analysis for illustration purposes.

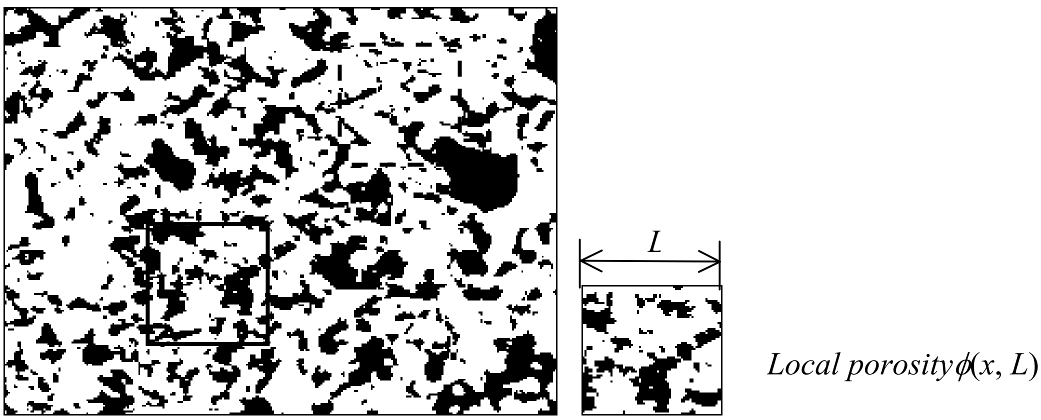

Figure 4.1 Schematic description of the measurement procedures in local porosity analysis. The linear dimension of the measurement square (centred at point x) is defined as field (probe) size L. The porosity within the measurement square is defined as local porosity $\phi(x, L)$. The measurement square is placed at all possible locations in the image frame.

A measurement square (defined as field or probe in image analysis) of linear dimension L was systematically placed in all possible locations within the image frame. A schematic description of measuring local porosity $\phi(x, L)$ in a measurement square (linear dimension of which is defined as field size L) is given in Fig. 4.1. Local porosity distributions were measured over a wide range of field size L from 9 to 66 μm.

4.2.1 Influence of L on local porosity distribution

Fig. 4.2 shows the local porosity distribution $\mu(\phi, L)$ for paste (w/c=0.6) at 14 days of hydration with field sizes L of 9, 38, 47 and 66 μm, respectively. The curve resembles the normal distribution to a closer extent as field size gradually increases to L_{RAE}. The μ curves exhibit the typical transfer stages between the limits L=0 and $L \rightarrow \infty$. The shape of μ curve depends strongly on L, revealing two competing effects [Hilfer, 1991]. At small L, the local geometries are simple in the rather small field, but the between-fields correlations are strong. When L is equal to the sample size, μ does not contain complex geometrical correlations because there is only one measurement cell. At large L, the local geometries are statistically uncorrelated but each one of them is nearly as complex as the whole pore space. There exists an intermediate length scale at which, on one hand the local geometries are relatively simple, whereas on the other hand the single-cell distribution function has sufficient non-trivial geometric contents to be a good approximation of the investigated structure.

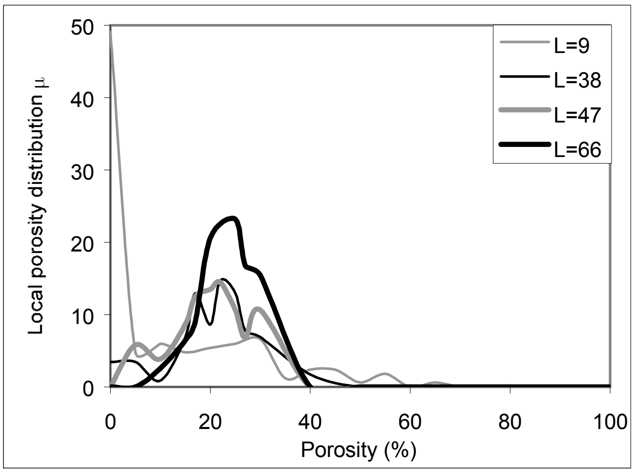

Figure 4.2 Local porosity distribution $\mu(\phi, L)$ for cement paste with w/c=0.6 at 14-day's hydration, at linear probe sizes L of 9, 38, 47 and 66 μm, respectively.

The μ curves in Fig. 4.2 manifest the changes imposed by the two competing influences at increasing L. For L significantly exceeding L_{RAE}, the μ curve should have a unique peak at the value of global porosity and a width approximating zero. This indicates that the paste approaches macroscopic homogeneity at $L \rightarrow L_{RAE}$. Because of stochastic influences the curve will have an increasing width at a declining L (as shown in Fig. 4.2), but the peak (though less pronounced and sometimes multi-peaked) should stay at the same porosity value because of its composition character. In the case of L=66 μm, the peak porosity for this paste is 25%. Direct measurement of global porosity by image analysis of the sample revealed a value of 24%. The values of global porosities revealed by LPT analysis are in good agreement with the results of the opening distribution indicated in Chapter 3 (see Table 3.3). Only when L is not sufficiently larger than the pore spacing (as in the case of L=9 μm), we will receive information from inside the representative element. Still, the average porosity pertaining to the μ curve will yield the global porosity to be the same. But statistical effects of probing will disturb stochastic information on density distribution of local porosity. To put it in a simple way, the closer the observation (when probe size is exceeding pore spacing), the more heterogeneous the structure will appear. Hence, observations on different levels of the microstructure will produce according to the theory systematically different information on the degree of heterogeneity, which will be discussed in section 4.3.

4.2.2 μ curves for pastes at different hydration times

The pore microstructure is changing during the hydration process since pore space is gradually filled up with hydration products. As a result, total porosity, critical pore size and mean pore size decrease with hydration time, while the pore size distribution becomes narrower, as earlier demonstrated in Chapter 3. Fig. 4.3 presents the local porosity distribution μ of a cement paste (w/c=0.6) at different hydration times, maintaining the same field size L=19 μm. The differences between a relatively mature paste (at 14-day's hydration) and early-age pastes (at 3- and 7-day's hydration, respectively) are clear. The shape of the μ curves for pastes at 3 and 7 days hydration are similar, with the curve for the 7-day's paste shifting to the left of the 3-day's curve. This shifting is due to the lower porosity in the 7-day's paste. If the field size L is close to L_{RAE}, the porosity distribution curve should resemble the normal distribution. The shape of the μ curve for paste at 14-day's hydration (Fig. 4.3) is far more deviating from the normal distribution than the other two pastes, indicating this paste to have the largest RAE. Correspondingly, the heterogeneity of porosity in cement paste is seemingly increasing during the hydration process, when based on probes of similar size.

A general trend in pore structure evolution during hydration is a significant decline in the volume of large pores, whereas the volume of small pores stays relatively constant. The reduction of the volume of large pores is predominant in the early stage of hydration. At first, hydration products are formed in larger pores and later on in the smaller ones, thus leaving initially the volume of small pores more or less constant [van Breugel, 1991]. This explains the similarity between the 3-day's and 7-day's curves. Once the larger spaces, *i.e.*, voids>0.13 μm, are filled, further hydration would affect the entire pore size distribution. This can account for the obvious difference between 14-day's paste and less mature pastes (at 3- and 7-day's hydration). Supporting experimental evidences can be found in Ye [2003], where it is stated that the permeability of 3-day's and 7-day's pastes (w/c=0.6) are $5.8\mathrm{x}10^{-8}$ and $1.1\mathrm{x}10^{-8}$ m/s, respectively, whereas the permeability for 14-day's paste is one order of magnitude lower, about $1.0\mathrm{x}10^{-9}$ m/s.

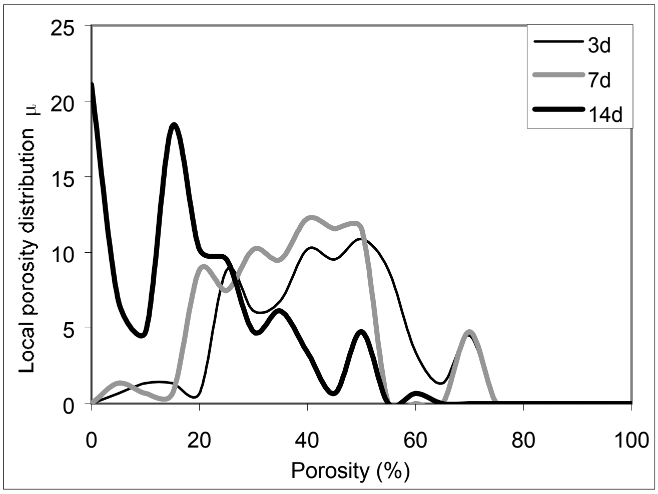

Figure 4.3 *Local porosity distribution μ for cement paste with a w/c=0.6 at 3, 7 and 14 days of hydration, respectively, at constant linear probe sizes L=19 μm.*

As a result of further hydration, the pore space gradually changes from a fully connected structure to a depercolated network with some isolated pores. In the viewpoint of statistics, the scatter of the porosity distribution is increasing during the hydration process due to the decline in the number of pore *features* observed in the investigated field of the section image. Therefore, for cement paste with 14-day's hydration, the scatter of the porosity distribution is larger than for less mature pastes. When observations are based on fields of similar size, this larger scatter corresponds to a seemingly more heterogeneous pore structure. This explains the increasing linear dimension of the RAE for porosity homogeneity during hydration.

Studying the heterogeneity of porosity in cement pastes hydrated to different extents requires modifying field sizes to the same proportion of the RVE/RAE. This renders possible properly comparing outcomes on the same level of microstructure unless the sample size considerably exceeds the linear dimension of the RVE/RAE. This will be discussed in detail in section 4.3. In other words, comparative study should be based on the respective characteristic length scale, which can be properly assessed as the minimum probe size $L_{\min}$ at which the μ curve can be approximated at a given probability level by the normal distribution function.

4.2.3 Local porosity distributions for pastes with different w/c ratios

The LPD curves for cement pastes with different w/c ratios are shown in Fig. 4.4 at their respective characteristic length scales. It can be seen that the pore space characteristics of cement paste with a w/c=0.4 at 3 days of hydration are almost equivalent to those of pastes with a w/c=0.6 at 7 days of hydration. The similarity in pore structure between cement pastes with a relatively low w/c ratio at an early age (say, 3 days hydration) and pastes with a higher w/c ratio at some weeks' hydration (one week or more) is supported by three-dimensional computer simulation results of Bentz and Garboczi [1991]. At the same hydration age, cement paste with a w/c=0.4 is more heterogeneous than the paste with a w/c=0.6 when based on the same probe size. This is reflected by the larger value of $L_{\min}$. This can be partly explained by the influence of the w/c ratio on the morphology of porosity. The higher the w/c ratio, the more space is available for the undisturbed growth of hydration products. Particularly in the early stage of hydration, when ettringite needles are formed, the available space determines the morphology of the hydration products, which in turn determines the morphology and distribution of porosity. So, for a cement paste with a higher w/c ratio, the spatial constraints to the hydration products are less, and, it is easier for cement paste to reach a relatively homogeneous distribution of porosity via dissolution and precipitation of the hydration products.

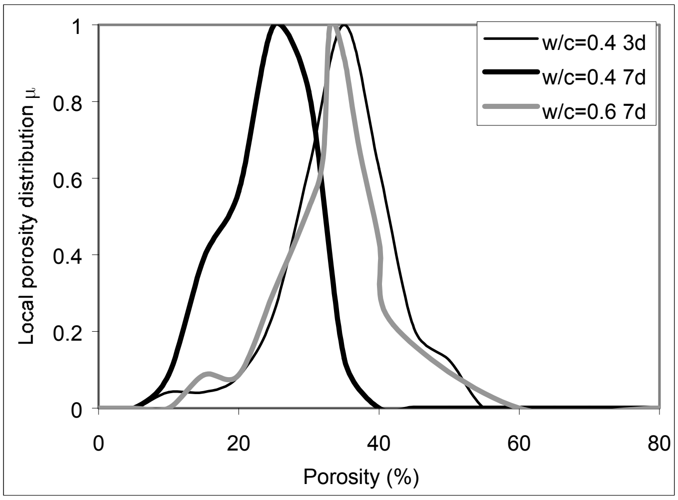

Figure 4.4 *Local porosity distribution μ for cement paste with a w/c ratio of 0.4, at 3- and 7-day's hydration, at their characteristic length scales L_{min}=40 and 45 μm, respectively; the μ curve for cement paste with a w/c of 0.6 at 7-day's hydration (L=45 μm) is also indicated for comparison purpose. The values of μ are normalised by their respective peak values.*

4.2.4 Local percolation probability

The LPD and local percolation probability are shown in Fig. 4.5 for cement pastes with w/c=0.4 at 3 days of hydration, at L=56 μm. The μ curve is rescaled so that its maximum equals 1. For this cement paste, the μ curve has its peak value at a porosity of 35%. The λ_3 curve ascends from zero to unity at increasing porosity, but its increase is not always strictly monotonous due to connectivity heterogeneities at intermediate scale levels. The local percolation probabilities are derived according to Eq. (4.6). The six local percolation functions λ_α provide useful information about the pore space. The λ_1 and λ_3 curves constitute lower and upper bounds, respectively, for the region inside which the connectivity increases from 'blocking' to 'fully connected'. If the band between λ_1 and λ_3 curves shifts to the left of the μ curve's peak, then the sample is well connected. The μ curve in Fig. 4.5 partially overlaps the band from λ_1 to λ_3, which indicates that the permeability of this paste is relatively low.

Fig. 4.5 reveals obvious changes in pore connectivity occurring over the 20 to 40% porosity range. This is in agreement with experimental results obtained by Parrott *et al*. [1984] and by Powers [1958]. Parrott *et al*. measured diffusion parameters at various ages for ordinary cement paste and found a large drop in diffusion coefficients when porosity decreased from 40 to 20%. Powers observed a sharp increase in permeability of various cement pastes as capillary porosity increased from 20 to 40%. The μ curve for mature paste shifts to the left of the λ_1 to λ_3 band. For pastes with a higher w/c ratio, the change from blocking to percolation occurs in the low porosity tail of μ, indicating a high degree of connectivity.

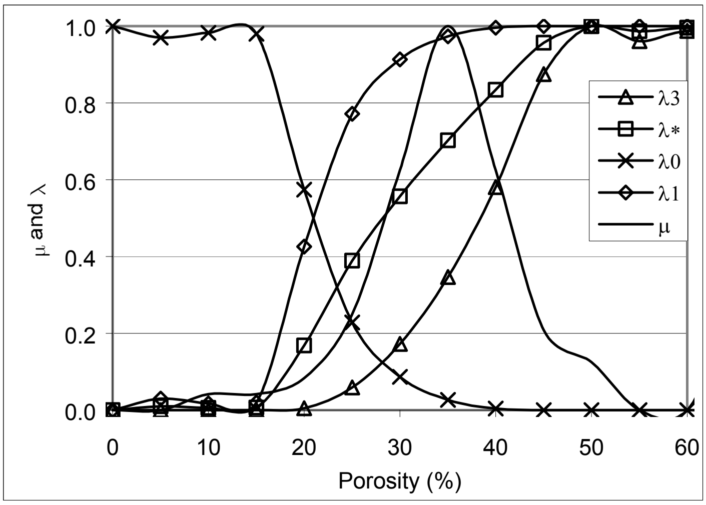

Figure 4.5 *Local porosity distribution μ and local percolation probabilities λ_α for cement paste with a w/c=0.4 at 3 days hydration, at the characteristic length scale L=40 μm; λ^* represents the local percolation probabilities in x, y and z direction (λ_x=λ_y=λ_z).*

4.3 Statistical concept of heterogeneity

The degree of heterogeneity for a given sample size depends on the type of geometric parameter, and on the sample size for a specific geometric parameter. A sample of (at least) the size of the RVE/RAE is necessary when an unbiased estimation of bulk features is pursued; then the material is considered at a macroscopic or engineering level. When the experimental design is based on volume or area elements of sub-representative size as to the property or geometric feature of interest, the associated amount of heterogeneity is a function of the size ratio of the sample and the RVE/RAE. This is denoted as the probing sensitivity. A logic consequence of the sketched stochastic heterogeneity concept is that comparison of different populations demands operating with similar probing sensitivity. This means the size ratio of the sample and the RVE/RAE should be constant. Only under such conditions are the heterogeneity influences normalised and separated from the mean estimates. Unfortunately, these fundamental requirements are rarely fulfilled by engineers in the field of material science.

Insight into the size of the RVE is therefore crucial for the sampling strategy, and thus for the economy of the experiment. When dealing with different populations, it is also a prerequisite for unbiased comparison of outcomes. In this section, the multi-stage sampling strategy (employed in local porosity analysis) and associated fundamentals will be briefly introduced. The cement pastes with a w/c ratio of 0.6 at different maturities (3, 7 and 14 days hydration, respectively) will be employed as an example in section 4.4 to illustrate the natural law of the statistical concept of heterogeneity by means of a proper comparison between the cement pastes on a similar level of microstructure.

4.3.1 Multi-stage sampling strategy

When the researcher is trying to assess the influences of a certain regime on the material of interest in the engineering construction, the material is moulded or shaped (*e.g.* by sawing) so it can be subjected to the regime at issue in a convenient way. In stochastic terms, the material in the construction constitutes the *population*, while a certain number of *identical* specimens can be seen as the *sample*. Specimens reveal fluctuations due to their restricted dimensions in material structure, and, as a consequence, also in their behaviour when subjected to the external regime. This is denoted as *between-specimens* scatter. A major part of the engineering research has this *first sampling stage* as a terminus. As an example, the average compressive strength of a series of specimens is seen in such research efforts as an unbiased estimate of the material strength in the construction, whereby reliability is associated with the aforementioned scatter.

However, with structural research, we have to add *additional sampling stages* as in this study; the specimens are cut to yield *sections*, of which location and orientation should be randomised, unless the researcher has strong arguments that allow the release of this requirement. Sections and associated images that can be visualised (by microscopy in this study) at the section surface have smaller dimensions than those of the specimens (at least to avoid disturbed boundary layers). These section images represent a set of different locations and orientations of a specimen body previously subjected to the regime. Similarly located and oriented section images of repeated experiments reveal *between-sections* scatter at the so-called *second sampling stage*. Of course, this equally holds for the result of the averaging operation over a set of sections randomised with respect to location and orientation.

In concrete technology, section areas are too large to be subjected to quantitative microscopy. Instead, fields (section images) significantly smaller than the section area are employed for that purpose. This is the *third sampling stage*, confronting the researcher with *between-fields* scatter, which depends, of course, on the size of the section images (263x186 μm in this study). The section images are finally submitted to stereological methods of quantitative image analysis. The procedure might be repeated randomly a number of times, revealing variation among the data. It can be imagined that the scatter will be directly governed by the extent of the geometrical parameter in the field and the grid line density. It is the fourth and last contribution in this *four-stage sampling strategy* to overall scatter. A schematic description of the four-stage sampling strategy is given in Fig. 4.6. In the LPT analysis, the fourth-stage scatter is dependent on the linear dimension of the measurement square.

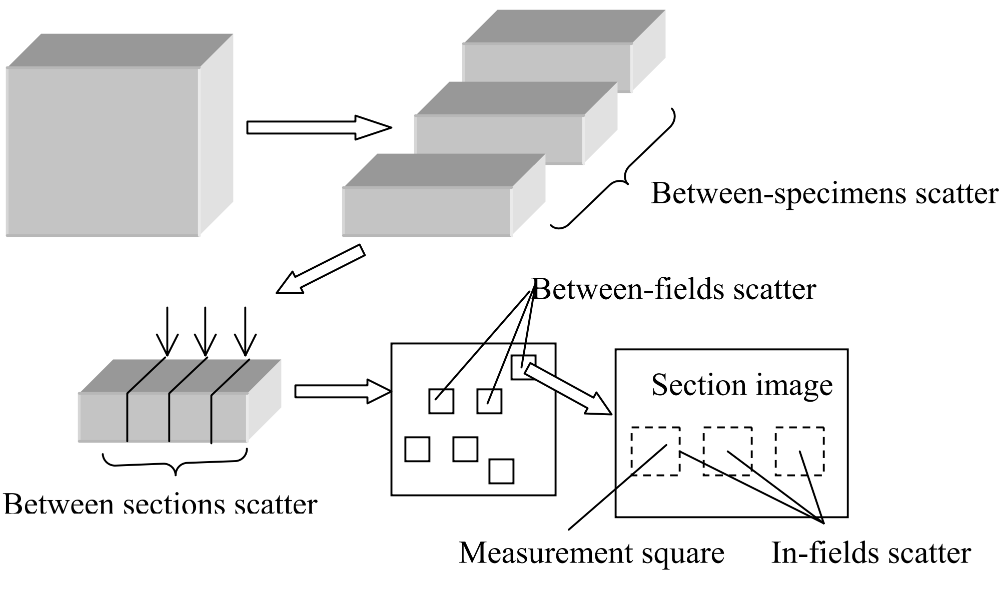

Figure 4.6 A schematic description of the four-stage sampling strategy. All the four stages contribute to the overall scatter. Local porosity analysis deals with the last stage.

The *reliability of the engineering estimate* for material behaviour (in terms of the observed geometric material parameters) under the external regime depends, of course, on the overall scatter, *i.e.* reflecting the four-stage sampling process involved in the research efforts. The average values of an arbitrary 3D geometric parameter of concrete will be quite alike when obtained from large volumes of the material. Thus, such volumes are defined as homogeneous for the very parameter. The differences between the average values (*i.e.*, scatter) will increase at declining size of the sample volumes. The sample volume for which the standard deviation in the global values of the selected geometrical parameter is still at an acceptable level is referred to as the RVE for that particular parameter; this RVE is said to be *homogeneous* as to the specific parameter. The same reasoning is followed when sections of similar size of the material are used for the assessment of 2D information on a certain geometric parameter. In this case, one of the equally sized area elements yielding an acceptable scatter level in the geometric data is defined as homogeneous for the associated parameter, and denoted by RAE.

This section focuses on the last stage in the aforementioned four-stage sampling process. Since the information on pore characteristics obtained in this way should be representative for the engineering level, where we are confronted with durability aspects of civil engineering structures in which the material is employed, extreme care should be bestowed on a careful design of the experiments involving all four sampling stages. It is noteworthy to remark that a more closer study of the various contributions to overall scatter (and, thus, to reliability of the estimates) will inevitably lead to the Golden Rule earlier formulated by Gundersen and Osterby [1981]: 'Do more less well'. This implies that in many cases an increase in the number of specimens is far more efficient in increasing reliability than selecting an excessive number of fields and, even more, in intensifying the image analysis operation. The latter, however, is the general trend because of the automation possibilities. Still, it will be the weakest link in such a chain that it disproportionately affects the reliability of engineering estimates. An optimised approach requires paying explicit attention to a design leading to equal contributions to scatter at the different sampling stages. Last, but far from least, the aforementioned fundamental requirements should be fulfilled. This aspect receives particular attention in this study, showing the major consequences of violating such requirements.

4.3.2 Level of microstructure for structural analysis

In an isotropic material, the representative element can be imagined as a cube in 3D space or a square in 2D. A simple statistical test can be employed to estimate the linear dimension L_{RAE} of the RAE [Stroeven *et al.*, 2002]. At a certain value of L, a series of local porosity data are recorded with average value of $\bar{x}$ and standard deviation σ. The coefficient of variation ε is defined as the ratio of σ and $\bar{x}$. The number of observations N can be calculated which is necessary to guarantee that the average value will be within an interval with acceptable range of deviation Δ at a given confidence level (90% in this study). Since it is equivalent to take N samples with area L^2 or to take a single sample with an area of NL^2, the linear dimension of RAE can be estimated to be $\sqrt{N}L$. Taking $\Delta=0.1\bar{x}$, the L_{RAE} is calculated for cement pastes with various w/c ratios at different degrees of hydration (Table 4.2). The linear dimension of RAE is averaged over the results obtained from different values of L (19, 38 and 66 μm, respectively). Once an RAE has been determined for a certain case (porosity in this study), its statistical heterogeneity can be explored.

Table 4.2 Comparison study on similar level of microstructure (w/c=0.6)

Hydration age (days)	3	7	14
L_{RAE} (μm)	202	267	441
L^* (μm)	33	40	66
Porosity $\bar{x}$ (%)	43.15	33.52	24.21
Porosity range (%)	8~73	9~53	10~37
Standard deviation σ (%)	9.75	7.46	5.42
Coefficient of variation ε (%)	22.6	22.3	22.4
χ^2_{exp} (16 classes, $\chi^2_{0.1,15}$=22.307)	14.73	10.86	11.55
χ^2_{exp} (20 classes, $\chi^2_{0.1,19}$=27.204)	18.59	13.02	21.12

Table 4.2 shows that the available images in this study (263 x 186 μm) are smaller than the RAE in two out of the three cases. This is due to the necessary resolution to detect pores with an area smaller than 0.1 μm^2. Simulation by Roelfstra [1989] demonstrated that diffusion (amount of water transferred over a certain distance through cement/concrete specimen per time unit) is structure-insensitive. When diffusion and permeability are of interest, the size of RAE can be *relatively* small. Therefore, it is reasonable to use the current image size to compromise between an acceptable representativeness of the section image and a satisfactory image resolution. On the other hand, a comparison of heterogeneity in porosity between cement pastes can be made as long as it is based on the same level of microstructure of different specimens (*i.e.* the same probing sensitivity), regardless of the specific RAE size.

Hydration will gradually transfer cement paste into a matured material with lower porosity. During the hydration process, the size of the RAE will gradually increase due to a declining number of pore *features* per unit of volume/area. When the structure of cement paste is modified by hydration, a similar level of the microstructure (same probing sensitivity) should be adapted for comparison purposes in experimental designs pursuing a study of the effects of such changes on porosity. Unless this is properly arranged, artificial effects will be mixed with fundamental ones.

Unfortunately, these fundamentals of the statistical concept of heterogeneity are ignored in the research of Biswal *et al*. [1998]. He defined the characteristic length scale as the minimum side length of the measurement cell when the local porosity distribution μ-curve vanishes at both ends of porosity (x-axis). He performed the comparison of different sandstone samples on their respective characteristic length scales and associated the width of μ-curve with the degree of heterogeneity of sandstones. The law of similar level of microstructure was also ignored in his work. The statistical concept of heterogeneity will be explored, on the basis of the porosity (composition aspect) distribution analysis data obtained in section 4.2.

4.4 Comparison study of cement pastes at different hydration stages

4.4.1 Comparison on similar level of microstructure

When L_{RAE} exceeds the image size as in this study, the same 'level of microstructure' (*i.e.*, the same coefficient of variation in the geometric parameter at issue) can be achieved by taking the ratio of L to L_{RAE} constant for all investigated specimens. This specific value of field size is denoted as the *proportional length scale L** (Table 4.2). Fig. 4.7 presents the measurements based on the same level of microstructure. The μ curves for three pastes (w/c=0.6, at 3, 7 and 14 days hydration) are normalised by their respective peak value such that all curves have a maximum value of 1. The curves resemble each other far more closely than in Fig. 4.3. The peak values of porosity of the three curves can be made to coincide when the aging effect is eliminated. Since the displayed measurements are based on an equal scatter of local porosity in the total sample images, theoretically, the three μ curves should be identical and conform to the normal distribution. The deviations from the normal distribution seem not to be too alarming, especially taking the limited (*i.e.* sub-representative) sizes of the sample images into account. Whether the deviations are significant or not can be checked by applying a χ^2-test. It is a standard statistics tool to evaluate differences between experimental distribution data and corresponding theoretical values. For details of this method the reader is referred to statistics textbooks, an example being the book by Hoel [1971].

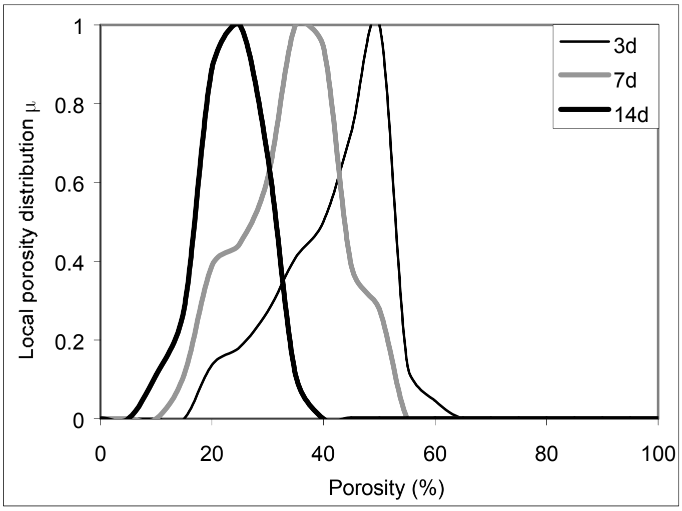

Figure 4.7 Local porosity distribution μ measured at the same level of microstructure: L=33, 40 and 66 μm for pastes (w/c=0.6) at 3, 7 and 14 days of hydration, respectively. The values of μ are normalised by their respective peak values.*

The local porosity data are collected into traditional histograms in the first step of χ^2-test. According to the rule of thumb, the number of classes n should roughly be the square root of the number of observations. Two values of n are taken into consideration, 16 and 20, respectively. In the case of n=16, the class intervals are 4.1, 2.8 and 1.7%, for 3-, 7- and 14-day's pastes, respectively. When $\overline{x}$ and σ are known, the theoretical value of relative frequency of occurrence f_{th} within a class can be calculated according to the normal distribution function. The measured frequency of occurrence is denoted as f_{exp}. The experimental value of χ^2 is calculated as:

$$\chi^2_{\exp} = \sum_{i=1}^{n} \left\{ \frac{(f_{\exp} - f_{th})^2}{f_{th}} \right\}_i \tag{4.7}$$

The results of χ^2–test are also listed in Table 4.2. In both cases of n=16 and n=20, the theoretical values of χ^2 exceed those of χ^2_{exp}. Hence, at the 90% probability level, there is no reason to reject the hypothesis that in all cases porosities were distributed according to the normal distribution, and as a consequence, Fig. 4.8 reflects the natural law of the statistical concept of heterogeneity. For L slightly smaller than L^*, the local porosity distribution might still be approximated at a high probability level by the normal distribution. So, the *characteristic length scale* can be properly assessed as the minimum probe size $L_{\min}$ whereby the μ curve can be approximated at a given probability level by the normal distribution function.

These observations are based on images made with the same optical resolution. The optical resolution governs the minimum geometrical dimensions incorporated in the quantitative image analysis studies. It should be noted that measurement sensitivity should also be adjusted to the size of the RAE to get an objective situation. Hence, the optical resolution of the SEM image should have been somewhat reduced during maturation, such that the ratio of minimum pore size detected to the L_{RAE} should have been similar for the pastes at different hydration stages. This would have made observations on the same level of the microstructure even more pronounced due to the extra reduction in total porosity (governed by image resolution) for more mature pastes.

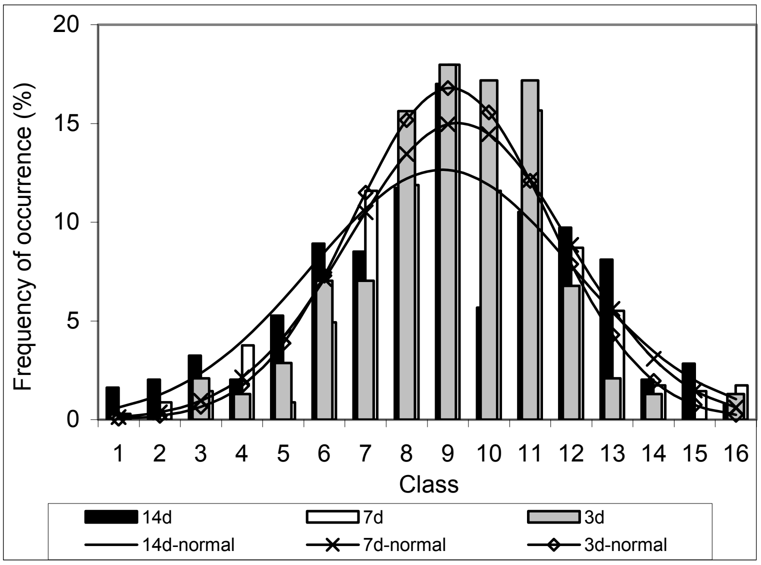

Figure 4.8 *Conventional histograms of relative frequency of occurrence in porosity distributions for pastes (w/c=0.6) at 3, 7 and 14 days of hydration, respectively. The experimental values are indicated as columns and the approximated normal distribution curves are shown as continuous lines.* χ^2*-tests revealed that local porosity distributions conform at 90% probability level to normal distributions.*

4.4.2 Reliability of 2D local porosity distribution

The conversion of the LPD from 3D to 2D measurement (section 4.1) is based on the stereological concept that the area fraction of porosity is an unbiased estimate of the volume fraction of porosity in a measurement cell of the same linear dimension. In this section, the reliability of this conversion will be explored in view of the statistical concept of heterogeneity and of the central limit theorem.

Virgin *et al*. [1996] studied the difference of the LPD obtained from 2D section plane and 3D reconstruction of the same porous medium (sandstone). Their investigation revealed that the LPD for a 3D porous medium and that for a 2D plane section through the medium are different at the same linear dimension of the measurement cells (squares in 2D). However, for homogeneous and isotropic media having finite correlation lengths, a good degree of correspondence between the two sets of local porosity distributions can be obtained by rescaling the lengths of measurement cells (squares), and the mapping associating corresponding distributions can be found from 2D observations alone. The agreement between associated distributions is good as long as the linear dimension of the measurement cells involved is somewhat larger than the correlation length, and it improves as the linear dimension increases. This phenomenon can be easily explained in view of the statistical concept of heterogeneity.

When the linear dimension of measurement cells (squares) exceeds that of the correlation length (characteristic length scale $L_{\min}$), the LPD from both 2D and 3D measurements approximate normal distributions to a sufficient extent such that the scatter between individual measurements is reduced to an acceptable level. A normal distribution has two independent parameters: the mean and the variance. When the measurement cell is large enough, corresponding to a low level of the microstructure, 2D and 3D LPD curves are expected to have the same mean according to the aforementioned stereological concept. The single parameter affecting the LPD curve, *i.e.*, variance, can be independently determined from correlation functions. Hence, a corresponding relationship between 2D and 3D LPDs can be established by matching their variances. This can be fulfilled theoretically by central limit theorems guaranteeing independence of the asymptotic LPD on the shape of the measurement cell [Hilfer, 1991].

The spatial correlations of the random geometry in homogeneous media decay with a finite correlation length. For such systems the central limit theorem can be applied to measurements of local porosity for sufficiently large measurement cells. For this purpose, a cubic measurement cell K of linear dimension L is partitioned into n cubic sub-cells $\{K_i\}$ of side length c. The number of sub-cells n is equal to $(L/c)^3$. The porosity in cell K can be obtained by averaging over the sub-cells, *i.e.*,

$$\phi(K) = \frac{1}{n}\sum_{i=1}^{n}\phi(K_i) \tag{4.8}$$

In the case of $L_{\min} << c << L$, the central limit theorem becomes applicable since $\phi(K_i)$ are weakly correlated random variables. The central limit theorem ensures existence of a number σ such that ($\overline{\phi}$ is bulk porosity)

$$\mu(\phi, K) \approx \frac{(L/c)^{3/2}}{\sqrt{2\pi\sigma}}\exp[-\frac{(\phi-\overline{\phi})^2(L/c)^3}{2\sigma^2}] \tag{4.9}$$

The accuracy of approximation increases with the value of L/c. In the limit $L/c \rightarrow \propto$ (with $c >> L_{\min}$), one has $\mu \rightarrow \delta(\phi - \overline{\phi})$, independent of dimension and shape of K. This implies for L/c sufficiently large but still finite, the form of LPD depends only on the bulk porosity and the variance of LPD can be expressed as $\sigma^2/(L/c)^3$. If the medium is isotropic, a sufficient condition for the equality of variance between 2D and 3D LPDs for the same medium is [Virgin *et al*., 1996]

$$\frac{L'}{c'} = \frac{\sigma'}{\sigma}(\frac{L}{c})^{3/2} \tag{4.10}$$

where L' is the linear dimension of the measurement square (2D) and L is the linear dimension of the measurement cell (3D) at the same variance level. This implies 2D and 3D LPDs for large measurement cells (squares) are simply related by rescaling the lengths. When L' is taken as $L^{3/2}$, the number of observations (sub-cells in 3D and sub-squares in 2D) is equal in the case of 2D measurement and 3D measurement. This reflects, in fact, the statistical concept of heterogeneity. Hence, the appropriate value of linear dimension of measurement cells can be estimated from measurement results of 2D LPD. On the other hand, this confirms that 2D LPD is a reliable representation of 3D LPD; the 2D measurements should be performed in a larger measurement square ($L' = L^{3/2}$, exceeding L at a similar variance level of local porosity distribution) in a comparative study with 3D measurement.

4.4.3 Second order stereology applied to porosity distribution

The stereological methods for estimating porosity and pore surface area are concerned with average or total quantities. These quantities can be considered as the 'first moments' of the corresponding distribution of the quantity. For example, the total porosity is a first-order summary of the distribution of local porosities. This feature of the methods has led them to be referred to collectively as 'first-order stereology'.

Parallel to the development of first-order stereology, there has been a growth in second-order stereology [Jensen *et al*., 1990], which is concerned with the statistical description of the spatial distribution of geometrical features. In both biomedicine and material sciences the spatial architecture of features within 3D space is often as important as the total quantity or density of the feature. For example, two systems may have a similar surface density but completely different spatial arrangements of the surface. The first-order methods shed little or no light on spatial architecture [Howard and Reed, 1998]. The quantitative methods capable of describing the spatial architecture of a 3D system are loosely referred to as second-order stereology. The readers are referred to Stoyan *et al*. [1987] for a full theoretical description of the methods.

In Chapter 3, first order stereological and mathematical morphological methods have been used successfully to experimentally assess the structural characteristics of pore space in cement paste. In doing so, total porosity, pore size distribution, critical pore size as well as pore distribution density have been quantified with respect to pore size, allowing a more accurate estimate of global mechanical and transport properties of cement paste. A more detailed study of the structural evolution of pore space additionally asks for quantitative measures of the porosity distribution on a local level. This is performed by means of the so-called local porosity analysis in section 4.2. As shown in Fig. 4.2, the LPD curve μ is strongly dependent on the probe size, of which the linear dimension is denoted as L. The pattern of changes of μ curve in shape at increasing probe size can be explained by second order stereological theory.

The cement paste with a w/c ratio of 0.6 at 14 days of hydration (of which the LPD curves at different values of L are shown in Fig. 4.2) is taken as an example. The area fraction of porosity for this paste is 21.6%, specific surface area S_V is 0.236 $\mu m^2/\mu m^3$ (see section 3.3), the pore size range is 0.1~10 μm (see Fig. 3.7, most of the pores are concentrated in the size range smaller than 5 μm) with the critical pore size of 2.03 μm (see section 3.4). The average pore spacing, *i.e.*, the mean intercept length $\overline{L}_3$ of solid phase (including hydration products and unhydrated cement) can be calculated by

$$\overline{L}_3 = 4\frac{V_V}{S_V} = 4\frac{1-p}{S_V}$$

$$\lambda = 4p / S_V \tag{4.11}$$

The calculation result is 13.29 μm. The average pore size can be calculated by $4p/S_V$ = 3.66 μm.

When the probe size is 1 pixel (0.185 μm), the pixel belongs to either pore space or solid phase; hence, porosity in a specified field is either 0 or 100%. This will lead to a LPD curve with non-zero values only at both ends of the x-axis (Fig. 4.9a). The value is 21.6% and 78.4%, respectively, at p = 0 and p = 100%. When L is far smaller than the average pore size, the value at both ends will decline, accompanied by a non-zero value appearing in the range of the x-axis because fields of this size probe areas contain both pore space and solid phase (Fig. 4.9b). As probe size L further increases to above the average pore size (but less than the average pore spacing), the curve will vanish at the p = 100% end of x-axis because it is nearly impossible for a field of this size to be encompassed in pore space (Fig. 4.9c). This statement is explicitly confirmed by the shape of the μ curve in Fig. 4.2, with L = 9 μm (3.66 < 9<13.26). When the probe size L exceeds the average pore spacing, the fields will explore at least two pore features; hence the μ curve vanishes at both ends of the x-axis (Fig. 4.9d) since it is impossible for the fields to exclusively cover pore space, or solid phase. This explains why the μ curves at L =47 μm and at L= 66 μm (Fig. 4.2) present (multiple) peaks but indicating zero-values at both ends of the x-axis. The multi peaks are associated with statistic fluctuations in the porosity distribution. When L exceeds the pore spacing to a significant extent, the curve will present only one peak, with the mode value corresponding to the global porosity.

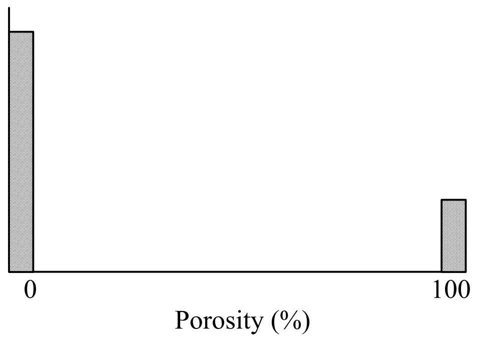

(a) L = 1 pixel (0.185 μm)

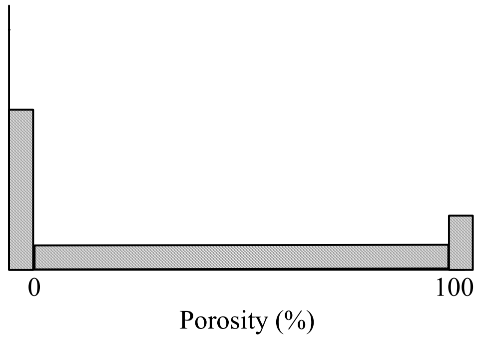

(b) L << average pore size

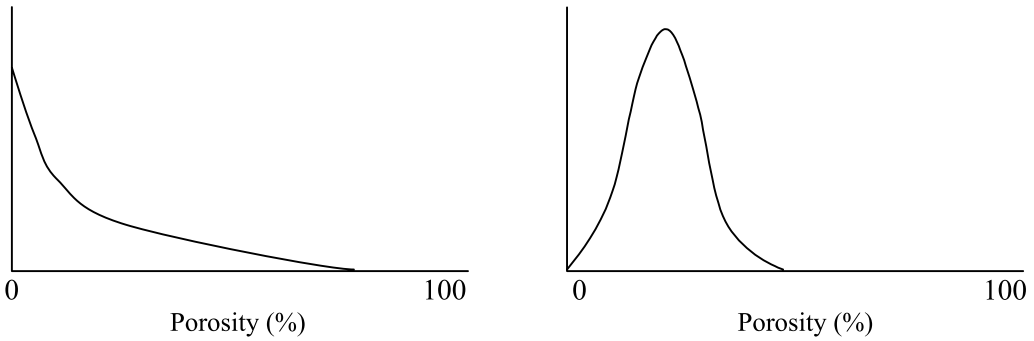

(c) pore size < L < pore spacing (d) average pore spacing $\ll L$

Figure 4.9 Scheme describing the influences of probe size L on the patterns of local porosity distribution curves. The vertical axis is porosity distribution. Two threshold values of probe size involved are average pore size and average pore spacing.

4.5 Configuration homogeneity

Section 4.4 deals with homogeneity of local porosity distribution in cement paste, which reflects the composition aspect of the materials. Some spacing parameters, including mean free spacing and nearest neighbour distance were introduced in Chapter 2. Configuration homogeneity of cement and concrete can be based on representative information as to the distribution of either one (or both) of these spacing parameters. In this section, the configuration homogeneity will be briefly discussed with a spacing parameter of moderate sensitivity to material configuration, *i.e.*, surface-to-surface spacing between nearest neighbouring particles. This spacing parameter is denoted as Δ_{3S} in three-dimensional space, and Δ_{2S} in a section plane of the material body. Although the centre-to-centre nearest neighbour spacing, Δ_3, is defined in stereological literature [Underwood, 1968], the surface-to-surface spacing may be more relevant for studying certain material properties. Therefore, surface-to-surface spacing Δ_{2S} is selected for illustration purposes.

This issue is approached by computer simulation on the basis of the SPACE system. Model concretes are generated with aggregate systems conforming to the Fuller type of volume-based size distributions. By using periodic boundary conditions for the reference frame (cubic container), the volume element will represent the bulk material (no boundary disturbances). The spatial dispersion of the aggregate grains in a mixtures is reflected by the distribution probabilities of Δ_{2S}, denoted as $f(\Delta_{2S})$. Serial sections of the model concretes were made in three orthogonal directions. Surface-to-surface distances between all nearest neighbours are determined in the section planes and thereupon classified according to their length. Sample areas of increasing extent are simulated upon averaging histogram data of the individual sections. Model concrete with 60% aggregate of 1~32 mm particles is simulated by Chen [2002]. The linear dimension of the cubic sample is 100 mm, yielding 100x100 mm section planes.

Simulation results on macro-, meso-, and micro-level will be presented. Fig. 4.10 shows the distribution curves $f(\Delta_{2S})$ at different sampling levels. A reference histogram is obtained by averaging over 40 section histograms (statistically independent section planes from three orthogonal directions), yielding an area element with linear dimensions of 4,000 mm, exceeding that of the RVE for configuration homogeneity (40~50 times the largest structural dimension of 32 mm). Hence, the reference histogram can be considered representing the configuration homogeneity of the aggregate grains. The data series 'M = 1' is the distribution histogram of an arbitrary section in the middle part of the concrete sample, while 'M = 4' represents the average results of four randomly selected sections. The differences between the histogram representing M section images and the reference one can be quantified by the well-known χ^2-test method introduced in section 4.4.

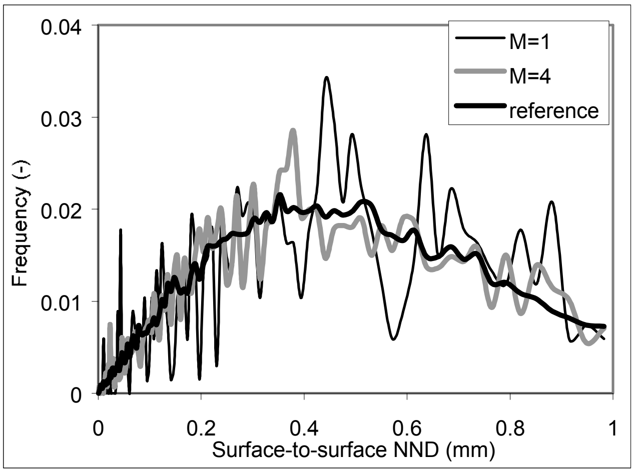

Figure 4.10 The distribution probability of surface-to-surface nearest neighbour spacing, $f(\Delta_{2S})$, at different sampling levels.

For this purpose, the information on the probability density function $f(\Delta_{2S})$ obtained from these measurements is plotted as a histogram with nine length classes. The length range is 0~1.0 mm, with an interval width of 0.1 mm for the first seven classes and 0.15 mm for the last two classes, so that the minimum frequency is at least at the 5% level. The frequency in class i for the reference histogram is denoted by $\overline{f_i}$. The corresponding frequency of a histogram averaged over M sections is indicated by f_i. Specific to the analysis of spacing homogeneity in this section, the χ^2-value can be defined by $\chi^2 = \sum_{i=1}^{9} (f_i - \overline{f_i})^2 / \overline{f_i}$. Successively adding sections ultimately leads to an average histogram that sufficiently resembles the reference histogram. The accompanying decline in χ^2-value at that stage is arriving at an acceptable limit defining the size of the RAE.

Fig. 4.11 presents the χ^2-values for the Δ_{2S} histograms at an increasing number of section planes (M) of 100x100 mm. These data can be approximated by a smooth curve of the hyperbolic type. Global extrapolation of the hyperbolic curve (taking 1.239 as an acceptable level, 7 degrees of freedom because the frequency of the 9th class was lower than 5%) would lead to M = 7~9. This implies an RAE for configuration-sensitive parameters with a linear dimension of about 300 mm. The value of $\overline{\Delta}_{2S}$ for this structure is 0.397 mm, *i.e.*, three times the value of $\overline{\Delta}_{3S}$ (0.126 mm). This indicates that nearest neighbours in space are more closely spaced than is reflected by the section plane pattern. This implies that for a certain aggregate grain, the nearest neighbouring particle in 3D space is not necessarily intersected by the investigated section plane; hence, the *range* of the Δ_{3S} distribution will be somewhat larger, supposedly resulting in a slightly enlarged RVE/RAE. By using $f(\Delta_{3S})$ for assessing configuration homogeneity, it could be expected that the linear dimension of the RVE will exceed the size of the RVE for structure-insensitive properties as given by the rule of thumb

(4 to 5 times of the maximum structural dimension) by one order of magnitude. This would be in accordance with the predictions of Brown [1965] for composition and configuration homogeneity of conglomerates associated with structure-insensitive and structure-sensitive properties respectively.

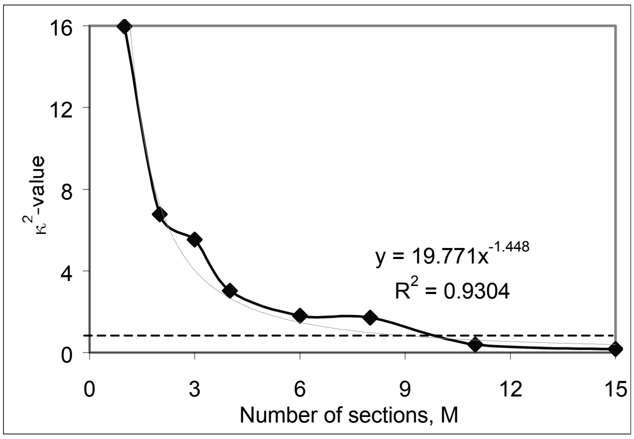

Figure 4.11 χ^2*-values show differences in* $f(\Delta_{2S})$ *as revealed by the reference histogram and by a histogram representing an increasing number (M) of section planes. The dash line corresponds to the acceptable level of* χ^2*-value of 1.239 (at a confidence level of 99%).*

4.6 Summary

Local porosity analysis proposed by Hilfer deals with porosity distribution fluctuations and local percolation probabilities in reconstructed 3D model of porous media. A 2D approach is developed in this study as an alternative to the 3D local porosity analysis. It is combined with quantitative image analysis and can be directly applied to specimen sections to characterise the 3D porosity distribution and percolation probability in cement pastes with various w/c ratios at different degrees of hydration. The conversion from 3D to 2D is based on two points: (1) area fraction of porosity is an unbiased estimate of volume fraction of porosity; (2) knowledge of porosity at the percolation threshold and quantitative empirical relationship between connectivity and porosity. Local porosity distribution and percolation probability curves are valuable sources of information for estimating permeability or diffusion quality of cement paste. LPT analysis provides a statistic estimation of the geometric characteristics of pore space, and therefore could be used to interpret and predict the permeability and other transport properties of cementitious materials.

Heterogeneity is a not a material characteristic. Instead, it is a stochastic concept governing the design of experiments; it inevitably results from sub-representative sampling procedures. Homogeneity of a geometric parameter or of the associated material property can only be achieved for volume elements that are large enough to reduce the between-samples scatter in the relevant parameter or property to an acceptable level. This is the so-called representative volume/area element (RVE/RAE). When the experimental design is based on volume or area elements of sub-representative size as to the property or geometric feature of interest, the associated degree of heterogeneity is a function of the size ratio of sample and RVE/RAE, which is defined as probing sensitivity in this study.

This implies biases to be similar when the size ratio (defining level of microstructure) is similar in comparative studies on cementitious materials with different sizes of RVE/RAE, *e.g.*, cement pastes of different maturities. Hence, the requirement of a constant size ratio of sample and RVE/RAE results in an experimental design encompassing different sample sizes adapted to the range of RVE/RAE sizes involved. When considered on fields of similar size, the linear dimensions of the RAE for porosity homogeneity increase with hydration time at a given w/c ratio and increase as the w/c ratio declines, corresponding to a more heterogeneous structure. When the comparison between various cement pastes is based on the same level of microstructure, however, the local porosity distribution curves can be approximated by normal distribution functions. These normal distribution curves are similar for various cement pastes, provided the age effects are eliminated and they are normalised by peak frequencies. This confirms that heterogeneity is not a material characteristic, but a function of the geometric material parameter at issue, of the microstructural level taken into consideration and of the linear dimension of the RAE involved.

Depercolation Threshold of Porosity

-Approach by morphological evolution during hydration-

In 1983, Dehoff [1983] pointed out the necessity of using serial sectioning for the evaluation of metallic microstructures. The reason is that, although some parameters like volume fraction or area of interfaces can be obtained directly from planar sections, and others such as particle size distribution or degree of anisotropy can be determined from planar sections with simplifying assumptions, there is a group of parameters that can only be obtained from a 3D representation of the microstructure [Alkemper and Voorhees, 2001]. This group includes the number of features per unit volume, connectivity of features, spatial distribution information, and the detailed shape of an element of the microstructure. Stereological theory can help to derive part of the structural information in this group from 2D sections of actual cement paste specimens, as demonstrated in Chapters 3 and 4. But complications arise when the researcher is interested in the connectivity and depercolation threshold of porosity in cement pastes.

Chapters 3 and 4 present the characterisation results obtained from SEM images of actual cement pastes by means of stereological analysis, of opening distribution technique and of local porosity analysis; these two chapters constitute the major experimental part of this study. The derived structural information, such as total porosity and pore distribution density, contains information about the pore connectivity, thus allowing for a comparative study of *pore connectivity* between cement pastes of different w/c ratios and of various extents of maturity (see Chapters 3 and 4).

However, a quantitative study of the *depercolation threshold of capillary porosity* and the influences of technical parameters thereupon can only be approached by computer simulation. Model cement pastes, when based on proper modelling concepts, provide relatively realistic 3D representations of the material and its structural development. In this chapter, the depercolation threshold of capillary porosity will be estimated in view of the morphological evolution of pore space during the hydration process in model cement pastes (generated with the SPACE system). The relevance of this chapter is derived from the intimate relationship between depercolation threshold and the water permeability of cementitious materials.

Section 5.1 briefly describes the definition of depercolation threshold of porosity and its relevance to transport properties of cementitious materials. Section 5.2 presents the research results of the NIST group on this subject, employing their digital-image-based model. This is a good reference to the simulation study with the SPACE system, although the latter is a continuum-based model. Section 5.3 describes the approach used in this study, *i.e.*, based on morphological evolution of pore structure during the hydration process. The influences of w/c ratio and cement fineness on depercolation threshold are discussed in section 5.4.

5.1 Definition of depercolation threshold of porosity (p_c)

The depercolation threshold of capillary porosity (p_c) is usually defined as the porosity at which the *volume fraction of connected pores* (known as connected porosity) in the cement paste decreases to zero. In the beginning of cement hydration, the pore space is entirely connected. During the hydration process, the volume fraction of the solid phase (consisting of unhydrated cement and hydration products) is continuously increasing as a result of cement hydration. The solid phase starts from individual spherical particles that gradually get inter-connected to form a microstructure network. The *porosity connectivity* of pore space (*i.e*., fraction of connected pores), decreases monotonically at a given w/c ratio as hydration proceeds, and parts of the capillary pore space become isolated. A point is reached for lower w/c ratios whereby pore connectivity drops rapidly during continuing hydration, ultimately leading to discontinuity in the capillary pore structure. The value of porosity p and degree of hydration α at which this occurs are denoted by p_c (depercolation threshold of capillary porosity) and α_c (the critical degree of hydration for depercolation), respectively. This depercolation threshold is associated with transport properties of cement paste and therefore directly related to the durability aspect of cementitious material.

5.2 Conventional approach to depercolation threshold of porosity

The computer simulation study on the depercolation threshold has been carried out by various researchers; a short review of their research findings is given in Chapter 1 (section 1.4). Although based on different modelling concepts (continuum-based model or digital-image-based model), the same approach to depercolation threshold is employed, *i.e*., the threshold is defined as the porosity at which the fraction of connected pores decreases to zero. Among these simulation studies representative is the extensive research on depercolation phenomenon conducted by the NIST group.

In the initial study of Bentz and Garboczi [1991], based on a simplified model of C_3S hydration only, a depercolation threshold of about 22% was identified for capillary porosity. The depercolation threshold of capillary porosity is found to be a function of technical parameters, among which cement PSD and w/c ratio are of significant importance. Using the most recent version of their microstructure model (digital-image-based model, see Chapter 1), Bentz *et al*. [1999] studied the depercolation for two cement PSDs (with median grain size of <5 μm> and <30 μm>, corresponding to a fine cement and a coarse one, respectively) at three different w/c ratios (0.246, 0.3 and 0.5). It was revealed that the cement PSD had a significant effect on the capillary porosity at which depercolation occurs. Compared to the effects of the PSD, those of the w/c ratio were of minor importance (see Fig. 5.1). A depercolation threshold of porosity of 18% was found for the coarse cement, while the threshold value was 22% for the relatively fine cement (Fig. 5.1).

Garboczi and Bentz [2001] also studied the capillary porosity depercolation for equal volume (EV) and equal number (EN) systems at the same w/c ratio of 0.3. In the EN case, equal numbers of each particle size were used, while in the EV case, equal volumes of particles were employed. The PSD functions of these two types of systems have been discussed in Chapter 2 (section 2.5). In both cases, only four sizes of particles were used, with diameters of 3, 9, 13, and 19 μm. The equal number case had a depercolation threshold of about 16%, whereas the threshold for the equal volume case was about 21%.

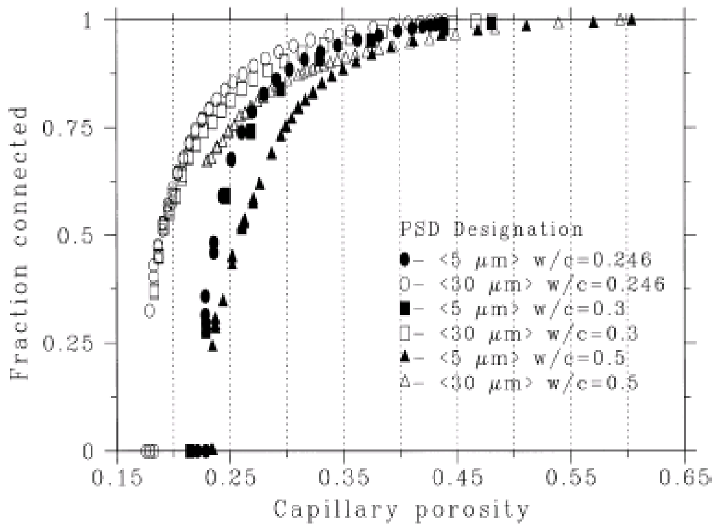

Figure 5.1 *Depercolation threshold for cement pastes with two different PSDs and for various w/c ratios. After Bentz et al. [1999].*

However, the research of Elam *et al*. [1984] revealed the depercolation threshold of a sphere-based (continuum) numerical model cement to be around 3~5%. Also based on the continuum-based model cement (HYMOSTRUC) composed of spherical cement particles, Ye [2003] reported that the depercolation of capillary pores cannot be realised because the pore structure remains highly interconnected even at the ultimate hydration stage. The obvious divergence between various research outcomes can at least partially be attributed to the characteristics of the various simulation models and to the digital resolution. This has been discussed in section 1.4.

The afore-mentioned conclusions are based on the conventional definition of p_c as the porosity at which the fraction of connected pores decreases to zero. In this study, the depercolation of pore space is studied in view of the morphological evolution of pore phase during hydration, employing the SPACE system.

5.3 Determination of p_c by morphological evolution

The volume fraction of solid phase, V_V, and porosity, p=1-V_V, can be easily determined for model cements at a specified hydration stage. Size and the spatial distribution of solid phase can be characterised by the mean intercept length of solid phase clusters $\overline{L}_3$ and the mean free spacing between solid clusters λ, respectively. The definitions of these stereological parameters can be found in Chapter 2. Mean free spacing λ is the direct representation of the average pore size and can be calculated according to Eq. (4.11). The specific surface area S_V can be obtained for hydrated model cements as described in section 3.3.

The change trend of λ represents the morphological evolution of pore space during the hydration process. From the viewpoint of morphological aspect, cement hydration and strength development of cement is in fact a geometrical problem. The hydration products gradually fill up the available pore space; hence, the hydration process is accompanied by a decreasing value of mean free distance between solid phase clusters (λ). At the final stage of hydration, the hydrating cement particles stop to 'grow' when there is no more space available; this stage is associated with the end value of λ. Since λ is a direct observation of the pore size, this point can be related to the depercolation threshold of capillary porosity. This concept is the basis of the new approach employed in this study, *i.e.*, to determine the depercolation threshold from the porosity at which λ arrives at a stable end value, instead of the porosity connectivity in the conventional method mentioned in section 5.2.

The evolution of mean free spacing λ during 10,000 hours of hydration is shown in Fig. 5.2 for model cement C342 (see Chapter 2) with various w/c ratios. Changes after 10,000 hours are only minor. A decreasing function of λ versus the hydration time could be expected. The starting point of the curve is the mean free distance in the initial packing structure, λ_0. It should be noted that the mean free distance drops rapidly in the first day (or so), and then gradually decreases to a certain value λ_{end} that only marginally diminishes at a further increase of hydration time. The critical point where the plateau is reached (the first point approaching λ_{end} within ±3% relative variation from the value of λ_{end}) corresponds to a porosity of 21% for w/c=0.3 paste. The parameters at depercolation for cement of various w/c ratios are presented in Table 5.1, and will be discussed in what follows.

The morphological evolution of cement Y420 (simulated by Ye [2003] with HYMOSTRUC, with a specific surface area of 420 m^2/kg) with a w/c ratio of 0.3 is also plotted in Fig. 5.2 as a comparison to that of C342 (generated with the SPACE system). The value of λ_0 is 5.7 μm for Y420, while the value for C342 (w/c=0.3) is 3.5 μm, although Y420 is finer than C342. This phenomenon can be partially explained by the big intervals of PSD for Y420, *i.e.*, 1 μm, while the PSD of C342 is a more continuous one with size intervals of 0.02 μm. On the other hand, the major difference between the two models is that HYMOSTRUC adopts a 'random packing' concept, whereas SPACE employs a 'dynamic mixing' algorithm to realize the densification of the cement particle system. The depercolation threshold value obtained in this study is in line with the NIST model. This can be partially attributed to the realistic simulation of packing structure in the fresh state of model cement. This also confirms the importance of packing structure in the fresh state to the microstructural development of cement during hydration.

5.4 Influences of technical parameters on p_c

5.4.1 Influence of the w/c ratio

Fig. 5.2 clearly reveals the curves of mean free distance versus hydration time to have similar shapes for various w/c ratios. For a higher w/c ratio, the mean free distance is larger at an equivalent hydration time because cement with higher w/c ratios starts from a less densely packed particle system. The time at which depercolation occurs t_c, as well as the critical hydration degree α_c, increase with w/c ratio, as demonstrated by the data presented in Table 5.1. It is interesting to note that the value of p_c is similar for cements with various w/c ratios (about 21% for C342). This indicates that the effect of the w/c ratio on the depercolation threshold is negligible, which is in agreement with the research outcomes of the NIST group. To give a better insight into the influence of the w/c ratio on the depercolation threshold, the mean free distance is plotted against the porosity in Fig. 5.3. The curves for the various w/c ratios slightly deviate from each other, suggesting a degree of self-similarity in the hydration process.

Table 5.1 Depercolation parameters of capillary porosity for paste C342

w/c ratio	p_c (%)	t_c (hrs)	α_c (-)	λ_0 (μm)	$\lambda_{end.}$ ($t = t_c$, μm)
0.3	21.1	126	0.42	3.5	2.0
0.4	21.3	631	0.57	4.6	2.6
0.5	23.4	7943	0.76	5.8	3.2

In the case of cement with a w/c ratio of 0.6, although the pore space also becomes less connected as hydration progresses, the depercolation threshold cannot be reached because the high initial porosity prevents closing off the water-filled pore space with hydration products. In this case, it is not possible for the cement to hydrate sufficiently to achieve depercolation of the capillary porosity. Bentz *et al*. [1999] reported that the depercolation curve (connected fraction versus capillary porosity) for a w/c ratio of 0.6 asymptotically approaches those of the lower w/c ratios. The cement with a w/c ratio of 0.6 had a final porosity of 26% at the ultimate hydration stage. According to Powers' model [1958], cement with a w/c ratio of 0.6 has an estimated final porosity of 25%. This accounts for the observation that the cement of a w/c=0.6 cannot depercolate because the porosity at complete hydration is still higher than the depercolation threshold.

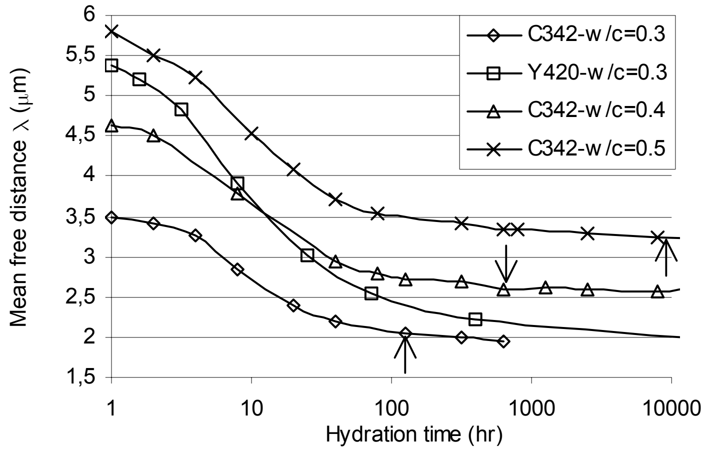

Figure 5.2 *Profile of morphological evolution of pore space in C342 (SPACE simulation, size range 1~45 μm), at w/c ratios varying between 0.3 and 0.5 (the depercolation threshold indicated with arrow); the change for model cement Y420 (HYMOSTRUC simulation, S_G=420m^2/kg, size range 2~45 μm) is also presented for comparison.*

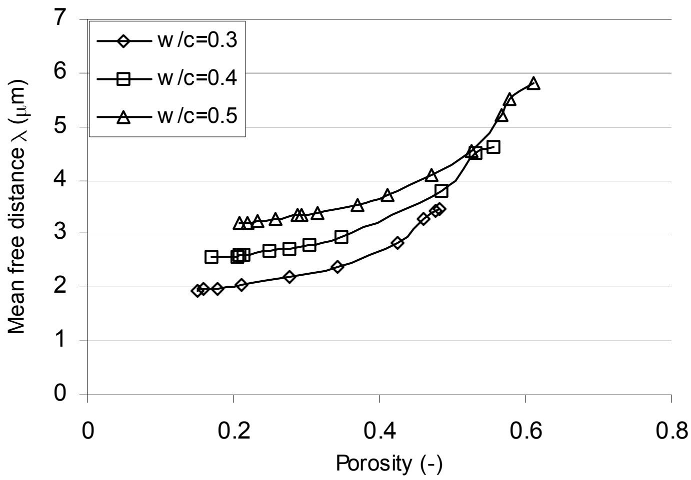

Figure 5.3 Influence of water cement ratio on the depercolation threshold of capillary porosity.

5.4.2 Influence of particle size distribution

The PSD and depercolation parameters for the three model cements C167, C342 and C605 (see Chapter 2), at a w/c ratio of 0.3 are given in Table 5.2 and Fig. 5.4. For coarser cement, the average inter-particle spacing is larger, such that more extensive hydration and longer hydration time is required to close off the capillary porosity. The finer cement hydrates far more rapidly, independently of w/c ratio; therefore, it reaches the depercolation threshold within a shorter period of time. Hence, when evaluating the depercolation of cement pastes of widely varying particle size distributions, one must be careful to distinguish the hydration kinetics effects from the micro-structural effects. For this purpose, the morphological evolution for the three cements is plotted in Fig. 5.4b against a micro-structural parameter, total capillary porosity, instead of plotting it against hydration time as in Fig. 5.4a. Eventually, for the lower w/c ratios such as 0.3, the hydration of coarser cement will catch up with that of the finer one, and the final mean free distance λ_{end} will be similar for the three model cements.

Table 5.2 PSD and depercolation parameters of the model cements (w/c=0.3)

Cement code		C167	C342	C605
PSD parameters	Size range (μm)	1~47	1~45	1~20
	a	1.836	1.083	1.193
	b	0.004	0.054	0.111
	Median diameter (μm)	17.6	10.6	4.2
Morphological parameters	λ_0 ($t = 0$, μm)	6.7	3.4	2.0
	λ_{end} ($t = t_c$, μm)	2.7	2.0	1.2
Depercolation	p_c (%)	7.9	21.1	31.8
	t_c (hrs)	794	126	40
	α_c (-)	0.52	0.42	0.33

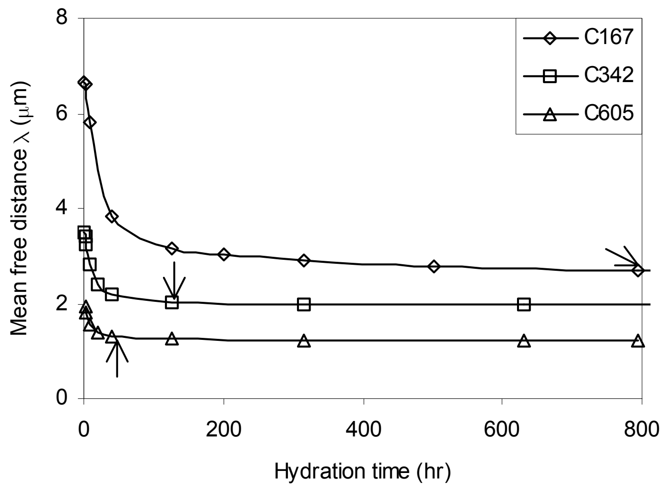

(a)

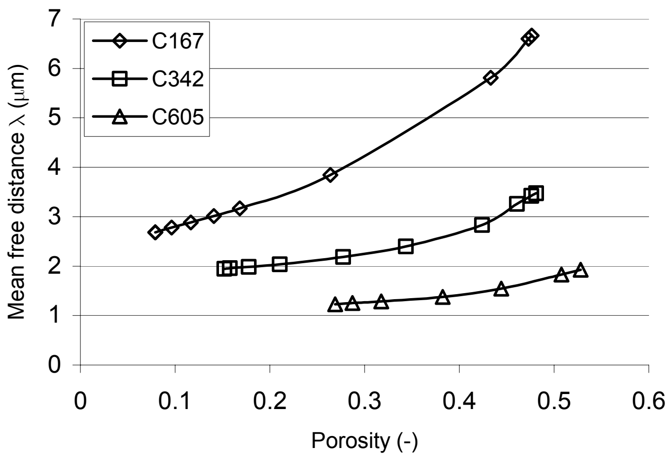

(b)

Figure 5.4 *Influence of PSD on depercolation threshold of pore space: (a) Evolution of mean free distance versus hydration time (the depercolation threshold indicated with arrow); (b) Evolution of mean free distance versus porosity.*

5.4.3 Analytical approach to the influence of PSD

As shown in Chapter 2, the initial mean free spacing (λ_0) in the fresh state of cement particle packing can be estimated from the specific particle size distribution (PSD) function in an analytical approach. The calculation can be performed for four types of PSD functions, *i.e.*, the Rosin-Rammler function, the Fuller function, equal volume (EV) and equal number (EN) mixtures. The calculation results can offer insight into the morphological evolution and the depercolation threshold of the pore structure in cement.

The minor influence of w/c ratio on p_c is reflected by the fact that curves for mean free spacing versus the capillary porosity to roughly merge into a single curve, for w/c ratios ranging from 0.3 and 0.5. This is corresponding to a common depercolation threshold of about 21%. In case of a higher w/c ratio, it takes more time to reach the depercolation threshold of porosity. This can also be explained from the morphological aspects. For example, in case of a model cement with a moderate fineness of 363 m^2/kg, the initial mean free spacing (λ_0) between cement particles is 4.58, 6.10, 7.63, 9.15 μm for a w/c ratio of 0.3, 0.4, 0.5, and 0.6, respectively (calculated according to equations in Chapter 2). Hence it is expected that the cement with a higher w/c ratio needs more time to reach a low value of λ that corresponds to the depercolation threshold of porosity. It has been observed that at higher w/c ratios (say, 0.6), the hydrating model cement is sometimes unable to achieve depercolation of the capillary porosity, especially in the case of relatively coarse cement. Even if the model cement hydrates completely, the final porosity is still higher than the depercolation threshold of porosity. This is because the spacing (dependent on cement PSD and w/c ratio) between cement particles is too large to be closed off by hydration products.

The different values of depercolation threshold for EV (21%) and EN (16%) cases reported by Garboczi and Bentz (section 5.2) can also be explained by the stereological parameters of these two systems. The mean intercept length of the EV mixture is 3.69 μm, and the mean free spacing between particles is 3.48 μm. For the EN mixture, the mean intercept length is 9.53 μm, the mean free spacing 9.00 μm. In the latter case, the average particle diameter heavily relies on the larger particles; so the average inter-particle spacing is much larger. As a consequence, the hydration process needs to be more advanced for closing off capillary pore space.

5.5 Summary

The mean free spacing between solid phase clusters, which can be determined in the continuous hydration process of model cement by stereological estimation, is a direct measure for the average pore size. The depercolation threshold of capillary porosity can be estimated within the framework of the morphological evolution of pore structure as hydration proceeds. The depercolation threshold of porosity is around 21~23% for cement paste with ordinary fineness. Cement PSD exerts significant influences on the depercolation threshold of capillary porosity. Finer cement has a higher threshold value because of two factors: (i) the inter-particle spacing is smaller, therefore it is easier for finer cement to close off pore space; (ii) at a given w/c ratio, the finer cement hydrates more rapidly, hence it takes less time to achieve depercolation of capillary porosity.

The influences of w/c ratio and cement fineness (Blaine specific surface area S_G) on depercolation threshold can be studied in an analytical approach on the basis of stereological relationships between initial mean free spacing (λ_0) and volume fraction of cement particles (V_V, corresponding to w/c ratio), and specific surface area of cement particles (S_V, closely related to cement fineness S_G). Combining Eq. (2.9) and Eq. (4.11) reveals a direct quantitative relationship:

$$\lambda_0 = 4\frac{1-(V_V)_{t=0}}{(S_V)_{t=0}} = 4\frac{1-(V_V)_{t=0}}{S_G \cdot \rho_{cem} \cdot (V_V)_{t=0}} \tag{5.1}$$

where t=0 indicated the fresh state of particle packing.

The w/c ratio is a composition parameter because it represents the volume fraction of cement particles in the material mixture, *i.e.*, $(V_V)_{t=0}$. To the contrary, when PSD is varied, spacing parameters including inter-particle spacing and nearest neighbour distances are involved; this constitutes a configuration issue. This explains the results revealed in this study: the particle size distribution of model cement has significant influences on the depercolation threshold of porosity, whereas the effect of the w/c ratio on this threshold is minor. Hence, the depercolation threshold of porosity is a structure-sensitive parameter.

The significant impact of cement PSD on depercolation threshold confirms the concept that depercolation phenomenon of pore space in cement pastes is a *geometry-related* rather than a chemistry-related process. Although depercolation of pore space *results* from increasing volumes of spatially dispersed hydration products, the depercolation threshold of pore space is *governed* by the *size and spatial distribution* of the particles at the initial packing state of the fresh cement.

Pore Structure in the Interfacial Transition Zone

Of particular interest in concrete technology is the so-called Interfacial Transition Zone (ITZ). The ITZ between aggregate and cement paste is a crucial element in mechanical (strength) as well as in transport systems (durability). Various experimental researches have been carried out as to the extent and the microstructure of the ITZ. The interest is derived from the recognition that in normal concretes the ITZ constitutes the weakest link in the mechanical system. However, the experimental investigations of different researches fail to provide consistent conclusions.

On the other hand, the quantitative structural analysis of the ITZ requires sampling in sections parallel to the interface. Experimentally, this would require a laborious process of physical sectioning and quantitative image analysis by point or line scanning operations. Instead, conventionally, narrow strips are subjected to image analysis procedures, as in the research work of Diamond and Huang [2001]. These strips run parallel to the interface, but are situated in the very section in which the gradient structure is investigated. The image analysis process can be automated, of course. A prerequisite in many cases is that the quality (contrast) of the image is enhanced by subjecting it to pattern recognition algorithms. This inevitably leads to extra scatter and even biases.

Conflicting experimental results as to the internal structure of the ITZ, as well as the labour intensive nature of experimental approach make it attractive to confront such observations with a *coherent picture* of the ITZ produced by computer simulation with the SPACE system. Under periodic boundary conditions, the simulated structure of cement particle dispersion in a cubic container can be considered as a representation of bulk paste material. When the container walls are specified as rigid surfaces, densification leads to disturbances in the particle packing near the wall. Cementitious materials can be considered to consist of particulate elements on various levels of microstructure. On a micro-level approach, the container wall can be conceived as aggregate surface. This allows for simulation of the ITZ between cement paste and aggregate grains.

In the present situation of model concretes generated in the SPACE system, the spatial distribution of all cement particles is known, so 3D structural information attributed to a section does not suffer from such inevitable experimental uncertainties. Thus, quantitative analysis of the gradient structure in the ITZ can be realised by section analysis (*i.e.*, determining V_V, A_A, L_A and S_V) of serial full sections parallel to the aggregate surface (*i.e.*, the container wall under rigid boundary conditions). The integrated stereological estimations in the SPACE system render possible visualization and characterisation of the gradient structure in the ITZ by section analysis of serial full sections (*i.e.*, the linear dimension of the section equal to that of the cubic container) parallel to the interface (aggregate surface).

In this chapter, the ITZ extent will be approached by computer simulation on the basis of composition and configuration parameters (section 6.1). In section 6.2, underlying mechanisms for strength improvement in Portland cement concrete associated with rice husk ash (RHA) blending are revealed in a computer simulation approach. Section 6.3 discusses the micro-structural development of the ITZ during hydration process, on the basis of the stereological parameters characterising the pore structure in the ITZ. These stereological parameters allow predicting mechanical and permeability properties in the ITZ of model concretes (Section 6.4).

6.1 The ITZ extent

Conventional experimental approaches to the ITZ extent considered either cement paste cast on the surface of a glass sheet/piece of stone, or a section through a concrete specimen. The first approach has the drawback of not properly simulating the conditions in the interior of the material; the second approach only provides off-equatorial particle sections yielding biased information on the ITZ thickness [Scrivener, 1989b]. Stroeven [2000a] demonstrated that the estimation of the ITZ extent by section measurement would be on average 50% too high. Indirect observations of the extent of the ITZ, such as by micro-hardness measurements, yield data at least partly influenced by the sensitivity of the technique. Some experimental investigations [Scrivener, 1999; Zimbelmann, 1985] showed that a lower w/c ratio would reduce the ITZ thickness and thereby contribute to the interfacial bond strength. In contrast, van Breugel [1991] and Garboczi and Bentz [1997] stated that the extent of the ITZ would not relate to the w/c ratio. Ollivier *et al*. [1995] found the extent of the ITZ equal to the mean diameter of the cement grains. This is deviating from the simulation results that the ITZ thickness is equal to the median size of the cement grains [Bentz and Garboczi, 1999].

The present study approaches this phenomenon by computer simulation with the SPACE system. The capability and advantages of this system for a realistic simulation of the particle packing have been discussed and demonstrated in Chapter 2. Three mixtures of different fineness levels, C167, C342 and C605 (used in Chapter 2), are taken as representative samples. The w/c ratios vary between 0.4 and 0.6. Details of the model cements and the PSD curves of the mixtures can be found in Chapter 2.

The extent of packing gradients in the fresh state was revealed to vary with changes in the material composition. In addition, Stroeven and Stroeven [2001] emphasized that the ITZ extent also depends on the configuration-sensitivity of the parameter characterising aspects of the material structure. This section gives particular attention to this fundamental aspect, and not to properly estimating the ITZ thickness of the model concretes. Morphological evolutions in the ITZ are quantified on the basis of the stereological parameters introduced in Chapter 2. This allows assessing the configuration sensitivity of the characterising parameter and its influence on the ITZ extent.

6.1.1 ITZ extent and material composition

The ITZ is commonly physically modelled around aggregate grains as a shell-like zone with a certain thickness. Segregation in the cement particle packing near a surface of aggregate grain is commonly expressed in terms of density or porosity data. This is a measure for structural *composition*. This section gives a short review concerning the dependence of the ITZ extent on the *material composition*, *i.e.*, associated with the volume fraction of cement particles (density) or porosity.

Previous study [Chen, 2002] learned that the ITZ thickness increased slightly with the w/c ratio. The *top point of the first ascending part* of the volume density curve of cement particles versus the distance to the interface is associated with the border of the ITZ. It was also found that the ITZ thickness corresponds to the mean diameter of cement particles. This implies finer cement to have a smaller extent of the ITZ. In addition, his research revealed that the ITZ extent was not related to the median diameter of cement particles.

Stroeven and Stroeven [2001] demonstrated the ITZ thickness in the lower range of w/c ratio (0.2-0.4) to be in the order of 1/3 of the maximum particle size. It is reported that the ITZ extent increased over the full range of w/c ratios (from 0.2 to 0.6) by a factor of about 2. Their results also revealed that porosity (interpreted as complementary to particle volume density) declined significantly faster away from the interface in case of finer cement, corresponding to a smaller extent of the ITZ. Due to a limited number of simulations, a quantitative relationship between the ITZ extent and the material composition cannot be established yet. But the SPACE simulation revealed trends consistent with experimental results published in the literature, *e.g*., see Scrivener [1999]. It can be concluded that computer simulation by the SPACE system provides a realistic representation of the ITZ microstructure.

6.1.2 ITZ extent and material configuration

However, a structure-sensitive property like crack initiation would basically appeal more to material configuration than to composition. The stereological descriptors L_A and $(S_V)_{pore}$, representing to some extent the morphology aspect of the material structure, will be employed for systematically studying the relationship between the ITZ extent and *material configuration*. In the SPACE system, these stereological parameters can be extracted from imaginary section planes of the ITZ parallel to aggregate surface.

The values of the mean intercept length of particles ($\overline{L}_3$) for the model concretes with a w/c ratio of 0.4 are shown in Fig. 6.1 over the distance to aggregate surface. If $\overline{L}_3$ is taken for characterising the ITZ extent, coarser model concrete has a wider ITZ, and the ITZ extent is related to both the mean diameter and the maximum size of cement particles. The influence of the w/c ratio on the ITZ thickness is much less pronounced than the cement fineness. Fig. 6.1 confirms that size segregation causes an accumulation of the smaller particles close to the aggregate surface.

Morphological evolution of the mixtures is shown in Figs. 6.2~6.4.

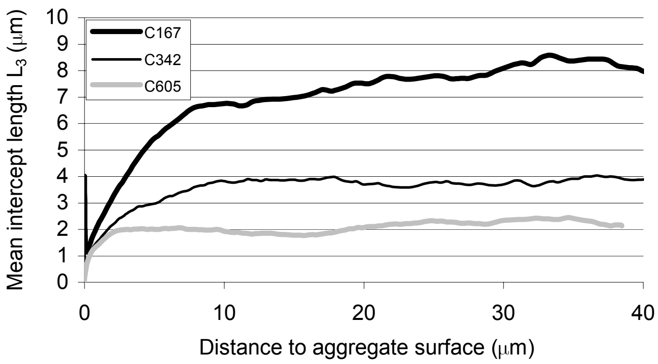

Figure 6.1 Mean intercept length of cement particles for w/c=0.4 mixtures with different finenesses, plotted as function of distance to the aggregate surface.

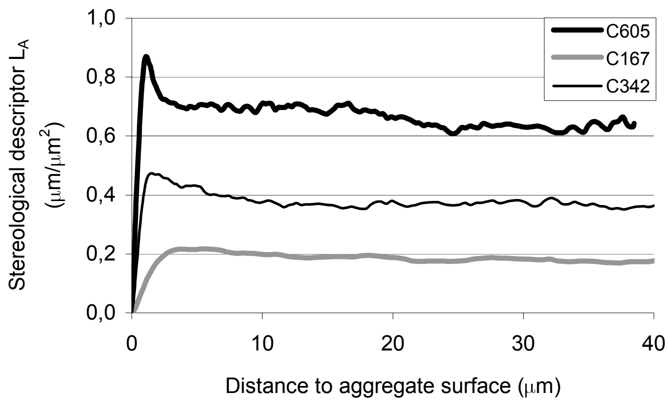

Figure 6.2 *Stereological descriptor L_A for model concretes of different fineness (w/c=0.4).*

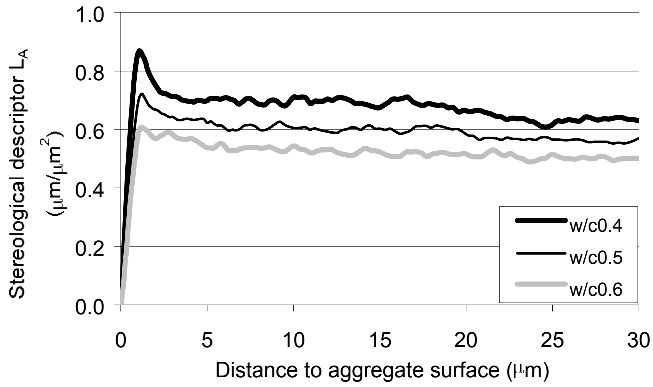

Figure 6.3 *Stereological descriptor L_A for model concrete C605 of different w/c ratios.*

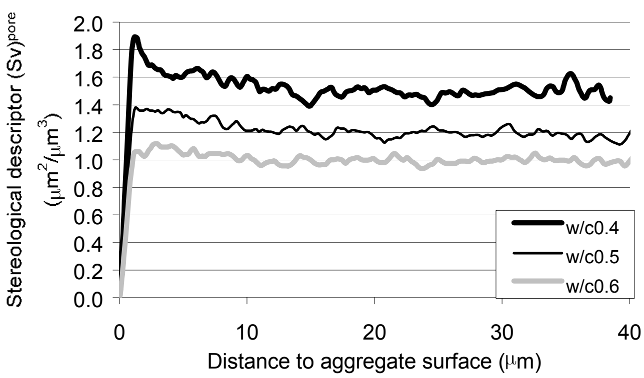

Figure 6.4 *Stereological descriptor $(S_V)_{pore}$ for model concrete C605 of different w/c ratios.*

Fig. 6.3 reveals that with a reduction in the w/c ratio, the L_A rises more steeply in the immediate vicinity of the aggregate surface to a level that significantly exceeds the bulk value (about 45% higher than bulk value for a w/c=0.4 concrete). For a mixture of a lower w/c ratio, the bulk value is gradually approached at a distance farther away from the interface. This is accompanied by a significant increase in the ITZ thickness. Although it is observed in some experiments that a lower w/c ratio reduces the ITZ extent, this is not the case if more configuration-sensitive parameters such as the morphological descriptors are adopted to characterize the material structure in the ITZ. The experimental outcomes of Diamond and Huang [1998] confirmed this conclusion. It can be expected that this phenomenon will be more pronounced at a lower w/c ratio between 0.2 and 0.3. Particularly under conditions relevant for HPC, the ITZ is significantly densified and the associated ITZ would have a thickness of the order of the maximum grain size of the cement.

6.2 Improvement of ITZ by gap-graded binder

It is generally assumed that the ITZ in concrete involves an approximately 30-50 μm wide zone around each aggregate grain [Scrivener, 1999]. Porosity in the ITZ increases as the aggregate interface is approached. Therefore, the ITZ is accepted to constitute the weakest link in the mechanical system. Hence, methods for upgrading concrete into the high strength or even high performance ranges should be in the first place effective in disproportionately improving the quality of the ITZ [Jiang and Roy, 1994]. A significant reduction in the w/c ratio (corresponding to lower porosity), rendered possible by the use of superplasticizer, has been demonstrated as a method for achieving this goal. Increasing the range of particle sizes in the binder by adding fine-ground fly ash or rice husk ash (RHA) also works out favourably [Fidjestøl and Frearson, 1994].

6.2.1 RHA as mineral admixture

RHA is a highly reactive pozzolanic material produced by controlled burning of rice husk. The utilization of RHA as a pozzolanic material to improve the ITZ microstructure in HPC provides several advantages, such as improved strength and durability properties, reduced materials costs due to cement savings, and environmental benefits related to the disposal of waste materials and to reduced carbon dioxide emissions. The reactivity of RHA is attributed to its high content of amorphous silica, and to its very large surface area governed by the porous structure of the particles [Mehta, 1994; Cook, 1984]. Generally, reactivity is favoured also by increasing the fineness of the pozzolanic material [Kraiwood *et al*., 2001; Paya *et al*., 1995].

Cements with a higher fineness are applied in HPC. Traditionally, HPC is produced of low w/c ratio mixtures (below 0.4), to which a superplasticizer and a fine-grained pozzolanic material are added. The limited available space in the fresh state of such low w/c ratio mixtures will be occupied by hydration products after hardening, which will also contain unhydrated cement regardless of the fineness of the cement [Taylor, 1997]. Based on computer simulation, Bentz and Haecker [1999] concluded that in this situation coarser cements could yield equivalent long-term performance as compared to finer cements. By blending finely ground RHA with such a coarser cement, higher packing densities near the aggregate grain interface can be expected, as a consequence, leading to improved behaviour of the blended systems. This is a strategy emphasized in this section. This section presents the results of a combined mechanical and computer simulation study on the effects of particle size ranges involved in RHA-blended Portland cement on compressive strength of gap-graded concrete in the HPC range.

6.2.2 Experimental

The experiments of RHA-blended cement concrete were conducted by Bui, for materials and experimental details, see Bui [2001]. A brief introduction will be given in this section to the experimental design and the outcomes of mechanical tests for RHA-blended cement concretes. Two kinds of ordinary Portland cement were employed, *i.e*. PC30 and PC40. The cements originated from one clinker source but were pulverized to different degrees of fineness. The Blaine specific surface area for PC30 and PC40 is 270 and 375 m^2/kg, respectively. A Vietnamese type of rice husks was incinerated in a drum incinerator for production of the RHA. The ash was finely pulverized using a vibrating ball mill after combustion. The mean diameter of the RHA particles is 5 μm. The aggregate for the mixtures consisted of a mixture of crushed basalt (9.5-19 mm) and of fine sand smaller than 0.6 mm (sand content of 30% by mass).

RHA was used to replace 10, 15 and 20% by mass of PC. The water to binder ratio involved was 0.3, 0.32 and 0.34, respectively. The superplasticizer was added to all mixtures to obtain high workability. Cubes of 100 mm in size were cast and compacted in two layers on a vibrating table. Each layer was vibrated for 10 seconds. The moulds were covered with polyethylene sheets after casting and moistened burlap for 24 hours. Thereupon, the specimens were de-molded and cured in water at a temperature of 20^{o}C until the day of testing. The compressive strength of the concretes was determined at 1, 3, 7, 28 and 90 days, using three specimens per test age.

Compressive strength data of RHA blended concrete are higher than those of the plain cement concrete, irrespective of w/b ratio and age. Compressive strength increases with blending percentage at corresponding values of w/b ratio and age. This trend is pronounced for replacement levels up to 20%. Fig. 6.5 presents relative compressive strength data, defined as the ratio of the compressive strength of the RHA-blended concrete to the strength of the plain cement concrete with the same binder content and cured to the same age. This ratio is denoted as *blending efficiency* in this study. It was found that the relative increase in compressive strength was 22% for the coarser cement compared to 10% for the finer one (at a PC replacement level of 20% by mass).

The strength increment for blended-cement concretes can be attributed to the fact that the RHA particles react with the abundant calcium ions in the ITZ to produce C-S-H, as opposed to the conventional precipitation of large CH crystals in the ITZ. However, it is noteworthy that the more favourable results for the coarser cement are considered to be due to the positive effect exerted by *gap grading*. Modern design of super HPC types reveals the *discontinuity in particle size ranges* of composing particle fractions to be of crucial importance for achieving optimum mechanical properties. Fundamental researches into the effects of replacing silica fume by inert carbon black have also demonstrated such particle packing efforts to prevail at lower w/c ratios [Goldman and Bentur, 1993].

The blending of RHA with the fine cement PC40 leads to less efficient particle packing due to the narrower particle size range when compared to the blending with the coarser PC30 cement. Hence, only a moderate contribution is given by the filler effect to early-age strength. To achieve optimum strength effects, the fineness of the RHA (or in general, the mineral admixture) should be attuned to that of the PC, *i.e.* the average grain sizes of PC and admixture should be quite distinct, yielding gap-graded blends. In a quantitative sense, roughly similar strength contributions at later ages come from the pozzolanic reaction. The physical contributions are different however, as a result of the better packing characteristics of the PC30 and the RHA. This is evidenced by the significant dependence of strength efficiency on blending percentage.

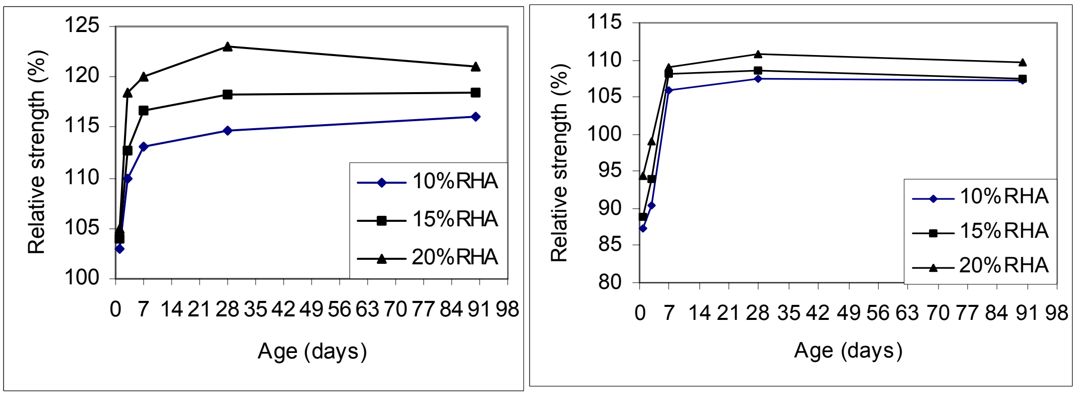

Figure 6.5 Relative strength of gap-graded concrete made with RHA-blended cement PC30 (left) and PC40 (right). The w/b ratio involved was 0.3. After Bui [2001].

6.2.3 Computer simulation approach

Mechanical experiments on RHA blended Portland cement concretes revealed that in addition to the pozzolanic reactivity of the RHA (chemical aspect), the particle grading (physical aspect) of cement and RHA mixtures also exerted significant influences on the blending efficiency. In HPC incorporating superfine particles, the filler effect has been demonstrated to be even more pronounced than the pozzolanic effect [Detwiler and Mehta, 1989]. Relevant to HPC, the packing characteristics of binder particles in the fresh state of concrete are of supreme importance because 'the idea behind concrete as a material is to attempt to reconstitute a solid rock from elements having complementary grading' [de Larrard and Malier, 1992]. Studying cement particle packing in the ITZ in the fresh state of concrete is therefore highly relevant. The *packing efficiency* of a mineral admixture can be expected to depend, therefore, on the average *fineness gap* between the particles of the mineral admixture and of the cement. This will be investigated in this section by employing the SPACE system for a computer simulation approach to this problem. The relative strength increase is higher for coarser cement, as shown in Fig 6.5. The gap-grading phenomenon is expected to be the underlying mechanism. This issue is also approached by computer simulation.

Model materials and methods

Relevant to the low w/c range in HPC, the w/b ratio of 0.30 of the experimental program is adopted for the simulation. This implies the volume fraction of *spherical* binder particles to occupy about 50% of the total container volume. The particle size distribution of the PC is made to closely match the so-called Rosin-Rammler size distribution function (see section 2.2). The constants *a* and *b* are derived from the experimental data of the cement particle size distribution. The simulation of the RHA particles is based on the sieve curve found in the experiments.

Table 6.1 presents some of the model data that characterize the particle mixtures used in the simulation experiments. The designed size range of the RHA is 0.18~11 μm. The upper border turned out to be 8.5 μm in the generated mixtures. The number in the code of model cements indicates the replacement level of RHA by mass (expressed in %). Partial replacement of the two types of PC with the relatively fine-grained RHA causes Blaine numbers to increase significantly, as shown in Table 6.1. Of course, the increase is largest for the coarser grained PC, *i.e.* 95 and 81% for PC30 and PC40, respectively, at a 20% PC replacement level. This refinement of the blended mixtures is also revealed by the cumulative fractional volume density curves presented in Fig. 6.6.

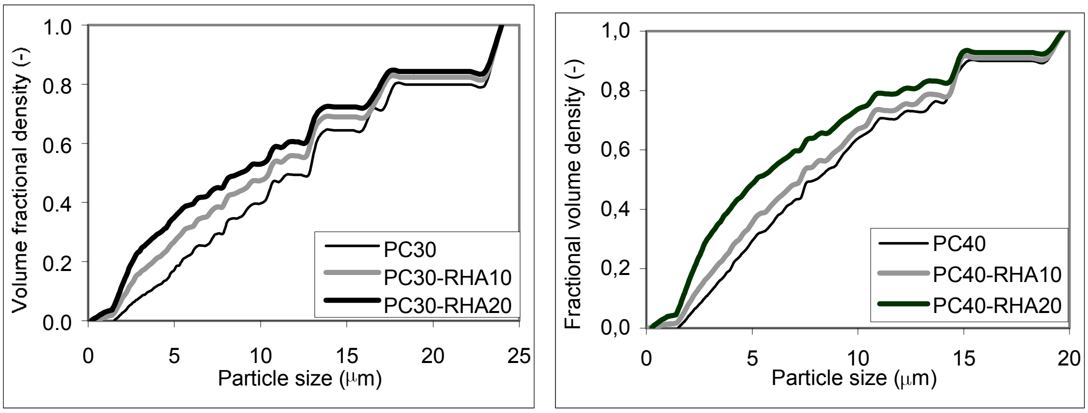

Figure 6.6 Cumulative volume fractional density of investigated mixtures for PC30 (left) and PC40 (right).

Table 6.1 Physical parameters of model cements

Model cement	Size range (μm)	Blaine specific surface area (m^2/kg)	Rosin-Rammler parameters
PC30	1.5~23.04	248	$a = 1.03$
PC30-RHA10	0.18~23	363	$b = 0.022$
PC30-RHA20	0.18~23	483	
PC40	1.5~18.93	329	$a = 1.10$
PC40-RHA10	0.18~19	431	$b = 0.045$
PC40-RHA20	0.18~19	594	

The model concrete containing binder particles is serially sectioned to derive information on the gradient perpendicular to the aggregate surface. Material properties depend on geometrical-statistical features of the material structure. Density is a relevant approach for assessing porosity when interested in certain concrete durability aspects. When strength is considered, a certain degree of structural sensitivity should be accepted. Only medium sensitivity will be encountered in the case of compression testing. The most relevant structural parameter is the mean free spacing λ. It is associated with S_V and L_A and can be calculated from Eq. (4.11). Following earlier studies [Stroeven and Stroeven, 2001], a global bonding capacity is used. When exceeded, the material is supposed to yield under compressive loadings. The global bonding capacity is - in analogy with van der Waals' physical bond concept - taken proportional to the reciprocal value to the third power of the mean free spacing (*i.e.* λ^{-3}).

Blending efficiencies for model concretes made with PC30 and PC40

Size segregation in the vicinity of a rigid interface, is shown in Fig. 6.7 for PC30 blended with 10% RHA. The successive size fractions - *only distinguished for illustration purposes* - have their peak contributions to the total volume fraction at distances from the rigid interface that are proportional to the average sizes involved in the particle fractions. The total fractional volume density curve does not reflect this size segregation phenomenon. Instead, it shows a steep ascending branch on the left that bends over to a plateau value on the right. The plateau value (bulk density) extends over most of the cube width. Although the ITZ has no distinct boundaries, the plateau value can be imagined to start at about 1/3 of maximum particle size, indicating the order of the ITZ thickness for compositional homogeneity.

The grading heterogeneity extends, however, outside this ITZ zone, as illustrated by the section patterns of Fig. 6.8, recorded at distances from the rigid interface of 1, 3, 8, 23.3 and 35 μm, respectively. It can be expected, therefore, that the ITZ thickness for *grading homogeneity* will considerably exceed the one for density. Fig. 6.9 shows the fractional volume density curves for the investigated cases, demonstrating blending to reduce porosity in the layer immediately bordering the interface surface. Also, a tendency of reduced ITZ thickness by blending is observed. This confirms the similar experiences when blending with silica fume. Bulk density is improved somewhat by blending, although only small differences were revealed between the two investigated partial PC replacement levels. No dramatic effects of the cement fineness on the blending efficiency as to the densification of the ITZ or bulk were found.

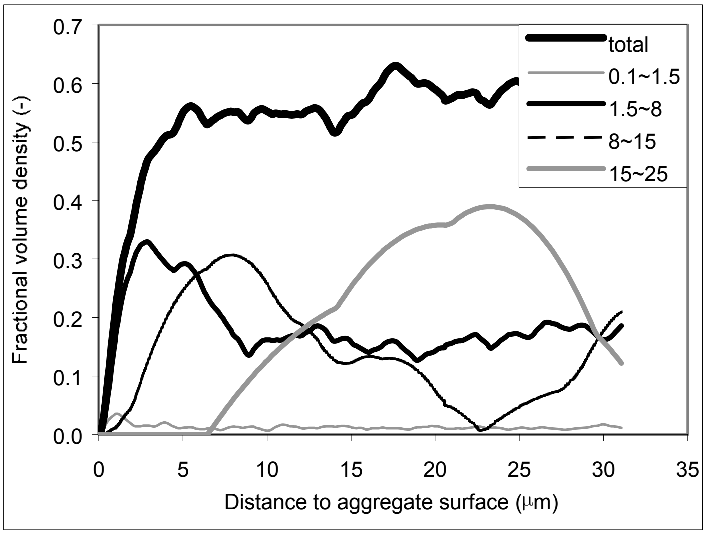

Figure 6.7 *Volumetric density of different size fractions (size range in μm) of particles from model cement PC30 with 10% RHA replacement.*

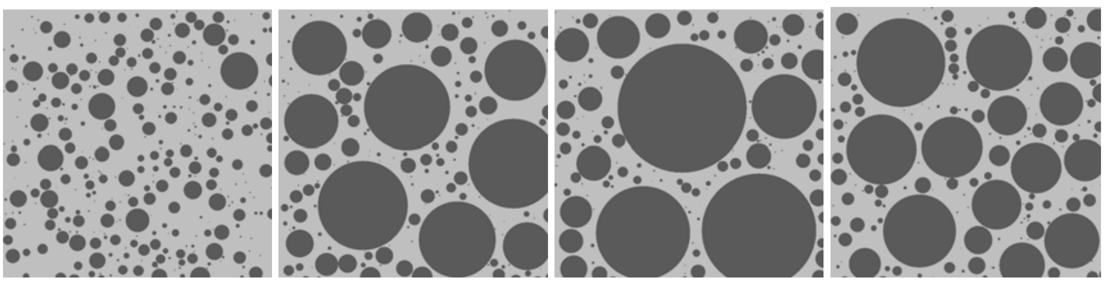

3.0 μm 8.0 μm 23.3 μm 35.0 μm

Figure 6.8 *Section images of model cement PC30 with 10% RHA replacement at specified distances from aggregate interface.*

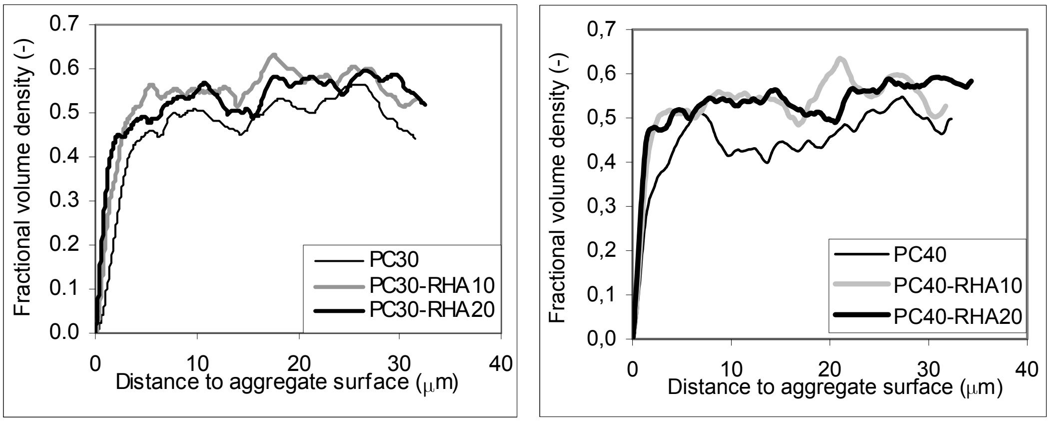

Figure 6.9 *Fractional volume density of model cements PC30 (left) and PC40 (right) as function of distance to aggregate interface.*

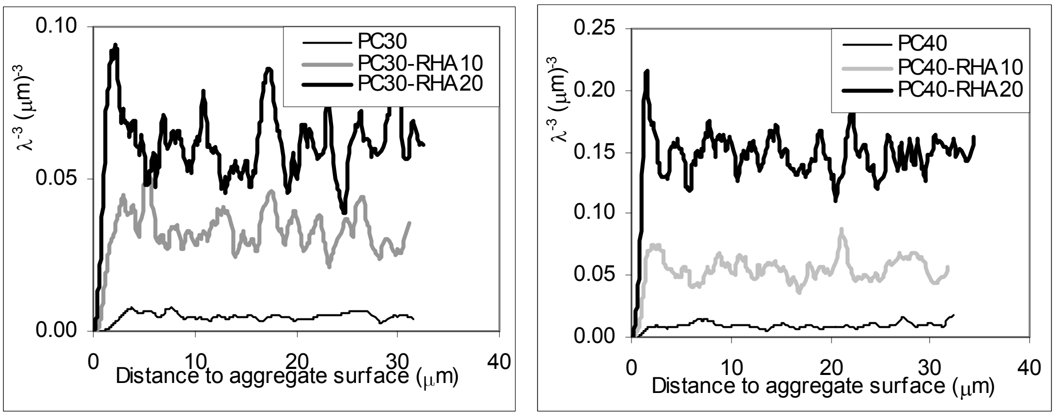

Figure 6.10 *Parameter proportional to global bond capacity of model cements as function of distance to aggregate interface.*

Fig. 6.10 presents the effects of blending on the global bonding capacity of the PC30 and PC40 model paste mixtures. The inter-particle bond capacity steeply rises in the immediate vicinity of the aggregate interface and exceeds bulk value to a considerable extent. At increasing distance to the interface, bulk value is gradually approached. This disproportional bond strength increase in the ITZ can be attributed to size segregation. The disproportional improvement of bond (compared to a situation without size segregation) in the part of the ITZ immediately neighbouring the interface surface is restricted to the range of w/c ratio between 0.2 and 0.3 (relevant for HPC).

In absolute terms, PC40 mixtures are superior in strength capacity, but even in Fig. 6.10 it is obvious that the improvements due to blending (denoted as blending efficiency) are larger in the case of the coarser grained PC30. This is convincingly demonstrated in Fig. 6.11, displaying the bonding capacity of the blended mixtures normalised by the bulk bonding capacity of the respective types of Portland cement. Specifically at the 10% partial replacement level, the blending efficiency of PC30 is roughly 60% exceeding that of PC40. This is in qualitative agreement with the mechanical experiments (see Fig. 6.5). These differences considerably declined at the 20% partial replacement level. It can be concluded that the mixture of the coarser grained PC and RHA provided better conditions for smaller

RHA particles to properly migrate through the ITZ towards the aggregate surface, leading to a more densely packed ITZ, but predominantly to reduced surface-to-surface spacing of binder particles.

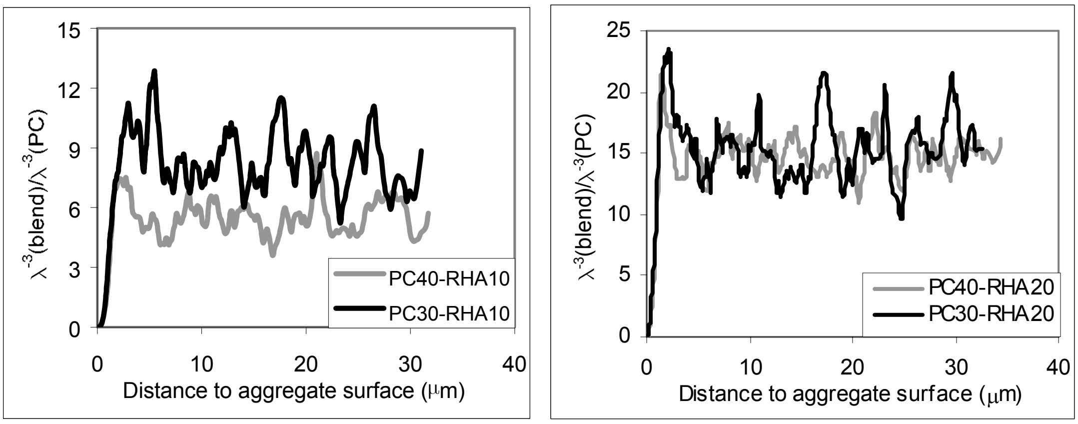

Figure 6.11 Parameter proportional to global bond capacity of blended model cements normalised by respective plain cement bulk value as function of distance to aggregate interface.

Since the global bonding capacity (supposed to be relevant for compressive strength testing) depends on local grading and spacing characteristics, the associated ITZ will extend over a larger distance from the rigid interface than in the case of density homogeneity. Because of its medium structure-sensitive character, bond estimates show a larger scatter than density estimates, as can be concluded from a comparison of Figs. 6.9 and 6.10. To establish a proper estimate of the ITZ thickness in the latter case, a series of similar simulations should be performed.

Proper dispersion of the RHA particles

Exploiting the gap-grading effect requires proper dispersion of the fine RHA particles. For illustration purpose, the RHA-blended coarser cement PC30 (level of replacement at 10%) was simulated in the case of insufficient dispersion of RHA particles. This is corresponding to poor workability conditions in concrete production. If proper migration of RHA particles can be realised, the smaller RHA particles tend to concentrate in the immediate vicinity of the aggregate surface (see Fig. 6.8, section image at distance of 3 μm), thereby disproportionately improving local bond capacity in the ITZ (Fig. 6.10).

However, if proper workability conditions are not met, compaction will be ineffective and RHA particles cannot migrate to the vicinity of the aggregate interface. This phenomenon is explicitly revealed by the differences of section images between the two cases (corresponding to poor and good workability, respectively) at the distance of 3 μm from the aggregate surface, although the bulk paste reveals similar patterns (Fig. 6.12).

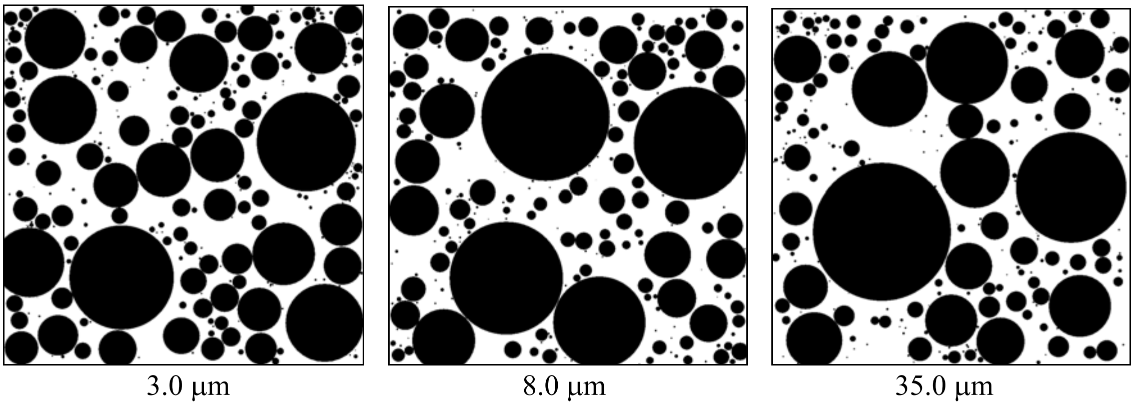

Figure 6.12 *Section images (at specified distances from aggregate surface) of model cement PC30 with 10% RHA replacement generated under the condition of insufficient dispersion of the fine RHA particles. This is corresponding to poor workability conditions in concrete production.*

Coordination number can be used to present the degree of dispersion of binder particles. A lower value of coordination number corresponds to a better-dispersed structure of the particle system. In the case of poor workability, the coordination number per particle is 0.32. The properly generated mixture yields a value of 0.003, indicating a well-dispersed system and a more homogeneous structure of particles. In the case of insufficient dispersion, RHA blending is not able to improve the ITZ microstructure since the mean free spacing λ will exceed the one of an efficiently blended cement. Fig. 6.13 presents the global bond strength (normalised by the bulk value of the plain cement) for the same mixture PC30-RHA10 (Fig. 6.11) in the case of insufficient dispersion of RHA particles.

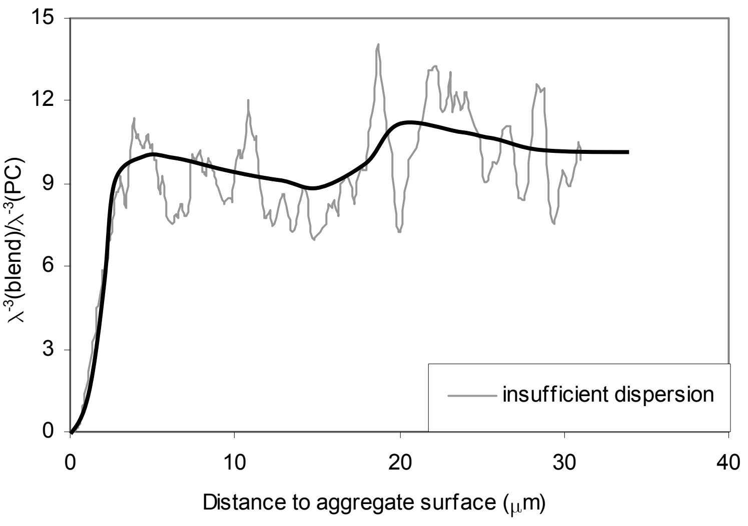

Figure 6.13 *Global bond strength (normalised by the bulk value of the plain cement) versus distance to the aggregate surface, for coarser cement PC30 at 10% replacement level under poor workability conditions (insufficient dispersion of RHA particles); Hand-drawn line reflects general features of bond strength.*

Comparing Fig. 6.13 with Fig. 6.11 confirms that when the RHA particles are agglomerated, they are less effective in improving the ITZ microstructure although the density curves are similar. If the RHA particles are properly dispersed, the bond strength presents relatively higher value in the ITZ within 8 μm away from the aggregate surface (Fig. 6.11). Fig. 6.13 reveals a sufficient amount of small particles not to have migrated to the part of the ITZ bordering the aggregate grain. This yields slightly higher bond capacity in the ITZ near the inner border (between 15~30 μm), but absence of the bond strength peak close to the interface. Hence, clustering of the fine RHA particles should be prevented, and the migration process should be facilitated by proper workability and compaction conditions in the concrete production process.

Conclusion

As a relatively soft and porous material, it is more cost effective to grind the RHA to a larger fineness than to do so with the Portland cement in gap-graded binder designs. An increased fineness of the RHA will ultimately result in a decline of water demand, and an enhanced filling capacity. Partial replacement of the PC with up to 20% RHA by mass yielded increased early-age compressive strength values only in the case of the gap-graded binder mixtures. RHA blending improved strength properties for both cement types (PC30 and PC40). However, the gap-graded binder PC30 gave rise to significantly higher relative strength values for comparable cases. The magnitude of this blending efficiency as to the compressive strength increases with the RHA content (in the studied partial replacement range). It is demonstrated by the computer simulation approach that the favorable results, particularly with the gap-graded binder, reflect improved particle packing (density and grading) leading to a decrease in porosity and particularly a decline in spacing between the binder particles. This inevitably results in more significant *physical* contributions to the strength, earlier demonstrated to be of significance in the lower range of w/c ratios. Moreover, this probably causes the development of a more homogenous microstructure of the hydrated cement paste in the ITZ, also yielding a more favourable situation for the development of *chemical* contributions to the strength.

6.3 Structural evolution during hydration

In the fresh state of particle packing, the 'wall effect' reflects the phenomenon of a reduced cement particle density, and thus a more porous ITZ. The porosity and microstructure in the ITZ have been studied extensively in experimental and computer modelling approaches. Some research outcomes revealed a pronounced increment of porosity within a few micrometers of the aggregate surface [Scrivener and Nemati, 1995]. Based on SEM observations and image analysis, Diamond and Huang [2001] found only slightly higher porosities in the ITZ.

It can be expected that after hydration, the porosity will still be affected by the packing discontinuity in the ITZ. Some researchers stated that while hydration does reduce the porosity near the aggregate interface, the ITZ still exists as a prominent microstructural feature exerting influence on strength and durability [Bentz and Garboczi, 1999; Scrivener *et al*., 1988]. Diamond and Huang [2001] argued, however, that there is no reason to assume significant negative effects of the ITZ on permeance or mechanical properties of concrete, even for concrete with water binder ratio of 0.5. Hence, as to practical implications for strength and permeability, a *communis opinio* is so far missing.

This section gives particular emphasis to the structural evolution of the ITZ during the hydration process. Based on the stereological estimation incorporated in the SPACE system, the morphological and structural evolution of the ITZ is quantified with *composite parameters* and *configuration parameters* for hardened concrete. This allows comparing properties of the ITZ in model concretes with experimental observations. Model concrete C342 with a w/c ratio of 0.3 is chosen as an example in this section, relevant to a low w/c range in HPC. The structural information is derived for two hydration stages (10 and 100 hours, respectively).

The average intercept length of cement particles in the vicinity of the aggregate surface is significantly smaller then that in the bulk paste, which demonstrates the higher concentration of finer particles in the ITZ (Fig. 6.1). A much higher w/c ratio is observed in the vicinity of the aggregate surface than in bulk paste. This phenomenon makes it plausible that the degree of hydration in this transition zone is higher than that in the bulk paste, as shown in Fig. 6.14.

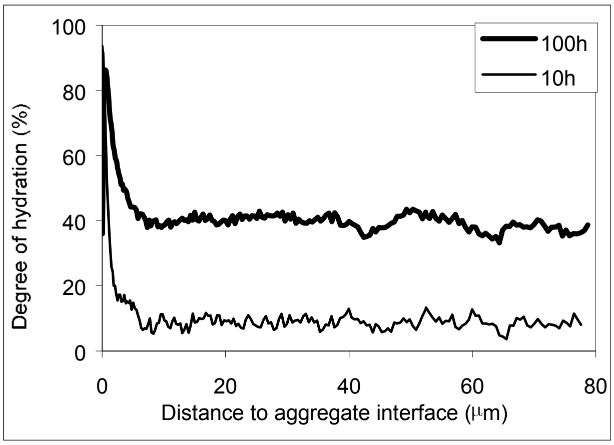

Figure 6.14 Significantly higher degree of hydration in the ITZ than in the bulk paste for model concrete matured for 10 hours and 100 hours, respectively.

Results of computer simulation as well as of experimental approaches confirmed the existence of a pronounced gradient of unhydrated cement starting from the bulk paste with progressively less residue cement as the aggregate surface is approached. The disproportionably higher degree of hydration can be additionally attributed to relatively abundant water and easier water supply in the more porous matrix-aggregate interfacial zone. It is observed that the hydration of cement in mortar and concrete proceeds faster than in neat paste. This can be attributed to an easier water supply via the porous matrix-aggregate interfacial zone. In addition, the higher connectivity of porosity accelerates the water supply in the ITZ. This disproportional higher degree of hydration in the vicinity of aggregates than in the bulk paste helps to offset the effects of a porous ITZ in the initial state of packing, especially in the case of a low w/c ratio.

Experimental techniques can only investigate the porosity gradient in the ITZ by analysing narrow strips at progressive distances from the aggregate perimeter. In the study of Diamond and Huang [2001], the width of strip is taken to be 10 μm. Their research outcomes indicated only slightly higher porosities inside the ITZ than in the bulk paste, even in the immediate vicinity (*i.e.* up to 5 μm) of the aggregate interface. Computer simulation provides for continuous monitoring of porosity as a function of distance to the aggregate surface.

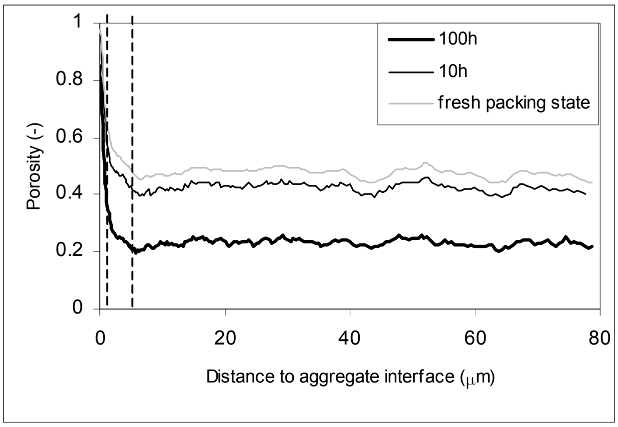

Figure 6.15 Porosity in the ITZ for model concrete matured for 10 hours and 100 hours, respectively. Bulk porosity is approached at a distance of about 6-8 μm away from aggregate surface (dashed line at the right).

The porosity gradient in the ITZ is presented in Fig. 6.15 for the fresh state of concrete as well as for the hardened material at 100-hour's hydration. Experimental research indicated that the porosity of the bulk paste in concrete decreases slightly between 3 and 100 days of hydration. Scrivener and Nemati [1995] also observed a negligible decline of bulk porosity in concrete (w/c ratio of 0.4) from 28 days to 1 year of hydration. Hence, the model structure at 100-hour's hydration is regarded representative of a mature concrete in this study. As presented in Fig. 6.15, the porosity is about 0.30 at 1.5 μm from the aggregate surface (dashed line at the left), while a bulk porosity of 0.24 is achieved at a distance of 6 μm (dashed line at the right) from the aggregate surface. Hence, the results of the SPACE simulation for a low w/c range support the findings of Diamond and Huang. The porosity gradients indeed confirm that the negative effects of the porous ITZ are less pronounced for a matured concrete with low w/c ratio.

Although the porosity in the ITZ is partly interconnected as observed by Scrivener and Nemati [1995], this percolative effect can be far outweighed by the increasing tortuosity due to aggregate grains [Marchand and Delagrave, 1999]. Stroeven [2000b] proved in a stereological approach that tortuosity of transport routes in concrete associated with the presence of aggregate grains is proportional to the volume fraction of supposedly spherical aggregates. Hence, in the low w/c ratio range, this increase of tortuosity can be significant enough to offset the percolation of porosities in the ITZ. This is in agreement with the experimental results of Jaiswal *et al*. [1997] who studied the influence of aggregate volume fraction on permeability of concrete: 'Tortuosity and ITZ both increase with volume fraction of aggregates. Tortuosity decreases and interfacial zone increases permeability but tortuosity dominates, at least until aggregates volume fraction of about 0.5'.

For a matured model concrete with w/c ratio of 0.3, higher porosity is found in zone in the immediate vicinity of the aggregate surface (within a distance up to 5 μm), see Fig. 6.15. Delagrave *et al*. [1998] indicated that in well-cured mortars of reasonably low w/c ratios (0.25~0.45), a front of dissolution of calcium hydroxide proceeds uniformly down the specimens, with no preferential leaching or decalcification around the aggregates ahead of the front. However, in the case of relatively high w/c ratios (say, 0.6), the porosity is highly interconnected in a region of at least 20 μm wide neighbouring aggregate surface [Scrivener and Nemati, 1995]. On the other hand, dissolution of some of the calcium hydroxide immediately surrounding aggregates may in fact open up channels of relatively easy transport and provide preferred sites for deposition of secondary reaction products. Hence, in this case, measures have to be taken to improve the ITZ microstructure and thereby reduce the detrimental effects of the ITZ on mechanical and durability properties of concrete.

Summarizing, the concentration of small particles near the aggregate grain surface leads to a more porous transition zone in the fresh state of concrete. The degree of hydration is therefore much higher in the ITZ than in the bulk paste. The combination of the non-uniform spatial size distribution of the cement particles (*i.e.* size segregation) and the non-uniform hydration rate in the ITZ will yield a slightly higher porosity in the ITZ for a mature concrete.

It is interesting to visualise the structure of hydrated model cement. For this purpose, seven parallel sections are produced at a distance of 0.5, 1, 3, 5, 10, 30 and 70 μm, respectively, from the imaginary aggregate interface. The section that lies 70 μm away from the aggregate surface represents bulk paste. Some of the representative section images are presented in Fig. 6.16. The black colour stands for unhydrated cement particles, the grey for hydration products, and white for pore space. The volume fraction of various phases at different distances from the aggregate surface, including unhydrated cement, hydration products and pore space, can be calculated from their area fractions on the section images. The calculation results are presented in Fig. 6.17. It is clear that in the immediate vicinity of the aggregate surface, the *volume fraction* of hydration products is higher than in the bulk, although the porosity is higher. This is due to the disproportionately high degree of hydration in this zone.

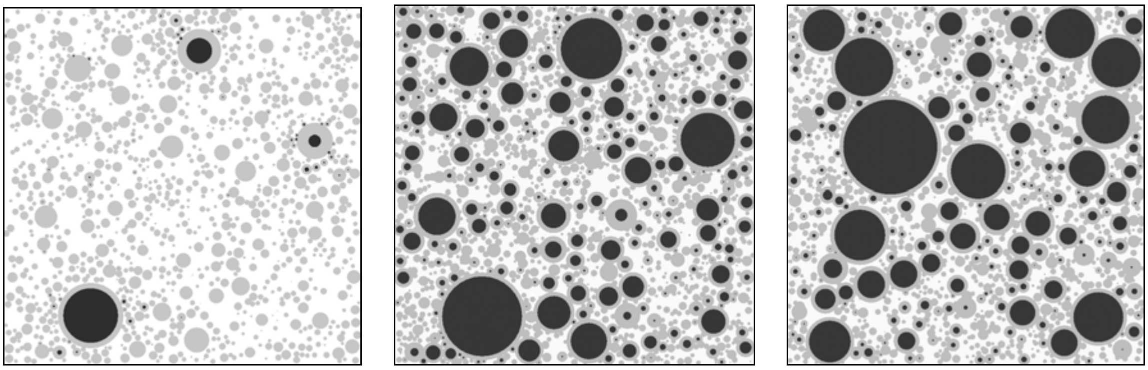

Figure 6.16 Section images of model concrete C342 hydrated for 100 hours. The distances from the aggregate surface are 0.5, 3 and 30 μm, respectively (from left to right).

The slightly higher porosity in the ITZ can be explained on the basis of arguments pertaining to the chemistry of cement hydration. The excess of space resulting from the 'wall effect' is filled in during hydration by calcium hydroxide (CH) deposits that are essentially non-porous. A significant part of it is anchored directly onto the surfaces of aggregate grains. Strong indications exist that the proportion of C-S-H per unit volume in the ITZ is as high as in the bulk paste. As a consequence, the larger space in the ITZ is filled up by through-solution deposits of C-S-H obtained from elsewhere in the hydrating material. As a result, the volume fraction of hydration products is higher in the ITZ than in the bulk paste (Fig. 6.17). SEM observations of Diamond and Huang [2001] showed that the area fraction of C-S-H is almost constant over distances ranging from 5 to 80 μm from aggregate surface. Thus, the higher volume fraction of hydration products in the ITZ can be attributed to the precipitation of CH in the immediate vicinity of the aggregate grain's surface.

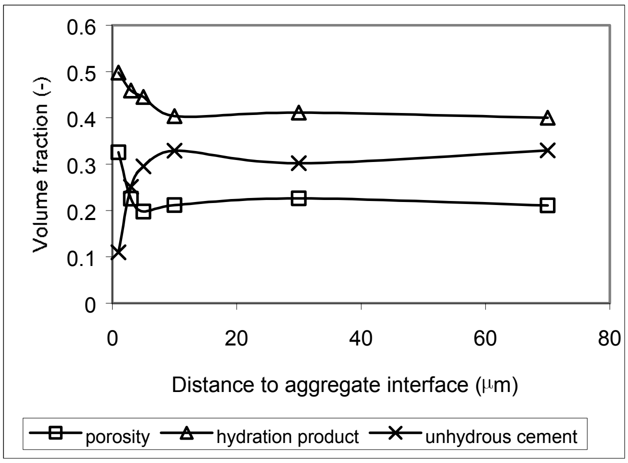

Figure 6.17 Volume fraction of different phases versus distance to the aggregate surface for the model concrete matured for 100 hours.

Both experimental observations [Scrivener *et al.*, 1988] and computer simulation [Bentz and Garboczi, 1999] reveal that ions with a relatively high mobility in cement paste pore solution, such as Ca^{2+}, Al^{3+}, SO_4^{2-}, tend to diffuse into the more porous ITZ (due to concentration gradients arising from the initial higher w/c ratio in the ITZ), resulting in the precipitation of CH and aluminate hydration products as ettringite. Because silicate ions have lower mobilities, they tent to form hydration products near their dissolution source. For a matured model C_3S paste (w/c=0.45, 77% hydration), the Ca/Si molar ratio seems to settle down to 3 (the expected bulk value) at a distance roughly corresponding to the average diameter of cement particles in the fresh state of packing. Approaching the aggregate surface, this ratio increases monotonically to a maximum value slightly larger than 5. This supports the hypothesis that calcium ions are diffusing into ITZ regions at a much faster rate than silicate ions. Hence, it is recommended to increase the amount of silicate ions in the ITZ. This can be realised by blending cement with mineral admixtures such as fly ash, silica fume and RHA (section 6.2).

6.4 Properties of the ITZ

The ITZ is seen as a packing discontinuity at the surface of aggregate particles. Mechanical or physical properties of cementitious materials, such as strength, fracture toughness, fracture energy, diffusivity or conductivity, will be (partly) governed by the grain-induced unevenness of the transport surface. This implies the intimate relationship between material properties and geometrical and morphological aspects of material structure. Some researchers even explicitly state that strength development is, in essence, a geometrical problem.

6.4.1 Mechanical properties

Bond strength in the ITZ of concrete in the high performance range was demonstrated to rise disproportionately over its bulk value in the fresh state due to the natural size segregation phenomenon (note that in this case w/c = 0.3), see Fig. 6.18. Relevant to the global bond capacity of concrete, the gradient over the ITZ of the configuration parameter λ^{-3} (see section

6.2) is studied in the *matured* state of the model concrete hydrated for 100-hours. The determination of mean free spacing λ is based on the specific surface area of solid phase (S_V), which is associated with the perimeter length of solid phase clusters (observed on section images) per unit test area (*i.e.*, area of section image), L_A (see section 3.3 for details). The section images (Fig. 6.16) are subjected to quantitative image analysis to determine L_A for the solid phase and thereby to calculate the mean free spacing λ according to Eq. (4.11).

The calculation results of λ^{-3} are normalised by their respective bulk values, to allow for a straightforward comparison of bond strength in the ITZ between the fresh and matured states of concrete. Fig. 6.18 reveals the disproportional bond strength increase in the very part of the ITZ neighbouring the aggregate interface to remain apparent throughout the hydration process. On the other hand, Fig. 6.17 reveals the volume fraction of solid phase (unhydrated cement plus hydration products) to be almost constant (apart from a very narrow zone immediately bordering the aggregate surface) as function of the distance to the surface. The volume fraction of solid phase significantly contributes to the physical aspect of concrete strength. Hence, the dominant effect of size segregation in the ITZ in concretes in the high performance range provides the ITZ with an inherent strength exceeding that of bulk, so that negative effects of the ITZ on mechanical properties of concrete can not be expected. Supporting experimental evidence can be found in the literature.

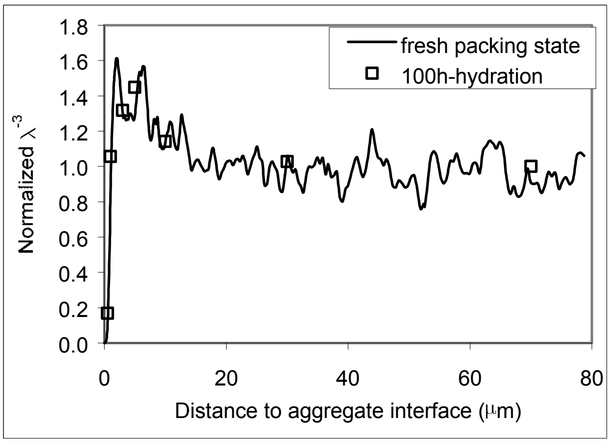

Figure 6.18 Disproportional bond strength increase in the ITZ remains throughout hydration process. The ITZ thickness exceeds that for porosity dramatically.

6.4.2 Tortuosity of transport path and permeability

The transport route in the ITZ is of significant importance because the water-born ions and molecules that transverse the material body are supposedly forced to go around the aggregate grains. According to the Carman-Kozeny model, permeability k of cement paste can be predicted on the basis of the geometrical properties of pore space by

$$k = -\frac{p(V_{pore} / S_{pore})^2}{2\beta} \tag{6.1}$$

where p is the porosity, V_{pore} and S_{pore} are the volume and the surface area of pore space, and β is the tortuosity of the transport route in the cement. Permeability is proportional to the second power of $V_{pore}/S_{pore}=\lambda/4$. Stroeven [2000b] demonstrated by a stereological approach that the tortuosity of transport paths in spherical aggregate concrete does not depend on the size distribution of the aggregate particles. Tortuosity of the transport route can be estimated only from a single morphological parameter, *i.e.* the volume fraction of aggregates, $\beta = 1+V_V/2$. Assuming this to hold for transport through the cement paste as well, Eq. (6.1) can be transformed into

$$k = \frac{(1-V_V)\lambda^2}{32+16V_V} \tag{6.2}$$

where $V_V = 1- p$ is the volume fraction of solid phase, and λ is the mean free spacing between solid clusters (reflecting average pore size).

The calculation results according to Eq. (6.2) are presented in Fig. 6.19 for the fresh and hardened state of cement paste, indicating that a bulk value of $1.5\text{x}10^{-13}$ m^2 is approximately achieved at a distance of 2.3 μm from the aggregate surface. Hence, higher permeability is restricted to the immediate vicinity of the aggregate surface. This does not give rise to a *continuous network system*. Similar normalised values are observed for the fresh state and for the hardened cement paste.

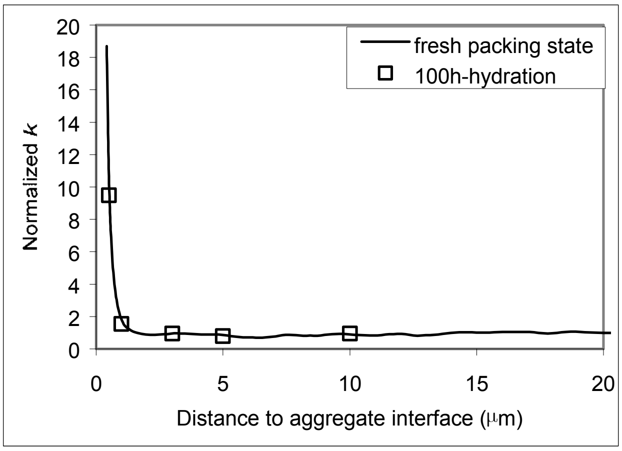

Figure 6.19 Permeability (normalised by respective bulk values) gradient in the ITZ for the fresh state of model concrete and hardened material hydrated for 100 hours.

6.4.3 Structure-insensitivity of permeability

It is generally assumed that for concrete in which adjacent ITZ aureoles significantly overlap, a continuous percolation network is established that will lead to high permeability and rapid diffusion of ions and other dissolved species [Synder *et al*., 1992]. Rangaraju [1999] studied the effects of the size distribution at constant volume fraction of sand on the permeability of concrete. The finer sands generate significantly larger volume proportions of ITZ, and closer grain-to-grain surface spacing, *i.e*., resulting in more overlap of aureoles. Nevertheless, rapid chloride permeability tests yielded almost identical results for all concretes with a given w/c ratio, regardless of the degree of overlap of the aureoles. This is an experimental verification of the model proposed by Stroeven [2000b] that yielded the tortuosity of transport paths in concrete not to depend on the size distribution of (spherical) aggregate grains. Details of the sieve curve of the aggregate do not exert influence on the transport phenomenon in concrete, provided the porosity (and volume fraction of grains) is similar.

For composition parameters such as porosity and cement permeability, the ITZ extent is estimated to be 5~8 μm (Figs. 6.15 and 6.19). The structure-insensitivity of permeability observed in this study is supported by the diffusion experiments of Roelfstra [1989]. However, the gradient of bond strength extends further away from the aggregate surface (to 35~40 μm) because the parameter λ^{-3} is sensitive to the packing configuration (Fig. 6.18). This confirms the dependence of the ITZ extent on the configuration-sensitivity of the investigated geometrical parameter or material property (see section 6.1).

6.5 Summary

The interfacial transition zone (ITZ) between aggregate and cement paste is a crucial element in mechanical as well as in transport systems. The extent of the ITZ depends on technological parameters such as w/c ratio and cement fineness, but also on the configuration-sensitivity of the characterising parameter. The thickness of the ITZ shell will be considerably smaller when derived from the density gradients instead of the configuration gradients. When morphological descriptors of the microstructure are taken to characterize the extent of the ITZ, mixtures with a lower w/c ratio and higher cement fineness show a more pronounced long-range fluctuating behaviour as a function of the distance to the aggregate surface.

The wall-effect limits the population of cement particles in the vicinity of the aggregate surface. In the low w/c ratio range, the combination of the non-uniform spatial size distribution of the cement particles (*i.e.* size segregation) and the non-uniform hydration rate in the ITZ will yield a slightly higher porosity in the ITZ than in the bulk paste for a matured concrete. The increase in bond strength in that part of the ITZ neighbouring the aggregate interface found in the fresh packing state (due to size segregation) is maintained throughout the hydration process. The relatively higher permeability in the ITZ is restricted to the immediate vicinity of the aggregate surface. So, a weaker and more porous spatial network structure will not be formed. Therefore, significant negative effects of the ITZ on permeability and mechanical properties of concrete in the lower w/c range (relevant to HPC) cannot be expected on structural arguments. In the relatively high w/c ratio range, the porosity is still more seriously affected by the packing discontinuity in the ITZ.

The microstructure of the ITZ can be largely improved by blending with rice husk ash (RHA). In the chemical aspect, the RHA particles react with the abundant calcium ions in the ITZ to produce C-S-H as opposed to the conventional precipitation of large calcium hydroxide (CH) crystals. This contributes to filling up the extra space in the ITZ. More important effects are due to the physical aspect: the fine RHA particles migrate through the structure network of large-particles into the vicinity of aggregate interface, leading to a densely packed ITZ and a disproportional bond strength increase in the ITZ neighbouring the aggregate surface. Simulation of the blended cements emphasizes the paramount importance of proper workability and compaction conditions. Only under such conditions can the optimum size segregation effects be achieved. This is stimulated by gap grading mechanisms.

Implications for Concrete Performance

The hydration reaction of cement results in a product consisting of solid and pore system. Thus pores are inherent to concrete. This pore system governs the most important properties of concrete, notably its strength and permeability. Capillary porosity and pore size of hardened cement paste depend on the technical parameters, including w/c ratio and cement PSD. A number of empirical relationships exist between concrete properties (mechanical and durability ones) and pore system characteristics, see *e.g*. [Taylor, 1997]. This allows for a direct prediction of concrete strength and permeability on the basis of structural information of pore space in cementitious materials.

In this chapter, these empirical equations will be briefly reviewed and upgraded for a better prediction on the basis of the characterising parameters obtained by stereological analysis and by mathematical morphology measurements in the previous chapters. Section 7.1 deals with various models for estimation of concrete strength. However, the mechanical aspect of concrete will not be elaborated in this study. More relevant to the durability aspect of cementitious materials, the existing models for predicting *cement permeability* will be discussed and refined on the basis of pore system characteristics derived for model cements (see Chapter 2) and for actual cement pastes (see Chapter 3) in sections 7.4 and 7.5.

7.1 Concrete strength

The w/c ratio is a technical parameter of paramount importance in cementitious materials. Some well-established quantitative relationships between strength and w/c ratio can be referred to the literature [Soroka, 1979; Popovics, 1981], which indirectly relate the strength of concrete with its pore system characteristics. However, a direct relationship is pursued to facilitate estimation of strength of in situ concrete from the knowledge of its pore system. Exploration in this field leads to prediction models of significantly different forms. The earlier linear relationship of the form $\sigma = \sigma_0 - Kp$ [Hasselman, 1963], the power exponent one of the form $\sigma = \sigma_0 (1-p)^K$ and the exponential equation expressed by $\sigma = \sigma_0 e^{-Kp}$ are demonstrated to be oversimplified in an extensive experimental program conducted by Kumar and Bhattacharjee [2003], revealing a coefficient of correlation around 0.5 between the prediction and experimental results. Older and Rößler [1985] assigned different coefficients to pores within different size ranges, but this type of model is proved to be unsuitable for correlating the in situ strength of concrete with the size distribution of the pore structure.

The proposal by Atzeni *et al*. [1987] related strength of cement paste to the porosity, strength at zero porosity σ_0 by a relatively practical relationship

$$\sigma = K\sigma_0 (1-p)/\sqrt{r_m} \tag{7.1}$$

where K is an empirical constant, r_m is the so-called mean pore radius, defined as

$$\ln r_m = \frac{\sum_{i=1}^{n} V_i \ln r_i}{\sum_{i=1}^{n} V_i} \tag{7.2}$$

where, for the continuous distribution curve divided into n discrete radii ranges, V_i is the increment of porosity corresponding to the i^{th} radius range represented by the mean radius r_i. The value of r_m can be easily calculated from the cumulative pore size distribution (opening distribution curve, see Chapter 3).

Kumar and Bhattacharjee [2003] extensively study the in situ strength of concretes designed to exhibit a wide variation in strengths. In addition to the w/c ratio and extent of maturity, different fineness levels of aggregate grains, different modes of compaction, curing periods as well as exposure conditions were involved to produce wide variations in pore structure (including apparent porosity and pore size distributions). They predicted the concrete strength under various technical conditions according to Eq. (7.1) and compared it with experimental data. Based on their research outcomes, they modified the basic model proposed by Atzeni *et al*. into a more comprehensive one for compressive strength,

$$\sigma = K f_a F \frac{1-p}{\sqrt{r_m}} \tag{7.3}$$

where F is the cement content of mix (related to the w/c ratio), expressed in fraction, K is a new empirical constant, f_a is a factor taking into consideration the aging effect. Other multiplying factors, reflecting various production conditions such as effects of temperature (f_T) and of exposure to acid environments (f_e), can be introduced and incorporated into Eq. (7.3). The value of f_a is unity for moist-cured 28-day-old concrete exposed to 26°C temperature. The ageing factor for 3-month-old concrete, *i.e.* 1.1, is determined by experimental observations. Different values of f_a can be associated with specific hydration stages. The coefficient of correlation of fitting to the experimental data by Eq. (7.3) is estimated to be 0.9, which shows a considerable improvement in the quality of prediction.

The tensile strength σ_t of concrete is dependent on the uni-axial compressive strength of the material; therefore, the same format can be written according to the Griffith's theory as in Eq. (7.4), relating σ_t to porosity p and mean pore size r_m,

$$\sigma_t = \sqrt{\frac{2E_0T_0}{\pi}} \frac{(1-p)}{\sqrt{r_m}} \tag{7.4}$$

where E_0 and T_0 represent the modulus of elasticity and specific surface energy of pore free solid, respectively. The effective modulus of elasticity and the effective specific surface energy will be lowered with the increase in porosity and therefore are taken as a linear relationship to E_0 and T_0: $E = E_0(1\text{-}p)$, $T = T_0(1\text{-}p)$. This allows predicting mechanical properties of cement and concrete.

Prediction of mechanical properties will not be elaborated here; the models and equation are presented just to indicate the quantitative relationship between concrete strength and pore structure characteristics.

7.2 Curability

Cement fineness has a significant influence on the depercolation threshold of the capillary porosity in cement paste (see Chapter 5). The pore structure in relatively fine cement depercolates at an earlier hydration stage, corresponding to a higher depercolation threshold of porosity. Bentz and Haecker [1999] discussed depercolation of porosity in terms of the 'curability' of concrete. Once the capillary porosity depercolates in a cement paste, the imbibitions of water to replace that lost due to chemical shrinkage during hydration slows down significantly, as the transport controlling mechanism shifts from the capillary pores to the much smaller gel pores. Thus, the longer it takes for the capillary porosity to disconnect, the longer one has to continue to add water to the interior of the concrete. This implies an increased 'curability' for the coarser cement systems. When the cement fineness level and details of PSD are known, the depercolation threshold of porosity can be estimated by computer simulation according to the approach proposed in Chapter 5. This is expected to offer some insight into concrete curability in the practice of concrete technology.

7.3 Diffusivity

Although diffusivity is not directly dependent on pore size, it is directly proportional to pore connectivity, which is higher in a paste with larger pores, such as the coarse cement C167. On the other hand, diffusivity is inversely proportional to pore tortuosity, which will decrease in systems with larger pores. For coarser cement, the pore size (represented by mean free spacing λ in Fig. 5.4) is larger than for finer cements at equivalent hydration time. As a result of higher pore connectivity and lower pore tortuosity in the coarser cement, its diffusivity is expected to be higher than in the case of finer cement.

For capillary porosities above the depercolation threshold, the relative diffusivities of the coarser cement C167 (the diffusion coefficient of an ion in the concrete relative to its value in free water) are about twice those of finer cement C342 with the same porosity. After the capillary porosity depercolates, the relative diffusivities of the two different systems are much more similar. On the basis of the estimation of depercolation threshold, the implications of pore structure characteristics can help to get a general idea about the differences in diffusivity between cement pastes on various cement fineness levels. However, the focus of this study is to predict water permeability of cement pastes on the basis of the structural information derived in the previous chapters.

7.4 Permeability of cement paste

The durability of cementitious material largely depends on the possibilities of penetration of hazardous ions into the porous material with water as a medium. Hence, the water permeability of the cementitious material is very crucial to its durability. The permeability of cement-based materials can be experimentally measured, but the accuracy of the results of these time-consuming experiments relies on the care bestowed on sample preparation and on the experimental conditions. Another deficiency of experimentally measuring permeability is that it is a time-consuming operation, especially for mature pastes and concretes. As an alternative, some models (see review in section 1.4) have been developed to relate water permeability to parameters characterising pore structure of cementitious materials. In this section, the permeability evolution of *model cement paste* will be discussed according to the Carman-Kozeny model. And for *actual cement paste*, permeability can be predicted on the basis of structural information derived from section image analysis of paste specimens (see Chapter 3).

7.4.1 Prediction for model cements with Carman-Kozeny model

The permeability of cement paste is closely correlated to pore size and pore connectivity. According to the Carman-Kozeny model, the water permeability k of cement paste can be predicted on the basis of the geometrical properties (porosity p and mean free spacing λ) of the pore space by Eqs. (6.1) and (6.2), *i.e.*, $k = \frac{(1 - V_V)\lambda^2}{32 + 16V_V}$ (see section 6.4). It is not difficult to depict the *gradual decline of permeability* for model cement pastes during the hydration process because the geometrical parameters involved in Eq. (6.2) can be continuously measured in the simulation system.

The estimated permeability for cement C342 with various w/c ratios is shown in Fig. 7.1 and the results for model cements with different finenesses are plotted in Fig. 7.2. The discrete points are experimental permeability results taken from the literature [Banthia and Mindess, 1989] for actual cements with moderate fineness. The mean free spacing (representing average pore size) has a pronounced influence on the transport properties of cement paste, as illustrated in Fig. 7.2. In contrast, for a given model cement (at specific fineness level), the differences in permeability between cement pastes of various w/c ratios are minor, as revealed in Fig. 7.1. The significant influence of mean free spacing (compared to that of w/c ratio) is a reflection of Eq. (6.2), where k is proportional to the second power of λ. It is clear that the permeability of C605 is much lower than that of C167 at the early hydration stages, and eventually reaches similar values of about 1×10^{-17} m^2 at low porosity. This is in agreement with the findings of Bentz *et al*. [1999].

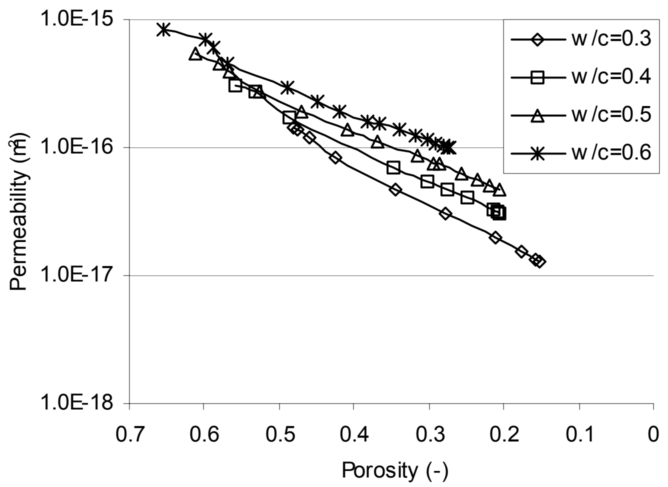

Figure 7.1 Predicted permeability of cement paste C342 with various w/c ratios.

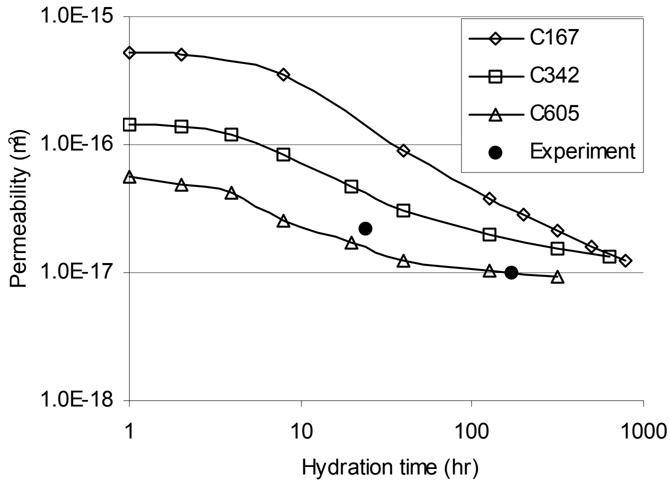

Figure 7.2 Influence of cement fineness on the permeability of cement paste.

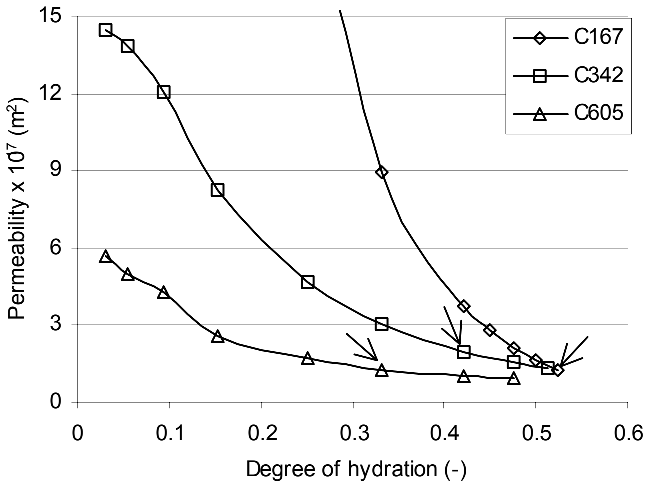

Figure 7.3 Predicted permeability of cement paste of different fineness levels, plotted versus degree of hydration.

The predicted permeability is plotted versus the degree of hydration of the model cements in Fig. 7.3 for comparison purposes. The permeability of cement C167 is so high that only a part of the curve relevant to depercolation threshold is visible. Powers *et al*. [1959] defined capillary pore discontinuity as the point at which the measured fluid permeability, as a function of the hydration degree α, showed a marked change in slope. The arrows in Fig. 7.3 indicate the depercolation threshold of porosity estimated in the morphological approach (see Chapter 5) for the respective model cements. It is clear that the depercolation threshold of porosity is indeed associated with an obvious change in slope of the permeability curve.

7.4.2 Prediction for actual cement pastes by General Effective Media theory

For *actual cement paste*, total porosity and critical pore size can be obtained by means of opening distribution measurement combined with section image analysis of cement paste specimens. Cement pastes at a specific hydration stage (stipulated in experimental standards, normally 3, 7, 14 and 28 days) can be subjected to the afore-mentioned mathematical morphology technique to derive the necessary structural information for the prediction of permeability (see Chapter 3).

One commonly accepted approach to permeability estimation is by application of the Katz-Thompson equation. However, it is found that the application of this model is far more difficult for cement pastes than for sandstones (see section 1.4). This is due to the extremely complex nature of pore structures in the cement paste, as can be convincingly demonstrated by visual means.

The difference in pore structure between stone and cement is the existence of gel pores. Powers *et al.* observed that the permeability of cement paste drops sharply when the capillary porosity of the sample is smaller than a critical value. This is due to the discontinuity of capillary pores by the hydration product when its capillary porosity is smaller than a critical value. In this situation, water has to pass through the gel pores whose size is more than one order smaller than the capillary pores size. Therefore, gel pores control the water permeability. It results in a much lower value. The gel pores do not exist in stone or rock.

Thus, the Katz-Thompson equation, which is successfully applied to stone and rock, is not appropriate to bi-pore structure (capillary pores and gel pores) cementitious materials with low permeability. When cement paste is very porous, capillary pores control the water permeability. However for low porosities, the model should consider the roles of both capillary pores and gel pores. In the present study, the General Effective Media (GEM) theory is used to predict the permeability of cement pastes.

General Effective Media theory

The GEM theory considers cement paste as a two-phase composite material consisting of high-permeability capillary pores and a low-permeability phase including C-S-H gel, CH, and unhydrated cement. Analogue to the overall conductivity of such a model material, the permeability will be governed by the volume fraction and the permeability of each phase. The detailed description of this theory can be found in McLachlan *et al.* [1990].

The GEM theory is a useful tool in predicting the permeability of cementitious materials. At a given w/c ratio and at a certain hydration stage, the overall permeability of cement paste can be estimated from data on porosity and critical pore size. The permeability of cement paste can be derived from the following equations:

$$\frac{(1-p)(k_l^{1/2}-k^{1/2})}{k_l^{1/2}+Ek^{1/2}}+\frac{p(k_h^{1/2}-k^{1/2})}{k_h^{1/2}+Ek^{1/2}}=0 \tag{7.5}$$

$$k_h=\frac{1}{226}l_c^{\,2}(1.8)(1-p_c)^2 \tag{7.6}$$

$$k_l=k_{C-S-H}(1-\frac{1-\phi_{C-S-H}}{1-\phi_c'})^2 \tag{7.7}$$

where k is the overall permeability of the cement paste, k_l is the permeability of the low-permeability phase, k_h the permeability of the high-permeability phase (namely, capillary pores), p is the total porosity of the cement paste, p_c = 0.18 is the critical value of capillary porosity for percolation, l_c is the critical pore size of the cement paste, E = (1- p_c)/ p_c is a constant, $k_{C\text{-}S\text{-}H} = 7 \times 10^{-23}$ m^2 is the permeability of the C-S-H gel [Powers, 1958], $\phi_{C\text{-}S\text{-}H}$ is the volume fraction of the C-S-H gel in the solid phase of the cement paste, which can be calculated from w/c ratio and porosity with the Powers' model, and ϕ_c' is the critical volume fraction of the C-S-H, taken as 0.17.

The calculated k (in m^2) is the intrinsic permeability of the cement paste. This material property is independent of the fluid used to measure it. Contrary, the permeability of the material is conventionally expressed in m/s in experiments, so it depends both on the material properties and on the fluid characteristics. To compare the predicted permeability with the experimental results, the intrinsic permeability (k in m^2) can be converted into the conventional permeability (k' in m/s) by the equation [Christensen *et al.*, 1996]: $k' = k\rho g/\eta$, where ρ (in g/cm^3) and η (in P) are the density and viscosity of the fluid, respectively, and g (in m/s^2) is the acceleration of gravity. This equation can be specified by $k' = 9.79 \times 10^6 k$ for water of 20°C.

Results and discussion

The values of porosity p and critical pore size l_c are determined by the stereological theory (area fraction of porosity) and mathematical morphology method (opening distribution), respectively (see Chapter 3). The cumulative pore size distribution is obtained by a series of opening operations; the critical pore size l_c is determined from the derivative of the pore size distribution curve. Based on these experimental data, the permeability of cement pastes is calculated according to Eqs. (7.5~7.7). The results are given in Table 7.1 for pastes of various w/c ratios at different hydration stages.

Table 7.1 Permeability of paste

w/c	Age (days)	Porosity p (%)	Critical size l_c (μm)	Permeability in (m^2)	Permeability in (m/s) *
0.4	3	34.50	1.847	7.40×10^{-16}	7.24×10^{-9}
	7	24.85	1.293	6.27×10^{-17}	6.14×10^{-10}
	14	15.53	1.108	1.20×10^{-21}	1.18×10^{-14}
0.5	3	33.18	2.586	1.23×10^{-15}	1.20×10^{-8}
	7	25.41	1.847	1.49×10^{-16}	1.46×10^{-9}
	14	18.46	1.478	6.12×10^{-19}	6.00×10^{-12}
0.6	3	41.40	3.694	5.95×10^{-15}	5.83×10^{-8}
	7	33.46	2.401	1.10×10^{-15}	1.08×10^{-8}
	14	23.68	2.032	1.07×10^{-16}	1.04×10^{-9}

* The intrinsic permeability (in m^2) is also converted into m/s for convenience in comparison with experimental data.

A study of Banthia and Mindess [1989] reveals that the water permeability of cement pastes with a w/c ratio of 0.35 was about 1×10^{-10} and 8×10^{-13} m/s, after 7 and 28 days of hydration, respectively. Halamickova *et al.* [1995] reported the permeability of cement pastes with a w/c ratio of 0.4 to be around 3.47×10^{-22} m^2 at 28 days. In the case of a w/c ratio of 0.5, Bier *et al.*

[1989] found the water permeability to be $2x10^{-10}$, $1x10^{-10}$ and $3x10^{-12}$ m/s, respectively, at 3, 7 and 14 days hydration. Ye [2003] presented a permeability of $3.28x10^{-8}$ m/s for a paste with a w/c of 0.6 at 3 days of hydration. The results of permeability experiments depend to some extent on the testing conditions, so an excellent agreement between the prediction and the experiment is not possible. However, a *relatively good consistency* is found between permeability estimated by the GEM theory and the experimental results.

It is interesting to compare the permeability estimation of GEM with that of the Katz-Thompson equation. Christensen *et al*. [1996] calculated the permeability of cement pastes (w/c=0.4) by the Katz-Thompson equation, yielding approximately $5x10^{-10}$, $2x10^{-11}$, and $1x10^{-11}$ m/s, at 3, 7 and 14 days, respectively. It is noteworthy that at 14 days hydration, the GEM theory gives a more reasonable estimation of $1.18x10^{-14}$ m/s (Table 7.1). This confirms that the GEM theory is more suitable for application to low-permeability materials like cement pastes at late stages of hydration.

7.5 Analysis of correlation between characterising-parameters and *k*

Conventional parameters for characterising pore structure in cement paste are porosity, critical pore size, pore size distribution. Another structural parameter, pore distribution density, is proposed in this study (see Chapter 3). These characterising parameters are related to the permeability of cement pastes. Total porosity and critical pore size are usually employed for the permeability prediction because they can be determined in experimental approaches or by image analysis, as in the Katz-Thompson equation. In this section, the degree of correlation between these characterising parameters and the cement paste permeability will be quantified on the basis of the so-called Grey System theory.

7.5.1 Analysis of correlation

The permeability data of cement paste obtained by experiments at different hydration ages are considered as the parent queue. The data of the pore distribution density, porosity and critical pore size at the corresponding hydration ages are considered as the individual child queues. The mean skeleton length $\bar{l} = (\sum_{i=1}^{N} l_i)/N$ and the sum of skeleton lengths $L_t = \sum_{i=1}^{N} l_i$ are also taken as child queues for comparison reasons. All data are normalised by the respective initial value (at 3 days hydration) of each queue to minimize data deformation. The degree of influence or contribution of these child queues for cement pastes with various w/c ratios is studied. The correlation degree represents the geometrical similarity between each child queue and parent queue. The child queue that is most similar in shape to the cement permeability curve has the highest correlation degree. The details of the correlation analysis by the Grey System theory can be found in [Deng, 1982].

7.5.2 Degree of correlation

Experimental data of permeability *k* are selected from literature [Bier *et al*., 1989]. The data of critical pore size, porosity and pore distribution density Γ_{3D} for cement pastes of various w/c ratios at different hydration times are taken from Chapter 3. The original data for analysis of correlation (parent queue and child queues) are listed in Table 7.2. The degrees of correlation of the various parameters versus permeability are given in Table 7.3. L_t and p reveal quite similar degrees of correlation since they are both largely dependent on the total amount of pores. It should be noted that Γ_{3D} has the highest degree of correlation with cement permeability in all cases.

Table 7.2 Parent queue and child queues in analysis of correlation for cement pastes with various w/c ratios

w/c ratio	Age (days)	Parent queue	Child queues				
		k (m/s)	$\bar{l}$ (μm)	L_t (μm)	Γ_{3D}	p (%)	l_c (μm)
0.5	3	2.0×10^{-10}	3.98	8777	1.80	33.19	2.59
	7	1.0×10^{-10}	3.85	6888	1.26	25.41	1.85
	14	3.0×10^{-12}	3.48	5459	0.93	18.46	1.48
0.6	3	3.3×10^{-8}	4.61	11627	2.68	41.40	3.69
	7	4.6×10^{-11}	3.69	8514	1.49	33.47	2.40
	14	1.2×10^{-11}	3.74	7283	1.26	23.68	2.03

Table 7.3 Degrees of correlation of different pore-characterising parameters

w/c ratio	Degree of correlation to paste permeability k				
	$\bar{l}$	L_t	Γ_{3D}	p	l_c
0.5	0.60	0.67	0.71	0.69	0.70
0.6	0.56	0.58	0.63	0.58	0.60

Table 7.3 shows that Γ_{3D} is the key factor with the strongest influence on the cement paste permeability. This is due to the fact that Γ_{3D} contains information on pore size as well as connectivity. A degree of correlation of porosity p lower than those of Γ_{3D} and l_c supports the statement that the pore structure has a pronounced influence on transport properties of cement pastes when the total porosity is constant. Supporting experimental evidences can be referred to Lange *et al.* [1989]. Therefore, Γ_{3D} is also an important factor for characterising pore structure and should be taken into account when predicting the permeability of cement pastes. The purpose of this analysis of correlation is to refine the empirical relationship between the pore structure and permeability of cement pastes. This may be realised by the integration of Γ_{3D} in the Katz-Thompson equation.

7.5.3 Refinement of Katz-Thompson equation

The Katz-Thompson equation is generally used to predict the permeability of porous materials. Christensen *et al.* [1996] directly applied the Katz-Thompson permeability theory [1986] to predict the water permeability (k) of ordinary Portland cement (OPC) paste by

$$k = \frac{1}{226} l_c^2 \frac{\vartheta}{\vartheta_0} \tag{7.8}$$

where l_c is the critical pore diameter. ϑ is the electrical conductivity of the sample, and ϑ_0 is the electrical conductivity of pore solution in the sample. Therefore, ϑ / ϑ_0 is the relative conductivity of the sample, which includes information of the connectivity of pore network. For ordinary Portland cement paste, this value can be calculated by Eq. (7.9), which was proposed by Bentz and Garboczi [1991]

$$\vartheta / \vartheta_0 = 1.8(p - p_c)^2 \tag{7.9}$$

Here p_c is the critical value of capillary porosity for percolation. Substituting Eq. (7.9) into Eq. (7.8), the Katz-Thompson equation for OPC paste can be obtained as follows

$$k = \frac{1}{226} l_c^{\,2} 1.8(p - p_c)^2 \tag{7.10}$$

Garboczi and Bentz [1996] modified the Katz-Thompson equation into

$$k = \frac{l_c^{\,2}}{226}[0.001 + 0.07p^2 + H(p - p_c) \cdot 1.8(p - p_c)^2]$$

$$\text{With } H(p - p_c) = \begin{Bmatrix} 1 & if \quad p > p_c \\ 0 & otherwise \end{Bmatrix} \tag{7.11}$$

Integration of $\Gamma_{3\mathrm{D}}$ into the Katz-Thompson equation leads to a refined quantitative relationship.

The refined equation is

$$k = \frac{l_c^{\,2.1}}{27800} \exp(1.7\Gamma_{3D})[0.001 + 0.07p^2 + H(p - p_c) \cdot (p - p_c)^{1.5}] \tag{7.12}$$

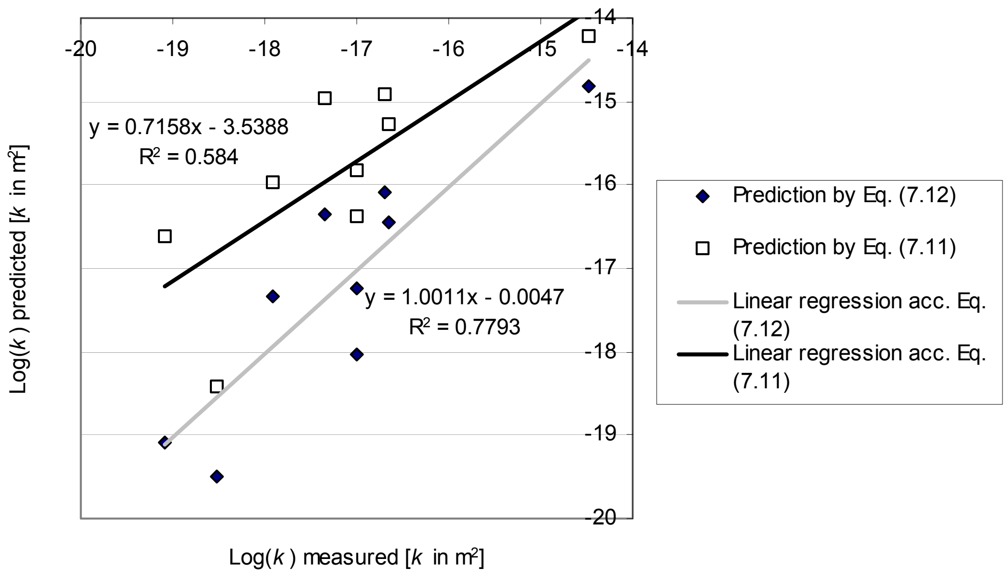

Figure 7.4 Comparison between refined equation and Katz-Thompson one for predicting permeability of cement paste (w/c=0.35, 0.5, 0.6, respectively).

The permeability of cement paste decreases very rapidly in the early period of hydration, covering a range of three orders of magnitude within 14 days. The Katz-Thompson equation cannot differentiate the permeability of cement paste at various hydration ages to a sufficient degree, as illustrated in Fig. 7.4. The factor $\exp(1.7\Gamma_{3D})$ proposed in the refined equation reinforces the differentiation capabilities. For instance, the value of this factor for cement paste with a w/c ratio of 0.6 are 95.5, 12.6 and 8.53, respectively, at 3, 7, 14 days of hydration. Hence, the prediction reveals to be in better agreement with experimental data, as was demonstrated by the coefficient of correlation R for the linear regression between prediction and experimental values in Fig. 7.4.

7.6 Summary

The Carman-Kozeny equation has been used to depict the continuous change of cement paste permeability for model cements of different w/c ratios and fineness levels. The involved structural information, *i.e.*, mean free spacing, can be measured for model cements throughout the hydration process. The estimation by the Carman-Kozeny equation is in good agreement with experimental measurements.

For actual cement paste specimens, the pore size distribution and the critical pore size can be characterised by means of the opening distribution technique as shown in Chapter 3. The water permeability of cement pastes can be estimated on the basis of porosity and critical pore size according to the GEM theory. Comparison with experimental data reveals that the GEM theory is especially useful for low-permeability materials like matured cement pastes. This is due to the modelling concept that takes the roles of both capillary pores and gel pores into consideration. This is of particular relevance to low-porosity and low-permeability materials such as cement pastes in late hydration stages.

A concept of 3D pore distribution density Γ_{3D} is proposed in this study; it is based on the stereological interpretation of quantitative image analysis data derived from 2D sections of cement specimens (see Chapter 3). In this chapter, the Grey System theory is used to analyse the degrees of correlation of various characterising parameters (including porosity, critical pore size, and pore distribution density) with cement paste permeability. The results of this analysis reveal Γ_{3D} to have the highest degree of correlation with cement permeability among the pore-characterising parameters. This can be attributed to the fact that Γ_{3D} contains information about pore size as well as pore connectivity.

The findings of this study support the Katz-Thompson equation for predicting cement permeability. The pore distribution density is integrated into the Katz-Thompson equation and a refined version of the Katz-Thompson equation is proposed for the purpose of improving the quantitative relationship between cement permeability and pore-characterising parameters. The prediction of cement paste permeability by the refined equation is in good agreement with the experimental results.

Overall Evaluation and Future Research

Quantitative characterisation of pore structure in cementitious materials has been and remains a focus of interest to researchers in the field of concrete technology. The interest arises from the high relevance of pore structure to a number of engineering properties of cementitious materials. This problem has been approached extensively by experimental techniques and by computer simulations. The subject of this study, *i.e.*, pore structure in cement and concrete, is nothing new; however, the highlight of this study is the application of stereological and mathematical morphological methods to model cements and to actual cement pastes which dramatically reduces the labour intensity of serial sectioning. This study developed a comprehensive methodological framework for characterising geometrical and morphological aspects of pore space in cementitious materials. The combination of image analysis and these quantification methods allows for the characterisation of the continuous morphological evolution of solid phase and pore space during the hydration process (Chapters 2, 3 and 6). On the basis of the derived structural information, a part of the mechanical and transport properties can be estimated for cement pastes and concretes (Chapter 7). In addition, the statistical concept of heterogeneity in concrete technology (Chapter 4) and depercolation threshold of porosity (Chapter 5) are explored in this study. The relevant research findings and conclusions are presented in the individual chapters. The last chapter provides a brief overall evaluation and suggestions for future research.

8.1 Overall evaluation

The morphological changes during hydration of the pore structure are assessed in this study by the developed methodological framework encompassing quantitative image analysis techniques, stereological estimation, and mathematical morphology methods. The research outcomes reveal that special attention should be directed to the following points.

8.1.1 Proper starting point for modelling

Numerical modelling of the micro-structural development of cementitious materials has experienced rapid improvement in the past decade. In addition to the SPACE system used in this study, representative models are HYMOSTRUC, the continuum-based model of Navi and Pignat and the digital-image-based model developed by Bentz *et al*. (see Chapter 1 for an overview). Most models put much emphasis on the simulation of cement hydration without serious considerations on the fresh state of particle packing, *i.e.*, just starting from a random-generator (RG) based packing structure. However, the application of HPC has confirmed details of particle packing to be of utmost importance. The influences of technical parameters (such as cement particle size distribution and w/c ratio) and dosage of superplasticizer are directly incorporated in the packing structure. The intrinsic phenomenon of particle clustering (flocculation) also deserves particular attention in the computer modelling of cement particle packing. Hence, a realistic simulation of the fresh state of packing is a proper starting point for structural modelling of cementitious materials. The SPACE system, based on a so-called dynamic mixing procedure, offers relatively realistic simulations of particle packing for the fresh state of cement and concrete, including the clustering phenomenon (see Chapter 2). The structural comparison between hardened cement pastes generated by SPACE and by the RG-based system confirms the importance of a good starting point in the modelling approach.

8.1.2 Application of stereological theory

The desire to understand the 3D microstructure of materials has led many scientists to use exhaustive serial sectioning. This is a classic technique dating back at least to the 19th century. Although recent development of computerized serial reconstruction allows different forms of surface and volume rendering, it doesn't avoid the major experimental problems associated with serial sectioning. The conventional approach, relevant to the study of pore structure in cement paste, is to derive information of individual pore features observed on each section and register the data into the computer, whereupon powerful algorithms are required to derive 3D structural information, such as total volume, surface area of pore space, as well as porosity connectivity. Avoiding this straightforward but laborious and time-consuming technique, the stereological theory is applied to cement pastes and model concretes for the characterisation of pore structure.

It is not only unsolved difficulties of a physico-chemical nature that pursues research towards a more stereological-oriented approach. The evident effect of the particles size distribution of the cement on structure formation (*i.e.*, the spatial position of hydrating particles and hydration products relevant to each other) also calls for increased attention to stereological considerations. Henk even explicitly states that the development of microstructure and strength is, in essence, a geometrical problem [van Breugel, 1991]. Stereology is a geometrical statistical tool for an objective quantitative analysis that enables an unbiased estimation of the 3D structural parameters, such as volume and specific surface area, from observations of lower dimensions. So much 3D information is readily available in single sections of representative size and can be assessed by stereological and mathematic morphological methods, that serial sectioning should be considered a method of last resort. Further, stereology is also at the basis of the proper design of experiments because this also relies on the geometrical statistical (*i.e.* sampling) strategy.

The emphasis on the stereological aspect does not suggest that physico-chemical aspects are of minor importance. The stereological-oriented approach allows the explanation of the effect exerted by particle size distribution and by w/c ratio on the structure formation and strength development that cannot be explained merely from physico-chemical considerations [van Breugel, 1991]. This conjecture is clearly demonstrated by the research outcomes in this study (see Chapters 2, 3 and 5). For example, w/c ratio is observed to exert minor impact on the depercolation threshold of capillary porosity whereas cement PSD has significant influences on the threshold value. The stereological approach (based on the evolution of mean free spacing during hydration process) employed in Chapter 5 reveals clearly that the depercolation threshold is structure-sensitive and is mainly governed by size and distribution of cement particles in the fresh state of packing structure. The w/c ratio is a composition parameter merely associated with the volume fraction of cement particles, so that cement pastes of various w/c ratios present similarity in the hydration process, revealing similar value of depercolation threshold although cement with higher w/c ratio needs more time to reach the depercolation threshold (see Figs. 5.2 and 5.3). In contrast, cement PSD is involved in configuration aspect of the material, its influence on the threshold value is much more pronounced (see Fig. 5.4). The stereological approach also allows for an analytical explanation of this interesting phenomenon, as demonstrated in Eq. (5.1).

8.1.3 Application of mathematical morphology

For actual cement pastes, only 2D sections are available for microscopic observation and for direct structural analysis. The pore features observed on section images are considered as individual objects in conventional methods (*i.e.*, so-called individual granulometric analysis) and the area histogram of these pore features are used directly as representations of pore size distribution. This is expected to be inappropriate in view of the complex and interconnected nature of pore structure. This study employs a mathematical morphology technique (*i.e.*, granulometric opening distribution) for the characterisation of pore size. Comparison of the opening distribution data with literature reveals satisfactory approximations to proper experimental findings by Wood's metal intrusion porosimetry (WMIP).

8.1.4 Implications for material property

In this study, the depercolation threshold of capillary porosity is determined in view of the morphological changes of pore space, instead of the conventional concept of connected porosity (Chapter 5). The results with respect to this threshold value and the influences of technical parameters (PSD and w/c ratio) on this value are found to be consistent with experimental findings and proper simulation researches available in the literature.

Furthermore, the opening distribution curves allow the derivation of quantitative information on porosity and critical pore size, which can be used for a relatively accurate and convenient prediction of the cement paste permeability by the general effective media (GEM) theory, especially for matured pastes. On the other hand, the 3D structural parameter derived in this study, *i.e.*, pore distribution density, allows for refining the empirical relationships for the permeability estimation. The accuracy of the prediction is obviously improved by incorporating the pore distribution density into the Katz-Thompson equation.

8.2 Future research

In this study, the relationship between cement paste permeability and pore structure is reviewed. In particular, the applicability of two physical models frequently used for estimating permeability of cement paste was discussed in Chapter 7, *i.e.*, the Carman-Kozeny equation and the Katz-Thompson equation. The former model provides a quantitative relationship between permeability and porosity, hydraulic radius and tortuosity of the transport path in cement paste. In the latter model, permeability is associated with critical pore size and porosity. Both equations have been proved to offer satisfactory estimations of permeability for sandstones and soils [Lebron *et al*., 1999]. However, the applicability cannot be extended to cement paste without significant modifications.

Christensen *et al*. [1996] employed the Katz-Thompson equation to predict the water permeability of cement pastes in high w/c ranges (above 0.47) and argued that the Katz-Thompson model provided a reliable estimation. However, the error of prediction increases dramatically in the case of a lower w/c range, especially for more mature conditions. A better approach in this case is the so-called General Effective Media theory, see Chapter 7. The overestimation by the Katz-Thompson equation is striking, usually of more than two orders of magnitude. In this study, a proposal is formulated for upgrading this relationship on the basis of the effective characterisation of pore morphology by means of the developed methodology. Deficiency of the Katz-Thompson equation can be compensated by incorporation of a stereological parameter derived from section image analysis, the so-called pore distribution density that contains information on pore size and pore connectivity (see Chapter 7).

Hence, it is not sufficient to encompass only pore size and porosity for an accurate prediction of cement paste permeability, particularly for matured pastes. An accurate estimation requires incorporating information on how the pores are interconnected, *i.e.*, topology characteristics of the pore structure. This requirement can be fulfilled by pore network modelling, which is constructed on the basis of pore size distribution and pore topology characteristics. As a morphological representation of the pore structure, this method has been used in soil technology [Vogel and Roth, 2001] and petroleum engineering for estimating hydraulic properties of porous media. Relevant to concrete technology, a similar modelling approach has been applied to *model cement paste* based on the serial sectioning technique [Ye, 2003]. This is not applicable to actual cement paste due to the extreme labour intensity. Mathematical morphology tools can be used in this case to derive the structural information of pore size distribution and pore topology that is necessary for constructing a pore network model.

The efforts in this study of applying mathematical morphological methods to structural analysis deal only with a small part of the characterisation of pore structure in cementitious materials. The application of mathematical morphology can be extended to more complex morphological aspects of cementitious materials, such as pore topology, pore network modelling and simulation of effective hydraulic properties. For an isotropic structure like ordinary cement paste, one single properly sampled section or a few sections can provide reliable information, provided the sampled size area is representative for the investigated parameter. This prevents appealing to serial sectioning, which requires dramatically high labour investments. On the other hand, the direct applicability to section images of specimens extracts the structural features of actual cement paste, thus being independent of the quality of the computer simulation. The quantitative simulation approach by means of pore network modelling to transport properties of cementitious materials is an interesting and promising tool for future research.

8.2.1 Pore scale topology

Besides porosity and pore distribution, the topology of pore space is a crucial property regarding flow and transport in porous media. The way in which pores are interconnected may be even more important than pore size and connected fraction of porosity. The Euler characteristic combines the basic topological measures (*i.e.*, number of isolated pores, number of redundant connections, number of enclosed cavities) into a measure of connectivity. The Euler characteristic may be deduced from the local geometry of the structure without explicitly counting the basic topological measures [DeHoff, 1987]. This is of practical importance in cement paste technology since a full 3D representation is hard to get.

Another approach towards the quantification of topology in porous media is the measure of percolation probabilities denoting the probability to find a continuous path through a sample of a given size. Percolation probabilities can be evaluated as a function of sample size and porosity. For isotropic structures as sandstone and ordinary cement paste, percolation probabilities provide the topological information required [Hilfer *et al.*, 1997]. This leads to connectivity functions related to the effective properties of cementitious materials.

In the context of mathematical morphology, a connectivity function can be derived from measurements of the Euler characteristic as a function of pore size [Vogel, 1997; 2002]. Starting with the largest pores, which may be isolated and not connected, the smaller pores are successively added which change the topology in a characteristic way, *i.e.*, accompanied by an increase in connectivity. This imaginary process of adding pores successively to the pore network is associated with the definition and determination of critical pore size (see Chapter 3). The connectivity function yields an integral description of the overall topology and should reflect the hydraulic behaviour of cementitious materials because it contains information on how pores of different sizes are interconnected.

8.2.2 Pore network modelling

Network models are idealized representations of the complex pore geometry that may be used to calculate effective hydraulic properties of porous media. This approach was introduced by Fatt [1956] and subsequently developed in different fields of material sciences, *e.g.*, petroleum engineering and soil hydrology. Network modelling has been demonstrated to be an efficient tool to investigate the effect of geometrical aspects on the effective behaviour of porous media [Friedman and Seaton, 1996].

The network model can be generated on the basis of the aforementioned connectivity function and the pore size distribution (obtained by morphological opening, see Chapter 3), which mimics the pore structure in terms of pore size and topology. Vogel and Roth [2001] successfully applied network modelling to clay soil and predicted hydraulic conductivity and the water retention characteristics of the soil. Comparison of the simulation with the experimental results reveals good agreement, indicating the hydraulic properties to be mainly governed by pore size distribution and topology.

This study explores the local percolation probabilities (related to connectivity function) and size distribution of pore structure in cement pastes (see Chapters 3 and 4), but their quantitative correlation to effective hydraulic properties remains to be solved. This requires the application of pore network modelling on the basis of pore size distribution and topology. This quantitative simulation approach to hydraulic properties of cementitious materials is an interesting and promising aspect for future research.

References

Alkemper J, Voorhees PW, 2001. Quantitative serial sectioning analysis. Journal of microscopy 201: 388-394.

Atzeni C, Massidda L, Sanna U, 1987. Effect of pore size distribution on strength of hardened cement pastes. In: Proceedings of 1st International RILEM Congress on Pore Structure and Material Properties, Paris, pp. 195-202.

Bágel L, Živica V, 1997. Relationship between pore structure and permeability of mortars. Cement and Concrete Research 27:1225-1235.

Banthia N, Mindess S, 1989. Permeability measurement on cement paste. In: Roberts LR, Skalny JP (eds.), Proceedings of Material Research Society Symposium 137, Boston, pp. 173-179.

Bear J, Bachmat Y, 1990. Introduction to Modeling of Transport Phenomena in Porous Media. Dordrecht: Kluwer Academic Publishers.

Bentz DP, 1997. Three-dimensional computer simulation of Portland cement hydration and microstructure development. Journal of American Ceramic Society 80 (1): 3-21.

Bentz DP, Garboczi EJ, 1989. A digitised simulation model for microstructural development. In: Mindess S (editor), Advances in Cementitious Materials. Westerville (Ohio): American Ceramic Society, pp. 211-226.

Bentz DP, Garboczi EJ, 1991. Percolation of phases in a three-dimensional cement paste microstructural model. Cement Concrete Research 21: 324-344.

Bentz DP, Garboczi EJ, 1992. Guide to Using HYDRA3D: A Three-dimensional Digital-Image-Based Cement Microstructural Model. NISTIR No. 4746, U.S. Department of Commerce, Washington.

Bentz DP, Garboczi EJ, 1999. Computer modeling of interfacial transition zone: microstructure and properties. In: Alexander MG (editor), Engineering and Transport Zone in Cementitious Composites, RILEM report 20. ENS-Cachan: RILEM Publishing, pp. 349-385.

Bentz DP, Garboczi EJ, Haecker CJ, Jensen OM, 1999. Effects of cement particle size distribution on performance properties of Portland cement-based materials. Cement Concrete Research 29: 1663-1671.

Bentz DP, Haecker CJ, 1999. An argument for using coarse cements in high performance concrete. Cement Concrete Research 29: 615-618.

Bentz DP, Mizzel S, Satterfield S, Davaney J, George W, Ketcham P, Graham J, Porterfield J, Quenard D, Vallee F, Sallee H, Boller E, Baruchel J, 2002. The Visible Cement Data Set. Journal of Research of the National Institute of Standards and Technology 107(2): 137-148.

Berryman JG, Blair SC, 1986. Use of digital image analysis to estimate fluid permeability of porous media: application of two-point correlation functions. Journal of Applied Physics 60: 1930-1938.

Berryman JG, Blair SC, 1987. Kozeny-Carman relations and image processing methods for estimating Darcy's constant. Journal of Applied Physics 62(6): 2221-2228.

Bier TA, Ludirdja D, Young JF, Berger RL, 1989. The effect of pore structure and cracking on the permeability of concrete. In: Roberts LR, Skalny JP (eds.), Proceedings of Materials Research Society Symposium 137, Boston, pp. 235-243.

Biswal B, Manwart C, Hilfer R, 1998. Three-dimensional local porosity analysis of porous media. Physica A 255: 221-241.

Bracewell R, 1999. The impulse symbol. In: The Fourier Transform and Its Applications, Chapter 5, 3rd edition. New York: McGraw-Hill, pp. 69-97.

Brach RM, 1991. Mechanical Impact Dynamics, Rigid Body Collisions. New York: John Wiley & Sons Inc.

Brown CB, 1965. Minimum volumes to ensure homogeneity in certain conglomerates. Journal of Franklin Institute 279: 189-199.

Bui DD, 2001. Rice Husk Ash as a Mineral Admixture for High Performance Concrete, PhD Thesis. Delft: Delft University Press.

Carman PC, 1939. Permeability of saturated soils and clays. Journal of Agriculture Science 29: 262-273.

Carpinteri A, Chiaia B, Invernizzi S, 1999. Three-dimensional fractal analysis of concrete fracture at the meso-level. Theoretical and Applied Fracture Mechanics 31(3): 163-172.

Carpinteri A, Chiaia B, Invernizzi S, 2000. Comments on ‘Direct fractal measurement of fracture surfaces’. International Journal of Solids and Structures 37: 4623-4625.

Chen H, 2002. Computer Simulation by SPACE of the Microstructure of the ITZ between Aggregate and Cement Paste, Report CM 2002-001. Delft: Delft University of Technology.

Cook DJ, 1984. Development of microstructure and other properties in rice husk ash - OPC systems. In: Proceedings the 9th Australasian Conference on the Mechanics of Structures and Materials. Sydney: University of Sydney, pp. 355-360.

Cooke RW, Seddon AE, 1956. The laboratory use of bonded-wire electrical resistance strain gauges on concrete at the Building Research Station. Magazine of Concrete Research 8(22): 31-38.

Christensen BJ, Mason TO, Jennings HM, 1996. Comparison of measured and calculated permeability for cement pastes. Cement Concrete Research 26 (9): 1325-1334.

Cui L, Cahyadi JH, 2001. Permeability and pore structure of OPC paste. Cement Concrete Research 31: 277-282.

De Larrard F, Malier Y, 1992. Engineering properties of very high performance concrete. In: Malier Y (editor), High Performance Concrete, From Materials to Structure. London: E&FN Spon, pp. 85-114.

Delagrave A, Marchand J, Pigeon M, 1998. Influence of the interfacial transition zone on the resistance of mortar to calcium leaching. In: Katz A, Bentur A, Alexander M, Arliguie G (eds.), The Interfacial Transition Zone in Cementitious Composites. London: E & FN Spon, pp.103-113.

Delesse M, 1848. Procédé mécanique pour déterminer la composition des roches. Annual Mines 13: 379-388.

DeHoff RT, 1983. Quantitative serial sectioning analysis: preview. Journal of Microscopy 131: 259-263.

DeHoff RT, 1987. Use of the disector to estimate the Euler characteristics of three dimensional microstructures. Acta Stereologica 6: 133-140.

DeHoff RT, Rhines FN, 1968. Quantitative Microscopy. New York: McGraw-Hill, pp. 442.

Deng J, 1982. Grey System Theory (in Chinese). Wuhan (China): Huazhong University of Science and Technology Press.

Detwiler RJ, Metha PK, 1989. Chemical and physical effects of silica fume on mechanical behaviour of concrete. ACI Material Journal 86: 609-614.

Diamond S, 2000. Mercury porosimetry; an inappropriate method for the measurement of pore size distributions in cement-based materials. Cement Concrete Research 30 (10): 1517-1525.

Diamond S, Huang J, 2001. The ITZ in concrete – a different view based on image analysis and SEM observations. Cement Concrete Research 23: 179-188.

Diamond S, Huang J, 1998. The interfacial transition zone: reality or myth? In: Katz A (editor), The Interfacial Transition Zone in Cementitious Composites. London: E & FN Spon, pp. 3-39.

Diamond S, Leeman ME, 1995. Pore size distributions in hardened cement paste by image analysis. In: Diamond S, Mindess S, Glasser FP, Roberts LW, Skalny JP, Wakeley LD (eds.), Microstructure of Cement Based Systems/Bonding and Interfaces in Cementitious Materials, Proceedings of Material Research Society 370, Pittsburgh, pp. 217-226.

Dullien FAL, 1979. Porous Media. New York: Academic Press.

El-Dieb AS, Hooton RD, 1994. Evaluation of the Katz-Thompson model for estimating the water permeability of cement-based materials from mercury intrusion porosimetry data. Cement Concrete Research 24: 443-455.

Elam WT, Kerstein AR, Rher JJ, 1984. Critical properties of the void percolation problem for spheres. Physical Review Letters 52: 1516-1519.

Fatt I, 1956. The network model of porous media. Petroleum Transport AIME 207: 144-159 (part I); 160-163 (part II); 164-181 (part III).

Fidjestøl P, Frearson J, 1994. High performance concrete using blended and triple blended cements. In: Malhotra VM (editor), High Performance Concrete, Proceedings ACI International Conference Singapore. Detroit: ACI, pp. 135-157.

Freudenthal AM, 1950. The Inelastic Behaviour of Engineering Materials and Structures. New York: Wiley.

Friedman S, Seaton N, 1996. On the transport properties of anisotropic networks of capillaries. Water Resources Research 32: 339-347.

Garboczi EJ, Bentz DP, 1996. Modelling of the microstructure and transport properties of concrete. Construction Building Materials 10: 293-300.

Garboczi EJ, Bentz DP, 1997. Analytical formulas for interfacial transition zone properties. Advanced Cement Based Materials 6: 99-108.

Garboczi EJ, Bentz DP, 2001. The effect of statistical fluctuation, finite size error, and digital resolution on the phase percolation and transport properties of the NIST cement hydration model. Cement Concrete Research 31: 1501-1514.

Garboczi EJ, Bentz DP, Martys NS, 1999. Digital images and computer modelling. In: Wong PZ (editor), Experimental Methods for Porous Media. New York: Academic Press.

Glagolev AA, 1934. Quantitative analysis with the microscope by the point method. Engineering Mining Journal 135: 399-400.

Goldman A, Bentur A, 1993. The influence of micro-fillers on enhancement of concrete strength. Cement Concrete Research 23: 962-972.

Gundersen HJG, 1988. The new stereological tools, Acta Microbiology and Immunology Scand 96: 379-394 and 857-881.

Gundersen HJG, Jensen EB, 1985. Stereological estimation of the volume-weighted mean volume of arbitrary particles observed on random sections. Journal of Microscopy 138: 127-142.

Gundersen HJG, Osterby R, 1981. Optimizing sampling efficiency of stereological studies in biology: or “Do more less well”. Journal of Microscopy 121 (1981) 65-73.

Halamickova P, Detwiler RJ, Bentz DP, Garboczi EJ, 1995. Water permeability and chloride ion diffusion in Portland cement mortars: relationship to sand content and critical pore diameter. Cement Concrete Research 25:790-802.

Hasselman DPH, 1963. Relation between effects of porosity on strength and Young’s modulus of elasticity of polycrystalline materials. Journal of American Ceramic Society 46(11): 564-565.

Hilfer R, 1991. Geometric and dielectric characterisation of porous media. Physics Review B 44: 60-75.

Hilfer R, 1992. Local porosity theory for flow in porous media, Physics Review B 45: 7115-7121.

Hilfer R, 1996. Transport and relaxation phenomena in porous media, Advances in Chemical Physics XCII: 299-424.

Hilfer R, Nøst B, Haslund E, Kautzsch TH, Virgin B, Hansen B, 1994. Local porosity theory for the frequency dependent dielectric function of porous rocks and polymer blends. Physica A 207: 19-27.

Hilfer R, Rage T, Virgin B, 1997. Local percolation probabilities for a natural sandstone. Physica A 241: 105-110.

Hoel PG, 1971. Introduction to Mathematical Statistics, 4th edition. New York: Wiley International Edition.

Holliday L, 1966. Geometric consideration and phase relationships. In: Holliday L (editor), Composite Materials. Amsterdam: Elsevier Publishing, pp. 1-27.

Howard CV, Reed MG, 1998. Unbiased Stereology: Three-Dimensional Measurement in Microscopy. Oxford (UK): BIOS Scientific Publishers.

Hu J, Stroeven P, 2002. Morphological analysis and modelling of cement structure. In: Setzer MJ, Auberg R, Keck HJ (eds.), From Nano-Structure and Pore Solution to Macroscopic Behaviour and Testing, Proceedings of 2nd International Essen Workshop on Frost Resistance of Concrete. Cachan: RILEM Publishing, pp. 29-36.

Hu J, Chen H, Stroeven P, 2003. SPACE simulation of particle flocculation in model cement. In: Yuan Y, Shah SP, Lu H (eds.), Proceedings of International Conference on Advances in Concrete and Structures, Xuzhou, China. RILEM Publications SARL (Pro 32), pp. 196-203.

Hughes DC, 1985. Pore structure and permeability of hardened cement paste. Magazine of Concrete Research 37 (133): 227-233.

Jaiswal SS, Igusa T, Styer T, Karr A, Shah SP, 1997. Influence of microstructure and fracture on the transport properties in cement-based materials. In: Brandt AM, Li VC, Marshall IH (eds.), Proceedings of Brittle Matrix Composites 5, Warsaw. Cambridge: Woodhead Publishing, pp. 199-220.

Jennings HM, Johnson SK, 1986. Simulation of microstructure development during the hydration of a cement compound. Journal of American Ceramic Society 69: 790-795.

Jensen EB, Kiêu K, Gundersen HJG, 1990. Second-order stereology. Acta Stereologica 9: 15-35.

Jeulin D, 2000. Random texture models for material structures. Statistics and Computing 10: 121-132.

Jeulin D, 2001. Models of Random Structure, lecture material for a summer course. Paris: École des Mines de Paris.

Jiang W, Roy DM, 1994. Strengthening mechanisms of high-performance concrete. In: Malhotra VM (editor), High Performance Concrete, Proceedings ACI International Conference Singapore. Detroit: ACI, pp. 753-767.

Johnson V, Anderson PJ, 1991. Particle packing and concrete properties. In: Skalny JP (editor), Materials Sciences of concrete II. Westerville (Ohio): American Ceramic Society, Science of Concrete.

Katz AJ, Thompson AH, 1986. Quantitative prediction of permeability in porous rock. Physics Review B 34 (11): 8179-8181.

Kendall MG, Moran PAP, 1963. Geometrical Probability. London: C. Griffin & Co.

Koenders EAB, 1997. Simulation of Volume Changes in Hardening Cement-based Materials, PhD thesis. Delft: Delft University Press.

Kumar R, Bhattacharjee B, 2003. Porosity, pore size distribution and in situ strength of concrete. Cement Concrete Research 33: 155-164.

Kolher R, 1981. A segmentation system based on thresholding. Computer Graphics and Image Processing 15: 319-338.

Kraiwood K, Chai J, Smith S, Seksun C, 2001. A study of ground coarse fly ashes with different finenesses from various sources as pozzolanic materials. Cement Concrete Composites 23: 335-343.

Lange DA, Jennings HM, Shah SP, 1989. The influence of pore structure on the properties of cement paste: Initial observations about research-in-progress. In: Roberts LR, Skalny JP (eds.), Proceedings of Materials Research Society Symposium 137, Boston, pp. 47-54.

Lange DA, Jennings HM, Shah SP, 1994. Image analysis techniques for characterisation of pore structure of cement-based materials. Cement Concrete Research 24 (5): 841-853.

Lebron I, Schaap MG, Suarez DL, 1999. Saturated hydraulic conductivity prediction from microscopic pore geometry measurements and neutral network analysis. Water Resource Research 35: 3149-3158.

Lu H, 1993. Introduction to Powder Technology (in Chinese). Shanghai (China): TongJi University Press.

Marchand J, Delagrave A, 1999. Influence of ITZ on ionic diffusion and leaching. In: Alexander MG, Arliguie G, Ballivy G, Bentur A, Marchand J (eds.), Engineering and Transport Properties of the Interfacial Transition Zone in Cementitious Composites. ENS-Cachan: RILEM Publishing, pp. 157-172.

McLachlan DS, Blaszkiewicz M, Newnham RE, 1990. Electrical resistance of composites. Journal of American Ceramic Society 73 (8): 2187-203.

Mecke K, Stoyan D, 2002. Morphology of Condensed Matter. Berlin: Springer Publishing.

Mehta PK, 1994. Rice husk ash – a unique supplementary cementing material. In: Malhotra VM (editor), Advances in Concrete Technology. Ottawa: Centre for Mineral and Energy Technology, pp. 419-444.

Myers EJ, 1963. Quantitative metallography of cylinders, cubes, and other polyhedrons. In: Proceedings of 1st International Congress for Stereology, Vienna, paper 15.

Navi P, Pignat C, 1996. Simulation of cement hydration and the connectivity of the capillary pore space. Advanced Cement Based Material 4 (2): 58-67.

Navi P, Pignat C, 1999. Three-dimensional characterisation of the pore structure of a simulated cement paste. Cement Concrete Research 29 (4): 507-514.

Nemati KM, 1994. Generation and Interaction of Compressive Stress-induced Microcracks in concrete, PhD thesis. Berkeley: University of California.

Older I, Rößler M, 1985. Investigations on the relationship between porosity, structure and strength of hydrated Portland cement pastes: ii. Effects of pore structure and degree of hydration. Cement Concrete research 15(4): 401-410.

Ollivier JP, Maso JC, Bourdette B, 1995. Interfacial transition zone in concrete. Advanced Cement Based Materials 2: 30-38.

Olson RA, Neubauer CM, Jennings HM, 1997. Damage to the pore structure of hardened Portland cement paste by mercury intrusion. Journal of American Ceramic Society 80 (9): 2454-2458.

Orange G, Dugat J, Acker P, 2000. New high performance concretes; damage resistance and micromechanical analysis. In: Rossi P, Chanvillard G (eds.), Fibre Reinforced Concretes, Proceedings of BEFIB 2000. Cachan: RILEM Publishing, pp. 781-790.

Parrott LJ, Patel RG, Killoh DC, Jennings HM, 1984. Effect of age on diffusion in hydrated Alite cement. Journal of American Ceramic Society 67: 233-237.

Paya J, Monzo J, Peris-Mora E, Borrachero MV, Tercero R, Pinillos C, 1995. Early-strength development of Portland cement mortars containing air classified fly ashes. Cement Concrete Research 25(2): 449-456.

Popovics S, 1981. New formulas for the prediction of the effects of porosity on concrete strength. ACI Material Journal 78(2): 127-129.

Powers TC, 1958. Structure and physical properties of hardened Portland cement paste. Journal of American Ceramic Society 41: 1-6.

Powers TC, Copeland LE, Mann HM, 1959. Capillary continuity or discontinuity in cement Pastes. PCA Bulletin 110: 3-12.

Rangaraju P, 1999. Mixture Proportioning and Microstructural Aspects of High Performance Concretes, PhD Thesis. West Lafayette: Purdue University Press.

Roelfstra PE, 1989. A Numerical Approach to Investigate the Properties of Numerical Concrete. Lausanne: EPFL-Lausanne.

Rosiwall A, 1898. Über geometrische Gesteinsanalysen. Ein einfacher Weg zur ziffermässigen Feststellung des Quantitätsverhaltnisse der Mineralbestandteile gemengter Gesteine. Verh. K.K. Geologie Reichsanst. 5: 143-175.

Saltikov SA, 1945. Stereometric Metallography. Moscow: Metallurgizdat.

Scheidegger AE, 1974. The Physics of Flow through Porous Media. Toronto: University of Toronto Press.

Scher H, Zallen R, 1970. Critical density in percolation processes, Journal of Chemical Physics 53 (9): 3759-3761.

Scrivener KL, 1989a. The use of backscattered electron microscopy and image analysis to study the porosity of cement paste. In: Roberts LR, Skalny JP (eds.), Proceedings of Material Research Society Symposium 137, Boston, pp. 129-140.

Scrivener KL, 1989b. The microstructure of concrete. In: Skalny JP (editor), Materials Sciences of concrete I. Westerville (Ohio): American Ceramic Society, pp. 127-161.

Scrivener KL, 1999. Characterisation of the ITZ and its quantification by test methods. In: Alexander MG (editor), Engineering and Transport Zone in Cementitious Composites, RILEM report 20. ENS-Cachan: RILEM Publishing, pp. 3-15.

Scrivener KL, Bentur A, Pratt PL, 1988. Quantitative characterisation of the transition zone in high strength concretes. Advances in Cement Research 1: 230-237.

Scrivener KL, Nemati KM, 1995. The percolation of pore space in the cement paste/aggregate interfacial zone of concrete. Cement Concrete Research 26: 35-40.

Scrivener KL, Pratt PL, 1984. Backscattered electron images of polished cement sections in the scanning electron microscope. In: Proceedings of 6th International Conference on Cement Microscopy, Albuquerque, pp. 145-155.

Serra J, 1982. Image Analysis and Mathematical Morphology. London: Academic Press.

Soroka I, 1979. Portland Cement Paste and Concrete. London: Macmillan.

Stauffer D, Aharony A, 1992. Introduction to Percolation Theory. London: Taylor and Francis.

Stoyan D, Kendall WS, Mecke J, 1987. Stochastic Geometry and its Applications. New York: John Wiley & Sons Inc.

Stroeven M, 1999. Discrete Numerical Model for the Structural Assessment of Composite Materials, PhD Thesis. Delft: Delft University Press.

Stroeven M, Askes H, Sluys LJ, 2002. A numerical approach to determine Representative Volumes for granular materials, in: Mang HA, Rammerstorfer FG, Eberhardsteiner J (eds.), Proceedings of 5th World Congress on Computation Mechanics, Vienna, proceedings published on CD.

Stroeven M, Stroeven P, 1996. Computer-simulated internal structure of materials. Acta Stereologica 15 (3): 247-252.

Stroeven P, 1973. Some Aspects of the Micromechanics of Concrete, PhD Thesis. Delft: Delft University Press.

Stroeven P, 1991a. Fractals and fractography in concrete technology. In: Brandt AM, Marshall IH (eds.), Proceedings of Brittle Matrix Composites 3. London: Elsevier Application Sciences, pp. 1-10.

Stroeven P, 1991b. Coastline-of-Britain aspects of damage in concrete-like composites. In: Simeonov Y (editor), Proceedings of 6th National Conference on Mechanics and Technology of Composite materials. Sofia: Bulgarian Academy of Sciences, pp. 259-361.

Stroeven P, 2000a. Analytical and computer-simulation approaches to the extent of the interfacial transition zone in concrete. In: Brandt AM, Li VC, Marshall IH (eds.), Proceedings Brittle Matrix Composites 6, Warsaw. Cambridge: Woodhead Publishing, pp. 465-484.

Stroeven P, 2000b. A stereological approach to roughness of fracture surfaces and tortuosity of transport paths in concrete. Cement Concrete Composites 22: 331-341.

Stroeven P, 2003. Implications of the law of aggregation of matter in concrete technology. In: Brandt AM, Li VC, Marshall IH (eds.), Proceedings Brittle Matrix Composite 7, Warsaw, Poland. Cambridge: Woodhead Publishing, pp. 129-142.

Stroeven P, Stroeven M, 1999. Assessment of packing characteristics by computer simulation. Cement and Concrete Research 29: 1201-1206.

Stroeven P, Stroeven M, 2001. Reconstruction by SPACE of the interfacial transition zone. Cement Concrete Composites 23: 189-200.

Struble LJ, Stutzman PE, 1989. Epoxy impregnation of hardened cement for micro-structural characterisation. Journal of Materials Science Letters 8: 632-634.

Stutzman PE, 1999. The Concrete Microscopy Library, imaging by Stutzman PE at NIST. http://cee.ce.uiuc.edu/lange/micro/.

Synder KA, Bentz DP, Garboczi EJ, Winslow DN, 1992. Interfacial zone percolation in cement-aggregate composites. In: Maso JC (editor), Interfaces in cementitious composites, RILEM Proceedings 18. E and FN Spon, pp. 259-268.

Taylor HFW, 1997. Cement Chemistry, 2nd edition. London: Thomas Telford.

Thomson E, 1930. Quantitative microscopic analysis. Journal of Geology 38: 193-222.

Tumidajski PJ, Lin B, 1998. On the validity of the Katz-Thompson equation for permeability in concrete. Cement Concrete Research 28(5): 643-647.

Underwood EE, 1968. Quantitative Stereology. Reading (MA): Addison-Wesley Publishing Company.

van Breugel K, 1991. Simulation of Hydration and Formation of Structure in Hardening Cement-based Materials, PhD Thesis. Delft: Delft University Press.

Virgin B, Haslund E, Hilfer R, 1996. Rescaling relations between two- and three-dimensional local porosity distributions for natural and artificial porous media. Physica A 232: 1-20.

Vogel HJ, 1997. Morphological determination of pore connectivity as a function of pore size using serial sections. European Journal of Soil Science 48: 365-377.

Vogel HJ, 2002. Topological characterisation of porous media. In: Mecke K, Stoyan D (eds.), Morphology of Condensed Matter. Berlin: Springer-Verlag.

Vogel HJ, Roth K, 2001. Quantitative morphology and network representation of soil pore structure. Advances in Water Resources 24: 233-242.

Wang Y, 1995. Microstructural Study of Hardened Cement Paste by Backscatter Scanning Electron Microscopy and Image Analysis, PhD thesis. West Lafayette: Purdue University.

Wang Y, Diamond S, 1995. An approach to quantitative image analysis for cement pastes. In: Diamond S, Mindess S, Glasser FP, Roberts LW, Skalny JP, Wakeley LD (eds.), Microstructure of Cement Based Systems/Bonding and Interfaces in Cementitious Materials, Proceedings of Material Research Society 370, Pittsburgh, pp. 23-32.

Wittmann FH, Roelfstra PE, Sadouki H, 1984. Simulation and analysis of composite structures. Material Sciences and Engineering 68: 239-248.

Willis KL, Abell AB, Lange DA, 1998. Image-based characterisation of cement pore structure using Wood's metal intrusion. Cement Concrete Research 28 (12): 1695-1705.

Ye G, 2003. Experimental Study & Numerical Simulation of the Development of the Microstructure and Permeability of Cementitious Materials, PhD Thesis. Delft: Delft University Press.

Ye G, Hu J, van Breugel K, Stroeven P, 2002. Characterisation of the development of microstructure and porosity of cement-based materials by numerical simulation and ESEM image analysis. Materials and Structures 35: 603-613.

Ye G, van Breugel K, Fraaij ALA, 2003. Three-dimensional microstructure analysis of numerically simulated cementitious materials. Cement Concrete Research 33: 215-222.

Zimbelmann R, 1985. A contribution to the problem of cement-aggregate bond. Cement and Concrete Research 15: 801-808.

Summary

Porosity and pore structure are of paramount importance with respect to the mechanical and durability properties of cementitious materials. The micro-structural development of cementitious materials and the relationship between structure and material properties have been extensively studied by experimental techniques and in computer modelling approaches. However, accurate quantitative characterisation of pore structure remains to be a challenge due to the complex and interconnected nature of pore network in cement pastes and concretes. The reliabilities of most experimental techniques are limited since the interpretation of experimental data is based on assumptions of pore geometry that are largely deviating from realistic situations. Numerical modelling of cement paste and concrete, when starting from non-realistic simulation of particle packing, cannot yield correct simulation results. This situation is pertinent to all commonly used systems that are making use of random generators. This inevitably leads to dramatic biases in the spatial dispersion of generated particles at densities relevant for cement and concrete. In the present study an appeal is therefore made to the SPACE system for the simulation of particle structures of cement and concrete in the fresh state and of cement hydration.

The morphological changes during hydration of pore structure are emphasized in this study as a function of technological parameters, including cement fineness (particle size distribution), water cement ratio and degree of hydration. These problems are approached by quantitative image analysis techniques, by stereological estimation, and by application of mathematical morphology methods. Stereological theory allows deriving 3D structural information including porosity and specific surface area from specimen sections, thus avoiding the extremely laborious approach by serial sectioning. Spacing parameters in stereological theory can be adopted to represent the spatial dispersion of solid phases, and thereby provide information on average pore size. In parallel, mathematical morphology measurements are performed on model cements and on section images of actual cement pastes for quantitative characterisation of pore size. The research outcomes can be summarized in two aspects, *i.e.*, computer simulation and experimental approach.

In computer simulation approach

Representative cements are selected from the model cements of different w/c ratios and particle size distributions (PSD), generated by Chen [2002] with the SPACE system. Important geometric parameters (average intercept length $\overline{L_3}$, nearest neighbour distance Δ_3, mean free spacing λ between cement particles) are measured by means of stereological algorithms integrated in the system for the fresh state of cement particle packing. The influences of PSD and w/c ratio on flocculation and on microstructure development of model cements are discussed in analytical approach. The morphological evolution during hydration of pore space is analysed on the basis of stereological theory since mean free spacing between solid phases is a direct representation of average pore size. The depercolation threshold of capillary porosity is associated with that value of porosity whereby the mean free spacing arrives at a stable value. The simulation results reveal a depercolation value of 21~23% for cement pastes on ordinary fineness level. Finer cement has a higher value of depercolation

threshold as a result of the higher hydration rate and the smaller inter-particle spacing, which make it easier for finer cement to close off the pore space. It is found that particle size distribution exerts significant influences on depercolation threshold, whereas the effect of w/c ratio is only minor. The results obtained by morphological method in this study are in good agreement with the simulation results of Bentz *et al*. [1999] as well as with the experimental outcomes of Parrott [1984] and Powers *et al*. [1959]. The relevance of studying the depercolation phenomenon is given by the close relationship between this parameter and transport phenomena in cement-based materials.

Porosity in the Interfacial Transition Zone (ITZ) between aggregates and cement paste would be of particular relevance for mechanical property (strength) and durability capability (permeability) of concrete. Morphological and structural evolution of the ITZ in SPACE-generated model concretes are stereologically quantified by means of composition parameters and configuration parameters. The extent of the ITZ depends on technological parameters, but also on type of the parameter characterising aspects of material structure. The ITZ thickness will be considerably smaller when derived from density (composition) gradients than from configuration gradients.

The ITZ is generally assumed to constitute the weakest link in the mechanical system in view of the higher porosity than bulk resulted from the 'wall effect' in cement particle packing. Experiments studies available in the international literature witness the favourable effects of adding fine-ground mineral admixtures to cement and concrete. This phenomenon is approached by simulation of rice husk ash (RHA) blended concrete in this study. The simulation results reveal gap grading in the binder to be one of the important underlying mechanisms. The gap graded binder mixture provides better conditions for the fine RHA particles to migrate into the vicinity of aggregate interface, thereby leading to a densely packed ITZ and significant improvement in mechanical performance of concrete. These findings are supported by experimental evidence from similar blending experiments.

Structural evolution of the ITZ is explored in the low range of w/c ratio (say, 0.3), relevant to high performance concrete (HPC). The simulation results reveal that relatively high values of porosity and permeability reported to occur in the ITZ for normal concrete qualities, are limited to the immediate vicinity of the aggregate surface in matured HPC. The disproportional bond strength increase that is detected in the ITZ remains apparent throughout the hydration process. Hence, there is no strong argument to assume significant negative effects of the ITZ on permeability and mechanical properties of concrete in this low w/c range.

<u>In experimental approach</u>

Only 2D section images were available for direct observation and quantitative analysis of actual cement pastes. By making use of SEM images of cement pastes provided by Ye [2003], characterisation of pore structure in hardening cement pastes is realised in this study by image analysis technique on the basis of stereological and mathematical morphological theories. Good agreement is found between section image analysis and computer simulation for stereological parameters such as L_A (perimeter of pore features per unit of test area) and S_V (surface area of pore space per unit of test volume), as well as for a structural parameter like critical pore size.

Pore size distribution curves are obtained by an opening operation of binary images of cement pastes representing different w/c ratios and different hydration stages. The opening distribution results are compared with literature data obtained by conventional mercury intrusion porosimetry (MIP), by Wood's metal intrusion porosimetry (WMIP) and other modeling approaches. The comparison study reveals good agreement between the pore size distribution obtained by mathematical morphology and by proper experimental technique, WMIP.

Relevant structural parameters of pore space are proposed and measured, including porosity, critical pore size l_c, and pore distribution density Γ_{3D}. Pore distribution density is a 3D parameter obtained on the basis of stereological theory, containing information about pore size and pore connectivity. The degree of correlation between these characterising parameters and experimental permeability k was analysed for the purpose of refining the current empirical relationship between pore structure and permeability. Grey system theory was used to evaluate the degree of correlation between k and characterising parameters of pore structure (including p, Γ_{3D}, l_c). The strongest correlation is found to occur between Γ_{3D} and k, followed by critical pore size l_c and porosity p versus k. The integration of Γ_{3D} into Katz-Thompson equation largely improves the prediction capability of this method.

Finally, the local porosity distribution and local percolation probability are analysed with 2D local porosity theory (LPT). 2D LPT is proposed in this study as a superior alternative for the 3D LPT method proposed by Hilfer [1991]. 2D LPT is directly applicable to section image of cement paste, since an appeal is made to stereological tools for data interpretation. To the contrary, 3D local porosity theory can only be applied to a reliable 3D representation (reconstruction) of material structure.

One of the underlying fundamental concepts of materials science, *i.e.* the statistic concept of heterogeneity is explicitly addressed in this study. It is elaborated with respect to composition (*i.e.*, porosity) and to configuration (spacing parameter) of cementitious materials, from which more generalized conclusions are drawn as to design and evaluation of experimental and computer simulation approaches. Among other things, the type of parameter used to define material structure governs linear dimension of the RVE. Also the level of the microstructure incorporated in the RVE is of crucial importance, since the ratio of smallest dimensions involved and the size of the RVE should be similar in a comparative study. Hydration induces continuous changes in the cement microstructure, yielding an RVE for more matured cement paste exceeding in size the one for young cement. When a comparative study would be based on similar volume (or area) elements, heterogeneity in the same type of parameter would, as a result, increase as a function of hydration time.

However, when a comparison between pastes at different hydration stages is performed on the same level of microstructure (at the same proportion to the representative RVEs), resulting in a similar coefficient of variation of the parameter at issue, the local porosity distribution curves would conform to the normal distribution function and when normalised would overlap each other, as demonstrated in this study. This reflects the natural law of the statistical concept of heterogeneity. Thus, this fundamental concept should be a leading principal in the design and evaluation stages of experimental as well as computer simulation studies.

Samenvatting

Met het oog op de mechanische eigenschappen en duurzaamheid van cementgebonden materialen zijn zowel de porositeit als de poriënstructuur van eminent belang. Microstructurele eigenschappen en de ontwikkeling daarin gedurende het verhardingsproces hebben daarom door de jaren heen uitgebreid aandacht gekregen, mede in de context van de relatie tussen materiaalstructuur en eigenschappen. De betreffende problemen zijn experimenteel benaderd of via computermodellering en -simulatie. Niettemin blijft de kwantitatieve karakterisering van de ruimtelijke netwerken van gedeeltelijk verbonden poriën in cementsteen en beton een uitdaging vanwege het complexe karakter van deze problematiek. De betrouwbaarheid van de meeste experimentele methoden is beperkt vanwege de noodzaak aannamen te doen aangaande de geometrie van de poriën; aannamen die de werkelijkheid echter aanzienlijk geweld aandoen. Numerieke modellering van cementsteen en beton kan doorgaans niet tot goede resultaten leiden, wanneer de deeltjespakking niet realistisch gesimuleerd kan worden. Dit laatste verschijnsel treedt op bij de meeste in gebruik zijnde simulatiesystemen die op de generatie van willekeurige getallen gebaseerd zijn. Daarom is in de onderhavige studie gebruik gemaakt van SPACE voor de simulatie van deeltjespakkingen bij jonge cement en beton en van hydratatie. De afwijkingen die in de ruimtelijke verdeling van de deeltjes bij conventionele systemen zou optreden bij de voor cement en beton relevante dichtheden is zeer aanzienlijk.

De evolutie in de poriënstructuur tijdens hydratatie is in deze studie bestudeerd als een functie van technologische parameters als cementfijnheid (korrelgrootteverdeling), water-cementfactor (w/c) en hydratatiegraad. Deze problemen zijn benaderd door gebruik te maken van kwantitatieve beeldanalyse, stereologische schattingstechnieken en methoden van de mathematische morfologie. Stereologische methoden maken het hierbij mogelijk 3D informatie betreffende de materiaalstructuur, zoals volumefractie en specifiek oppervlak van poriën, uit doorsnedenbeelden af te leiden. Stereologisch gedefinieerde afstandsparameters zijn gehanteerd om de ruimtelijke verdeling van vaste fasen te karakteriseren teneinde informatie te verkrijgen over de gemiddelde poriegrootte. Bovendien zijn metingen met behulp van de mathematische morfologie parallel uitgevoerd op modelcementen en op doorsnedenpatronen van echte cementsteen om poriegrootte kwantitatief te kunnen definiëren.

De onderzoeksresultaten kunnen worden gerubriceerd in twee categorieën, namelijk die welke verkregen zijn met behulp van computersimulatie en die welke resulteren uit experimentele aanpak.

<u>Computersimulatie</u>

Representatieve voorbeelden van cementen gemaakt met verschillende water-cementfactoren (w/c) en korrelverdelingen (PSD) zijn geselecteerd uit een groot aantal door Chen [2002] met SPACE gegenereerde modelcementen. Door middel van in SPACE geïntegreerde algoritmen zijn voor jonge cementen belangrijke geometrische parameters gegenereerd, zoals de gemiddelde doorgangslengte $\overline{L}_3$, de afstand tot de naaste buur Δ_3 en de gemiddelde onbelemmerde afstand tussen deeltjes λ. De invloed van de korrel-grootteverdeling en de

water-cementfactor op cementclustering en op de daaropvolgende fase van microstructurele evolutie zijn in een analytische benadering geëvalueerd en becommentarieerd. De morfologische veranderingen in de porieruimte zijn geanalyseerd met behulp van de hierboven aangeduide gemiddelde onbelemmerde ruimte tussen vaste fasen. De depercolatiedrempel voor capillaire porositeit kan geassocieerd worden met die waarde voor de porositeit waarbij de gemiddelde onbelemmerde afstand een stabiele waarde bereikt. De simulatieresultaten leveren een depercolatiewaarde op van 21 ~ 23% voor cementsteen waarbij een cement met normale fijnheid is gebruikt. Meer fijnkorrelige cementen leiden tot hogere depercolatiewaarden vanwege de hogere hydratatiesnelheid en de geringere korrelafstanden, waardoor het afsluitingen van poriën wordt bevorderd. Het onderzoek toont aan dat de korrelgrootteverdeling aanzienlijke invloed uitoefent op de depercolatiewaarde, terwijl de invloed daarop van de water-cementfactor gering is. Deze resultaten blijken zowel goed overeen te komen met uitkomsten van simulaties van Bentz *et al*. [1999], als van experimenten van Parrott [1984] and Powers *et al*. [1959]. De relevantie van deze studie naar depercolatie ligt in de nauwe relatie met transportfenomenen in cementgebonden materialen.

Mechanische eigenschappen (sterkte) en duurzaamheid (dichtheid) van beton worden in bijzondere mate beïnvloed door de porositeit in de overgangszone tussen toeslagkorrels en cement (ITZ). Morfologische en structurele veranderingen in deze overgangszone die het gevolg zijn van technologische parametervariaties zijn stereologisch vastgesteld aan met SPACE gegenereerde korrelstructuren. De veranderingen in deze grenslaag zijn gevisualiseerd met behulp van samenstelling - zowel als opbouwparameters. De dikte van de overgangszone hangt van de gekozen technologische parametercombinatie af, maar ook van het type parameter waarmede de bewuste korrelstructuur wordt gekarakteriseerd. Zo is de gevonden dikte van deze grenslaag bij een samenstellingparameter aanzienlijk kleiner dan bij een opbouwparameter. Dit wordt weerspiegeld door de gradiënten in de twee soorten parameters, waarbij de randstoring in het geval van een opbouwparameter zich relatief ver zal uitstrekken vanaf het korrel - cement grensvlak.

Van de overgangslaag (ITZ) wordt algemeen aangenomen dat deze bij gewone betonsoorten de zwakste schakel vormt in het micromechanisch systeem vanwege de relatief hoge porositeit die het resultaat is van zogenaamde wandeffecten in de korrelpakking. In de internationale literatuur beschreven experimentele onderzoekingen laten het gunstig effect zien van fijnkorrelige minerale toevoegingen aan beton. Dit fenomeen is in deze studie onderzocht door simulatie met SPACE van beton waarin een deel van de Portland cement (PC) was vervangen door rijstkafas (RHA). De resultaten tonen het belang aan van duidelijk verschillende gemiddelde korrelgrootten van PC en RHA. Anders gezegd, de verdelingskrommen van de korrelgrootte moeten elkaar zo weinig mogelijk overlappen (principe van *gap grading*). Onder dergelijke omstandigheden kunnen de fijnere RHA korrels makkelijker migreren door het korrelskelet van PC deeltjes in de nabijheid van toeslagkorrels, waardoor een dichtere overgangszone wordt gevormd met duidelijk verbeterde mechanische eigenschappen. Een en ander wordt ondersteund door onderzoekresultaten op beton gebaseerd op dezelfde combinatie van binderelementen.

De structuurontwikkeling in de overgangszone is eveneens geëxploreerd bij lage water-cementfactoren (ongeveer 0.3), relevant voor beton met hoge duurzaamheid (HPF). De simulatieresultaten tonen aan dat de relatief hoge porositeit en permeabiliteit die zich bij normale betonsoorten in de overgangszone manifesteren zich voor HPC beperken tot de onmiddellijke nabijheid van het grensvlak in het verharde materiaal. De vastgestelde disproportionele verhoging van de hechtingssterkte bij jonge beton in de overgangszone bij de onderzochte lage water-cementfactoren blijft behouden gedurende het verhardingsproces. Hieruit zijn geen argumenten af te leiden die de hier en daar in de internationale literatuur gesuggereerde negatieve effecten van de overgangszone op permeabiliteit en mechanische eigenschappen van betonsoorten met lage water-cementfactoren zouden kunnen ondersteunen.

Experimenten

In dit onderzoek kon slechts gebruik gemaakt worden van 2D doorsnedenpatronen van "echte" cementgebonden materialen voor directe waarnemingen en uitvoering van kwantitatieve beeldanalyse. Aanvullend stonden SEM-opnamen ter beschikking vervaardigd door Ye [2003]. Bovengenoemd materiaal werd in deze studie onderworpen aan beeldanalysetechnieken op basis van methoden uit de stereologie en de mathematische morfologie. Een goede overeenkomst is gevonden tussen experimenteel en via computersimulatie bepaalde waarden voor stereologische parameters zoals L_A (lengte van de omtrek van poriën per eenheid van oppervlakte) en S_V (poriënoppervlakte per eenheid van testvolume), zowel als voor een structurele parameter als kritieke poriegrootte.

Poriënverdelingen zijn verkregen door toepassing van een *opening* operator op binaire beelden van cementsteen, vervaardigd met verschillende water-cementfactoren en met verschillende rijpheid. Deze uitkomsten zijn vergeleken met in de open literatuur beschikbare resultaten van porositeitmetingen met kwik (MIP) en met "Wood's metal" (WMIP) en van andere methoden. Een grote mate van overeenstemming kon worden vastgesteld tussen de computersimulatie-uitkomsten en de resultaten bereikt met WMIP.

Deze studie maakt het mogelijk bepaalde structuurparameters voor het karakteriseren van porieruimte aan te bevelen. Dit betreft de kritieke poriegrootte l_c en de porieverdelingsdichtheid Γ_{3D}. De porieverdelingsdichtheid is een langs stereologische weg bepaalde 3D parameter welke informatie bevat betreffende grootte van poriën en de graad van verbondenheid binnen het poriënsysteem. De correlatiegraad tussen deze, de structuur beschrijvende parameters en de experimentele waarde van de permeabiliteits-coëfficiënt k is in deze studie onderzocht met het oog op verfijning van de huidige empirische betrekking tussen porositeit en permeabiliteit, de zogenaamde Katz-Thompson vergelijking. Met behulp van de theorie van grijze systemen zijn bovenstaande correlaties geanalyseerd voor porositeit, p, Γ_{3D} en l_c. De hoogte van de correlatie-coëfficiënt nam af voor de combinaties k en Γ_{3D}, via k en l_c tot tenslotte k en p. De integratie van Γ_{3D} in de Katz-Thompson vergelijking zou de voorspellende waarde van de methode sterk kunnen verbeteren.

Tenslotte zijn de locale porositeitsverdeling en de locale percolatiekans geanalyseerd met behulp van de 2D locale porositeitstheorie (LPT). 2D LPT wordt in deze studie aanbevolen als een verbeterd alternatief voor de 3D LPT, zoals voorgesteld door Hilfer [1991]. 2D LPT kan direct worden toegepast op doorsnedenbeelden van cementsteen, aangezien de bij de data-interpretatie een appèl wordt gedaan op stereologische methoden. Daarentegen kan 3D LPT slechts effectief worden ingezet wanneer een betrouwbare 3D representatie van de materiaalstructuur ontwikkeld is.

Een van de onderliggende, fundamentele materiaalconcepten, namelijk dat van de statistische heterogeniteit, krijgt expliciet aandacht in deze studie. Het wordt toegepast op onderzoek aan zowel een samenstellingparameter als een opbouwparameter. Belangrijke conclusies voor de inrichting en opzet van studies van experimentele aard of die zich baseren op computersimulatie worden getrokken. De grootten van de representatieve volume-elementen (RVE) zijn daarbij gekoppeld aan de structuurparameter die wordt geanalyseerd. Ook het niveau van de microstructuur, geïncorporeerd in the RVE, is van eminent belang, omdat bij vergelijkende studies de minimumafmetingen hiervan en de grootte van de RVE gekoppeld dienen te zijn. Hydratatie induceert continue veranderingen in de cementsteen. Dit heeft tot gevolg dat de RVE voor rijpere cementsteen grotere afmetingen bezit dan die voor jongere cementsteen. Daardoor zal bij volume-elementen van gelijke grootte de parameter, waarmede beoogd wordt hydratatie-effecten op de materiaalstructuur zichtbaar te maken, een grotere heterogeniteit vertonen bij een rijpere cementsteen.

Wanneer derhalve cementsteen op verschillende tijdstippen op hetzelfde niveau van de microstructuur onderzocht wordt (bij zelfde afmetingsverhouding tot de RVE), blijkend uit een zelfde variatiecoëfficiënt van de bewuste parameter, dan ontstaan gelijksoortige normale verdelingskrommen voor de locale porositeitwaarden, die het natuurlijke heterogeniteitconcept bevestigen. Dit is in de onderhavige studie uitgewerkt. Dit concept zal daarom een leidend principe dienen te zijn bij het ontwerpen en uitvoeren van zowel experimenten als computersimulatiestudies.

(Dutch translation by Piet Stroeven)

Relevant Publications

Journals

- Stroeven P, Hu J, 2004. Stereological tools: strong and mature, but almost terra incognito in concrete technology. Journal of Materials Science, submitted for publication.
- Stroeven P, Hu J, Chen H, 2004. Size effect as globalisation anomaly. Cement Concrete Research, submitted for publication.
- Hu J, Chen H, Stroeven P, 2004. Spatial dispersion of aggregate in concrete: a computer simulation study. Computers & Concrete, accepted for publication.
- Bui DD, Hu J, Stroeven P, 2004. Particle size effect on the strength of rice husk ash blended gap-graded Portland cement concrete. Cement Concrete Composites, in press.
- Hu J, Stroeven P, 2004. Local porosity analysis of pore structure in cement paste. Cement Concrete Research, in press.
- Hu J, Stroeven P, 2004. Depercolation threshold of porosity in model cement; approach by morphological evolution during hydration. Cement Concrete Composites 27 (1): 19-25.
- Hu J, Stroeven P, 2004. Properties of the interfacial transition zone in model concrete. Interface Science 12 (special issue on interfaces in cementitious materials): 387-395.
- Hu J, Stroeven P, 2003. Application of image analysis to assessing critical pore size for permeability prediction on cement paste. Image Analysis & Stereology 22 (2): 97-103.
- Ye G, Hu J, van Breugel K, Stroeven P, 2002. Characterisation of the development of microstructure and porosity of cement-based materials by numerical simulation and ESEM image analysis. Materials and Structures 35: 603-613.

Conferences

- Stroeven P, Hu J, 2005. Reliability of quantitative image analysis of images evaluated by Underwood approach. In: Proceedings of the 9th European Congress on Stereology and Image analysis, May 10-13, Poland, submitted for publication.
- Hu J, Stroeven P, 2005. Size effect in structural analysis of cementitious materials. In: Proceedings of the 9th European Congress on Stereology and Image analysis, May 10-13, Poland, submitted for publication.
- Stroeven P, Hu J, 2005. Damage evolution in compressed concrete. In: Proceedings of the 11th International Conference on Fracture, March 20-25, Italy, accepted for publication.
- Stroeven P, Chen H, Hu J, Zheng J, 2004. ITZ in plain and fibre concrete. In: Proceedings of 6th RILEM Symposium on Fibre-Reinforced Concretes BEFIB' 2004, September 20-22, Italy, accepted for publication.
- Hu J, Stroeven P, 2004. Size characterisation of pore structure for estimating transport properties of cement paste. In: Tadeu A, Atluri SN (eds.), Proceedings of International Conference on Computational & Experimental Engineering and Sciences (ISBN: 0-9657001-6-X), Portugal, paper (ID 146) available on proceedings CD.

- Hu J, Mu R, Stroeven P, 2004. Stereological methodology for damage analysis - application to free-thaw cracking in cement paste. In: Walraven J, Blaauwendraad J, Scarpas A, Snijder B (eds.), Proceedings of 5th International PhD Symposium in Civil Engineering, June 16-19, Delft. Leiden: A.A. Balkema Publishers, pp. 41-48.
- Stroeven P, Hu J, Bui DD, 2004. Particle packing efficiency in concrete. In: Mahmud HB, Akib SM, Ramen S (eds.), Proceedings of 8th International Conference on Concrete Engineering and Technology (CONCET), Malaysia, paper (ID C37) available on proceedings CD.
- Hu J, Stroeven P, 2004. Analysis of correlation between paste permeability and pore structure. In: Mahmud HB, Akib SM, Ramen S (eds.), Proceedings of 8th International Conference on Concrete Engineering and Technology (CONCET), Malaysia, paper (ID C13) available on proceedings CD.
- Stroeven P, Hu J, 2003. Partial cement replacement - effects of particle size. In: Ghavami K (editor), Proceedings of Inter American Conference on Non-Conventional materials and Technologies in the Eco-Construction and Infrastructure (IAC-NOCMAT 2003), Brazil, November 13-16.
- Hu J, Stroeven P, 2003. The extent of the Interfacial Transition Zone; approach by computer simulation. In: Yuan Y, Shah SP, Lu H (eds.), Proceedings of International Conference on Advances in Concrete and Structures, Xuzhou, China. RILEM Publications SARL (Pro 32), pp. 228-235.
- Hu J, Chen H, Stroeven P, 2003. SPACE simulation of particle flocculation in model cement. In: Yuan Y, Shah SP, Lu H (eds.), Proceedings of International Conference on Advances in Concrete and Structures, Xuzhou, China. RILEM Publications SARL (Pro 32), pp. 196-203.
- Hu J, Stroeven P, 2003. The influence of particle size distribution on the microstructure of model cement. In: Brandt AM, Li VC, Marshall IH (eds.), Proceedings Brittle Matrix Composite 7, Warsaw, Poland. Cambridge: Woodhead Publishing, pp. 143-152.
- Hu J, Stroeven P, 2003. Structural evolution during hydration of the interfacial transition zone in model concrete. In: Liu G, Wang D (eds.), Proc. 11th International Congress for Stereology, Beijing, pp. 14.
- Hu J, Stroeven P, 2002. Morphological analysis and modeling of cement structure. In: Setzer MJ, Auberg R, Keck HJ (eds.), From Nano-Structure and Pore Solution to Macroscopic Behaviour and Testing, Proceedings of 2nd International Essen Workshop on Frost Resistance of Concrete. Cachan Cedex: RILEM Publishing, pp. 29-36.
- Stroeven P, Stroeven AP, Hu J, 2002. Particle orientation in ‘Natural’ concrete samples from Antarctica; analysed by automated and macula procedures. In: AMAS Workshop on Image Analysis in Investigation of Concrete SIAIC’02, Warsaw, October 21-23, pp. 55–63.
- Ye G, van Breugel K, Hu J, 2002. Numerically simulated pore structure and its potential application in high performance concrete. In: Proceedings of 3rd DIANA World Conference on Finite Elements in Civil Engineering Applications, Tokyo, October 9-11, pp. 141-148.

Curriculum Vitae

Name:	Jing Hu
Date of birth:	March 8, 1976
Place of birth:	Danjiangkou, Hubei Province, China

2000 - 2004	PhD study at Materials Science and Sustainable Construction Section, Faculty of Civil Engineering and Geosciences, Delft University of Technology, The Netherlands
1997 - 2000	Graduate study of Materials Science at Wuhan University of Technology, China
1993 - 1997	Undergraduate study of Materials Engineering at Wuhan University of Technology, China